The background of the cover is a high-magnification photomicrograph of a volcanic rock. It shows a complex network of dark, irregular veins and fractures cutting through a lighter, more crystalline groundmass. Some of the veins appear to contain elongated, dark mineral grains. The overall texture is highly irregular and fractured.

VOLCANIC TEXTURES

A guide to the interpretation
of textures in volcanic rocks

J. McPHIE
M. DOYLE
R. ALLEN



VOLCANIC TEXTURES

A guide to the interpretation of textures in volcanic rocks

J. McPHIE • M. DOYLE • R. ALLEN

Volcanic Textures is designed for use by exploration geologists, graduate students and other earth scientists with an interest in physical volcanology, especially those engaged in mapping and interpreting volcanic sequences. It is the first in a series to be published by the Centre for Ore Deposit and Exploration Studies at the University of Tasmania that is designed to communicate the latest results of research on ores and their geological environment.

The book provides a practical guide to the description and interpretation of important textures in lavas, syn-volcanic intrusions and a wide variety of volcanoclastic deposits. Many examples come from the Cambrian Mount Read Volcanics, the submarine volcanic host sequence to several world-class polymetallic massive sulfide ore deposits in western Tasmania. These are compared with younger analogues and contrasting subaerial sequences in the USA, Japan, New Zealand, Italy, Central America and South America.

Volcanic Textures contains 46 thematic plates comprising 330 colour photographs, each accompanied by a description

and, where appropriate, an interpretation. The plates are complemented by text that reviews relevant genetic processes and facies relationships. Part 1 gives an introduction to terminology, field identification techniques and classification. Part 2 describes selected textures, components and structures in volcanic deposits. Part 3 focusses on lavas, shallow intrusions and related autoclastic deposits. Part 4 covers pyroclastic and other volcanoclastic deposits with emphasis on transport and depositional processes. Part 5 outlines the textural effects of hydrothermal alteration, especially in the vicinity of massive sulfide ore deposits, using examples in the Mount Read Volcanics.

Jocelyn McPhie lectures in physical volcanology at CODES, University of Tasmania, and conducts field-based research on both subaerial and submarine volcanic sequences. Mark Doyle is a Research Assistant also at CODES. Rod Allen is a Consultant, Volcanic Resources Limited, based at Uppsala, Sweden and has established expertise in the textural effects of alteration in mineralised volcanic terranes.

ISBN 0-85901-522-X



9 780859 015226

Volcanic Textures

A guide to the interpretation of textures in volcanic rocks

J. McPhie

M. Doyle

R. Allen



Centre for Ore Deposit and Exploration Studies
University of Tasmania

The publication of this book would not have been possible without strong support given by the following organisations:

Government of Tasmania
Australian Research Council
University of Tasmania
Aberfoyle Resources
Pasminco Exploration
Renison Goldfields Exploration
BHP Minerals
Geopeko Pancominental Mining
WMC Exploration

©1993 CODES Key Centre

This book is copyright. Apart from any fair dealing for the purposes of private study, research, criticism or review as permitted under the Copyright Act, no part may be reproduced, stored in a retrieval system, or transmitted, in any form or by any means electronic, mechanical, photocopying, recording, or otherwise without prior written permission. Inquiries to be made to CODES Key Centre, University of Tasmania, GPO Box 252C, Hobart, Tasmania 7001.

National Library of Australia Cataloguing-in-Publication entry

McPhie, Jocelyn.

Volcanic textures: a guide to the interpretation of textures in volcanic rocks.

Bibliography. Includes
index. ISBN 0 85901 522 X.

1. Volcanic ash, tuff, etc. 2. Petrofabric analysis.

I. Doyle, M. (Mark). II. Allen, R. (Rodney Leslie), 1958- . III. University of Tasmania. Centre for Ore Deposit and Exploration Studies. IV. Title.

552.2

Design and desktop publishing by June Pongrarz.

Printed and bound in Tasmania by the Tasmanian Government Printing Office.

Contents

Acknowledgements	ix
------------------------	----

Part 1. Interpreting textures: terminology and techniques

The imprint of genetic processes on textures in volcanic deposits	1
Emphasis and organisation	1
An approach to the genetic interpretation of textures in volcanic deposits	3
Two textural categories: coherent volcanic and volcanoclastic	3
Descriptive nomenclature for coherent volcanic and volcanoclastic deposits	7
Graphic logging technique	12
Important textures and structures	15
A summary of the essential features of the seafloor massive sulfide environment.....	15
Introduction to the Mount Read Volcanics15

Part 2. Common components, textures and structures in volcanic deposits

Phenocrysts and porphyritic texture	21
Crystals and crystal fragments.....	22
Vesicles.....	22
Volcanic glass.....	23
Devitrification	24
Spherulites.....	24
Lithophysae.....	25
Micropoikilitic texture.....	25
Perlite	25
Pumice and scoria	27
Achneliths, bombs and blocky juvenile clasts.....	27
Glass shards.....	28
Lithic fragments	29
Accretionary lapilli	29
Fiamme and pseudofiamme.....	30
Flow foliations	30
Joints	31

Part 3. Lavas, syn-volcanic intrusions and related volcanoclastic deposits

Autobreccia.....	54
Talus.....	54
Hyaloclastite	54
Peperite	57
Pillow lavas	58
Subaqueous basaltic lava flows	60
Subaqueous silicic lava flows, domes and syn-volcanic intrusions	61
Subaqueous silicic lava flows and extrusive domes	61
Subaqueous partly extrusive cryptodomes	64

Subaqueous syn-volcanic sills and dykes	64
Volcaniclastic deposits associated with silicic lava dome eruptions in shallow water	65
Case Study: Partly extrusive, submarine, dacite cryptodome, Sock Creek South, western Tasmania.....	66
Subaerial silicic lava flows and domes	66
Subaerial basaltic lava flows	69
Andesitic lavas.....	71

Part 4. Pyroclastic, resedimented volcaniclastic and volcanogenic sedimentary deposits

Genetic classification of volcaniclastic deposits	94
Explosive eruptions and pyroclastic deposits.....	95
Explosive magmatic eruptions.....	95
Phreatomagmatic eruptions.....	96
Phreatic or steam eruptions	96
Resedimented syn-eruptive volcaniclastic deposits	96
Volcanogenic sedimentary deposits	97
Transport and deposition of volcaniclastic particles	97
Mass movement and mass-flow deposits.....	98
Primary pyroclastic flow deposits.....	99
Definition and genesis.....	99
Transport and depositional processes	99
Characteristics of pyroclastic flow deposits	100
Components.....	100
Types of deposits	100
Textures and internal organisation of depositional units	102
Grade	104
Geometry and aspect ratio	104
Dimensions of pyroclastic flow deposits	105
Proximal to distal textural variations	105
Compositional zonation.....	105
Significance of pyroclastic flow deposits.....	105
Subaqueously-emplaced pyroclast-rich mass-flow deposits.....	106
Transgression of shorelines by pyroclastic flows.....	106
Welded ignimbrite interbedded with submarine sedimentary sequences.....	106
Non-welded, pyroclast-rich, submarine mass-flow deposits.....	107
Significance	108
Water-supported and gravity-driven volcaniclastic mass flows and their deposits	109
Turbidites.....	111
Low-density turbidity currents	111
High-density turbidity currents	111
Volcaniclastic turbidites.....	112
Significance	112
Cohesive debris flows, volcaniclastic debris flows and their deposits.....	112
Lahars	113
Volcaniclastic grain-flow deposits.....	114
Volcanic slides, volcanic debris avalanches and their deposits.....	114
Massive sulfide clast-bearing submarine volcaniclastic mass-flow deposits	116
Traction transport and volcaniclastic traction current deposits.....	117
Tractional sedimentary structures.....	117
Characteristics	117
Significance.....	118
Pyroclastic surges and their deposits	118

Characteristics.....	118
Dimensions of pyroclastic surge deposits	119
Significance	119
Suspension transport and volcanoclastic suspension deposits	120
Pyroclastic fall deposits	120
Characteristics.....	120
Water-settled pyroclastic fall deposits.....	121
Suspension sedimentation associated with subaqueous volcanoclastic mass flows.....	121
Sedimentation in volcanic terranes.....	122

Part 5. Alteration: an integral part of textural evolution

Alteration events in the Mount Read Volcanics.....	165
Alteration of lavas, shallow intrusions and related autoclastic breccias.....	166
Original texture	166
Glassy margins	166
Mixed glassy and spherulitically devitrified zones	167
Spherulitic or microlitic cores of lavas and shallow intrusions.....	167
General trends and implications	168
Alteration of pumiceous deposits	168
Originally glassy and permeable deposits	168
Phyllosilicate alteration	168
Two-phase feldspar and phyllosilicate alteration	168
General trends and implications	169
References	181
Index	191

List of Plates

Plate 1—Evenly porphyritic and volcaniclastic textures.....	34
Plate 2—Vesicles and volcanic glass.....	36
Plate 3—Spherulites and lithophysae.....	38
Plate 4—Micropoikilitic texture in rhyolite.....	40
Plate 5—Perlite.....	42
Plate 6—Pumice, scoria, bombs and juvenile blocks.....	44
Plate 7—Shards, lithic fragments and accretionary lapilli.....	46
Plate 8—Flow foliations.....	48
Plate 9—Columnar joints, "tiny normal joints" and tortoise shell joints.....	50
Plate 10—Autoclastic breccia and talus.....	72
Plate 11—Hyaloclastite.....	74
Plate 12—Hyaloclastite.....	76
Plate 13—Hyaloclastite varieties and feeder dykes.....	78
Plate 14—Peperite (intrusive hyaloclastite).....	80
Plate 15—Pillowed lava flows and pillows.....	82
Plate 16—Rinds and crusts on pillow lobes.....	84
Plate 17—Pillows.....	86
Plate 18—Products of silicic lava dome eruptions in shallow water: Bunga Beds, NSW.....	88
Plate 19—Subaerial lava flows and domes.....	90
Plate 20—Textures in glassy, subaerial rhyolitic lava.....	92
Plate 21—Three types of pyroclastic flow deposits.....	124
Plate 22—Geometry and components of pyroclastic flow deposits.....	126
Plate 23—Vapour-phase crystallised and slightly welded ignimbrites.....	128
Plate 24—Welding and granophyric crystallisation textures in ignimbrite.....	130
Plate 25—Lithophysae and Spherulites in welded ignimbrite.....	132
Plate 26—Heat retention in pyroclastic flow deposits and high-grade ignimbrite.....	134
Plate 27—Welded ignimbrite in the Mount Read Volcanics.....	136
Plate 28—Subaqueously emplaced pyroclastic flow deposits: northern Wales, UK.....	138
Plate 29—Volcaniclastic turbidites.....	140
Plate 30—Syn-eruptive submarine volcaniclastic megaturbidite.....	142
Plate 31—Volcaniclastic megaturbidites.....	144
Plate 32—Submarine, lithic-rich, volcaniclastic mass-flow deposits.....	146
Plate 33—Components in subaqueous, volcaniclastic mass-flow deposits.....	148
Plate 34—Deposits from subaqueous volcaniclastic debris flows.....	150
Plate 35—Deposits from subaerial lahars and volcaniclastic debris flows.....	152
Plate 36—Subaerial grain-flow and volcanic debris-avalanche deposits.....	154
Plate 37—Massive sulfide clasts in submarine volcaniclastic mass-flow deposits.....	156
Plate 38—Traction current structures in volcanogenic sediments and pyroclastic surge deposits.....	158
Plate 39—Subaerial pyroclastic fall deposits.....	160
Plate 40—Textures and structures in volcaniclastic deposits from suspension, flotation and traction.....	162
Plate 41—Syn-eruptive volcaniclastic deposits from shallow submarine explosive activity.....	164
Plate 42—Altered coherent lava and related breccia.....	170
Plate 43—Pseudobreccia and altered volcanic breccia.....	172
Plate 44—Altered devitrified silicic lava.....	174
Plate 45—Altered pumiceous volcaniclastic deposits.....	176
Plate 46—Altered and deformed pumiceous volcaniclastic deposits.....	178

Acknowledgements

Production of this book has depended on generous financial support from sponsors of the Key Centre for Ore Deposit and Exploration Studies, in particular, the Tasmanian Department of Mines, Aberfoyle Resources, BHP Exploration, CRA Exploration, Geopeko, Pancontinental, Pasmirico, RGC Exploration and Western Mining Corporation.

Although the material presented comes principally from the collections of JMcP and RLA, we made use of some thin-sections, hand specimens and photographs contributed by colleagues: Stephen Abbott, Guillermo Alvarado, David Cooke, Keith Corbett, Bruce Gemmell, Bruce Houghton, John Waters, Matthew White and Colin Wilson. We are further indebted to Aberfoyle Resources and Pasminco for use of many samples from drillcore stores at Hellyer and Rosebery.

Professor Ross Large initiated the project and provided much appreciated encouragement throughout its realisation. The first draft was substantially revised after reviews by Stuart Bull and Ross Large (CODES), Fergus Fitzgerald (Pasminco Exploration), Malcolm Howells (British Geological Survey), Noel White (BHP) and Hiromitsu Yamagishi (Geological Survey of Hokkaido).

The production team included June Pongratz (design and desktop publishing), Jeanette Hankin and Kirsty Whaley (typing), Debbie Harding (draughting), Simon Stephens and Naomi Deards (thin-section and slab preparation), Fred Koolhof (technical advice and some photography) and Alison Jones (final editing).

Part 1. Interpreting textures: terminology and techniques

The important task of exploring for base metal ore deposits in ancient submarine volcanic sequences begins with geological mapping, which in turn depends on correct identification of outcrops and hand specimens. The text and illustrations that follow are designed to help meet this significant challenge, by providing a guide to the interpretation of common textures and structures in volcanic deposits. *Volcanic deposits* include consolidated volcanoclastic and coherent volcanic rocks, and unconsolidated volcanoclastic aggregates. The examples used are principally from the Mount Read Volcanics in western Tasmania, a deformed, Cambrian, largely submarine volcanic sequence that hosts major massive sulfide deposits (Large, 1992). We have also included, for comparison, examples from other well-exposed and younger, submarine volcanic sequences, and from subaerial volcanic sequences.

The imprint of genetic processes on textures in volcanic deposits

The development of textures in volcanic deposits can be considered in terms of three main stages:

- (1) creation of original textures by eruption and emplacement processes;
- (2) modification of original textures by syn-volcanic processes (oxidation, degassing, hydration, vapour-phase alteration, high-temperature devitrification, hydrothermal alteration);
- (3) modification by post-volcanic processes (hydration, devitrification, hydrothermal alteration, diagenesis, metamorphism, deformation, weathering).

Of overriding importance in the creation of original textures in primary volcanic deposits is the eruption style, in particular whether explosive or effusive (Fig. 1). Explosive eruptions produce a wide variety of *pyroclastic* deposits. Effusive eruptions produce *lava flows* and *lava domes* that comprise coherent and autoclastic facies. A third category of "volcanic" deposits is created by the syn-volcanic emplacement of *cryptodomes*, *dykes* and *sills*, and also includes coherent and autoclastic facies. In active volcanic terranes, whether subaerial or subaqueous, diverse volcanoclastic deposits are generated by non-volcanic processes, specifically by resedimentation coeval with or independent of eruptions and by weathering, erosion and reworking of pre-existing volcanic deposits. These are sometimes referred to as *secondary* volcanoclastic deposits, whereas undisturbed pyroclastic and autoclastic deposits are *primary*. Mechanisms of particle transport and deposition are of great importance in the creation of original textures and structures in pyroclastic, resedimented and volcanogenic sedimentary deposits. Lavas, syn-volcanic intrusions and many types of primary pyroclastic deposits are hot at the time of

emplacement or deposition. Their original textures are almost invariably modified by processes related to cooling. All types of volcanic and volcanoclastic deposits, particularly those that initially contained volcanic glass, can be subject to post-volcanic textural modification.

Emphasis and organization

This guide emphasises the principal genetic processes responsible for the creation of original textures, and the most common syn-volcanic modifications. The organization of the plates and text reflects a process-oriented classification (Fig. 1) that also includes volcanoclastic deposits generated by resedimentation and by purely sedimentary processes. The classification shows the main transport and deposition mechanisms involved in the formation of pyroclastic, resedimented volcanoclastic and volcanogenic sedimentary deposits. It is very important to appreciate that similar mechanisms operate in each of these categories and, hence, similar textures and structures may result.

Components, textures and structures (Part 2) are inherent properties of volcanic deposits and provide the basis for descriptive nomenclature. Some give tight constraints on genetic interpretations but many merely suggest a number of equally valid alternatives. The selection of components, textures and structures in Part 2 is not comprehensive but instead concentrates on features that help distinguish volcanoclastic from coherent volcanic deposits, that survive in ancient sequences and can be recognized in outcrop or hand specimen with a hand lens. Part 3 of the guide describes structures and facies associations in the products of effusive eruptions (lava flows and lava domes) and syn-volcanic, high-level intrusions (sills, dykes, cryptodomes). These are typically associated with autoclastic deposits that are generated by non-explosive fragmentation (quenching, autobrecciation). Part 4 deals with volcanoclastic deposits produced by explosive eruptions (primary pyroclastic deposits), their syn-eruptive resedimented equivalents, and volcanoclastic deposits resulting from surface processes operating on pre-existing volcanic sequences (volcanogenic sedimentary deposits). Correct interpretation of these deposits relies on recognition of (1) structures and lithofacies characteristics that indicate transport and depositional processes; (2) textures and structures that indicate whether or not the particles were hot when deposited; (3) textures of constituent particles that indicate clast-forming processes. Finally, in Part 5, the alteration textures in volcanic sequences that host massive sulfide deposits are reviewed, using examples from the Mount Read Volcanics. An important aim of this part is to show that unraveling the complex web of interrelated processes involved in alteration of volcanic

deposits is critically dependent on knowledge of the original textures and how they form.

The essential features of the four main genetic categories considered here — lavas and syn-volcanic intrusions, pyroclastic deposits, resedimented

volcaniclastic deposits and volcanogenic sedimentary deposits — are summarized in Figures 2, 3, 4, 5. Explanations of all the terms used on these figures for textures, components and processes are given in the corresponding part of the text.

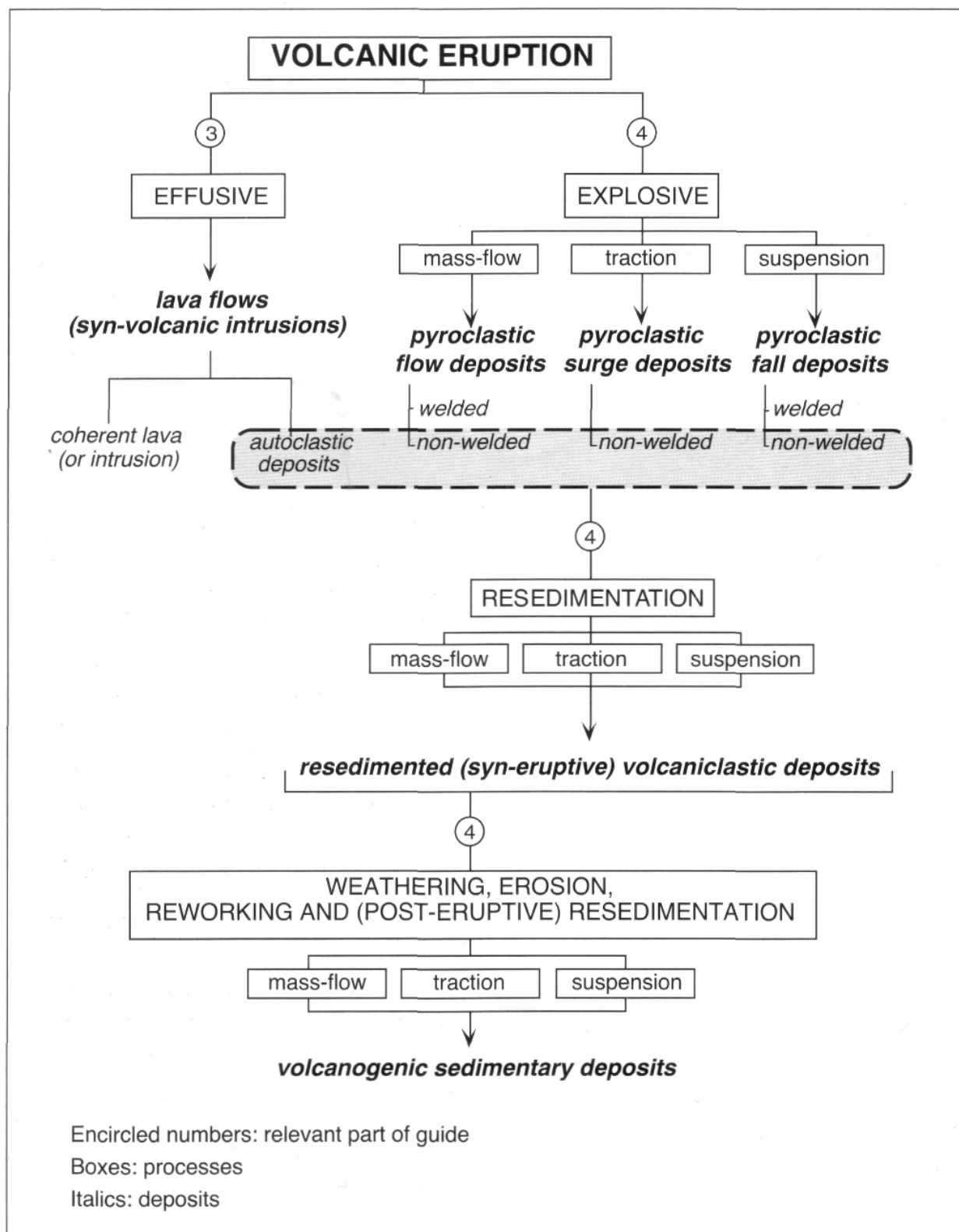


Fig. 1 Genetic classification of volcanic deposits.

An approach to the genetic interpretation of textures in volcanic deposits

Identification and interpretation of volcanic textures involves a blend of process-oriented volcanology and sedimentology, and primarily depends on careful observations made at a range of scales. Proficiency improves dramatically with an awareness of genetic processes and by adopting a systematic approach to description. We therefore emphasize:

- (1) the use of appropriate terminology for the accurate field description of volcanic deposits;
- (2) recording outcrop and drillcore sections by means of graphic logs;
- (3) identification of original volcanic textures, and discrimination of these from textures attributable to alteration, deformation and/or metamorphism;
- (4) recognition of textures and structures diagnostic of emplacement processes, in particular, coherent facies (lavas, intrusions) versus volcanoclastic facies (autoclastic, pyroclastic, resedimented, volcanogenic sedimentary);
- (5) recognition of outcrop features diagnostic of particular depositional settings, in particular, subaerial versus subaqueous environments, and relatively deep versus relatively shallow subaqueous settings.

Two textural categories: coherent volcanic and volcanoclastic

The diverse genetic processes involved in the formation of volcanic deposits result in original textures that can be classified into either of two categories: *volcanoclastic* or *coherent*. The term "volcanoclastic" is descriptive and applies to deposits composed predominantly of volcanic particles (Fisher, 1961). The particles may be any shape and size. No specific clast-forming processes, transport and depositional processes, or settings are implied. Textures in volcanoclastic deposits encompass enormous variation but, in general, are characterized by the presence of separate particles or fragments, of mixtures of a few or many different particle shapes, sizes and types, or, in many cases, of bedding or other sedimentary structures indicating particulate transport and deposition. The four main genetic categories of volcanoclastic deposits (autoclastic, pyroclastic, resedimented and volcanogenic sedimentary) each have sets of distinguishing features and numerous further subdivisions (Parts 3 and 4).

Coherent volcanic textures form from cooling and solidification of molten lava or magma. The most ubiquitous hallmark is porphyritic texture, especially the presence of evenly distributed, euhedral crystals that have narrow size ranges. Aphyric, aphanitic and totally glassy textures are also coherent. Vesicles, flow foliations, spherulites and lithophysae are common in deposits with coherent textures, though not independently diagnostic, and also occur in volcanoclastic deposits. Coherent textures occur principally in lava flows and in intrusions.

There are two additional textural categories that can be

useful, particularly in ancient sequences in the early stages of mapping or logging and in strongly altered rocks. *Apparent volcanoclastic* textures are very common in altered coherent lavas and intrusions, as a result of patchy or domainal alteration or fracture- and joint-controlled alteration (Part 5). The apparent textures in many cases superficially resemble welded ignimbrite or coarse lithic breccia. Some unaltered microspherulitic or micropoikilitic lavas and intrusions also display apparent volcanoclastic textures, and resemble well-sorted, massive sandstone. *Apparent coherent* textures are best developed in some very densely welded primary pyroclastic deposits, especially rheomorphic and lava-like ignimbrites (Part 4). In these, the glassy pyroclasts have completely coalesced and are no longer separately distinguishable, and crystal particles are dominantly complete euhedra. Fine-grained, massive or planar laminated volcanoclastic deposits, such as shard-rich mudstone, may display apparent coherent textures as a result of recrystallization during diagenesis and alteration.

In order for the field geologist to proceed further to appropriate descriptive terminology and, thereafter, to genetic interpretation, it is necessary first to make a decision regarding the textural category, that is, whether volcanoclastic or coherent. As more information becomes available from mapping or thin-section studies, and understanding increases, that initial decision should be reviewed and evaluated.

Descriptive nomenclature for coherent volcanic and volcanoclastic deposits

Isolated outcrops and hand specimens of ancient volcanic rocks rarely exhibit clear and unambiguous evidence of their origins. Because uncertainty is part of the practical reality of working on volcanic sequences, it is advisable to begin with lithological and lithofacies terminology, until there is adequate justification for applying terms that have genetic implications. *Lithological* terminology provides information on composition, components and grain size. *Lithofacies terminology* provides information on facies characteristics evident at outcrop scale in the field, such as structures, internal organization and geometry. *Genetic* terminology provides information on eruption and emplacement processes for primary volcanic and volcanoclastic deposits, and on subsequent redeposition, erosion, transport and depositional processes for resedimented and volcanogenic sedimentary deposits. It also takes into account facies geometry and facies associations at a range of scales, from single eruptive or sedimentation units to entire volcanic centers.

Existing descriptive lithological classifications actually involve implicit distinctions between deposits with coherent and volcanoclastic textures and, in this respect, are also genetic. Having decided whether the texture is coherent or volcanoclastic or, in difficult cases, apparent coherent or apparent volcanoclastic, it is then possible to build descriptive names using combinations of lithological and lithofacies terms (Tables 1, 2). The

naming scheme should be adapted to suit the aims and scale of the textural analysis, the range of compositional variation present, and the state of preservation of the volcanic sequence.

In naming coherent volcanic deposits, the emphasis in available classifications is on chemical composition which, of course, can only be roughly guessed in the field. In most cases, it is possible to distinguish mappable units, so long as the terminology is used con-

LAVAS AND SYN-VOLCANIC INTRUSIONS

coherent facies

- porphyritic texture (evenly distributed euhedral crystals) or aphanitic
- high T devitrification textures common in groundmass (spherulites, lithophysae, micropoikilitic texture)
- internally massive or flow foliated
- non-vesicular ↔ vesicular {
 - pumiceous
 - scoriaceous

 coherent facies

autoclastic facies:

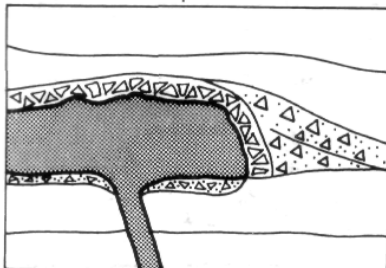
 jigsaw-fit texture

 jigsaw-fit texture, sediment matrix

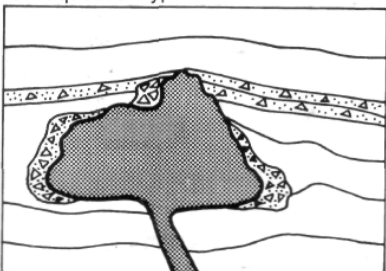
 resedimented

silicic:

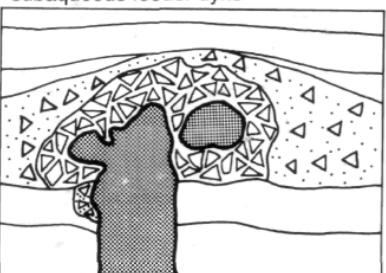
subaerial or subaqueous lava



subaqueous cryptodome



subaqueous feeder dyke



basaltic autobreccia



pillow lava

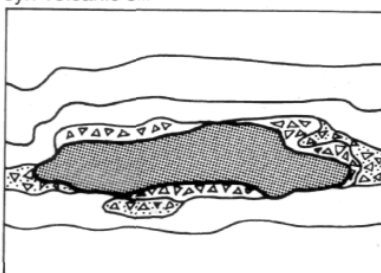


pillow fragment breccia



enclosing sequences

silicic or basaltic:
syn-volcanic sill



autoclastic facies

- monomict
- clasts with porphyritic texture or aphanitic texture
- abundant jigsaw-fit texture

autobreccia

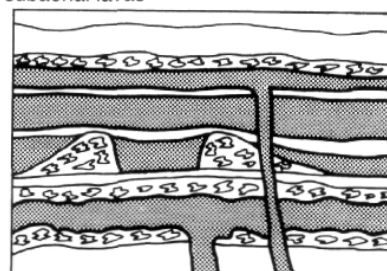
- slabby, flow foliated clasts with jagged ends; ragged or blocky, massive clasts
- clast margins not quenched
- pumiceous or scoriaceous clasts common
- low proportion of clasts finer than 2 mm
- separate crystal fragments uncommon

hyaloclastite breccia

- blocky clasts with curvilinear surfaces
- clast margins have (or had) glassy groundmass; clast interiors glassy or crystallised
- "tiny normal joints" along clast margins
- very coarse sand to granule size (1–4 mm) matrix may be abundant
- separate crystal fragments can be abundant
- pumiceous or scoriaceous clasts may be present

basaltic:

subaerial lavas



subaqueous lavas

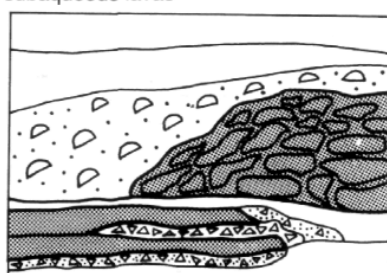


Fig. 2 Characteristics of coherent and autoclastic facies of lavas and syn-volcanic intrusions (Part 3).

sistently, regardless of the absolute accuracy of the terms. If necessary, the composition subdivisions shown in Table 1 can be made more precise by adding percentage limits for the phenocryst abundances. Adjustments can be made to how terms are used, if and when accurate modal or chemical analyses become available. For deposits with coherent and apparent

coherent textures, genetic interpretation will seek to discriminate between lavas, syn-volcanic intrusions, post-volcanic intrusions and very densely welded pyroclastic deposits, and will depend on additional detailed information on textures in thin-section, contact relationships and geometry.

PYROCLASTIC DEPOSITS

deposits from explosive magmatic and phreatomagmatic eruptions:

- composed of crystals, pumice or scoria clasts, other less vesicular juvenile clasts, lithic fragments
- pumice or scoria and other juvenile clasts show porphyritic texture, or are aphanitic
- abundant crystal fragments in matrix
- lithic clasts sparse to abundant

explosive magmatic

- abundant bubble-wall glass shards in matrix
- pumice or scoria clasts usually have wispy or ragged margins, and lenticular, platy or blocky shapes
- accretionary lapilli occur
- welded or non-welded

phreatomagmatic

- abundant blocky and splintery glass shards
- pumice or scoria and other juvenile clasts are typically blocky; curvilinear surfaces common
- accretionary lapilli common
- usually non-welded
- dominantly ash and fine lapilli

deposits from phreatic eruptions:

- composed of lithic pyroclasts; hydrothermally-altered clasts common
- accretionary lapilli common
- small volumes ($< 1 \text{ km}^3$), limited extent ($\leq 2 \text{ km}$ from source)
- mainly fall and surge deposits
- non-welded

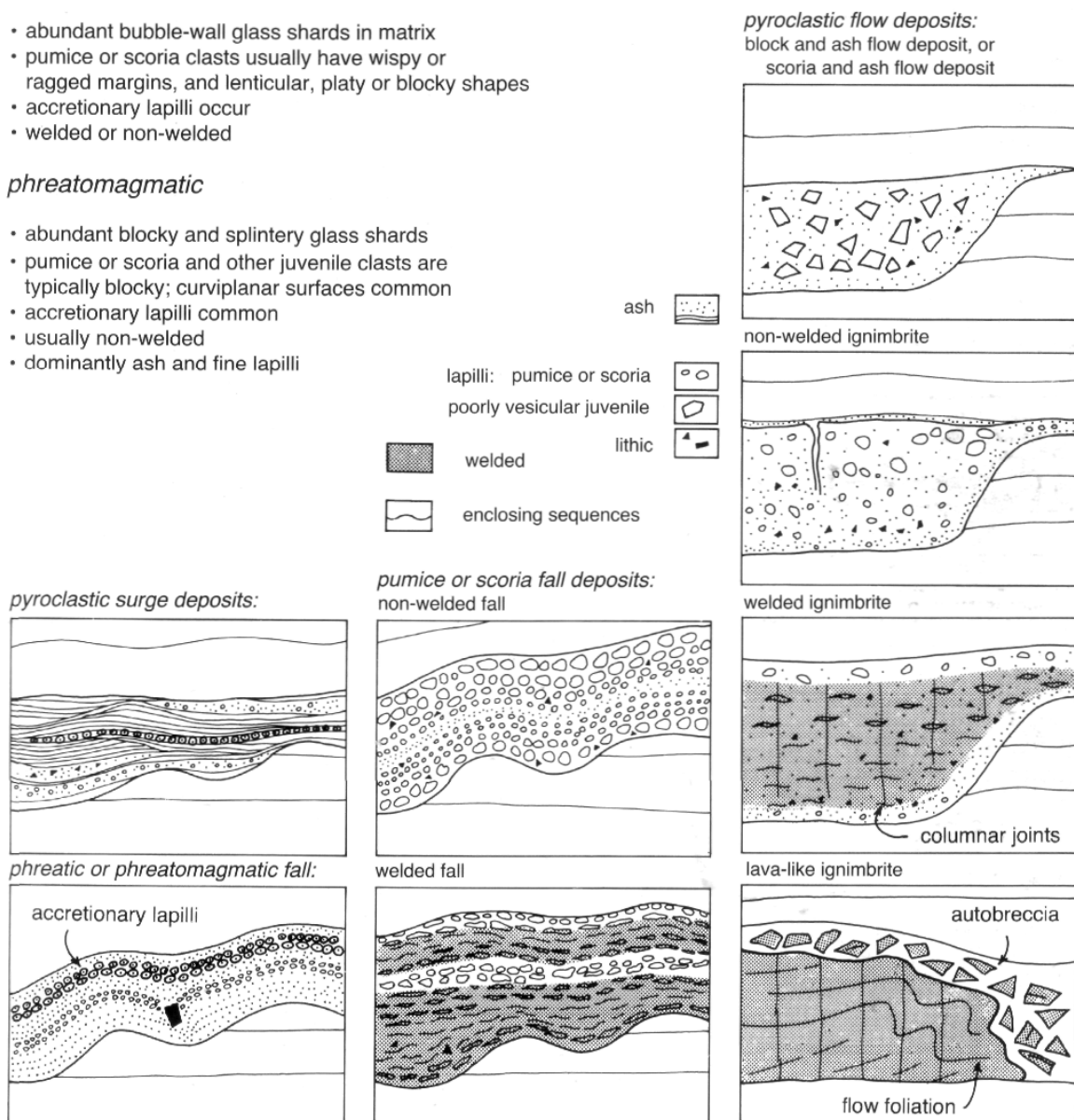


Fig. 3 Characteristics of deposits from explosive eruptions (primary pyroclastic deposits) (Part 4).

The problem of in-built genetic interpretation is more serious for naming deposits with volcanoclastic textures. There is no terminology that applies generally to all volcanoclastic deposits without genetic implications. Relatively non-genetic terms have been borrowed from sedimentology (Fisher, 1961) (Table 2) and, for that reason, are far from satisfactory. In other contexts, these terms are used for epiclastic deposits, and in volcanic terranes, only some of the volcanoclastic deposits have that origin. Furthermore, if these terms are used in a general descriptive sense, they are no longer effective as terms specifically for volcanogenic sedimentary

deposits. Nevertheless, the borrowed terms are the best currently available and will remain so, until the nomenclature problem is solved by agreement among volcanologists and sedimentologists. Out of necessity, the borrowed terms are used in the scheme for building descriptive names for volcanoclastic deposits (Table 2). For these deposits, genetic interpretation seeks to discriminate between four main categories that are based on fragmentation and transport processes — autoclastic, pyroclastic, resedimented syn-eruptive volcanoclastic, and volcanogenic sedimentary (epiclastic volcanic). In each case, there are finer scale genetic

RESEDIMENTED SYN-ERUPTIVE VOLCANICLASTIC DEPOSIT

- dominated by texturally unmodified juvenile clasts
- narrow range of clast types and composition
- sedimentation units and successions of units are compositionally uniform or show systematic changes
- bedforms indicate rapid deposition (mass-flow deposits common)

resedimented autoclastic deposits:

shallow subaqueous:

- mixture of autoclastic and pyroclastic particles
- combination of mass-flow and traction current bedforms
- dominated by clasts coarser than ~2 mm

deep subaqueous:

- poorly vesicular, quenched lava clasts dominant
- mainly mass-flow bedforms
- may have primary dips up to ~25°
- granule - cobble size clasts dominant
- associated with in situ hyaloclastite and coherent lava

resedimented pyroclastic deposits:

- composed of pyroclasts

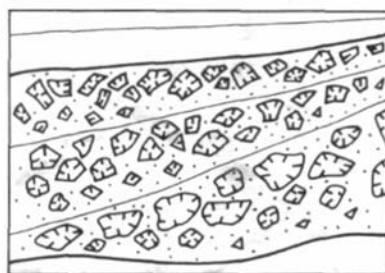
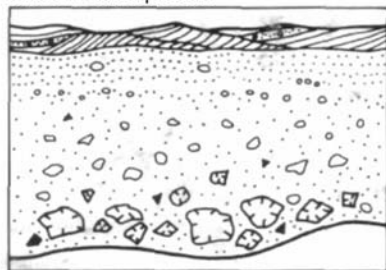
subaerial and shallow subaqueous:

- combination of mass-flow, hyperconcentrated flow and traction current bedforms
- depleted in fine ash

deep subaqueous:





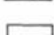
- very thick mass-flow sedimentation units that consist of a massive, crystal- and lithic clast-rich base and a normally graded or stratified, pumice- and shard-rich top
- intraclasts present near base of mass-flow units
- laminated, shard-rich units (settled from suspension)

resedimented autoclastic deposits: shallow subaqueous

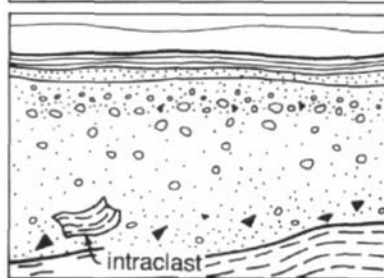
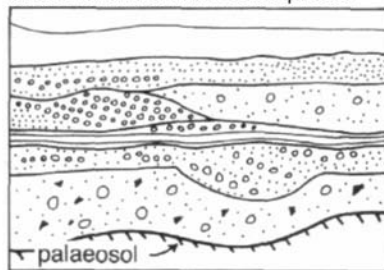


deep subaqueous

clast types:

-  pumice
-  lithic
-  poorly vesicular, quenched juvenile
-  sand and finer, juvenile
-  enclosing sequences

resedimented pyroclastic deposits: subaerial and shallow subaqueous



deep subaqueous

Fig. 4 Characteristics of resedimented syn-eruptive volcanoclastic deposits (Part 4).

VOLCANOGENIC SEDIMENTARY DEPOSIT

mixture of volcanic and non-volcanic clasts
volcanic clasts comprise different compositions and types
volcanic clasts rounded
moderate to good sorting (according to clast density)

subaerial and shallow subaqueous deposits:

- dominated by traction current bedforms

deep subaqueous deposits:

- dominated by mass-flow
- bedforms medium-very thick tabular beds

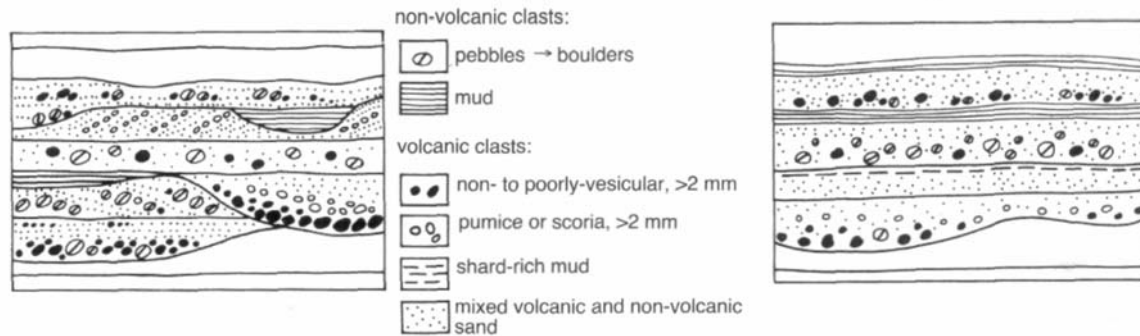


Fig. 5 Characteristics of volcanogenic sedimentary deposits (epiclastic volcanic deposits) (Part 4).

interpretations that imply eruption styles, transport and deposition mechanisms, and depositional environments (Parts 3 and 4). Lithological terms used for primary pyroclastic deposits (Fig. 6; Table 3) are well established, but their use presupposes that interpretation. Note, in particular, that "tuff" is reserved for primary pyroclastic deposits. "Tuffaceous" implies the presence of pyroclasts and is commonly applied to reworked and resedimented pyroclast-rich deposits. There is, at present, no adequate terminology for autoclastic deposits, nor for resedimented syn-eruptive pyroclastic and autoclastic deposits. The terms given in Table 3 are merely those that are frequently used, with some modifications added here for consistency with established grain size classifications of pyroclastic and volcanogenic sedimentary deposits.

Ancient volcanic sequences may contain non-primary mineral assemblages, as a result of hydrothermal alteration or metamorphism. The distinction between these origins is critically important in mineral exploration. For both coherent volcanic and volcanoclastic deposits, descriptive terminology can include alteration mineralogy and distribution (Tables 1,2). Omission of the alteration term implies that the deposit is essentially unaltered. Alteration minerals frequently encountered in volcanic host sequences to massive sulfide deposits are listed below:

Chlorite — a particularly common metamorphic phase in andesitic and basaltic volcanics, but also an important hydrothermal alteration phase in silicic (rhyolitic or dacitic) volcanics in the footwall of volcanic-hosted massive sulfide (VHMS) deposits;

Sericite — results from metamorphism of silicic volcanics, especially volcanoclastic deposits; it is also a major, regionally extensive hydrothermal alteration phase in the footwall of VHMS deposits and related chemical sediments;

Silica — generally typical of hydrothermal alteration of

all compositions but not a common metamorphic phase; **Pyrite** — an important hydrothermal alteration phase that is extensively developed in the footwall of many VHMS deposits;

Carbonate — frequently associated with metamorphism of dacitic, andesitic and basaltic volcanics, and also results from hydrothermal alteration of volcanics in close proximity to VHMS deposits;

Epidote — uncommon as a hydrothermal alteration phase, but typical of metamorphosed andesitic and basaltic volcanics.

Other, less common alteration phases that may be associated with VHMS deposits are albite, K-feldspar, hematite and a variety of clay minerals.

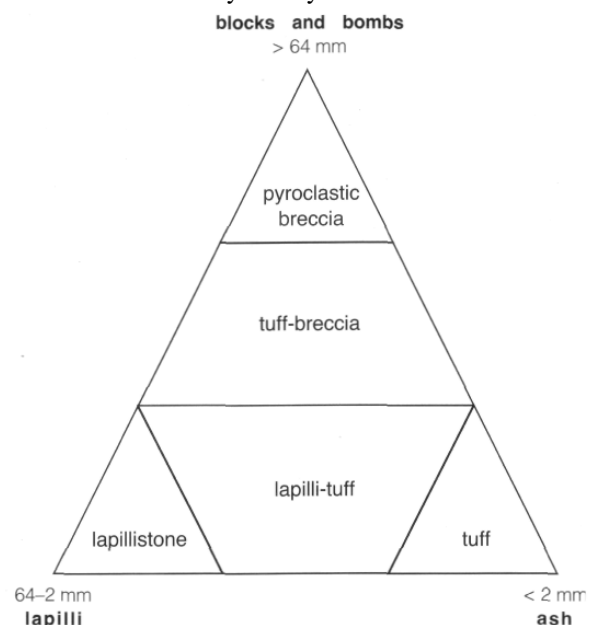


Fig. 6 Grain size terms used for primary pyroclastic rocks (Fisher, 1966b).

Descriptive names for coherent lavas and intrusions

Ideal combination: ④ + ③ + ② + ①
 alteration texture lithofacies term composition

e.g. sericitic, highly quartz-phyric, coarse, flow-banded rhyolite
moderately vesicular, poorly olivine-phyric, fine, columnar jointed basalt

Minimum: ② + ① e.g. blocky jointed rhyolite; massive basalt

 ③ + ① e.g. hornblende-phyric andesite; aphanitic dacite(?)

 ④ + ① e.g. sericite-silica rhyolite(?); chlorite-epidote andesite(?)

① COMPOSITION

a. estimate based on phenocryst assemblage:

- *rhyolite*: K-feldspar \pm quartz (\pm Ca-poor plagioclase \pm ferromagnesian phase: biotite, amphibole, pyroxene, fayalite)
- *dacite*: plagioclase \pm ferromagnesian phase: biotite, amphibole, pyroxene \pm quartz (\pm K-feldspar)
- *andesite*: plagioclase \pm ferromagnesian phase: biotite, amphibole, pyroxene (\pm olivine)
- *basalt*: pyroxene + Ca-rich plagioclase \pm olivine

b. for aphanitic samples, estimate based on colour:

- *rhyolite(?)*, *dacite(?)* : pale grey, pink, cream, pale green
- *andesite(?)*, *basalt(?)* : dark grey, dark blue, dark green, dark purple

② LITHOFACIES

- massive or flow-foliated, flow-banded, flow-laminated
- jointing: columnar, radial columnar, concentric, tortoise shell, blocky, prismatic, platy
- pillows or pseudo-pillows

③ TEXTURE

- porphyritic:
 - a. phenocrysts
 - type (*quartz-phyric ... , pyroxene-phyric ... , etc.*)
 - abundance (*poorly ... , moderately ... , highly ...*)
 - size (*fine ≤ 1 mm, medium 1–5 mm, coarse ≥ 5 mm*)
 - b. groundmass
 - glassy, cryptocrystalline, microcrystalline, very fine grained
- aphanitic: uniformly microcrystalline
- aphyric: no phenocrysts present
- glassy: composed of volcanic glass
- non-vesicular or vesicular (or amygdaloidal): sparsely ..., moderately ..., highly ..., pumiceous ..., scoriaceous ...
- spherulitic, microspherulitic, lithophysae-bearing

④ ALTERATION

- mineralogy: chlorite, sericite, silica, pyrite, carbonate, feldspar, hematite ...
- distribution: disseminated, nodular, spotted, pervasive, patchy ...

Table 1 Descriptive names for coherent lavas and intrusions.

Graphic logging technique

Graphic logging is pictorial representation of sections through sedimentary and/or volcanic sequences. The aim is to record the variations in textures, structures, bedforms, grain size, and contact relationships by a schematic, simplified, pictorial summary. Graphic logging is an especially effective way of representing this information for drillcore sections. The log should remind the observer, at a glance, of the actual deposit

appearance and, therefore, requires disciplined observations, focusing on internal variations, the nature and position of contacts, and relationships between successive parts of the sequence. This style of logging is not only a thorough system for documenting sedimentary and volcanic sequences, but also steers observations toward those features that aid interpretation of emplacement processes and depositional environments. Most standard exploration drill log forms and data sheets are designed for

computer applications and are not suitable for textural analysis and volcanological interpretation.

The format for graphic logs is simple: the vertical axis indicates the depth or thickness and the horizontal axis shows the average grain size. Adjacent space is used for recording younging direction indicators, measurements of structures, maximum particle size, sampling information and a succinct lithological description. Ordinary field notebooks and standard logging forms can both be adapted to this format (Figs 7, 8). Symbols (Fig. 9) are used on graphic logs to convey two sorts of information: composition and texture. Composition symbols represent interpreted chemical composition,

phenocryst size and abundance, and are used for both coherent facies and juvenile, essentially monomict clastic facies. Texture symbols represent the appearance of the volcanic units, including different sorts of components, their distribution and approximate relative abundance. Massive coherent lavas and intrusions can be portrayed just by composition symbols. Juvenile clast-rich volcanoclastic deposits and lava- or intrusion-related in situ breccia can be shown by combinations of composition and texture symbols. Many texture symbols also imply grain size, as they do in sedimentological logs. The symbols for sedimentary structures and for non-volcanic sedimentary rocks are those commonly used in sedimentology.

GRAIN SIZE	VOLCANICLASTIC DEPOSITS IN GENERAL and VOLCANOGENIC SEDIMENTARY DEPOSITS	AUTOCLASTIC DEPOSITS			RESEDIMENTED AUTOCLASTIC DEPOSITS
		Hyaloclastite	Autobreccia	Mixture or uncertain origin	
< 1/16 mm	volcanic mudstone	fine hyaloclastite	?	autoclastic mudstone	resedimented fine hyaloclastite, resedimented autoclastic mudstone
1/16-2 mm	volcanic sandstone	hyaloclastite sandstone		autoclastic sandstone	resedimented hyaloclastite sandstone, resedimented autoclastic sandstone
2-4 mm	volcanic conglomerate, volcanic breccia	granular hyaloclastite	granular autobreccia	granular autoclastic breccia	resedimented granular hyaloclastite, resedimented granular autobreccia, resedimented granular autoclastic breccia
4-64 mm		hyaloclastite breccia	autobreccia	autoclastic breccia	resedimented hyaloclastite breccia, resedimented autobreccia, resedimented autoclastic breccia
>64mm		coarse hyaloclastite breccia	coarse autobreccia	coarse autoclastic breccia	resedimented coarse hyaloclastite breccia, resedimented coarse autobreccia, resedimented coarse autoclastic breccia

GRAIN SIZE	PYROCLASTIC DEPOSITS		PYROCLAST-RICH DEPOSITS	
	Unconsolidated tephra	Consolidated pyroclastic rock	RESEDIMENTED SYN-ERUPTIVE	Post-eruptive resedimented or reworked, or uncertain origin
< 1/16 mm	fine ash	fine tuff	resedimented ash-rich mudstone	tuffaceous mudstone
1/16-2 mm	coarse ash	coarse tuff	resedimented ash-rich sandstone	tuffaceous sandstone
2-64 mm	lapilli tephra	lapillistone (or lapilli tuff or tuff-breccia)	resedimented pyroclast-rich lapillistone, resedimented pumice lapillistone, resedimented pumice and lithic lapillistone	tuffaceous conglomerate, tuffaceous breccia
> 64mm	bomb (fluidal shape) tephra, block (angular) tephra	agglomerate (bombs present), pyroclastic breccia	resedimented pyroclast-rich breccia, resedimented pumice breccia, resedimented pumice and lithic breccia	

Table 3 Grain size-based genetic nomenclature for common types of volcanoclastic deposits. Modified from Fisher (1961) and Schmidt (1981).

The top or base of a section is the most obvious but not always the easiest place to begin logging. A far better approach is to review quickly the entire section, in order to find the least complicated parts, and to start there. Having logged these parts, it is usually possible to progress to adjacent, more difficult intervals until the log is complete. Complex contacts or relationships can be deciphered by constructing supplementary logs at larger scales. The accompanying description consists of lithological and lithofacies terms that summarize essential features and complement the graphic log with additional information; for example, percentage abundances of important components such as phenocrysts, or types of lithic clasts present. In general, each depositional or emplacement unit is logged then described more or less in turn, so it is imperative to devote time to locating contacts. For altered rocks, the description also includes a summary of alteration mineralogy and textures. Graphic logging is very versatile and can be adapted to cater for any special features and relationships. However, it is important to be consistent.

Important textures and structures

A small number of textures and structures are particularly important in deciphering genetic processes and/or setting of volcanic deposits. Early identification of these features thus greatly accelerates progress toward volcanological interpretations; for example:

Porphyritic texture — found in lavas, syn-volcanic intrusions, lava-like ignimbrites and clasts derived from these deposit types (1.1, 1.2);

Spherulites, lithophysae and micropoikilitic texture — indicating high-temperature devitrification of coherent volcanic glass (3, 4, 25.1-2);

Perlite — indicating hydration (or quenching?) of coherent volcanic glass (5, 27.2, 42.6-7);

Accretionary lapilli — formed by subaerial explosive eruptions but may be redeposited and reworked (7.6-8, 22.6, 38.1, 39.6, 40.1);

Flow foliations — found in lavas, syn-volcanic intrusions, and rheomorphic and lava-like ignimbrites (8, 26.3-5);

Columnar joints — found in lavas, syn-volcanic intrusions and primary volcaniclastic deposits (mainly pyroclastic) that are emplaced hot (9.1-3, 26.1-2);

Pillows — found in lavas emplaced subaqueously and intrusions emplaced into wet sediment (15, 16, 17);

Graded bedding — indicating sedimentation from mass flows or suspension (18.1, 30, 31.1, 32.1, 34.2-3);

Planar thin bedding — indicating suspension or traction current deposition (38.1, 38.8, 39.2, 39.5, 40.5-7);

Cross stratification — indicating traction current deposition (38, 40.8, 41.3).

Many components and textures are not strongly diagnostic of particular origins. The most frequently misinterpreted are:

Vesicles — found in lavas, intrusions and non-welded or

very densely welded pyroclastic deposits (2.1-5, 20, 17.2);

Pumice and scoria — produced in abundance by both effusive and explosive eruptions (6.1-7, 20);

Glass shards — found in hyaloclastite, primary pyroclastic deposits, syn-eruptive resedimented volcaniclastic and volcanogenic sedimentary deposits (7.1-3, 12.4, 23, 30. IB);

Fiamme — found in diagenetically compacted, non-welded, primary and secondary pumiceous deposits, and in welded primary pyroclastic deposits (both fallout and flow deposits) (24.1-3, 26.5, 45.7, 46.2);

Pseudo-fiamme — found in a wide variety of deformed and altered volcanic deposits (44.5).

A summary of the essential features of the sea-floor massive sulfide environment

As presently understood, volcanic-hosted massive sulfide mineralization forms in "relatively deep" sea water and is at least spatially associated with volcanic sequences. Although absolute water depths are not easily constrained, appropriate environments are well below storm wave base and are here simply referred to as "deep". The sedimentary and volcanic processes that operate in deep marine settings differ from those that operate in shallow marine and subaerial settings.

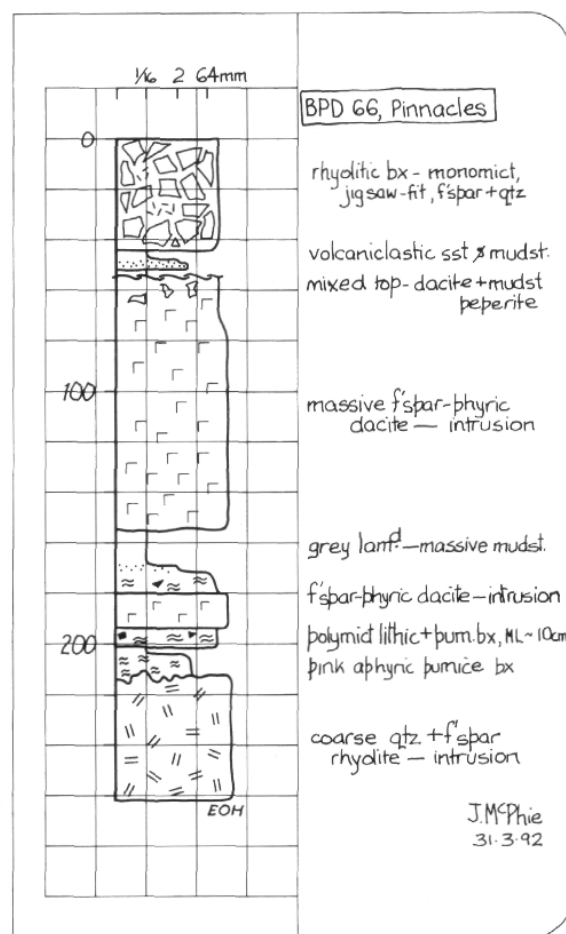


Fig. 7 Example of a drillcore graphic log drawn directly in a field notebook. J. McPhie (unpub. data).

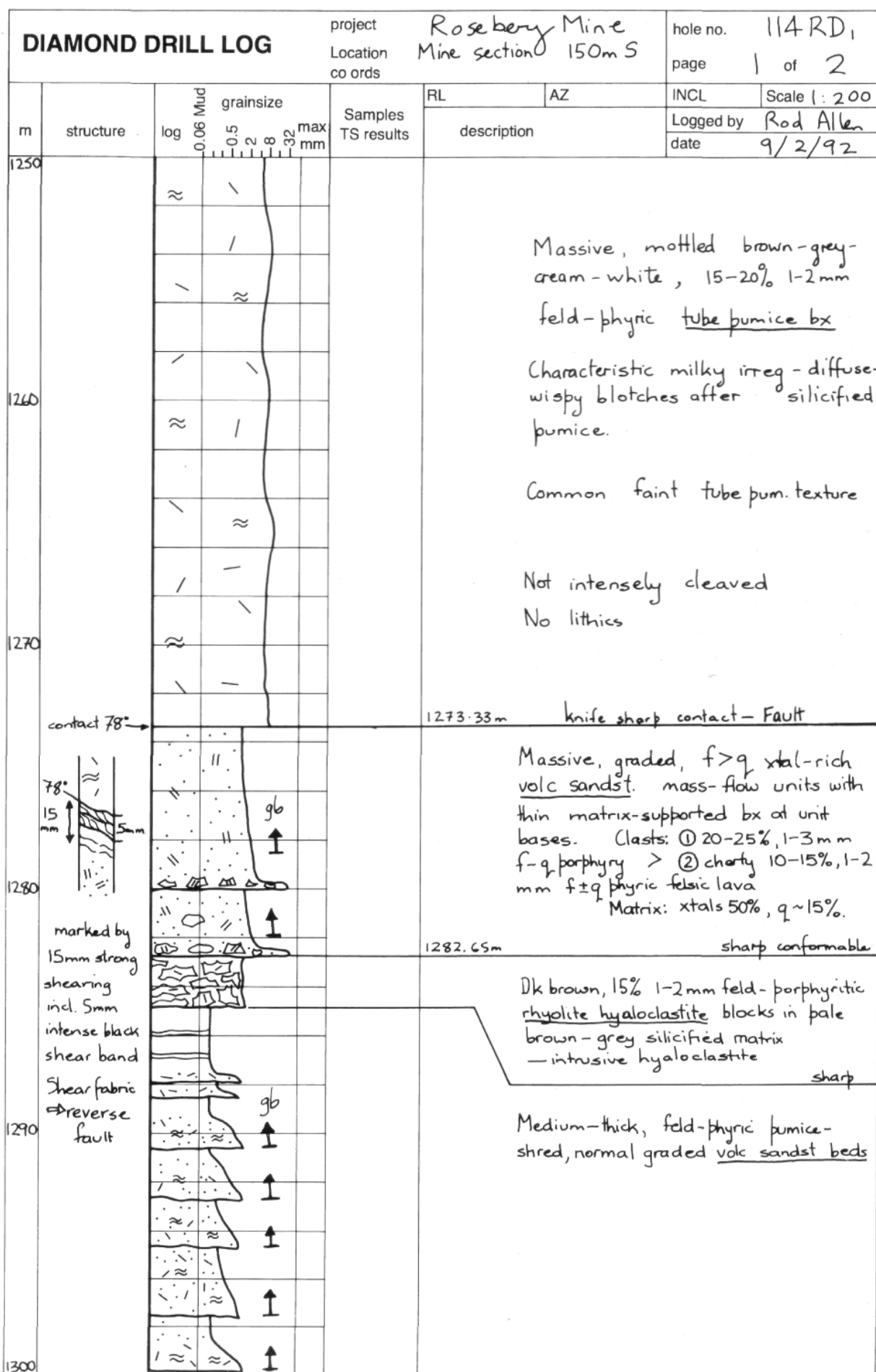


Fig. 8 Example of a graphic log that uses a modified standard logging sheet. R. Allen (unpub. data).

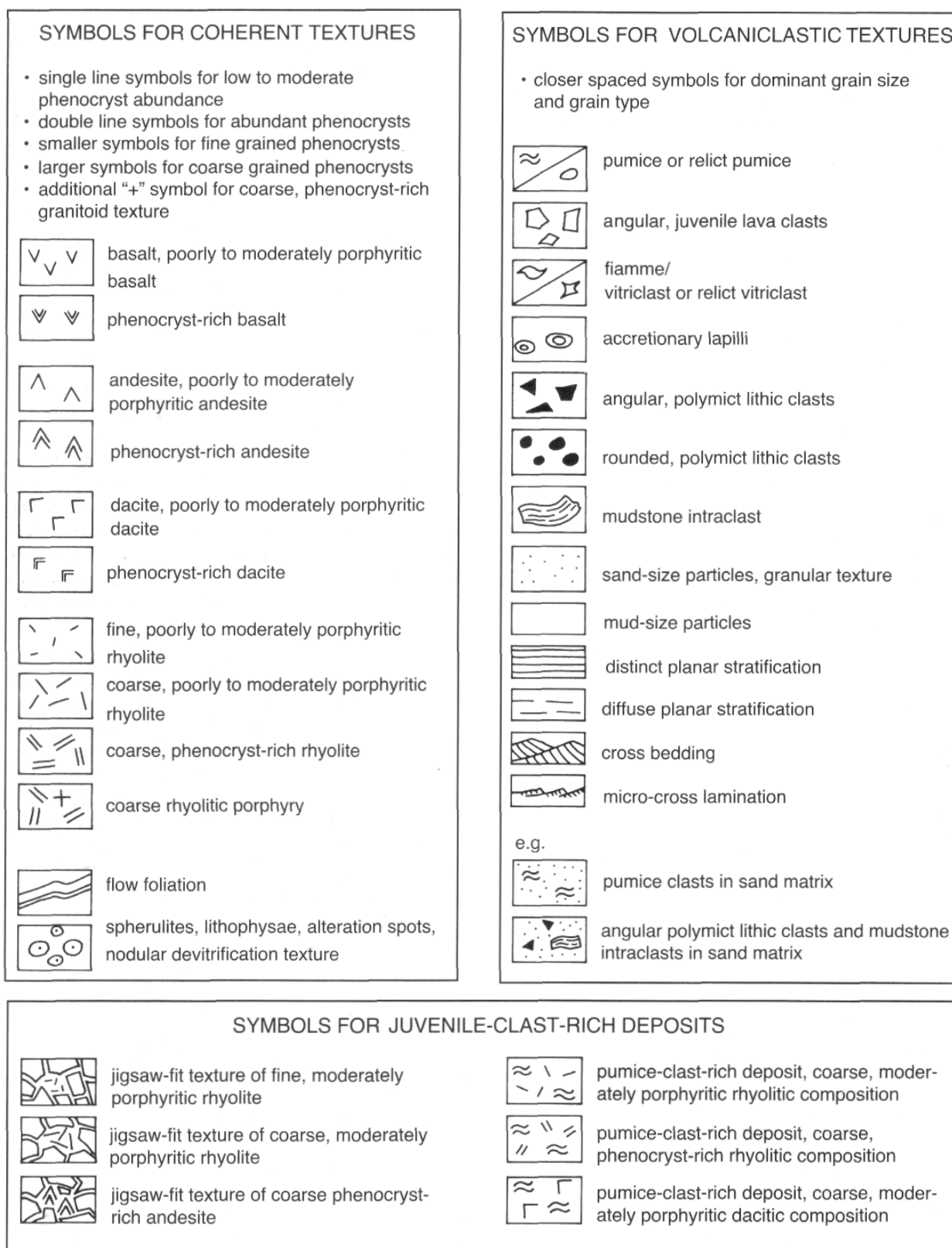


Fig. 9 Recommended composition and texture symbols for graphic logging of volcanic deposits.

Deep submarine volcanic sequences contain deposits from both intrabasinal and extrabasinal (subaerial) or basin-margin (shallow marine) eruptive centers, and are normally mixtures of volcanic and non-volcanic deposits. They include the products of both effusive and explosive eruptions. Syn-volcanic sills, dykes and cryptodomes may be just as common as lava flows. Intrusions and lava flows are associated with

hyaloclastite and peperite, and can develop pillowed and lobate forms. Most clastic deposits, both volcanoclastic and non-volcanic, are emplaced by water-supported mass flows and by fallout from suspension in the water column. Water-supported mass flows are a particularly important means by which subaerially and shallow subaqueously erupted pyroclasts are transported to deep submarine depositional settings, and by which

intrabasinal hyaloclastite is resedimented. Both syn-eruptive and post-eruptive volcanoclastic mass-flow deposits can occur, and are usually associated with volcanoclastic mudstone and siltstone formed by settling from suspension. Studies of ancient sequences suggest that, in general, welded pumiceous pyroclastic deposits are uncommon in below-wave-base environments and restricted to special circumstances that allow heat retention and primary transport in a deep subaqueous setting.

Non-volcanic facies are typically interbedded with the volcanic facies, and are especially important in constraining the depositional environment in cases where the volcanic facies are dominated by very thick massive lavas, intrusions and/or volcanoclastic deposits. Non-volcanic sedimentary facies mainly comprise turbidites and hemi-pelagic mudstone, together with minor biogenic, biochemical and chemical sedimentary deposits. Fossils in intercalated sedimentary facies may also provide independent constraints on the water depth of the depositional setting. In general, the non-volcanic sedimentary facies lack abundant or large traction structures, such as cross bedding, scours, or channels.

Introduction to the Mount Read Volcanics

The Mount Read Volcanics, western Tasmania, consist of compositionally and texturally diverse, Middle to Late Cambrian lavas and volcanoclastic rocks (Corbett, 1992). The volcanics have been affected by regional deformation and metamorphism, and locally hydrothermal alteration is intense. These volcanics are famous worldwide for the abundance and richness of deposits of massive sulfides that they contain (e.g. Mount Lyell, Hercules, Rosebery, Que River, Hellyer — Solomon, 1989; Large, 1992) (Fig. 10). They present a considerable but typical challenge for mapping, textural interpretation and volcanic facies analysis. The Mount Read Volcanics comprise the following lithostratigraphic units: the Central Volcanic Complex, the Western volcano-sedimentary sequences, the Eastern quartz-porphyritic sequence and the Tyndall Group (Corbett, 1992) (Fig. 10). Lavas and syn-volcanic intrusions of the Mount Read Volcanics are predominantly rhyolites and dacites, with locally abundant andesites and basalts, that conform to calc-alkaline trends on geochemical variation diagrams (Crawford et al., 1992).

The principal volcanic facies in the Mount Read Volcanics are (McPhie and Allen, 1992):

Silicic, intermediate, and mafic lavas — lavas are common in the Central Volcanic Complex and occur at many localities in the Western volcano-sedimentary sequences;

Syn-eruptive volcanoclastic deposits — two main types of subaqueous, juvenile clast-rich, volcanoclastic mass-flow deposits occur; one is dominated by poorly- or non-vesicular, blocky lava clasts and related to the subaqueous emplacement of lava flows and lava domes; the other contains abundant silicic pumice clasts produced by subaerial or shallow subaqueous explosive

eruptions and redeposited into deeper water settings;

Syn-volcanic intrusions — largely conformable, emplaced into and locally mixed with wet, unconsolidated host sediments, forming peperite and sill complexes.

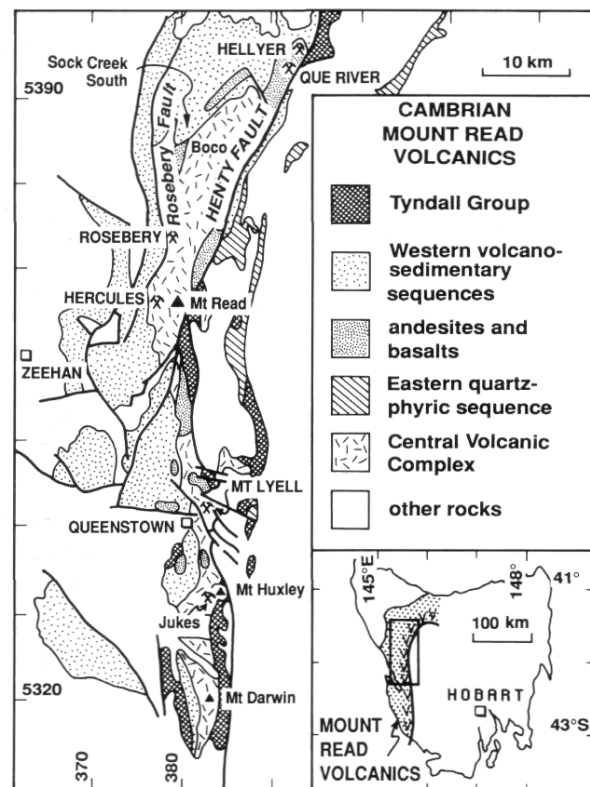


Fig. 10 Distribution of the principal lithostratigraphic formations and major massive sulfide deposits in the Cambrian Mount Read Volcanics of western Tasmania. Modified from Corbett (1992).

These volcanic facies are interbedded with sedimentary facies comprising laminated or massive, black mudstone and graded bedded sandstone turbidites of mixed volcanic and metasedimentary Precambrian basement provenance. Middle Cambrian trilobites and other marine fossils are sparsely distributed in the sedimentary facies (Corbett, 1992).

Given this selection of facies with which to work, an attempt has been made to reconstruct the Cambrian facies architecture of the Mount Read Volcanics (Fig. 11). The best correlation framework for reconstructing facies architecture is provided by volcanic facies that are erupted in large volumes, deposited rapidly, and widespread. Mass-flow-emplaced pumiceous volcanoclastic facies generated by large-magnitude explosive eruptions are the obvious first choice. Some examples in the Mount Read Volcanics have been traced for over 12 km along strike and reveal the presence of syn-volcanic faults that created important sediment traps and environments favorable to sulfide mineralization.

The volcanic host sequences to two massive sulfide deposits in the Mount Read Volcanics, Hellyer and Rosebery-Hercules, are featured in many of the plates (Figs 12, 13). The Hellyer deposit is a typical mound-style (Kuroko type), polymetallic, sea-floor massive

sulfide deposit containing 16 million tonnes grading 7% lead, 13% zinc, 0.4% copper, 160 ppm silver and 2.3 ppm gold (McArthur and Dronseika, 1990). The massive sulfide body is located between a footwall sequence of feldspar-phyric andesitic lavas, with minor volcanoclastic units, and a hangingwall sequence of pillow basalt and black mudstone (Fig. 12). Immediately along strike, the ore position is represented by coarse, polymict, volcanic lithic-rich, mass-flow-emplaced breccia and laminated volcanoclastic mudstone and sandstone (Waters and Wallace, 1992). The massive sulfide body is underlain by an alteration pipe which displays a series of alteration zones and related stringer mineralization (Gemmell and Large, 1992).

The Rosebery deposit is a 25 million tonnes massive sulfide ore body, grading 4.2% lead, 13.8% zinc, 0.6%

copper, 136 ppm silver and 2.4 ppm gold. The deposit comprises a number of sheet-like ore lenses hosted in massive to laminated, pumiceous, rhyolitic sandstone and siltstone, above a footwall of very thick, mass-flow-emplaced pumice breccia (Allen and Cas, 1990; McPhie and Allen, 1992). The footwall sequence is altered and locally strongly deformed to quartz-sericite and chlorite schist containing disseminated pyrite. The hangingwall sequence is dominated by variably crystal-rich or pumiceous volcanoclastic sandstone, and in places includes thin intervals of black mudstone (Fig. 13).

Both these deposits and others in the Mount Read Volcanics were described by Large (1992) and in related papers in the *Economic Geology* Special Issue (1992) on "Australian volcanic-hosted massive sulfide deposits and their volcanic environment".

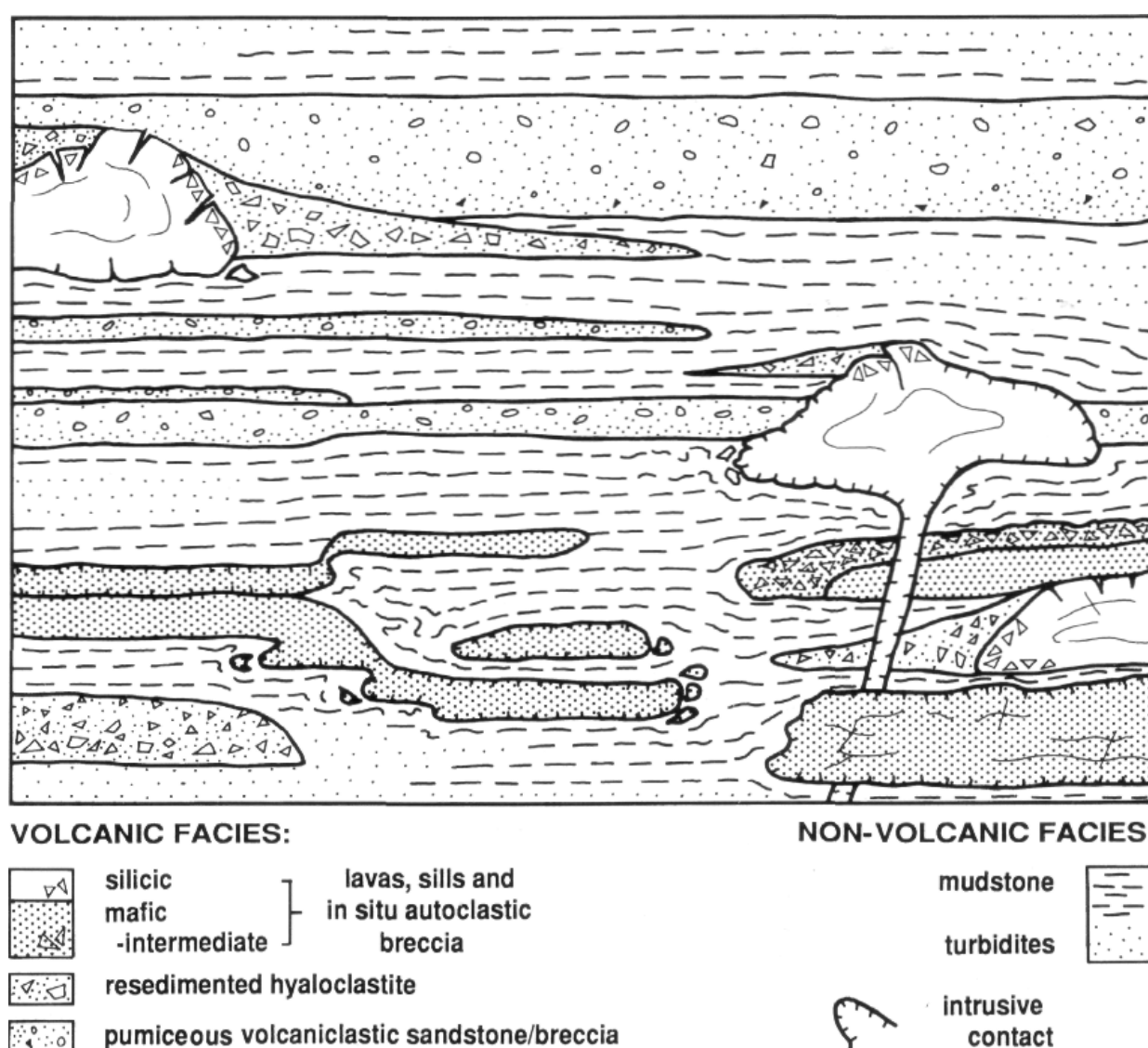


Fig. 11 Schematic facies architecture of submarine volcanic sequences, such as the Mount Read Volcanics, western Tasmania. Volcanoclastic mass-flow deposits include resedimented hyaloclastite from intrabasinal lava flows and domes, and thick, tabular units of pumice breccia that provide good markers for correlation. There are considerable regional variations in relative proportions of lava flows, sills and volcanoclastic units, and in volcanic versus non-volcanic facies. Modified from McPhie and Allen (1992).

Plates :

Graphic log :

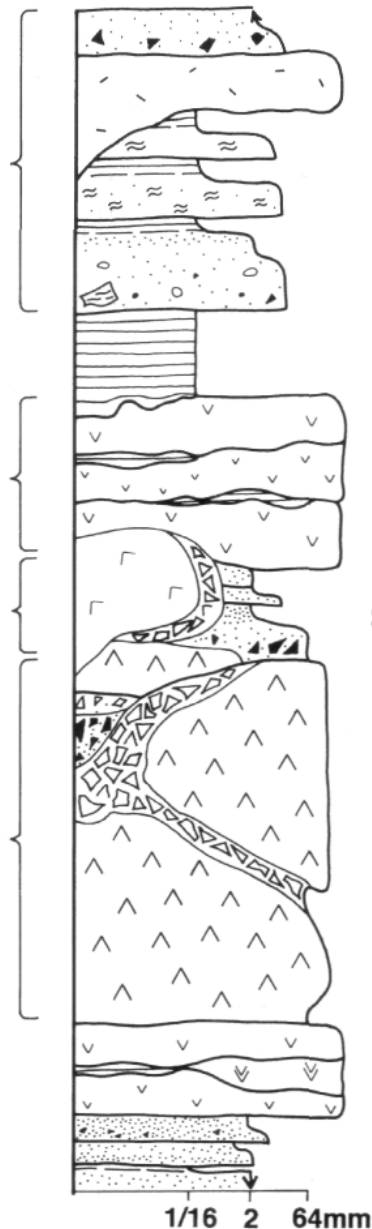
Hellyer stratigraphy :

3.5
33.3, 33.4
33.7, 33.8
45.2

12.8
14.5-14.8
15.5, 15.6
42.8

29.1
33.5
37.5
42.7

12.5
43.4, 43.5



Southwell Sub-group
very thick, massive to graded
pumice breccia; flow banded
rhyolite; volcanic lithic breccia
and conglomerate; black pyritic
and grey micaceous mudstone

Que River Shale
black mudstone

Hellyer Basalt
massive and pillow basalt,
hyaloclastite breccia, peperite;
black mudstone

"mixed sequence"
massive dacite, autoclastic breccia; polymict volcanic
breccia, graded volcanic sandstone; massive sulfide

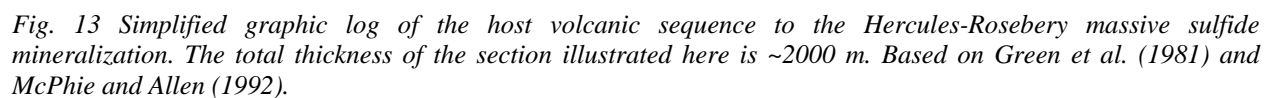
"feldspar-phyric sequence"
massive, feldspar-phyric
andesite; autoclastic breccia;
minor polymict volcanic
breccia

"lower basalt"
pillow basalt, basaltic hyaloclastite

Animal Creek Greywacke
graded, micaceous sandstone
turbidites

Fig. 12 Simplified graphic log of the host volcanic sequence to the Hellyer massive sulfide ore body, western Tasmania. The total thickness of the section illustrated here is ~2400 m. Based on Waters and Wallace (1992) and Corbett and Komyshan (1989).

Hercules-Rosebery stratigraphy :



Part 2. Common components, textures and structures in volcanic deposits

Here we describe and illustrate components, textures and structures commonly encountered in volcanic rocks. The presentation is not comprehensive; rather, we emphasise features that are important for description and interpretation, and that usually survive diagenesis, moderate hydrothermal alteration, low-grade regional metamorphism and deformation. Most can be observed in outcrop or in hand specimens using a hand lens. In isolation, few components, textures or structures are uniquely diagnostic of genetic processes. However, combinations of features provide the basis for distinguishing volcanoclastic deposits from coherent lavas and intrusions, which is the first important step towards interpretation of emplacement processes and setting.

Phenocrysts and porphyritic texture (1)

Porphyritic texture consists of relatively large, euhedral or subhedral *phenocrysts* dispersed in much finer grained or glassy *groundmass* (1.1-2, 8.1). It is characteristic of coherent lavas, syn-volcanic intrusions and clasts derived from these (Part 3). It is one of the most important criteria for distinguishing coherent facies from pyroclastic, resedimented volcanoclastic and volcanogenic sedimentary deposits. *Glomeroporphyritic* texture consists of a small number of phenocrysts clustered together and is also typical of coherent lavas and syn-volcanic intrusions.

Porphyritic texture is generally interpreted to form in magmas that have cooled and solidified in two stages. Some crystals grow during early, slow, subsurface cooling of magma. When the magma erupts, it consists of these already solid crystals (phenocrysts) suspended in melt. Following eruption, relatively rapid solidification of the melt results in formation of the groundmass. In some cases, the melt is chilled to volcanic glass, with or without quench crystals; otherwise the melt crystallizes to a fine-grained aggregate of interlocking crystals.

Phenocryst abundance in coherent lavas and syn-volcanic intrusions ranges from very sparse (1 volume %) up to about 55 volume %. The size range is similarly broad, from about 1 mm to 3 cm. Phenocryst mineralogy, abundance and distribution are, in most cases, reasonably constant within single lava flow emplacement units. These features, therefore, provide a means of distinguishing and mapping different units in a sequence of lavas, and are also the most reliable basis for estimating chemical composition in the field.

Because phenocrysts grow relatively slowly and are suspended in the melt, they are typically euhedral or subhedral, complete and unbroken. However, the original shapes of phenocrysts can be modified if the

chemical or physical environment changes. The main shape-modifying processes are partial resorption, which results in embayed and rounded outlines, and reaction with the melt, which generates rims of fine-grained minerals around the phenocrysts. Quartz phenocrysts in silicic lavas and syn-volcanic intrusions commonly show the effects of resorption. They typically have a bipyramidal habit but are embayed and partly rounded. During rise and eruption of the quartz phenocryst-bearing magma, SiO_2 solubility in the melt increases as the pressure decreases and, as a result, quartz phenocrysts that were initially in equilibrium with the melt are partially resorbed.

Resorption embayments and reaction rims are frequently interpreted to reflect disequilibrium between crystals and melt, and are especially important in the recognition of *xenocrysts*. These are crystals which did not crystallize from the host magma but were accidentally incorporated from a foreign source, such as disintegrating wall rocks. Xenocrysts can comprise mineral phases incompatible with, or atypical of the host magma composition. Mixing of porphyritic magmas shortly prior to eruption also results in disequilibrium textures, complex phenocryst assemblages and heterogeneous phenocryst distributions.

Even in undeformed lavas and intrusions, phenocrysts are sometimes cracked and broken apart (44.2). All the fragments derived from one phenocryst commonly form a cluster that displays jigsaw-fit texture, although some fragments may be rotated and separated from the rest. Phenocrysts in magmas break as result of shear during flowage, rapid vesiculation of the enclosing melt, or pressure release during rise and eruption. In situ fragmentation of phenocrysts may also be caused by quenching and hydration of the host lava or syn-volcanic intrusion.

In most cases, porphyritic texture can be recognized with confidence in the field, in small outcrops and hand specimens, and confirmed readily by examination of thin-sections. However, it is imperative to include all available lithofacies information before concluding that a porphyritic sample belongs to a coherent lava or intrusion or related autoclastic facies. Euhedral, evenly distributed apparent phenocrysts also occur in some lava-like and rheomorphic welded pyroclastic deposits (Henry et al., 1988) (1.4). Although produced by pyroclastic eruptions, the vitriclastic texture in these deposits is almost completely overprinted by welding and high-temperature devitrification of glassy components. Rheomorphic and lava-like pyroclastic rocks at present are known only in subaerial volcanic sequences. Many examples have peralkaline compositions and/or can be inferred to have erupted at

unusually high temperature. Apparent porphyritic texture can also occur in non-welded pumice-rich deposits in which alteration and diagenetic compaction mask the outlines of porphyritic pumice clasts (45.5-6; Part 5).

Crystals and crystal fragments (1)

Crystals and crystal fragments are found in a wide variety of volcanoclastic deposits (1.3, 25.3-4, 32.4-5). They are ultimately derived from porphyritic magmas and from crystalline or porphyritic country rock. Both primary volcanic and surface sedimentary processes of fragmentation can effectively separate crystals from their host, and concentrate them in crystal-rich volcanoclastic deposits (Cas, 1983).

Whole crystals and crystal fragments are liberated during explosive eruptions of porphyritic magma. A small proportion of crystal fragments in pyroclastic rocks may be derived from the disintegration of igneous and metamorphic wall rocks. In pyroclastic deposits, angular fragments of euhedral crystals are typically more abundant than complete euhedral crystals, and show a relatively wide grain size range, the upper limit of which is determined by the maximum phenocryst size in the porphyritic source magma. Crystal fragments, especially euhedra, may have a thin partial selvage of glassy pumice or scoria. Some crystals within pumice or scoria clasts are fractured in situ, and the fragments show jigsaw-fit texture.

Quench fragmentation of porphyritic magma is another means of generating free crystals and crystal fragments, and these can be significant in the coarse sand- and granule-size components of hyaloclastite, especially resedimented hyaloclastite. In situ quench fragmentation of porphyritic lavas commonly affects phenocrysts, producing jigsaw-fit or near jigsaw-fit, monomineralic crystal fragment clusters. Subsequent alteration and deformation of quench-fragmented phenocrysts and glassy groundmass may result in an apparent pyroclastic texture.

Crystals in volcanogenic sedimentary deposits may be derived by reworking and resedimentation of non-welded, crystal-bearing pyroclastic or autoclastic deposits, and by surface weathering and erosion of crystal-bearing volcanic rocks, such as porphyritic lava or crystal-rich welded ignimbrite. Crystal fragments of either origin become increasingly rounded by surface processes, and evidence of the original clast-forming mechanisms may be destroyed. Note that some primary phenocrysts are rounded prior to eruption, due to magmatic resorption.

Crystal fragments are typically confined to, and may dominate the sand or coarse ash grain size of volcanoclastic deposits. The mineral assemblage represented by crystals and crystal fragments in volcanoclastic deposits, especially pyroclastic and mass-flow resedimented syn-eruptive volcanoclastic deposits, strongly reflects that present in the porphyritic source

magma(s), and gives a useful, though rough guide to the source composition. However, the original total abundances and relative proportions of each phase are usually significantly modified during fragmentation and transportation, and are not easily inferred from the abundances and relative proportions of crystal components in the final volcanoclastic deposit. That limitation aside, data on the assemblage, total abundance, relative abundance, size and shape of crystal fragments can provide a very effective and reliable basis for distinguishing and mapping volcanoclastic units in the field. These parameters are approximately constant, or else vary systematically within single emplacement units in primary pyroclastic deposits and also, commonly, within mass-flow resedimented volcanoclastic deposits. Systematic variations in the crystal fragment population may reflect compositional zonation in the source porphyritic magma and/or sorting of crystal fragments according to size or density during transport and deposition (especially common in fallout deposits).

Vesicles (2)

Volatiles exsolved from lavas, shallow intrusions and densely welded tuffs accumulate in bubbles called *vesicles*, that may be permanently entrapped on solidification and preserved. Vesicles are also formed by steam bubbles enclosed in some fine-grained, moist ash deposits generated by explosive eruptions (Lorenz, 1974; Rosi, 1992). *Amygdales* are former vesicles that have been partially or completely infilled with secondary minerals.

Vesicles are common in silicic, intermediate and mafic lava flows, in both subaerial and subaqueous settings (2.1-4, 6.4, 17.4, 20). Variations in their size, shape and abundance in lavas reflect the interplay of several controls, including original magma volatile content and viscosity, rates of decompression and diffusion, coalescence and interference of adjacent vesicles, and deformation during flowage. Some subaerial basaltic flows consist of an upper and sometimes lower vesicle-rich zone, separated by a poorly vesicular interior. The upper zone is broader, more vesicular and contains larger bubbles than the lower zone, probably as a result of coalescence of rising bubbles during solidification (Sahagian et al., 1989). Dimroth et al. (1978) noted an equivalent increase in vesicularity towards the tops of subaqueous basaltic sheet flows in the Archean of Quebec, Canada. A different pattern occurs in "spongy" pahoehoe (Walker, 1989b): vesicles are spherical and increase in size and abundance symmetrically inward from the margins to the centers of lava flow units (19.6). This distribution is interpreted to result from vesicle growth and coalescence in static lava that has appreciable yield strength, and is principally developed in medial to distal parts of subaerial basaltic flows.

Pipe vesicles are slender cylindrical cavities up to several millimeters across and tens of centimeters in length (16.1, 17.2). They are commonly found near the bases of subaerial pahoehoe lava flows (Waters, 1960;

Walker, 1987a; Wilmoth and Walker, 1993), occur in dykes and sills (Walker, 1987b), and are radially distributed in the interiors of pillow lobes (Jones, 1969; Easton and Johns, 1986; Kawachi and Pringle, 1988; Yamagishi et al., 1989; Walker, 1992). Adjacent pipe vesicles in flows occasionally coalesce upward forming an inverted Y; few subdivide upward. In subaerial lava flows, pipe vesicles appear to be restricted to sheets emplaced on very gentle slopes ($< 4^\circ$; Walker, 1987a). Philpotts and Lewis (1987) and Godinot (1988) attributed pipe vesicles to the exsolution of gas into bubbles that are attached to the zone of solidification. As this zone advances into the cooling lava, bubbles continue to grow, forming pipes perpendicular to the solidification front.

Vesicle size and abundance in subaqueously erupted lavas are also affected by the confining pressure exerted by the water column (McBirney, 1963). In some cases, vesicularity of subaqueous lava flows increases systematically upward through continuous sequences comprising multiple flows, presumably in response to decreasing confining pressure (Moore, 1965; Jones, 1969; Moore and Schilling, 1973; Cousineau and Dimroth, 1982). In studies of ancient volcanic sequences, such trends may be useful indicators of shoaling or deepening palaeoenvironments. However, because controls other than water depth are important, vesicularity alone is unreliable as a means of determining absolute water depth, of comparing depths of emplacement of separate lava sequences, and of detecting changes in depth in sequences comprising flows of different composition.

Volcanic glass (2)

Rapid quenching of silicate melts produces solid *volcanic glass*. Volcanic glass may be non-vesicular, partly vesicular or highly vesicular (pumiceous or scoriaceous) (2.5-6, 20, 44.3). Hand specimens of glassy volcanic rocks have distinctive conchoidal fracture surfaces and glassy luster. In thin-section, unmodified volcanic glass is isotropic. However, in some cases quenching includes a short period of very rapid crystallization, and the glass is crowded with quench crystals (20, 25.3). The crystals formed during quenching have a variety of distinctive shapes (e.g. skeletal, dendritic or sickle shapes; plumose or stellate bundles; laths with swallowtail terminations; rods or chains — Joplin, 1971; Bryan, 1972; Cox et al., 1979; Swanson et al., 1989); they may be aligned parallel to flow directions at the time of solidification of the melt. They are found in both non-vesicular and pumiceous, coherent lava flows and in fresh pyroclastic pumice. Quench crystals are commonly, but not invariably microscopic (crystallites, microlites). Quench olivine in some ultramafic lavas forms large (up to a few cm) skeletal bladed crystals (*spinifex* texture).

Crystallization of abundant microlites occurs in response to high degrees of undercooling and supersaturation. Swanson et al. (1989) suggested that such drastic undercooling accompanies early degassing

(loss of H₂O vapour) of silicic melts prior to eruption. Some microlite-poor — microlite-rich banded lavas are, in fact, mixtures of two magma compositions (Gibson and Nancy, 1992), one of which crystallized microlites in the process of attaining thermal equilibrium.

Once formed, both the texture and composition of volcanic glass may be partially or completely modified by a variety of processes. On further slow cooling, or later reheating, primary volcanic glass may devitrify (Lofgren, 1971b). Hydration of volcanic glass generates perlitic fractures. Diagenesis, metamorphism and/or hydrothermal alteration convert the glass to aggregates of new mineral phases such as clays, zeolites, sericite or chlorite.

There are two common types of basaltic glass (Peacock and Fuller, 1928; Fisher and Schmincke, 1984; Heiken and Wohletz, 1985) (2.5, 16.1). *Sideromelane* is isotropic, transparent, colorless or yellow, pristine glass. *Tachylite* is actually partly crystalline and contains abundant Fe-Ti oxide microlites that cause opacity. Low-temperature hydration and alteration of sideromelane converts it to resinous, yellow or brown *palagonite*, with changes to H₂O, FeO/Fe₂O₃, MgO, Na₂O, and some trace elements. Tachylite is less susceptible to alteration because it is composed largely of crystals. Palagonitization of basaltic glass may be very rapid (occurring within years), especially in ash deposits subject to wet and warm conditions, for example, near hydrothermal systems (Heiken and Wohletz, 1985; Jakobsson and Moore, 1986; Farrand and Singer, 1992). More advanced alteration and metamorphism convert palagonite to smectites, ferric oxides, zeolites or chlorite, depending on the pore fluid composition and temperature.

Silicic glass (*obsidian*) is usually transparent, and pale to dark grey or black in hand specimen (20.2-3, 44.3). Diagenesis, low-grade metamorphism and hydrothermal alteration convert silicic glass to fine-grained clays and zeolites. Alteration of silicic glass may involve an initial stage of dissolution of the glass by high pH (> 9) pore fluid, followed by precipitation from solution of fine-grained new minerals. In many cases, silicic glass in ancient volcanic rocks is represented by phyllosilicates (chlorite, sericite) or fine-grained quartz-feldspar aggregates.

Rates of alteration of glassy volcanic rocks are strongly controlled by porosity. Glassy particles in non-welded volcanoclastic rocks are especially susceptible to alteration. Joints, perlitic cracks and quench fractures in coherent glassy lavas and intrusions commonly focus alteration processes.

Devitrification (3, 4)

Glasses are thermodynamically unstable and will eventually devitrify or be replaced by alteration minerals such as zeolites, phyllosilicates or palagonite. Devitrification involves the nucleation and growth of crystals in glasses at subsolidus temperatures. It is a

process that accompanies cooling of hot, coherent glass and, hence, affects lavas, shallow intrusions and densely welded pyroclastic deposits. At least in principle, primary, high-temperature devitrification is distinct from crystallization in response to metamorphism, hydrothermal alteration or weathering. Spherulites, lithophysae, orb texture and micropoikilitic texture composed of fine-grained quartz and feldspar are characteristic products of high-temperature devitrification of silicic glass (Lofgren, 1971a, b). Subsequent recrystallization to a mosaic of quartz and feldspar can destroy or modify the original devitrification textures.

Lofgren (1971a, b; 1974) artificially generated many of the devitrification textures found in natural rhyolitic glasses and identified important controls on the rate and products of devitrification. The rate of devitrification is dependent on temperature and on the presence and composition of aqueous solutions (Marshall, 1961; Lofgren, 1970). In particular, below about 300°C or under dry conditions, or if only pure water is present, rates of devitrification are very slow. The presence of alkali-rich solutions increases devitrification rates by four to five orders of magnitude (Lofgren, 1970). OH in these solutions helps to transform polymeric chains of SiO₂ into separate SiO₄ tetrahedra and allows more rapid diffusion of Na and K; both changes promote crystallization of quartz and feldspar. In addition to the textural changes noted above, devitrification results in significant changes in the bulk rock chemistry, particularly affecting SiO₂, H₂O, Na₂O, K₂O and Al₂O₃ contents (Lipman, 1965; Lofgren, 1970) and, in some cases, trace and rare earth element abundances (Weaver et al., 1990).

Lofgren (1971b) distinguished two textural associations among the devitrification products of silicic glasses. *Glassy-stage texture* consists of glass that contains isolated spherulites (spherulitic obsidian) (44.3). Perlitic fractures and a variety of quench crystallites may be present in the glassy portions. This textural stage reflects rapid cooling and low-temperature (200°C) hydration of relatively dry magma. Devitrification is complete in *spherulitic-stage texture*, in which former glass is crystallized to spherulites and/or micropoikilitic texture (3.2, 4). Relatively slow cooling and

maintenance of higher temperatures, or the presence, of aqueous solutions, especially alkali-rich solutions, favor the development of spherulitic-stage textures. Lofgren (1971b) predicted that glass subject to prolonged heat, pressure and solutions would be granophyric, consisting of fine, equigranular quartz and feldspar, and lacking in textural evidence of the former presence of glass. Central parts of very thick (several tens to hundreds of metres), densely welded ignimbrites commonly display granophyric texture due to slow cooling and crystallization of the formerly glassy components (welded shards and pumice) (24.3-4, 28.5).

Spherulites

Spherulites consist of radiating arrays of crystal fibres (3.1-6, 8.2, 25.3, 25.6, 44.3-7). Each fibre is a single crystal that has only slightly different crystallographic orientation from adjacent crystals. Spherulites are a characteristic product of the high-temperature devitrification of natural glass. In formerly glassy silicic igneous rocks, crystal fibres consist of alkali feldspar and/or quartz (or cristobalite). In mafic rocks, spherulite fibres consist of plagioclase and/or pyroxene.

Spherulites are not spherical throughout their growth history (Lofgren, 1971a; 1974). Lofgren (1971a) demonstrated that the morphology of spherulites in rhyolitic glasses varied according to the temperature of formation (Fig. 14). Spherulites formed at high temperatures (700°C) consist of open clusters of widely spaced crystal fibres. At low temperatures (<400°C), spherulites comprise bundles of radiating fibres. Bow-tie-shaped sheafs of fibres characterize intermediate temperatures of formation (400°-650°C). In addition, crystal fibre width increases with increasing temperature of formation. The internal crystal fibre structure can be recrystallized to a quartz-feldspar mosaic as a result of later alteration, metamorphism or deformation.

Spherulites typically have diameters of 0.1-2.0 cm but may be much larger (e.g. 10-20 cm in welded ignimbrite — Steven and Lipman, 1976). Isolated spherulites are commonly spherical. Adjacent spherulites may impinge on each other and produce elongate trains of spherulites, often aligned along flow layering.

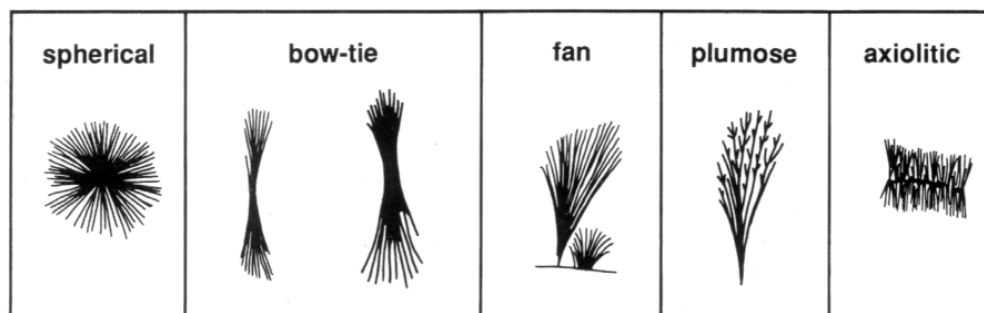


Fig. 14 Spherulite morphologies. Outlines of spherical spherulites are often irregular due to impingement on adjacent spherulites. Bow-tie spherulites consist of two conical bundles of fibres joined at their apices. Plumose spherulites are open, coarse and commonly fan shaped. Fibres in axiolitic spherulites radiate from a line. Modified from Lofgren (1974).

Lithophysae

Lithophysae are spherulites that have a central vug (Wright, 1915; Ross and Smith, 1961) (3.7, 25.1). They begin to grow at an early stage in the cooling history, when the hot glass is still able to deform plastically, and involve nucleation of spherulites on small vesicles. As spherulitic crystallization proceeds, the vesicles are expanded by the exsolving volatiles. The vugs vary from circular to star shaped, and may remain open or be lined or filled with minerals such as agate or chalcedony. Lithophysae range up to larger diameters than spherulites, reaching a few tens of centimeters across. As for spherulites, lithophysae are characteristic products of high-temperature devitrification of coherent silicic glass, and are found in formerly glassy lavas and welded pyroclastic deposits.

Micropoikilitic texture

Micropoikilitic texture consists of small (<1 mm), commonly irregular crystals of one mineral that completely enclose even smaller crystals of another mineral. Micropoikilitic texture comprising optically continuous quartz that encloses laths or spherulites of feldspar is especially common in rhyolites (4) and has been generated artificially in devitrification experiments on rhyolitic glass (Lofgren, 1971b). The same texture was termed *snowflake* texture by Anderson (1969). The optically continuous quartz patches may include several spherulites or be densely crowded with feldspar crystals, so that only a few small inclusion-free areas of quartz are left. The result in hand specimen is a finely granular texture (4.1).

An incipient stage in development of micropoikilitic texture in rhyolite involves poorly segregated quartz-rich patches in the groundmass (4.3-4). Under crossed nicols these patches extinguish concurrently. Further development is reflected in the formation of more pronounced boundaries, visible in both plane polarized light and with crossed nicols (4.5). Abundant feldspar laths that are enclosed in the micropoikilitic quartz show no preferred orientation. In addition, feldspar (and sericite after feldspar) is concentrated at the margins of quartz-rich patches.

In some instances, the cores of the micropoikilitic quartz crystals are free of inclusions and very distinct (4.1-2). The cores extinguish concurrently with the remainder of the micropoikilitic quartz and commonly have highly irregular outlines. Sericite (after feldspar) is concentrated in the interstices between micropoikilitic quartz. The granular ("sugary") texture of the hand specimen (4.1) resembles well-sorted sandstone.

Micropoikilitic texture results from initial devitrification of cooling glass, and develops in both coherent glassy rocks (lavas and shallow intrusions) and densely welded ignimbrites (Anderson, 1969; Lofgren, 1971b). The texture occurs mainly in rocks of silicic composition. Lofgren (1971b) considered that micropoikilitic texture develops through primary devitrification, especially in glasses that have relatively high water contents or are

cooled (or reheated) slowly.

Perlite (5)

Perlite is volcanic glass in which there are abundant, delicate, intersecting, arcuate and gently curved cracks that surround cores of intact glass, generally less than a few millimetres across (2.6B, 5, 27.2D, 42.2, 42.6-7). Perlitic cracks develop in response to hydration of the glass. Hydration involves the diffusion of water into the solid glass, accompanied by a volume increase. Strain associated with hydration is released by means of perlitic cracks. In *classical perlite*, the cracks are distinctly arcuate and concentrically arranged around spherical, non-hydrated cores (Ross and Smith, 1955; Friedman et al., 1966; Allen, 1988) (5.1). In strongly flow-banded glassy lava, perlitic fractures form a roughly rectilinear network, comprising cracks that are subparallel and strongly oblique to the banding (*banded perlite*) (Allen, 1988) (5.2). Hydration occurs after emplacement and late in the cooling history of the glass, or else after complete cooling to surface temperatures. Although perlitic fractures are not primarily the result of cooling (cf. Marshall, 1961), residual stress acquired during cooling is probably partly released when they form (Allen, 1988).

Perlitic fractures can develop in any hydrated coherent glass, including that in glassy lavas, shallow intrusions and densely welded pyroclastic deposits. They may occur in the glassy domains between spherulites in partially devitrified obsidian. Although most commonly found in hydrated silicic glass, perlitic fractures also occur in mafic and intermediate composition glasses. Perlite is usually recognizable with a hand lens but, in some cases, may only be evident in thin-section. Under favorable circumstances, an identical but much larger texture (*macro-perlite*) can be recognized in outcrop (42.6). Yamagishi and Goto (1992) described macro-perlite with cores up to about 6 cm across in Late Miocene submarine rhyolite. They concluded that the macro-perlite formed before other columnar and polygonal joints that also occur in the rhyolite, and primarily as a result of quenching rather than hydration. The rhyolite is apparently not hydrated and does not show micro-perlitic cracks.

Hydration initially affects outer surfaces of glassy lava flows (or shallow intrusions), margins of cracks or joints in glassy lava flows and densely welded pyroclastic deposits, or surfaces of glassy clasts in volcanoclastic aggregates. Hydration proceeds inward along a hydration front defined by strain birefringence, a change in the colour of the glass, and a change in the glass index of refraction (Ross and Smith, 1955; Friedman et al., 1966; Lofgren, 1971b). The water content of obsidian is typically less than 1 wt%, and is considered to be an original component of the magma (Ross and Smith, 1955; Friedman and Smith, 1958). The higher water content of perlite (up to about 5 wt%) is attributed to addition of "secondary" water from external sources, such as ground water or surface water. Measurable changes in alkali contents and in the

FeO/Fe₂O₃ ratio may also accompany hydration (Lipman, 1965; Noble, 1967). The rate of hydration is higher at higher temperatures and in the presence of alkali-rich solutions (Lofgren, 1970), and is also dependent on the glass composition, especially the water content (Friedman and Long, 1976).

Relict perlitic fractures are commonly present in ancient, altered, formerly glassy volcanic rocks. The texture is accentuated by crystallization of secondary minerals in the cracks and by narrow zones of devitrification in the adjacent glass (Marshall, 1961). Alteration of glassy perlitized volcanic rocks can also be focused along the perlitic fractures (42.6-7). In strongly altered rocks, relict perlitic fractures are difficult to recognize and easily overlooked or misinterpreted. Allen (1988) described false pyroclastic textures in altered perlitized lavas from Benambra, Victoria. In these rocks, cusped shard-like shapes are defined by phyllosilicate alteration of parts of the original arcuate perlitic fracture network, or else by the siliceous segments remaining between the altered perlitic fractures (Fig. 15). Correct identification as coherent, formerly glassy lava is favored where there is a gradation from the apparent shard texture to less altered perlite and an association with euhedral, evenly distributed phenocrysts (Allen, 1988).

Pumice and scoria (6)

Pumice is highly vesicular volcanic glass (with or without crystals) (6.1-5). The term *scoria* is usually used for pumice of mafic to intermediate composition (6.6-7). *Reticulite* (thread-lace scoria) is an

exceptionally porous type of mafic scoria (porosity up to 98%).

Vesicles in pumice and scoria vary widely in both size and shape, even in the products from one eruption. Tube pumice is characterized by vesicles with extremely elongate cylindrical shapes that have subparallel alignment, imparting a silky or fibrous or woody texture to the pumice (6.1-3, 46.3-4). Tube pumice forms when vesicles are stretched during flow of vesiculating magma and usually involves silicic compositions, because these typically have appreciable yield strength (Heiken and Wohletz, 1991). Mixed or "streaky" pumice consists of clots, bands, or layers of two or more magma compositions (e.g. rhyolite-basalt) and is especially common in deposits from some small-magnitude pyroclastic eruptions (6.5). The phenocryst content of pumice and scoria ranges from zero to very abundant (more than 40 volume %). Phenocrysts in pumice and scoria have the same textural characteristics as phenocrysts in non-vesicular or sparsely vesicular lavas, being euhedral, evenly distributed and ranging up to about 3 cm in size. A small proportion of phenocrysts within pumice or scoria can be fragmented in situ.

Pumice and scoria pyroclasts are formed by explosive disruption of vesiculating magma. Subaerial coherent lava flows are, in most cases, partly pumiceous or scoriaceous, and are associated with pumiceous or scoriaceous autoclastic deposits (2.1, 20.1, 20.4). Parts of subaqueous silicic lava flows, domes, cryptodomes and associated hyaloclastite can also be pumiceous (Kato, 1987; 1988).

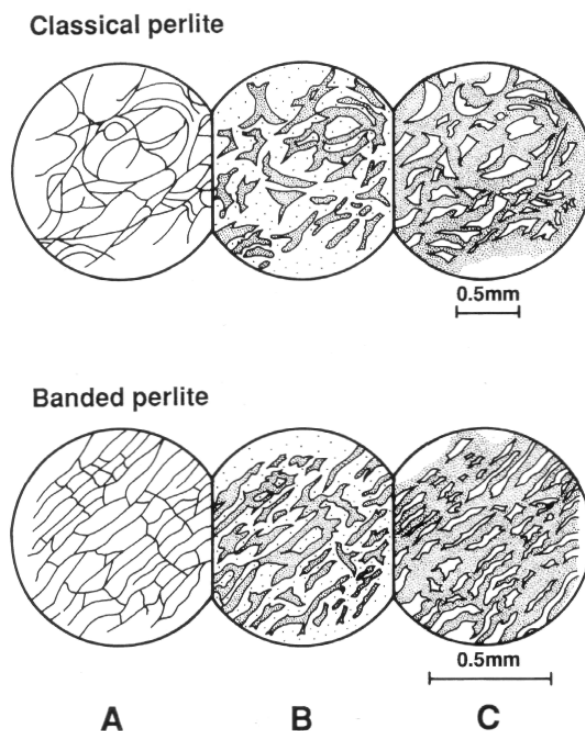


Fig. 15 (A) Original fracture patterns for classical perlite (top) and banded perlite (below). (B) False vitriclastic texture; apparent shards are phyllosilicate-altered sections of the perlitic fractures. (C) False vitriclastic texture; apparent shards are defined by interconnected phyllosilicate alteration along the perlitic fractures. Modified from Allen (1988).

Unmodified pyroclastic pumice or scoria fragments have equant, elongate, platy or irregular shapes, bounded by rough, ragged surfaces. Pumice and scoria lapilli in pyroclastic flow and surge deposits can be appreciably rounded due to abrasion during transport (21.4, 22.7). Autoclastic pumice fragments are blocky or prismatic with planar to curvilinear surfaces. Quench-fragmented tube pumice commonly breaks along surfaces normal to the elongation of the tube vesicles (*woody pumice*). Autoclastic scoria fragments associated with a'a lava have ragged, twisted, spinose shapes. Transport and reworking of pyroclastic or autoclastic pumice and scoria by wind or water result in well-rounded shapes.

Pumice and scoria fragments commonly have densities less than that of water (1.0 g/cm^3) and may float. If pumice fragments from subaerial eruptions are transported to shorelines or deposited on water, they can be transported by flotation in surface currents for thousands of kilometers prior to becoming waterlogged and sinking. Lava domes erupted underwater, for example in caldera lakes or the sea, sometimes have a pumiceous carapace that breaks up into very large blocks, which are buoyant, at least temporarily (Reynolds et al., 1980; Clough et al., 1981; Wilson and Walker, 1985) (40.3-4). Experiments conducted by Whitham and Sparks (1986) suggested that, following an initial rapid uptake of water, cold pumice clasts absorb water slowly, the rate depending on the pumice clast size, initial density, the size and distribution of vesicles, and the extent to which vesicles are interconnected. Conversely, hot pumice clasts can sink immediately, even though they are less dense than water. At low temperatures ($<150^\circ\text{C}$), gas in vesicles contracts and water is drawn in. At higher temperatures, gas within vesicles is flushed out, as absorbed water is converted to steam. On cooling, the steam condenses, more water is absorbed, and eventually the pumice sinks.

Pumice and scoria are prone to alteration and textural modification, even in young deposits. Glass, especially vesicular glass, is rapidly devitrified, crystallized and/or altered. The new minerals may faithfully preserve the vesicular texture or else destroy it completely. Pumice and scoria fragments in strongly welded pyroclastic deposits are compacted to discs of dense glass that may be subsequently devitrified or altered (24.1-2). Pumice and scoria clasts in non-welded pyroclastic deposits and in volcanogenic sediments are commonly flattened parallel to bedding, during diagenesis and lithification (Branney and Sparks, 1990) (45.1-4). If the vesicles are infilled and the glass replaced by silica or feldspar soon after emplacement, then the primary texture can be preserved. Weathering and/or alteration of compacted, matrix-poor pyroclastic deposits, rich in porphyritic pumice or scoria clasts, can obscure clast boundaries and result in an apparent evenly porphyritic texture, similar to that displayed by porphyritic coherent lavas and intrusions (45.5-6). Tectonic deformation commonly results in cleavage-parallel flattening and alignment of relict pumice or scoria clasts, overprinting

any original bedding-parallel foliation.

Achneliths, bombs and blocky juvenile clasts (6)

In explosive eruptions of low viscosity magmas, some pyroclasts are ejected in a molten condition and drawn out into elongate ribbons or aerodynamically-shaped *achneliths* and *bombs* (Macdonald, 1972; Walker and Croasdale, 1972; Williams and McBirney, 1979) (6.8, 39.7-8). These may solidify before deposition and retain their distinctive shapes, or else be flattened into irregular rounded disks on impact. More viscous, degassed and/or chilled magma breaks up into ragged or angular, poorly or non-vesicular, blocky pyroclasts that, in some cases, can be difficult to distinguish from non-juvenile accessory lithic fragments or juvenile clasts produced by non-explosive autoclastic fragmentation. Explosive magmatic and phreatomagmatic eruptions that accompany extrusion of silicic lava domes and flows generate non- to moderately vesicular, angular, blocky pyroclasts, some of which may be flow banded. In some cases, the interiors of bombs and juvenile blocks continue to vesiculate after deposition, causing the chilled outer surfaces to crack in a *breadcrust* pattern (6.8).

Bombs, achneliths and juvenile blocks are important components of welded and non-welded, proximal, subaerial fallout deposits, especially those involving basaltic magma. Bombs are, however, not restricted to subaerial settings. They occur in shallow marine volcanoclastic deposits, as a result of direct fallout from mildly explosive pyroclastic eruptions in shallow water (Staudigel and Schmincke, 1984; Dimroth and Yamagishi, 1987) (13.1), or as a result of downslope resedimentation of primary deposits from littoral or shallow-water fire-fountain eruptions (Dolozzi and Ayres, 1991). Basaltic "welded frothy agglutinate" (Gill et al., 1990), "bombs" and "glassy spatter" (Smith and Batiza, 1989) apparently also occur in modern, deep submarine ($>1700 \text{ m}$) settings, and have been interpreted as proximal deposits from submarine, mildly explosive lava fountaining, associated with especially high effusion rates.

Non-vesicular to moderately vesicular juvenile clasts are generated in abundance by autobrecciation and quench fragmentation of active lava flows and domes (10, 19.1). Clasts produced by quench fragmentation are characteristically blocky and bounded by curvilinear surfaces; margins of such clasts are usually glassy and cut by "tiny normal joints" (Yamagishi, 1987) (9.6). Clasts produced by autobrecciation are typically flow-banded slabs with uneven, angular ends, and/or massive, irregular blocks. The clasts may remain in situ, be re-incorporated into the lava, or be reworked and redeposited by sedimentary processes.

Juvenile magmatic clasts in resedimented syn-eruptive deposits commonly retain their original shape sufficiently well for the clast-forming processes to be established. However, non-welded juvenile magmatic clasts that are reworked and transported by traction

currents rapidly lose the distinctive shapes that allow the original clast-forming process to be determined. Clasts of volcanic rock generated by post-eruptive weathering and erosion of lava flows and domes, and incorporated in volcanogenic sedimentary deposits, will be, in general, significantly rounded. They can be difficult to distinguish from other lava clasts that were formed initially by primary autoclastic fragmentation and subsequently rounded.

Glass shards (7)

Shards are small (generally <2 mm) particles of volcanic glass (7.1-3, 23.2-3). The term is applied to particles generated by explosive fragmentation of magma or lava, by non-explosive quench fragmentation of magma or lava, and by attrition of glassy clasts during transportation (Fisher and Schmincke, 1984; Heiken and Wohletz, 1991). Glass shards or formerly glassy shards commonly dominate the ash grain size class of primary and resedimented pyroclastic deposits, and can also be abundant in volcanogenic mudstone and sandstone.

Three main types of shards are formed from explosive magmatic eruptions (Heiken, 1972; 1974; Fisher and Schmincke, 1984; Heiken and Wohletz, 1991) (7.1-2): *Cusped*, X- or Y-shaped shards — fragments of junctions between vesicles;

Platy shards — flat or curvilinear fragments of the walls separating adjacent large vesicles;

Pumice shards — fragments of microvesicular glass ("micro-pumice").

All three commonly occur together in deposits from a single explosive magmatic eruption. These shapes are significantly modified if the shards remain hot and plastic after deposition. Load compaction of hot, plastic glass particles results in progressive flattening and moulding together of adjacent shards (welding compaction) (24.1-2, 25.3, 27.1B, 27.2C). Shards at the upper and lower margins of rigid particles (crystals and lithic clasts) are typically the most strongly deformed and may be stretched or folded. Particles generated by explosive eruptions involving low viscosity magmas (e.g. mafic and/or high-temperature and/or peralkaline magmas) can stick together on contact (agglutinate) and deform readily during transport and deposition (Branney and Kokelaar, 1992). Matrix textures in such deposits resemble the groundmass textures in coherent lava flows, and separate shards may not be discernible.

Shards in deposits from phreatomagmatic eruptions have diverse shapes, and a significant proportion are more blocky to equant and less vesicular than those from "dry" explosive magmatic eruptions (Heiken, 1972; 1974; Wohletz, 1983) (2.5, 7.3). In these eruptions, shard shape is complexly dependent on the physical properties of the melt (viscosity, surface tension, and yield strength), the rate of heat energy release, and the vesicularity of the melt prior to interaction with external water. Bubble-wall shards are generated if the magma is significantly vesicular prior to

mixing with external water. Simultaneous quenching and spalling may produce blocky or splintery shards. Magma particles that remain ductile develop smooth fluidal surfaces during turbulent mixing with water or steam. The influence of water during phreatomagmatic eruptions usually fluctuates. The resulting deposits commonly include shard shapes typical of both explosive magmatic and phreatomagmatic fragmentation processes.

Glass shards may be an important component of autoclastic deposits, especially hyaloclastite. Shards generated by quench fragmentation have blocky, cuneiform or splintery shapes, and surfaces are planar or curvilinear (12.4). Hyaloclastite shards are typically non-vesicular or poorly vesicular, and shard surfaces cut across vesicles. Basaltic hyaloclastite shards are especially prone to alteration and, even in young deposits, sideromelane is commonly replaced by palagonite.

Deposits composed mainly of glass shards or formerly glassy shards, have *vitriclastic* texture in thin-section (23.1B, 24.2B, 30.1B). The texture can survive the effects of devitrification and diagenetic or hydrothermal alteration of the glass. Axiolitic fibres are especially characteristic of relatively high-temperature devitrification of shards in welded pyroclastic deposits that have cooled slowly (25.4B). In these, shard outlines are typically well preserved. Shard outlines can also remain after alteration of the glass to palagonite, zeolites, quartz or feldspar, and are most easily recognized in plane polarized light. Alteration of shards to "weak" phyllosilicates is less favorable for long-term preservation of the distinctive shard shape, and dissolution of glass in warm porous pyroclastic deposits can result in complete obliteration of the vitriclastic texture.

Lithic fragments (7)

Lithic fragments are clasts derived from pre-existing rocks, including both volcanic and non-volcanic types. They are an important and common component of volcanoclastic aggregates (7.4). In general, but not invariably, lithic fragments are absent or sparse in lava flows and syn-volcanic intrusions (7.5). In volcanic terranes, the two main processes that produce lithic fragments are explosive eruptions, and surface weathering and erosion of pre-existing rocks (volcanic and non-volcanic). Fragments produced by the latter process are genuine epiclasts.

Three types of lithic fragments occur in pyroclastic aggregates (Wright et al., 1980) (22.3-5, 25.4A, 26.3, 39.3-4):

Accessory lithic pyroclasts — fragments of country rock dislodged from the conduit walls and vent during explosive eruptions;

Accidental lithic clasts — fragments eroded or collected from the substrate by pyroclastic flows or surges;

Cognate lithic pyroclasts — juvenile fragments derived from solidified parts of the erupting magma, such as

degassed crusts on lava ponded in the vent, or magma chilled against the conduit walls, or portions of the magma already crystallized in the magma chamber.

In ancient primary and resedimented pyroclastic rocks, the three types can be difficult to distinguish. Cognate and accessory lithic pyroclasts are typically angular, whereas the roundness of accidental lithic clasts varies widely and depends on their source and prior transportation history. Accessory lithic pyroclasts are commonly, but not invariably volcanic. Cognate lithic pyroclasts are co-magmatic with other juvenile pyroclasts but differ texturally, depending on their source. Those derived from early-crystallized portions of the magma consist of aggregates of interlocking, medium- or coarse grained crystals (25.4A). Those derived from chilled and degassed portions of the magma are non- or poorly vesicular, and glassy or very fine grained. Accidental clasts can be composed of any rock type or of unconsolidated cohesive sediments.

Surface processes (mass-wasting, physical and chemical weathering, erosion) also generate lithic clasts that may subsequently be incorporated into volcanogenic sedimentary deposits, or into pyroclastic flow and surge deposits, or into lava flows. In subaerial volcanic terranes, surface processes are a very important source of lithic clasts. In subaqueous settings, the principal non-volcanic lithic-clast-forming process is mass-wasting; for example, gravitational collapse of unstable parts of lava domes and flows, and rockfall adjacent to active fault scarps.

Lithic fragments generated by mass-wasting are in most cases angular and may exhibit in situ fracture patterns. Reworking of epiclastic lithic fragments generally results in appreciable rounding. Autoclastic fragments and volcanic lithic pyroclasts that are subsequently reworked and rounded become texturally indistinguishable from volcanic lithic epiclasts. Precisely constrained facies relationships may be the only means of recognizing the primary volcanic origin of such clasts once they are incorporated in volcanogenic sedimentary deposits.

Accretionary lapilli (7)

Accretionary lapilli are spheroidal lapilli-sized aggregates of ash, recorded sizes of which range from 3 or 4 mm to more than 10 cm (7.6-7). There are two textural types of accretionary lapilli (Moore and Peck, 1962; Reimer, 1983; Schumacher and Schmincke, 1991):

- (1) those with a core of coarse-grained ash, surrounded by a rim of finer grained ash (*rim-type*); rims may be graded, with grain size decreasing towards the margin, or else consist of alternating layers of fine- and very fine-grained ash; in some cases, lapilli have multiple rims but lack a well-defined core;
- (2) aggregates of relatively coarse ash without a finer grained rim (*core-type*).

Small (<1 mm) vesicles frequently occur in the coarser

ash cores of accretionary lapilli. *Armoured* or *cored lapilli* consist of crystal-, pumice-, or lithic-fragment nuclei coated by fine to coarse ash (Waters and Fisher, 1971) (7.8). Large accretionary structures, termed *armoured mud balls* (Dimroth and Yamagishi, 1987), occur in some Miocene submarine volcanoclastic mass-flow deposits in Japan. These have a mudstone intraclast nucleus that is surrounded by concentric shells of pumiceous ash, and are 6-10 cm in diameter.

The formation of accretionary lapilli usually involves suspended ash and moisture. Suspended ash particles begin to aggregate as a result of electrostatic attraction and particle collision, and are held together by surface tension of condensed moisture, electrostatic forces, particle interlocking and growth of new minerals as the condensed moisture evaporates (Reimer, 1983; Schumacher and Schmincke, 1991; Gilbert et al., 1991). Electrostatic attraction is especially important in the formation of fine-grained outer rims. Accretionary lapilli also form when rain falls through an otherwise "dry" ash cloud (Walker, 1971; Macdonald, 1972). Some accretionary lapilli are thought to develop when raindrops, moist lithic clasts or crystal fragments fall on and roll across freshly deposited ash (Walker, 1971; Reimer, 1983).

Most accretionary lapilli form in subaerial environments. They are common in a wide variety of primary pyroclastic deposits, especially those from phreatomagmatic eruptions; for example, surge deposits of tuff rings; pyroclastic flow and fall deposits from large silicic, phreatomagmatic eruptions (phreatoplinian eruptions); fall deposits from ash clouds that accompany pyroclastic flows and surges (co-ignimbrite and co-surge ash). Accretionary lapilli have also been recorded in gas segregation pipes in ignimbrites (Self, 1983) (22.6) and in subvolcanic intrusive breccia complexes (Wormald, 1992). The best guide to interpreting the origins of accretionary lapilli is the field relationships. Details of their internal structures and grain size characteristics may help in determining their mode of formation (Schumacher and Schmincke, 1991).

Accretionary lapilli in fall deposits (co-surge, co-ignimbrite, phreatoplinian) are commonly concentrated in layers within discrete, widespread ash beds (39.6). The lapilli are well-sorted, may be flattened parallel to bedding, and are either whole or broken in situ. Relatively loose packing of ash particles in the lapilli results in high porosity and low density. In surge deposits, accretionary lapilli may be concentrated on the lee-side of obstacles and dune crests (Fisher and Waters, 1970) and armoured lapilli are common. Accretionary lapilli may be generated in relatively dilute ash clouds that are associated with pyroclastic flows, and deposited in ash-rich beds at the tops of the related flow deposits. Accretionary lapilli within pyroclastic flow deposits are usually widely dispersed and may be broken or abraded (McPhie, 1986). Packing of ash particles in accretionary lapilli found in pyroclastic surge and flow deposits is relatively tight and results in somewhat higher densities. Although formed principally in subaerial environments,

accretionary lapilli may be deposited, redeposited or reworked in subaqueous settings. Fresh accretionary lapilli that are rapidly cemented and hardened can survive immersion in water and can be preserved in water-settled fall deposits (Fiske, 1963) (40.1) and syn-eruptive subaqueous volcanoclastic mass-flow deposits (Heinrichs, 1984; Dimroth and Yamagishi, 1987). Subaerially deposited accretionary lapilli may be reworked by fluvial processes (Self, 1983) (38.1) and/or redeposited to subaqueous settings (Bateson, 1965).

Fiamme and pseudofiamme

The term *fiamme* has been applied to glassy lenses with flame-like shapes in welded pyroclastic deposits (24, 26.5, 28.5). Alignment of the long dimensions of the glassy lenses defines a bedding-parallel foliation attributed to welding compaction of presumed formerly vesicular juvenile clasts (*eutaxitic* texture). The term is now widely used for both glassy and devitrified lenticular juvenile fragments, regardless of the fragments having been originally vesicular or non-vesicular. Furthermore, foliated lenticular juvenile fragments are not restricted to welded pyroclastic deposits but also occur in diagenetically compacted, non-welded, primary pyroclastic deposits and pumice- or scoria-rich, resedimented and reworked volcanoclastic deposits (45.1-4). Here, *fiamme* refers to lenticular to disc-shaped juvenile volcanic fragments that define a pre-tectonic foliation. The fragments may or may not have wispy, flame-like ends. The preferred shape and orientation of the fragments is most commonly due to welding or diagenetic compaction. In carefully studied ancient examples of diagenetically compacted pumice-rich deposits, many *fiamme* are compacted single pumice clasts, whereas some comprise compacted aggregates of a few pumice clasts (Allen, 1990; Allen and Cas, 1990).

We emphasize restriction of *fiamme* to confirmed juvenile fragments that define a confirmed pre-tectonic foliation. Foliated lenticular apparent clasts are common in altered and deformed volcanic sequences (Part 5). In cases where lenticular apparent clasts are the result of alteration and deformation, or in cases where the origin is uncertain, the terms *pseudofiamme* or *fiamme-like lens* can be used.

Flow foliations (8)

Flow foliations are common in silicic and intermediate coherent lava flows, domes, sills and dykes, and in strongly rheomorphic tuffs (8, 20.2, 26.3, 44.3, 44.7). Foliations form in response to laminar flowage. In lavas, development of foliation begins during flow in the conduit and continues during extrusion and outflow. In rheomorphic ignimbrites, foliations develop during and after the pyroclastic flow has begun to deflate, deposit and weld. In rheomorphic fallout tuffs, foliations develop only after the process of welding is well advanced.

In relatively viscous lavas and rheomorphic tuffs, foliations generated during laminar flowage are

preserved and record the history of internal deformation and movement of the mass. Foliations are defined by variations in composition, vesicularity, crystallinity, grain size, spherulite and lithophysae abundance, the degree of devitrification or colour, and/or by extremely flattened *fiamme* or by parting surfaces. Flow foliations may be laterally continuous over several metres and, although typically sub-millimeter to centimeter in width, bands up to several metres wide have been reported (Christiansen and Lipman, 1966).

At the vent, an emerging lava inherits a near-vertical foliation in response to shear stresses along the conduit walls. Shear stresses at the lava flow base accompany lava advance, and cause the flow layering to rotate towards horizontal, so that horizontal layers propagate upward through the flow as it moves forward (Fink, 1983). Foliation rotation is restricted to the plastically deforming parts of the flow, so the brittle crust retains its original vertical foliation. Close to vents, foliations in lavas generally dip steeply inward and have strikes that are broadly arcuate around the source (Christiansen and Lipman, 1966; Fink and Manley, 1987; Duffield and Dalrymple, 1990). In more distal parts of flows, foliations are subhorizontal near the base, and upward become more steeply inclined.

Mesoscopic folds (dimensions of millimeters to tens of metres) may be present locally or throughout flow-foliated volcanic rocks (8.3, 8.6, 26.3-4). Axial planes of flow folds lie subparallel to the foliation plane, and fold axes are perpendicular to the direction of flow. Fold vergence and "rolling" directions of rigid inclusions (e.g. foreign rock fragments, early-formed spherulites) within a flow give the local direction of flowage (Fig. 16). However, rotation of fold axes, due to changing internal body forces, and reversals of the mean flow direction are both possible and result in considerable scatter in fold axes orientations. If there are enough measurements and they are evenly distributed, then the mean orientation of fold axes can be used to estimate the direction of flowage (Christiansen and Lipman, 1966; Benson and Kittleman, 1968; Wolff and Wright, 1981). Flowage directions indicated by flow folds and lineations are sensitive to underlying slopes, especially in distal portions and rheomorphic tuffs (Wolff and Wright, 1981).

Flow foliations and flow folds in strongly rheomorphic tuffs and lava-like tuffs are very similar to those in lava flows (e.g. Schmincke and Swanson, 1967; Wolff and Wright, 1981; Henry et al., 1988; Henry and Wolff, 1992) (26.3-4). Flow foliations, therefore, are not indicative of a specific eruption mechanism, although they do reliably indicate that the final stages of emplacement involved non-particulate flow. Other lithofacies and textural criteria must be assessed in order to distinguish lavas from rheomorphic or lava-like tuffs, and to distinguish rheomorphic fallout tuff from rheomorphic ignimbrite.

In areas of strong alteration, planar flow banding in aphanitic lavas or sills may resemble bedding in fine

volcaniclastic rocks. Correct interpretation depends on: (1) a search for features such as flow folds, relict phenocrysts, spherulites or lithophysae (or altered equivalents), and columnar jointing; (2) mapping the

lithofacies geometry and contacts; (3) study of thin-sections in order to distinguish formerly vitriclastic from devitrified or recrystallized, coherent textures.

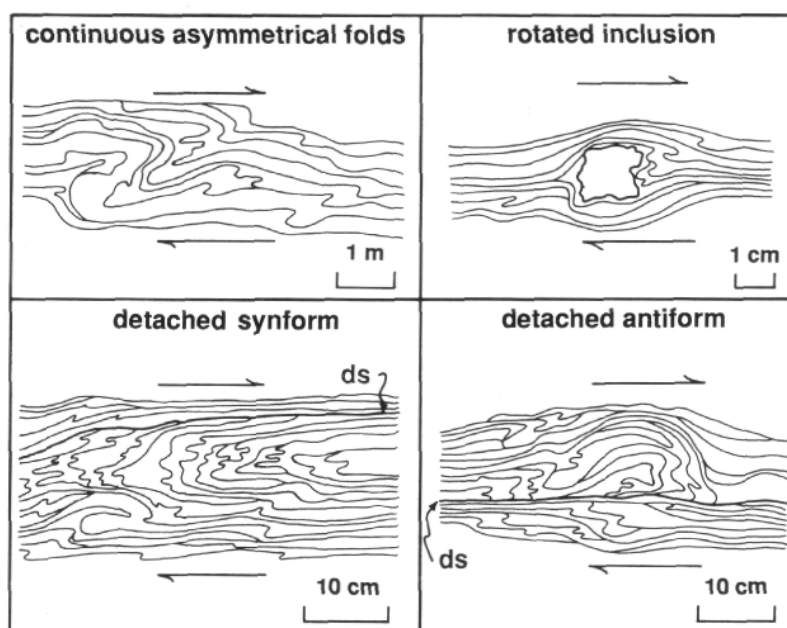


Fig. 16 Folded flow foliations in a rhyolite lava that indicate the local sense of relative movement. Detached synforms closely resemble detached antiforms. In synforms, the detachment surface is at the top of the fold. In antiforms, the detachment surfaces is at the base. ds: trace of detachment surface. Modified from Christiansen and Lipman (1966).

Joints (9)

Contraction that accompanies cooling of hot volcanic deposits and high-level intrusions produces a variety of more or less regular joints: columnar joints, radial columnar joints, concentric joints, tortoise shell joints, "tiny normal joints" and quench fractures. Joints and fractures related to cooling are very conspicuous features of lavas, especially those emplaced under water, and they strongly influence the shapes of clasts in associated autoclastic deposits.

Columnar joints divide the affected rock into elongate prismatic units or columns (9.1-4, 13.7, 19.2, 22.2, 26.1-2). Joints that define the sides of the columns are continuous and dominant over joints that cut across the prisms (Spry, 1962). Columns typically have hexagonal shapes in cross-section, although 3-, 4-, 5- and 7-sided columns are relatively common. Column diameters range from a few centimeters to several metres. The surfaces of some columns are striated by alternating smooth and rough zones, each a few centimeters wide and oriented normal to the column axis (chisel marks — Spry, 1962; Ryan and Sammis, 1978). Grain size and composition of the centers and margins of separate columns are uniform, or else show only very minor changes (Spry, 1962; Macdonald, 1968).

Columnar jointing occurs in coherent igneous bodies (lava flows, lava lakes, domes, sills, dykes), in both subaerial and subaqueous settings, and in a wide range of magma compositions. Parts of ignimbrite sheets can

be columnar jointed, especially the densely welded and vapour-phase crystallized zones (26.1-2). In some cases, columnar joints in ignimbrite are rectangular rather than hexagonal in cross-section.

The pattern of jointing in columnar-jointed sheets can be organized into two or three distinct zones (Waters, 1960; Spry, 1962) (Fig. 17; 9.5). Regular, well-developed, wide columns in the basal zone or lower colonnade are oriented perpendicular to the flow base. The overlying entablature consists of thinner, less regular columns in complex arrangements. An upper zone of regular columns (upper colonnade) oriented normal to the top cooling surface may overlie the entablature. No significant compositional variations occur between the various zones (Spry, 1962). The boundaries of the entablature are typically very distinct, and could easily be mistaken for flow unit contacts. Although the colonnade-entablature pattern is most commonly associated with basaltic lavas, it also occurs in some peralkaline silicic sheets (comendite — Schmincke, 1974).

Cooling of magma results in increases in the viscosity and in contraction. When thermally induced stresses exceed the tensile strength, intersecting contraction fractures form at right angles to surfaces of equal tensile stress (Spry, 1962). The fractures migrate inward from the cooling surface, most probably by incremental fracturing events which are recorded by complementary subhorizontal joints or by striated zones on the fracture surface (Ryan and Sammis, 1978). In magma bodies

that have simple and regular geometries, the surfaces of equal stress are parallel to isothermal surfaces, and columns form perpendicular to both. Thus, columns are typically perpendicular to the contacts of sheets (tabular flows, sills, dykes). Cooling of more complexly shaped bodies results in columns that are perpendicular to the surfaces of equal stress but not to isothermal surfaces.

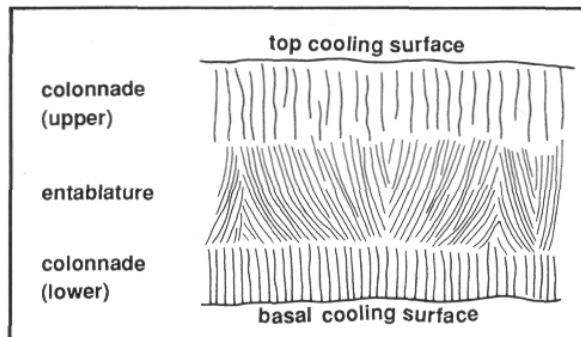


Fig. 17 Zones of jointing commonly developed in basaltic lava flows. Modified from Spry (1962).

Radial columnar joints develop in lava that cools in pillows, lobes, tubes, pipes and the top parts of feeder dykes (Yamagishi, 1987; Yamagishi et al., 1989) (9.3-4, 15.7, 16.1, 17.6). The axes of the columns are radially arranged, like the spokes of a wheel, and cross-section dimensions of the columns gradually diminish inward from outer surfaces. Radial columnar joints within pillows and lava lobes produce a polygonal pattern where they intersect curved outer surfaces.

Concentric joints may occur in pillows, lava lobes and feeders, in addition to radial columnar joints (13.3-4). These develop approximately parallel to flow layering and to the curved margin of the lava body, and at right angles to radial columnar joints. Concentric joints also occur within ellipsoidal lava clasts (concentric pillows) in one type of hyaloclastite (Yamagishi, 1987).

Tortoise shell joints outline equant, polyhedral blocks which, in two dimensions, define a polygonal pattern, similar to the polygonal pattern seen in cross sections through columnar and radial columnar joints (9.7, 17.4).

"Tiny normal joints" characteristically develop adjacent to chilled surfaces, and in many, though not all cases, coincide with glassy margins (9.6). They extend for less than a few centimeters inward away from the chilled surface and are closely spaced (about 1-2 cm apart).

Joints in the interiors of subaqueously emplaced intermediate and silicic lavas and feeder dykes are distinctive (Yamagishi, 1987; 1991; Yamagishi and Goto, 1992). These commonly display relatively continuous, smoothly curved, intersecting quench fractures that outline polyhedral blocks (pseudo-pillows) in three dimensions (9.6, 17.7). In many cases, pseudo-pillows are internally jointed as well, in tortoise shell or radial columnar joint patterns (Fig. 18). In addition, "tiny normal joints" oriented at right angles to the pseudo-pillow surfaces are typically present. Clasts

derived from disintegration of pseudo-pillows have equant blocky, prismatic or polyhedral shapes and are bounded by distinctive curvilinear joint surfaces.

"Tiny normal joints" and tortoise shell joints also occur in rapidly chilled juvenile blocks in subaerial pyroclastic and autoclastic deposits, and curvilinear joints also occur in subaerial lavas. Therefore, in ancient volcanic sequences for which the depositional setting is not clear, joint patterns should be interpreted with care and in the context of other lithofacies information.

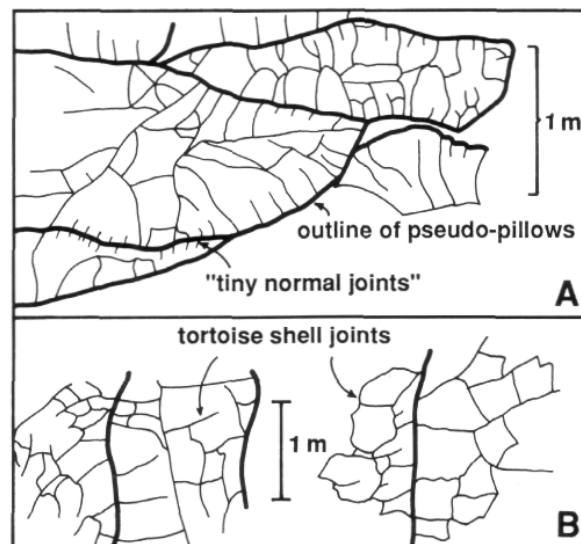


Fig. 18 Field sketches of cooling joints in a high-level, andesitic dyke, Oshinkoshin Dyke, Pliocene, Shiretoko, Japan. (A) Pseudo-pillows with marginal "tiny normal joints" and internal tortoise shell joints. (B) Tortoise shell joints between through-going master joints.

Plate 1 — Evenly porphyritic and volcaniclastic textures



1. Evenly porphyritic texture in coherent dacite

A. This sample shows porphyritic texture comprising evenly distributed, moderately abundant, euhedral plagioclase phenocrysts (**P**), in a much finer groundmass. Porphyritic texture is characteristic of coherent lavas and shallow intrusions.

Mount Read Volcanics, Cambrian; specimen 71425, Pieman Road, western Tasmania.



B. The groundmass of the porphyritic dacite in **1.1 A** consists of fine-grained quartz, feldspar, chlorite and carbonate. Plagioclase phenocrysts (**P**) are prismatic but their shapes are slightly modified by alteration. Plane polarised light.

Mount Read Volcanics, Cambrian; specimen 71425, Pieman Road, western Tasmania.



2. Phenocryst-rich porphyritic andesite

A. Medium to coarse, euhedral, evenly distributed phenocrysts are abundant in this andesite. Most conspicuous are black hornblende (**H**) phenocrysts whereas pale feldspar phenocrysts are harder to distinguish from the fine-grained groundmass.

Mount Read Volcanics, Cambrian; specimen 75868, Anthony Road, western Tasmania.



B. Although altered, the plagioclase (**P**) and hornblende (**H**) phenocrysts are euhedral and unbroken. Chlorite completely replaces some relict phenocrysts of a ferromagnesian phase (probably also hornblende). The groundmass consists of fine-grained feldspar and sericite. Plane polarised light.

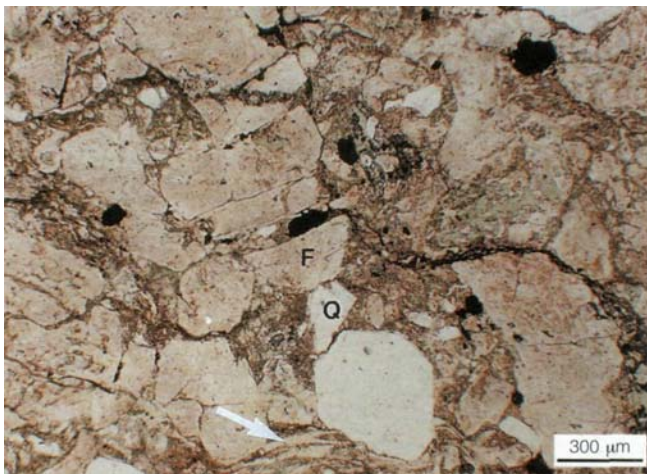
Mount Read Volcanics, Cambrian; specimen 75868, Anthony Road, western Tasmania.



3. Volcaniclastic texture in crystal-rich sandstone

A. Abundant crystal fragments (feldspar and quartz) occur together with scattered volcanic lithic fragments (**L**) in this crystal-rich sandstone. Unlike phenocrysts in coherent lavas or intrusions, the feldspar crystal fragments are angular, unevenly distributed and range from almost complete, millimeter-sized euhedra to sub-millimeter chips and splinters.

Mount Read Volcanics, Cambrian; specimen 91-9B, Cradle Mountain Link Road, western Tasmania.



B. A thin-section of the crystal-rich sandstone (**1.3A**) shows the uneven distribution, angular shape and broken condition of the crystal components, all hallmarks of volcaniclastic texture. Abundant feldspar (**F**) and less abundant quartz (**Q**) crystal fragments are locally closely packed, with only minor fine, chloritic and quartzofeldspathic matrix. Another important indicator of volcaniclastic origin is the presence of relict shards (arrow). Plane polarised light.

Mount Read Volcanics, Cambrian; specimen 91-9B, Cradle Mountain Link Road, western Tasmania.



4. Apparent porphyritic texture in crystal-rich ignimbrite

A. The most conspicuous feature of this hand specimen is the apparent porphyritic texture, comprising abundant, evenly distributed, mostly euhedral feldspar (**F**) crystals. Although the crystal abundance is high, the texture in hand specimen alone could reasonably be interpreted as that of a coherent lava or intrusion.

Rhyolitic base of ignimbrite P1, 14.1 Ma; Anden Verde, Gran Canaria, Canary Islands.



B. The sample in **1.4A** in fact comes from crystal-rich welded ignimbrite. In outcrop, the scattered lithic fragments (dark brown and grey) and subtle foliation (arrow) of flamme are important clues that a volcaniclastic origin is correct. (The matrix also contains abundant welded shards — **2.6B**.)

Rhyolitic base of ignimbrite P1, 14.1 Ma; Anden Verde, Gran Canaria, Canary Islands.

Plate 2 — Vesicles and volcanic glass



1. Vesicular subaerial rhyolitic lava

Substantial parts of the Little Glass Mountain subaerial rhyolite consist of finely or coarsely vesicular, pumiceous lava. Here, coarsely vesicular lava is interlayered with poorly vesicular obsidian. Both show coherent porphyritic texture comprising fine, sparse, euhedral phenocrysts (feldspar, pyroxene) in glassy, microlite-bearing groundmass.

Little Glass Mountain rhyolite flow, 1100 a; Medicine Lake Highland volcano, California, USA.



2. Vesicular submarine basaltic lava

This sample of vesicular basaltic lava comes from the sea-floor at about 2400 m water depth and is possibly part of a sheet flow. The hackly and conchoidally fractured glassy upper part contains moderately abundant, very irregular vesicles. The lower surface of the sample is the roof of a very large cavity that was presumably initially steam-filled (cf. gas blister in subaerial pahoehoe) and later invaded by sea water.

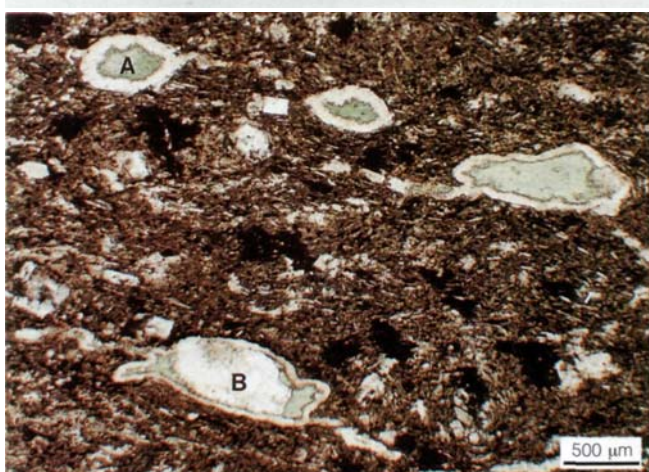
Holocene(?) basaltic lava flow, Manus Spreading Centre (2400 m below sea level), Papua New Guinea.



3. Flow-aligned amygdalites in devitrified dacite

Well-developed flow foliation is accentuated by lenticular, quartz-filled amygdalites (A) in much finer groundmass. On weathered surfaces, the amygdalites form a prominent lenticular foliation and resemble silicified flattened relict pumice lenses.

Mount Read Volcanics, Cambrian; specimen 76760, Burns Peak, western Tasmania.



4. Concentrically zoned amygdalites in thin-section

Amygdalites in this finely porphyritic basalt are aligned within the trachytic-textured groundmass. The amygdalites are filled with quartz, carbonate, or zones of quartz-chlorite (A), quartz-chlorite-quartz (B), quartz-chlorite-carbonate, or quartz-chlorite-epidote. Plane polarized light.

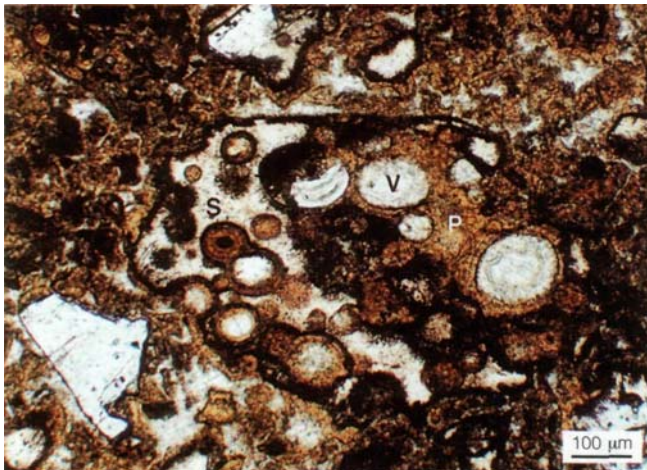
Mount Read Volcanics, Cambrian; specimen 100801, Mount Black, western Tasmania.



5. Partly palagonitised basaltic volcanoclastic sandstone

A. Volcanic glass (or relict glass) is a very common component of a wide variety of primary, resedimented and reworked volcanoclastic deposits. The most abundant grains in this fine to coarse volcanoclastic sandstone are made of tan palagonitised basaltic glass. Other components are plagioclase-phyric basalt grains (black) and sparse crystal fragments. The sample comes from a 10 m thick, graded bedded submarine sequence of resedimented, possibly phreatomagmatic basaltic debris.

Woolnorth Tuff, Tertiary; specimen CGI, Cape Grim, northwestern Tasmania.



B. Sideromelane (**S**) is inclusion-free, fresh basaltic glass that is clear and isotropic in thin-section. Alteration of sideromelane produces yellow-brown or yellow-orange palagonite (**P**). In the sample shown in **2.5A**, palagonite forms rims around the vesicles and along the margins of blocky sideromelane shards. Vesicles (**V**) are lined with radially fibrous zeolite and infilled by massive zeolite. Plane polarised light.

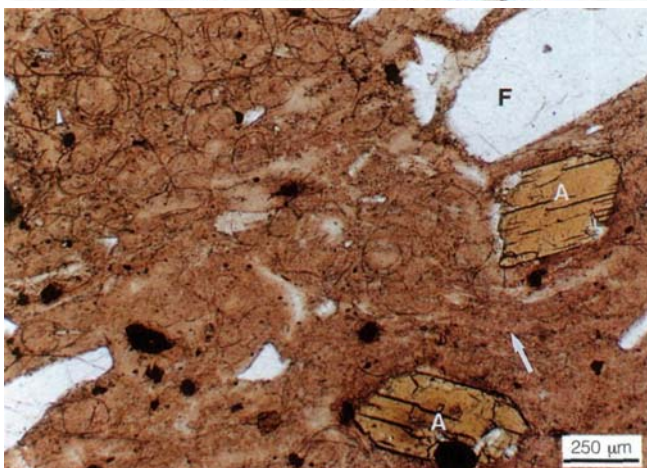
Woolnorth Tuff, Tertiary; specimen CGI, Cape Grim, northwestern Tasmania.



6. Glassy crystal-rich ignimbrite

A. The abundant feldspar crystals and crystal fragments (**F**) in this rhyolitic ignimbrite are separated by black glassy matrix. Dark lithic fragments (**L**) are also present.

Rhyolitic base of ignimbrite P1, 14.1 Ma; Anden Verde, Gran Canaria, Canary Islands.



B. In thin-section, densely welded glass shards (arrow) are evident in the matrix of the sample shown in **2.6A**. Welding compaction of the glass shards has produced coherent glass with perlitic fractures (probably due to hydration following welding). The glass shards are strongly deformed, especially near crystal fragments (feldspar, **F**; amphibole, **A**). Plane polarised light.

Rhyolitic base of ignimbrite P1, 14.1 Ma; Anden Verde, Gran Canaria, Canary Islands.

Plate 3 — Spherulites and lithophysae



1. Spherulites in Palaeozoic, flow-banded rhyolite

Pinkish, isolated and coalesced, spherical spherulites up to about 4 cm across are locally arranged in trains that help define flow bands (F) in this outcrop of coherent rhyolite.

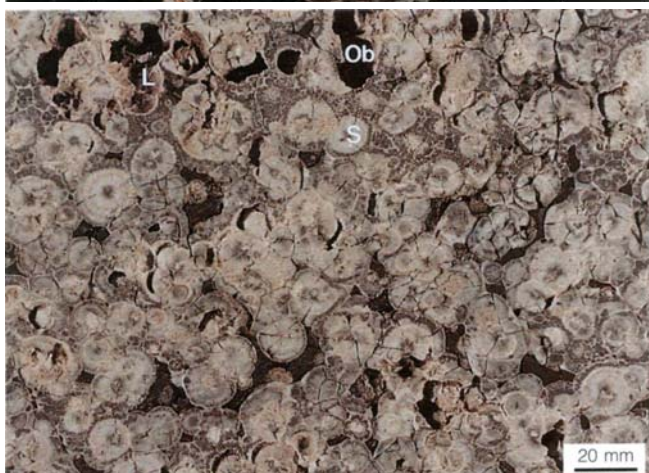
Bulgonunna Volcanic Group, Late Carboniferous; Wyarra Creek, northern Queensland.



2. Spherulites in Quaternary, devitrified rhyolitic lava

The well-defined spherulites in this feldspar-phyric subaerial rhyolite are sufficiently large for the radiating crystallites to be easily distinguished. Cusped areas of obsidian (Ob) remain between larger coalesced spherulites. Pale brown patches of closely-packed microspherulites (arrow) have irregular bulbous margins.

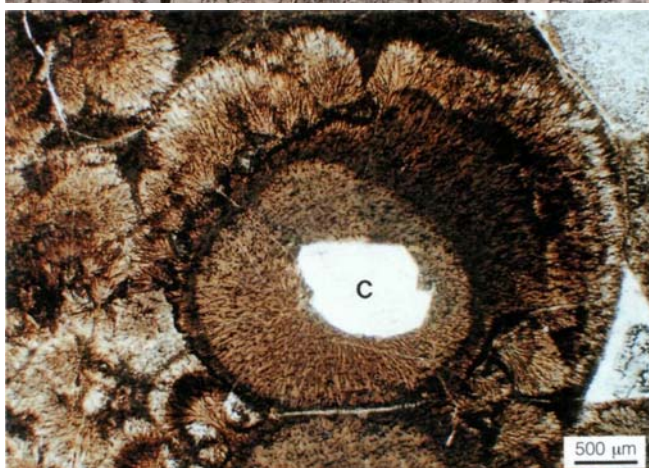
Ngongotaha lava dome, <140 ka; Hendersons Quarry, Rotorua caldera, New Zealand.



3. Spherulites and obsidian in rhyolite

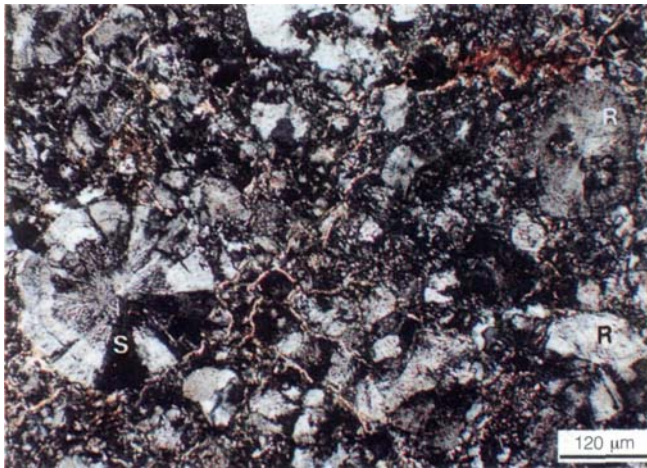
A. This rhyolite is substantially devitrified. It consists almost entirely of large spherulites (S) and lithophysae (L) within patches of coalescing microspherulites. Obsidian (Ob) is restricted to small, cusped areas. Concentric zones within the large spherulites reflect variations in the packing of radial fibres and the abundance of very fine inclusions. The textural and compositional contrasts produced by such primary devitrification strongly influence the textural effects of subsequent hydrothermal alteration or metamorphism.

Ngongotaha lava dome, <140 ka; Hendersons Quarry, Rotorua caldera, New Zealand.



B. In thin-section, spherulites such as those illustrated in 3.3A consist of radial crystal fibres. This example has grown on a cluster of plagioclase crystals (C). Fan- to sheaf-shaped microspherulites occur around the margin of the central spherulite. Plane polarised light.

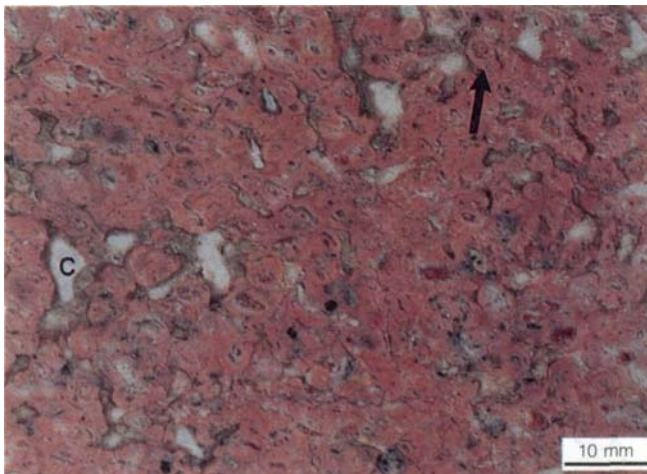
Ngongotaha lava dome, <140 ka; Hendersons Quarry, Rotorua caldera, New Zealand.



4. Spherulites in thin-section

An isolated spherulite (**S**) consists of intergrown radiating quartz and feldspar crystal fibres, and displays radial extinction. Concentric zoning in spherulites is caused by variation in the packing of fibres. Partial recrystallisation (**R**) to interlocking anhedral quartz and feldspar has destroyed some microstructures in several other spherulites. A mosaic of anhedral quartz and feldspar (possibly recrystallised microspherulites), with subordinate sericite occurs between the spherulites. Crossed nicols.

Mount Read Volcanics, Cambrian; specimen 74573, Silverfalls Road, western Tasmania.



5. Altered spherulitic rhyolite

This texture is interpreted to result from alteration and recrystallisation of spherulitically devitrified rhyolite. Former spherulites are now pink-grey bulbous aggregates of anhedral quartz and feldspar. Some relict spherulites retain concentric zonation (arrow). Cuspate patches of chlorite and calcite (**C**) that occur between closely packed spherulites are probably the result of alteration of former obsidian (cf. **3.3A**).

Mount Read Volcanics, Cambrian; DDH MAC22 (410 m), Hellyer mine, western Tasmania.



6. Nodular devitrification structures in flow-banded rhyolite

Nodular- to cauliflower-shaped, aggregates of anhedral quartz (**Q**) are similar to coalesced spherulites in less altered rhyolites (cf. **3.2**, **3.3A**). The quartz nodules are surrounded by smaller, recrystallised spherulites which impart a granular texture. Flow bands (**F**) can be traced through some quartz nodules, although elsewhere flow bands wrap around them.

Berserker Beds, Early Permian; Mount Chalmers, Queensland.



7. Lithophysae in densely welded ignimbrite

The lithophysae consist of star- and shell-shaped cavities surrounded by a border of pale, fine crystal fibres. Pale purple, devitrified welded ignimbrite occurs between the lithophysae. In this case, growth of the lithophysae clearly postdates welding compaction and predates final solidification of the welded pyroclastic deposit. One lithophysal cavity is partly filled with a lobe of the welded matrix (arrow) squeezed in while the mass was still ductile.

Tuff of Blue Creek, 6 Ma; Snake River Plain, Idaho, USA.

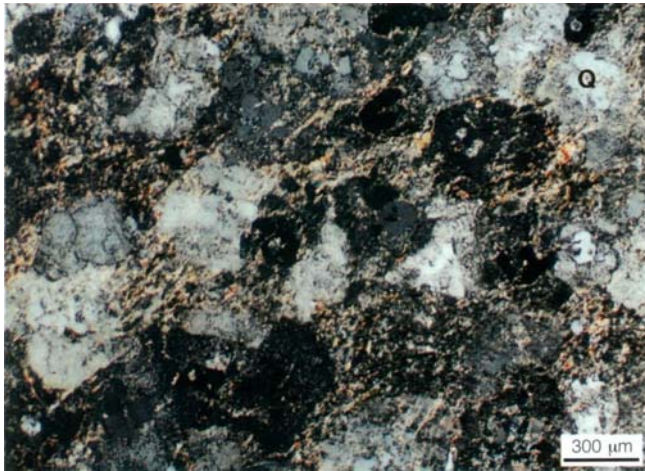
Plate 4 — Micropoikilitic texture in rhyolite



1. Altered rhyolite with micropoikilitic texture

This massive rhyolitic lava consists of extensively sericitized feldspar phenocrysts (**F**) in a granular groundmass. The granular texture in the groundmass is imparted by micropoikilitic quartz that encloses very fine, sericitized feldspar laths (cf. 4.2), and is similar to that observed in hand specimens of microspherulitic samples.

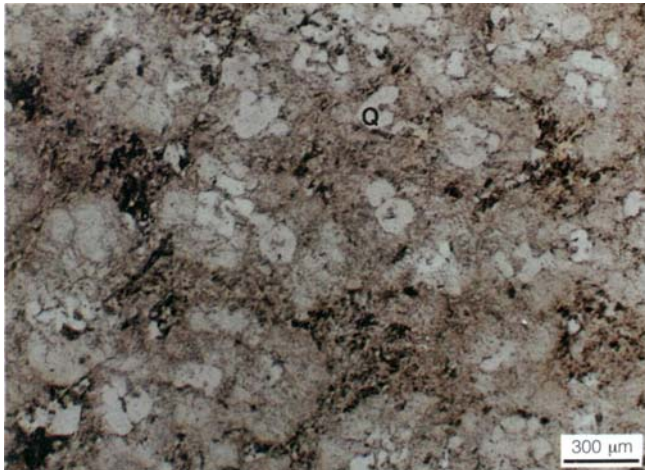
Mount Read Volcanics, Cambrian; specimen 74269, Jukes Proprietary prospect, western Tasmania.



2. Micropoikilitic texture in thin-section

A. Well-developed micropoikilitic texture in this sample consists of small irregular quartz cores (**Q**) in quartz-rich patches with boundaries clearly defined by concentrations of sericite. The quartz cores are optically continuous with the remainder of the quartz-rich patches. The quartz cores may represent an initial stage in the development of granophyric texture. Lofgren (1971b) predicted, but did not observe, a gradation between micropoikilitic and granophyric texture. The granular texture of the hand specimen (4.1) is the result of micropoikilitic devitrification. Crossed nicols.

Mount Read Volcanics, Cambrian; specimen 74269, Jukes Proprietary prospect, western Tasmania.



B. In plane polarised light, the quartz cores (**Q**) are clearly distinguishable within the micropoikilitic quartz-rich patches.

Mount Read Volcanics, Cambrian; specimen 74269, Jukes Proprietary prospect, western Tasmania.



3. Flow-banded rhyolite with micropoikilitic texture

Euhedral feldspar and embayed quartz phenocrysts are evenly distributed in this devitrified flow-banded rhyolitic lava. Flow bands are defined by alternating siliceous, micropoikilitic-textured layers, and slightly more phyllosilicate-rich layers evident in thin-section (4.4A, 4.4B). The flow foliation is deflected around an ellipsoidal lithophysa (L) that consists of a chlorite core (formerly a cavity) and a rim of fibrous feldspar crystallites.

Mount Read Volcanics, Cambrian; specimen 41092, Mount Darwin, western Tasmania.



4. Micropoikilitic texture in thin-section

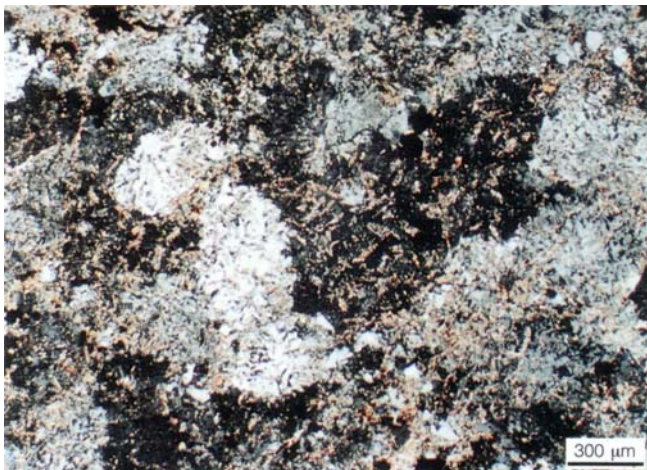
A. In thin-section micropoikilitic texture comprises patches of optically-continuous quartz enclosing variably oriented, sericitized feldspar laths (arrow). Crossed nicols.

Mount Read Volcanics, Cambrian; specimen 41092, Mount Darwin, western Tasmania.



B. In plane polarized light, the boundaries between quartz patches are marked by a concentration of fine sericite flakes (arrow).

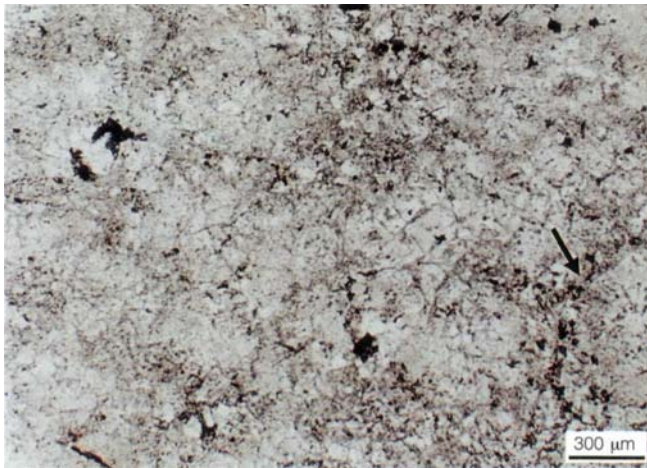
Mount Read Volcanics, Cambrian; specimen 41092, Mount Darwin, western Tasmania.



5. Micropoikilitic texture in thin-section

A. Micropoikilitic texture is very well-developed in this rhyolitic lava. Feldspar laths enclosed by micropoikilitic quartz are extensively replaced by sericite. Crossed nicols.

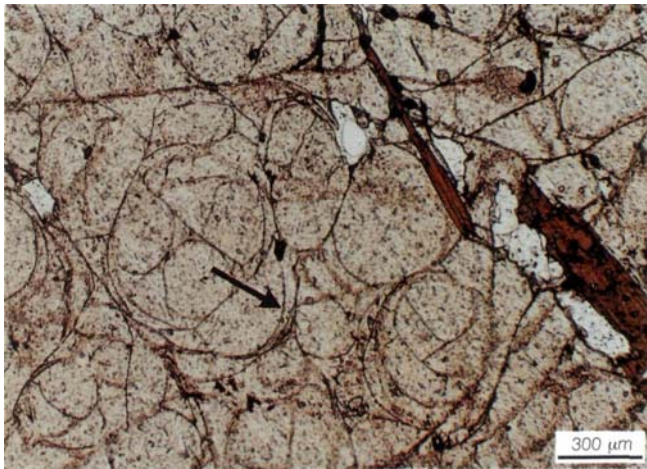
Mount Read Volcanics, Cambrian; specimen 41340, east Darwin area, western Tasmania.



B. In plane polarized light, boundaries between quartz-rich patches are defined by the concentration of fine sericite and opaque grains (arrow).

Mount Read Volcanics, Cambrian; specimen 41340, east Darwin area, western Tasmania.

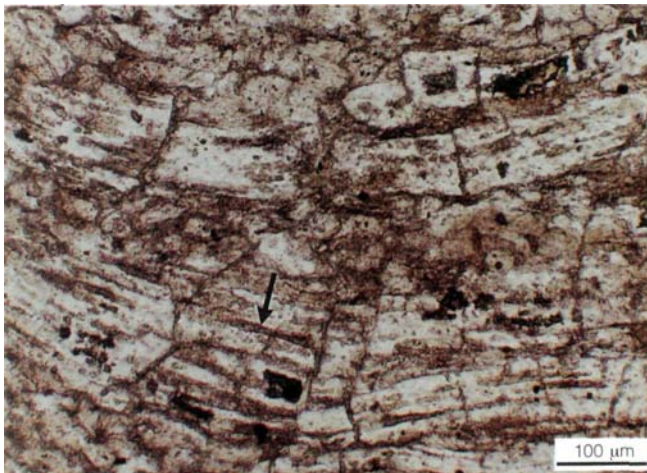
Plate 5 — Perlite



1. Classical perlite in thin-section

The glassy groundmass of this rhyolite shows classical perlitic fractures, comprising arcuate, overlapping and intersecting cracks (arrow). Sparse phenocrysts of clear plagioclase and brown biotite, and faint flecks in the glass (feldspar microlites) define a subtle flow foliation, which is overprinted by the perlitic fractures. Plane polarized light.

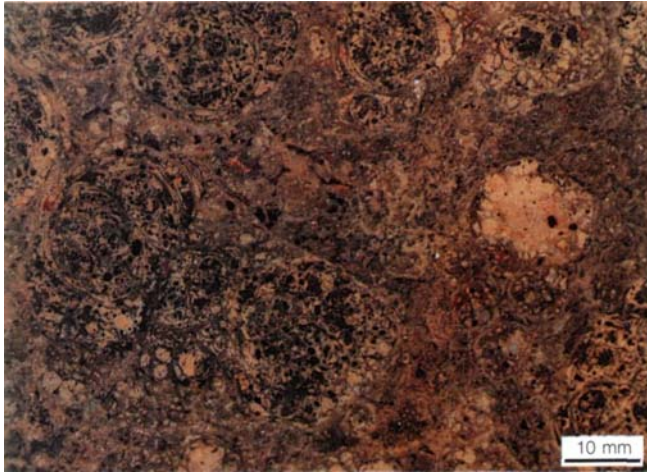
Glassy rhyolite, Pleistocene; Cala de Gaetano, Ponza, Italy.



2. Banded perlite in thin-section

The formerly glassy groundmass of this strongly flow-foliated dacite contains rectilinear fractures (arrow) typical of banded perlite. The fractures are preserved by a thin, infilling layer of sericite and chlorite. Most of the glass has recrystallized to a mosaic of quartz and feldspar; some has been replaced by sericite and chlorite. Plane polarized light.

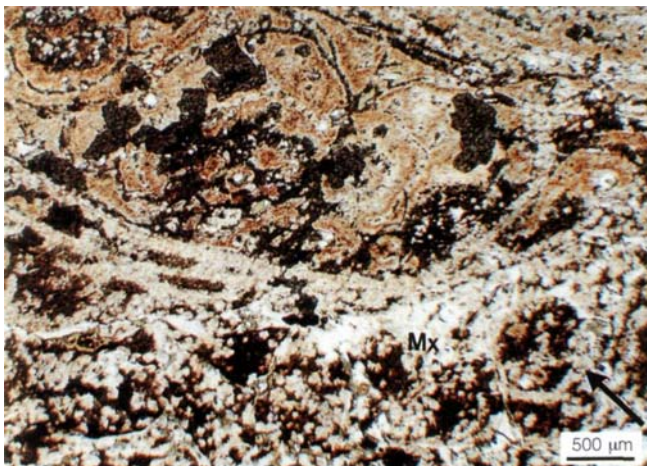
Mount Read Volcanics, Cambrian; specimen 401117, Pieman Road, western Tasmania.



3. Relict perlite

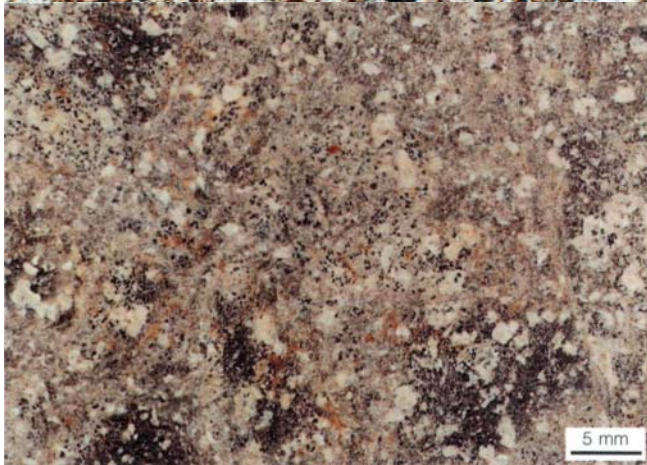
A. Relict classical perlite is well-developed within clasts in this hand specimen of formerly glassy, in situ dacitic hyaloclastite.

Mount Read Volcanics, Cambrian; specimen C101159, Sock Creek, western Tasmania.



B. In thin-section, the relict perlitic fractures in **5.3A** are outlined by sericite and confined within the centers of clasts. Other arcuate fractures oriented subparallel to clast boundaries may be quench fractures. The granular-textured apparent matrix (**Mx**) consists of finely intergrown quartz, feldspar and phyllosilicates. In places, the apparent matrix contains ghosts of former perlitic fractures (arrow), and may have been originally composed of glass but has been more strongly altered. Plane polarized light.

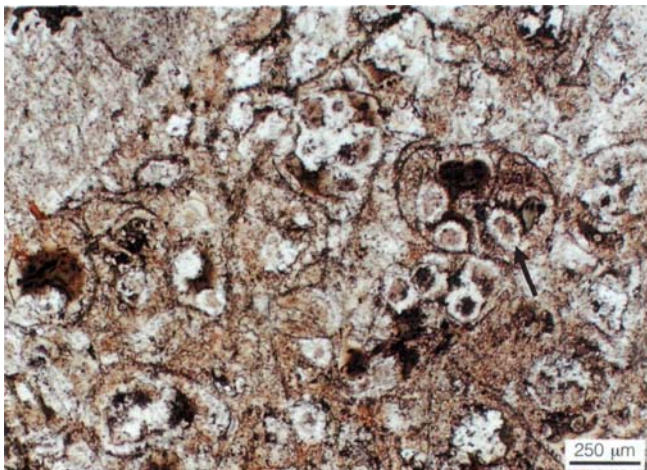
Mount Read Volcanics, Cambrian; specimen C101159, Sock Creek, western Tasmania.



4. Relict perlite in dacite

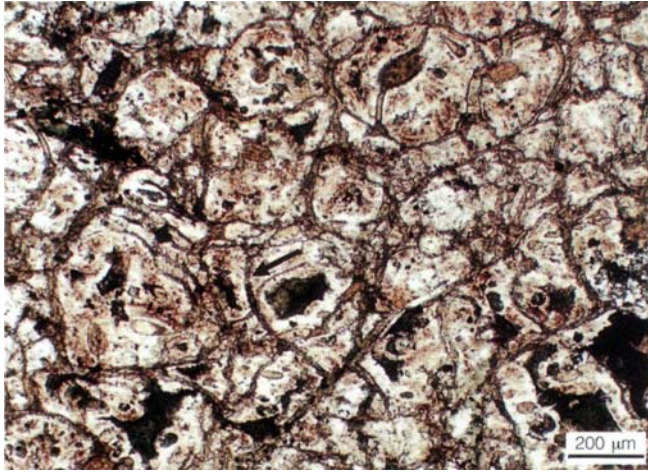
A. Relict perlitic fractures in this hand specimen of feldspar-phyric dacite are defined by chlorite. Although recognizable with a hand lens, they require a careful search.

Mount Read Volcanics, Cambrian; specimen 401242, Murchison Highway, western Tasmania.



B. In thin-section, well-developed relict perlitic fractures are ubiquitous in the formerly glassy groundmass of the dacite in **5.4A**. Fractures are defined by chlorite, and the glass has been replaced by quartz, feldspar, sericite and epidote. The groundmass also contains partially recrystallized spherulites (arrow). Plane polarized light.

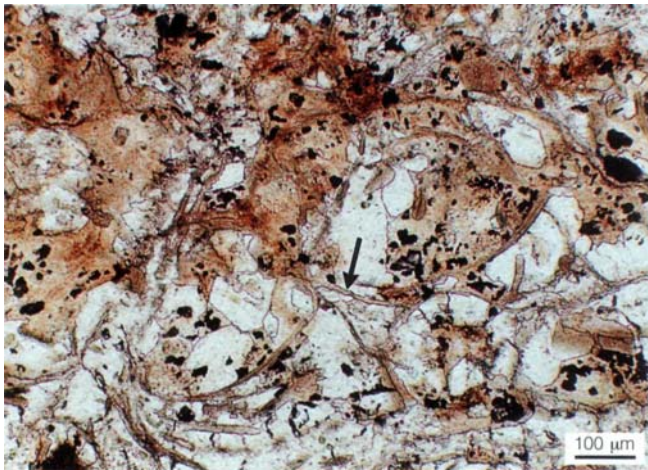
Mount Read Volcanics, Cambrian; specimen 401242, Murchison Highway, western Tasmania.



5. Relict classical perlite in dacite

Relict classical perlite fractures (arrow) are here strongly defined by chlorite. The remainder of the originally glassy groundmass has been recrystallized to fine quartz and feldspar, or else replaced by chlorite. Plane polarized light.

Mount Read Volcanics, Cambrian; specimen 401163, Pieman Road, western Tasmania.

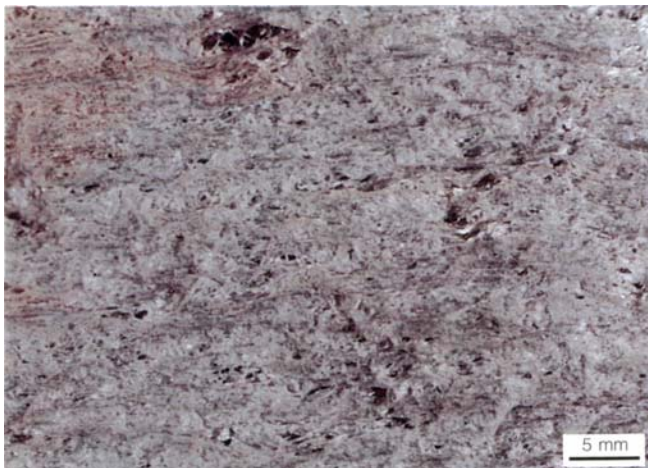


6. Relict perlite in thin-section

Recrystallization of glass in ancient volcanics can effectively obscure evidence of perlitic fractures. The texture is barely recognizable in this formerly glassy rhyolite. The perlitic fractures (arrow) are infilled with sericite, whereas the interstitial glass has recrystallized to quartz and feldspar, or has been replaced by phyllosilicates. Plane polarized light.

Mount Read Volcanics, Cambrian; specimen 401223, Boco Road, western Tasmania.

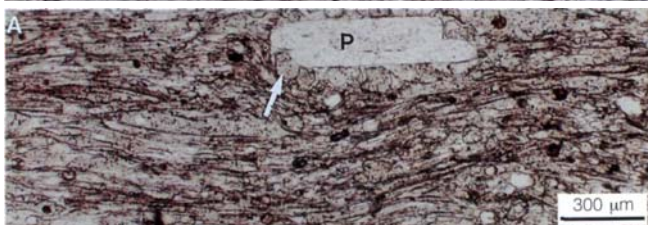
Plate 6 — Pumice, scoria, bombs and juvenile blocks



1. Rhyolitic tube pumice

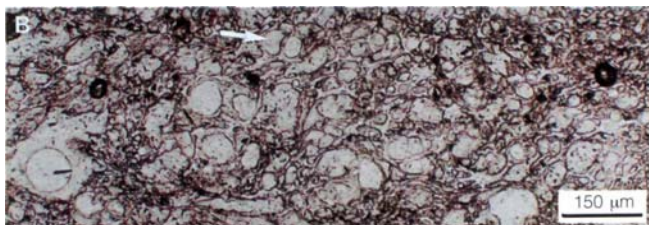
Rhyolitic tube pumice has a silky, fibrous or "woody" texture that results from the subparallel alignment of extremely elongate cylindrical vesicles. This pumice is composed of fresh, rhyolitic glass.

Pumice block from the AD 1912 plinian eruption of Novarupta; Valley of Ten Thousand Smokes, Alaska, USA.



2. Rhyolitic tube pumice in thin-section

A, B. These photomicrographs show the **6.1** tube pumice in thin-sections cut parallel (A) and perpendicular (B) to the tube elongation direction. In (A) there is a very strong foliation defined by the elongate tube vesicles except immediately adjacent to



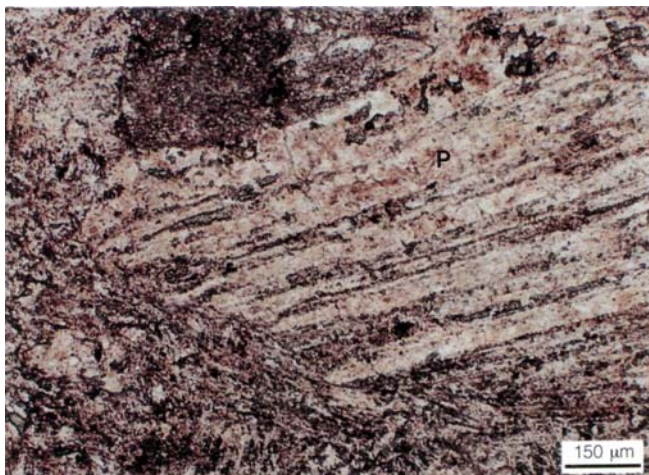
the plagioclase phenocryst (**P**), where round vesicles occur (arrow). In (B) the cross-section shape of the tube vesicles is round to oval (arrow) and no foliation is apparent. Mounting medium infills the vesicles. Plane polarised light.

Pumice block from the AD 1912 plinian eruption of Novarupta; Valley of Ten Thousand Smokes, Alaska, USA.

3. Relict tube pumice in thin-section

Unflattened tube vesicles are clearly evident in the relict pumice clasts (**P**) in this altered rhyolitic pumice breccia. Quartz and albite have infilled vesicles and replaced the formerly glassy vesicle walls, ensuring preservation of the tube vesicle structure. Pumice which is replaced by phyllosilicate minerals and flattened during diagenesis or tectonic deformation may be unrecognizable as relict pumice, or else resemble welded pumice. Plane polarized light.

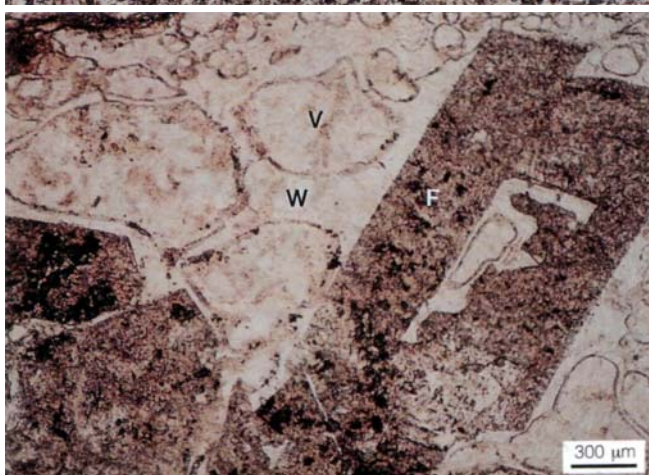
Mount Read Volcanics, Cambrian; specimen R3, Hercules mine haulage road, western Tasmania.



4. Round vesicles in porphyritic pumice in thin-section

This sample of tube pumice contains large round vesicles (**V**) adjacent to euhedral feldspar phenocrysts (**F**). Away from crystals, there is a transition to tube vesicles. Initially, vesicles in magmas are more or less spherical. Those that nucleate and grow adjacent to crystals are protected from stretching during flow of the vesiculating magma. In this example, the vesicles have been infilled and vesicle walls (**W**) replaced by albite. Plane polarized light.

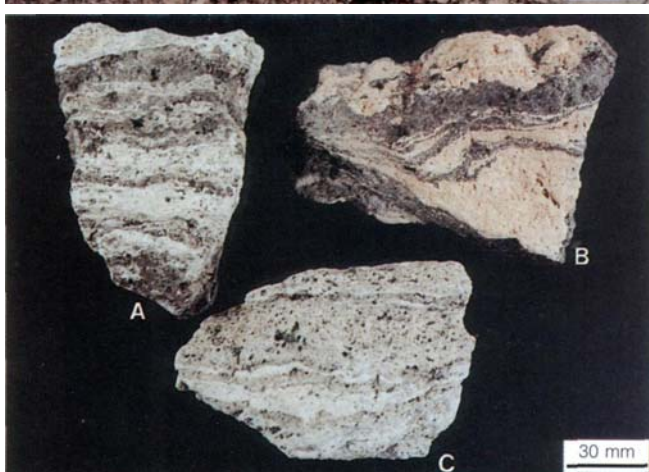
Mount Read Volcanics, Cambrian; footwall of Rosebery massive sulfide deposit, DDH LB271 (130.5 m), western Tasmania.



5. Compositionally banded, "streaky" pumice

These pumice blocks are combinations of: (**A**) pale grey dacite and dark grey andesite; (**B**) pink rhyolite and dark grey andesite; and (**C**) very pale grey rhyolite and pale grey dacite. The three magma compositions were mingled shortly before and during eruption, and the pyroclastic deposits (both fallout and flow), as well as single juvenile clasts such as these, show complex compositional variations.

Pumice blocks from the AD 1912 plinian eruption of Novarupta; Valley of Ten Thousand Smokes, Alaska, USA.

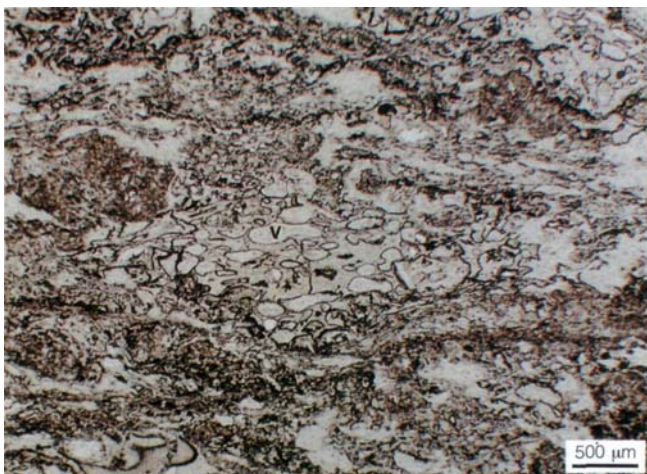




6. Subaerial basaltic scoria

Basaltic scoria lapilli dominate this near-vent subaerial fallout deposit. The red colour is a result of thermal oxidation, a process that reflects cooling of the hot lapilli while in contact with air. The irregular shapes of the lapilli are the result of tearing apart of vesiculating magma.

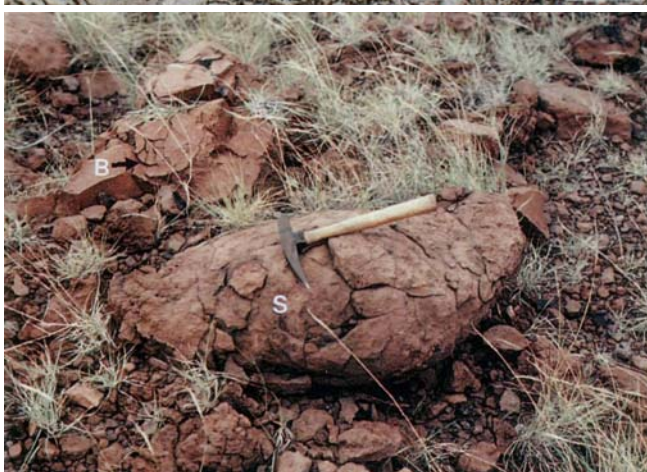
Basaltic lapilli breccia, Miocene; Porto Santo, Madeira Archipelago, Portugal.



7. Altered scoria in thin-section

Ragged scoria grains are abundant in this sample of metamorphosed basaltic volcanoclastic sandstone. The scoria grains and ovoid vesicles (V) within them are outlined by a fine, opaque mineral. The vesicles are infilled by delicately fibrous sericite or by albite. Apart from scoria grains, the sandstone contains scattered crystal and lithic fragments and fine, recrystallized matrix. Plane polarized light.

Mount Read Volcanics, Cambrian; specimen 91-109B, Henty River, western Tasmania.

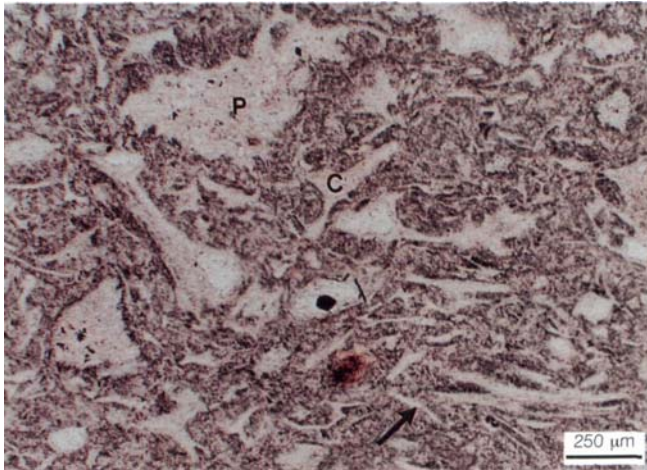


8. Near vent bomb and juvenile block

These juvenile basaltic pyroclasts are part of a bomb and block field, deposited near vent by ballistic fallout. The spindle bomb (S) has been shaped by surface tension during flight. Adjacent is a large, angular block with a partly bread-crust surface (B). Bread-crust fracturing is caused by vesiculation and expansion of the hot clast interior beneath a chilled crust.

Telica composite volcano, Nicaragua; deposits from the AD 1982 eruption.

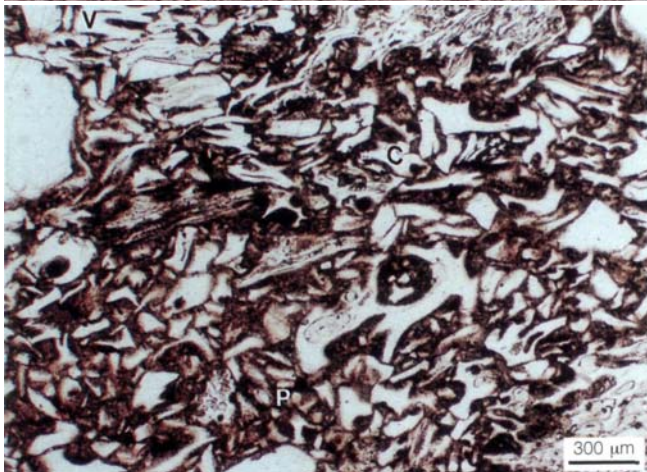
Plate 7 — Shards, lithic fragments and accretionary lapilli



1. Bubble-wall shards in thin-section

This photomicrograph shows the typical shapes of pyroclastic cuspsate (C), platy (arrow) and pumice (P) shards in thin-section. The shards were formerly glassy and are now composed of albite. The delicate spines and cusps on bubble-wall and pumice shards are undeformed and indicate that the deposit was originally non-welded. Plane polarized light.

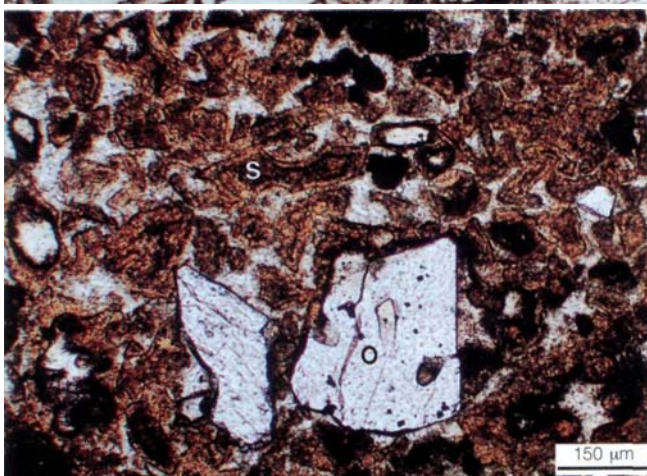
Mount Read Volcanics, Cambrian; specimen V405, Winter Brook, western Tasmania.



2. Glass shards in thin-section

Most of these glass shards have cuspsate (C) and platy (P) shapes, but a few microvesicular pumice shards (V) are present. The shards are largely undeformed and the sample is texturally only slightly welded (sintered). Light brown, glassy fine ash fills the interstices between the shards. Plane polarized light.

Bishop Tuff, 0.74 Ma; specimen BT2, Long Valley caldera, California, USA.



3. Basaltic shards in thin-section

Although these formerly glassy (sideromelane) basaltic shards (S) are altered to palagonite, the blocky shapes and round vesicle outlines are distinct. Other primary components are olivine crystals and crystal fragments (O). The shards and crystal fragments are cemented by fibrous and massive zeolite. Plane polarised light.

Woolnorth Tuff, Tertiary; specimen CG1, Cape Grim, northwestern Tasmania.



4. Lithic fragments in volcanic breccia

The most abundant lithic fragment type in this polymict volcanic breccia is quartz- and feldspar-phyric rhyolite (arrow). The rhyolite fragments are blocky and have curvilinear margins that show little sign of modification during transport. They may have been generated by autoclastic fragmentation of rhyolite lava, but have been mixed with other lithic fragment types and with granular, lithic- and crystal-rich matrix (M) during subsequent resedimentation.

Mount Read Volcanics, Cambrian; Anthony Road, western Tasmania.



Lithic fragments are typically only very minor components of coherent lavas. They may be volcanic or non-volcanic and, in many cases, can be linked with conduit wall-rock or substrate lithologies. This photograph shows a basalt inclusion in rhyolite lava. The inclusion may be a foreign lithic fragment but another possibility is that it is derived from incomplete mingling of mafic and rhyolitic magmas prior to eruption.

Boyd Volcanic Complex, Late Devonian; Bunga Head, New South Wales.



6. Accretionary lapilli

The conspicuous ovoid shaped features in these samples are accretionary lapilli. The lapilli are only a few millimeters across and closely packed in the bottom right sample. In the sample on the left side, the lapilli are flattened and compacted. All three samples come from different parts of a widespread unit of subaerial rhyolitic fallout tuff.

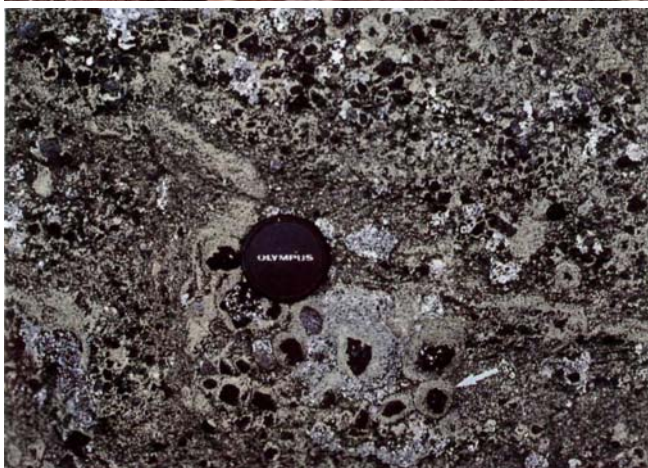
Cana Creek Tuff, Currabubula Formation, Late Carboniferous; Cana Creek, New South Wales.



7. Reworked accretionary lapilli

Accretionary lapilli are composed of concentric shells of fine and coarse ash. Fresh accretionary lapilli can be rapidly cemented or indurated, and remain intact during erosion and reworking. The scattered accretionary lapilli in this volcanoclastic sandstone have been eroded from primary deposits and their fine-grained outer rims are partly abraded. The host sandstone is a subaerial mass-flow deposit generated during the explosive eruption that also produced the accretionary lapilli-bearing fallout deposits (7.6; McPhie 1987).

Cana Creek Tuff, Currabubula Formation, Late Carboniferous; Cana Creek, New South Wales.

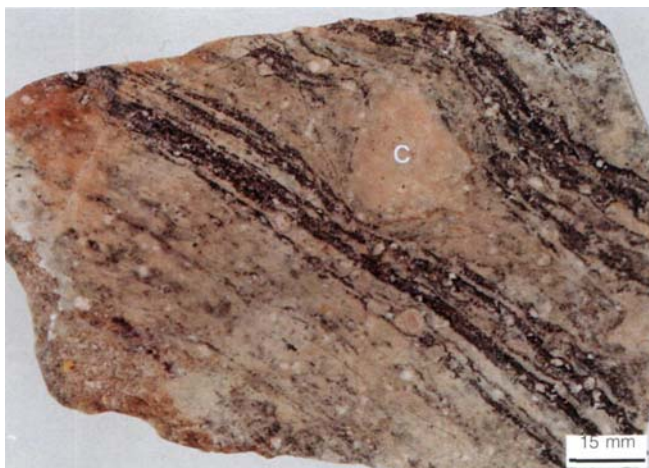


8. Armoured lapilli

These armoured lapilli consist of nuclei of black basaltic scoria lapilli coated by pale, coarse ash of the same composition. They occur in phreatomagmatic surge deposits in the rim beds of a tuff cone.

Cape Bridgewater volcano, ~4 Ma; Cape Bridgewater, Victoria

Plate 8 — Flow foliations



1. Flow banding in recrystallized submarine rhyolitic lava

The flow foliation in this feldspar-phyric rhyolitic lava consists of pale siliceous bands alternating with darker, more phyllosilicate-rich bands. Flow bands wrap around a pink, silicic lava clast (C). In thin-section, the phyllosilicate-rich bands comprise isolated and coalescing, variably recrystallized spherulites and patches of interlocking quartz and feldspar in a phyllosilicate-rich matrix. The siliceous bands consist of isolated spherulites, dispersed in a fine-grained mosaic of quartz and feldspar.

Mount Read Volcanics, Cambrian; specimen 76771, Chester mine area, western Tasmania.



2. Flow banding in devitrified subaerial rhyolitic lava

Devitrification of this flow-banded, feldspar-phyric rhyolitic lava has generated large, isolated aggregates of coalesced spherulites (arrow). The flow bands have been deflected around the spherulitic masses, implying that the spherulites formed while the lava was still ductile, probably during flowage. A sinistral sense of rotation is implied by the geometry of the flow laminations.

Ngongotaha lava dome, <140 ka; Hendersons Quarry, Rotorua caldera, New Zealand.



3. Flow folds in a rhyolite dyke

These continuous, even flow bands are in rhyolite within a dyke. The flow bands define asymmetrical flow folds that suggest a dextral sense of shear.

Rhyolite dyke, Bulgonunna Volcanic Group, Late Carboniferous; near Desmond Creek, northern Queensland.



4. Dacitic lava with planar flow banding

Even, continuous, planar flow banding in this submarine, dacitic lava flow superficially resembles sedimentary bedding. However, the rock has an evenly porphyritic texture characteristic of coherent lava and locally grades into in situ hyaloclastite breccia.

Hornblende dacite, 6 Ma; Kariba, Hokkaido, Japan.



5. Planar flow banding in recrystallized dacitic lava

Planar, laterally continuous flow banding is particularly well-developed in this evenly porphyritic, feldspar-phyric dacite. The flow bands accommodate the prominent siliceous boudin-like structures which are probably the result of nodular devitrification and overprinting siliceous alteration.

Mount Read Volcanics, Cambrian; Mount Huxley, western Tasmania.



6. Flow folds in a rhyolite dyke

Highly contorted flow bands occur here in a fine-grained, sparsely porphyritic rhyolite dyke. Flow bands are defined by varying spherulite and phyllosilicate content, and in the degree of recrystallization.

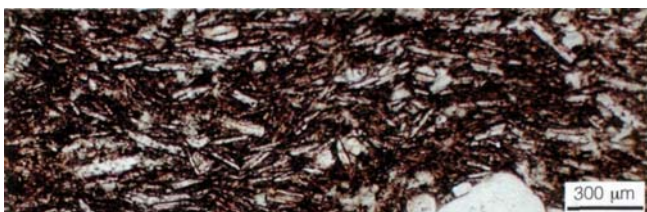
Rhyolite dyke associated with the Lower Rhyolitic Tuff Formation, Ordovician; Llanberis Pass, northern Wales, UK.



7. Planar flow lamination in altered dacite

Flow lamination (arrow) comprises pink siliceous domains that alternate with pale green domains. Dark green, phyllosilicate stringers (S) transect the flow foliation and overprint any pre-existing flow laminae.

Mount Read Volcanics, Cambrian; DDH SCS2 (102.2 m), Sock Creek South, western Tasmania.



8. Trachytic texture in basalt in thin-section

Clinopyroxene and plagioclase phenocrysts are set within a finer grained groundmass of strongly flow-aligned plagioclase laths, exemplifying trachytic texture. Plane polarized light.

Mount Read Volcanics, Cambrian; DDH MC-1D (256.9 m), Mount Charter, western Tasmania.

Plate 9 — Columnar joints, "tiny normal joints" and tortoise shell joints



1. Columnar-jointed dacite

Regular columnar joints in this coherent dacite have column axes that plunge at 50° to the left side of the picture. Palaeocooling surfaces of columnar-jointed sheets are typically oriented more or less at right angles to the plunge of the columns. In this case, the palaeocooling surface is inferred to dip at $\sim 40^\circ$ to the right side of the picture. Note geological hammer for scale (arrow).

Mount Read Volcanics, Cambrian; Jukes Proprietary prospect, western Tasmania.



2. Columnar jointing in submarine andesitic lava

Columnar joints shown here in cross-section have hexagonal outlines. These columnar joints occur in andesitic lava that solidified within a submarine feeder tube.

Maori Bay pillow lava flow, Nihotupu Formation, Miocene; Muriwai, New Zealand.



3. Jointing in submarine andesitic lava feeder tubes

This cliff provides a cross-section through a large, former feeder tube now filled by columnar-jointed andesite and surrounded in part by cogenetic pillow lava lobes. Columnar joints in the feeder tube radiate outward from the centre, remaining perpendicular to the isothermal surfaces present during cooling. The cliff is approximately 25 m high.

Maori Bay pillow lava flow, Nihotupu Formation, Miocene; Muriwai, New Zealand.



4. Radial columnar joints in basaltic pillow lobe In cross section, this basaltic pillow lobe exhibits radial columnar joints (**J**). The columnar joints transect the pillow rind and are perpendicular to the continuously curving outer surface. The pillow core is massive and vesicular.

Basaltic lava, Recent; Reiljannes Peninsula, Iceland.



5. Columnar joints in subaerial basaltic lava

Jointing patterns in this exposure define two distinct zones: the thin, lower colonnade (C) comprises well-developed wide columns, oriented at right angles to the flow base; the overlying entablature (E) is much thicker and consists of less regular, narrow, fanning columns. The height of the exposure is approximately 15 m.

Junction Butte Basalt, 2 Ma; near Tower Falls, Yellowstone, Wyoming, USA.



6. "Tiny normal joints" and pseudo-pillow

The hammer rests on a clast of hornblende dacite, about 1 m across, that is bounded by curvilinear surfaces along which there are "tiny normal joints" (arrow). These joints typically develop perpendicular to surfaces that have been chilled. The clast is a pseudo-pillow (cf. 17.7) derived from disintegration of relatively viscous, quench fragmented submarine lava.

Green Tuff Belt, Miocene; Teine Olympia Road, Hokkaido, Japan.



7. Tortoise shell joints

The pattern of intersecting, broadly curving joints shown here is known as tortoise shell jointing. On two-dimensional surfaces, the joints outline equant polygons with straight to broadly curved sides. In three dimensions, the joints define equant polyhedral blocks. They develop in response to contraction during cooling.

Oshinkoshin basaltic andesite dyke, Pliocene; Oshinkoshin waterfall, Shiretoko Peninsula, Hokkaido, Japan.

Part 3. Lavas, syn-volcanic intrusions and related volcanoclastic deposits

As magma rises to shallow levels prior to an eruption it may become saturated in volatiles, as a result of decompression, and/or as a result of crystallization of anhydrous phases (Sparks, 1978; Burnham, 1983). If volatile contents are very low, or if volatiles are able to escape from the magma, an effusive eruption will occur, generating lava flows or domes. Several processes are involved in degassing of magmas:

- (1) minor, magmatic-volatile-driven explosive eruptions;
- (2) the steady loss of gas and condensates through fractured, permeable conduit wall rocks, in some cases associated with shallow hydrothermal systems;
- (3) vesiculation prior to eruption and during outflow;
- (4) formation, passive rise and escape of bubbles from the magma in the conduit.

Vigorous but short-lived explosive activity (1) and gas loss through permeable conduit walls (2) are very common precursors and accompaniments to eruptions of subaerial intermediate and silicic lavas (Ncwhall and Melson, 1983; Taylor et al., 1983; Eichelberger et al., 1986; Heiken and Wohletz, 1987). Detailed studies of textures and H₂O contents in high-viscosity silicic flows and domes (Eichelberger et al., 1986; Fink and Manley, 1987) and low-viscosity basaltic flows (Mangan et al., 1993; Wilmoth and Walker, 1993) suggested that volatiles are lost rapidly but non-explosively by vesiculated lava (3). This mechanism requires that the vesicles are interconnected (important in high-viscosity flows), or else are able to rise and escape (important in low-viscosity flows). The fourth process is mainly confined to low-viscosity magmas (mostly basaltic), and can extend to mild fountaining and emission of sprays of fluid magma that coalesce and recombine to form coherent lava when deposited on the vent rim (fountain-fed lava flows — Wilson and Head, 1981).

The physical properties of magmas (composition, temperature, viscosity, volatile content, phenocryst content) have a major influence on the internal textures, facies geometry and facies associations of lavas and syn-volcanic intrusions. Other important controls are, for lavas, the circumstances of eruption, such as discharge rate, vent character, substrate gradient and subaerial versus subaqueous setting (Walker, 1973b; Hulme, 1974; Moore et al., 1978; Wilson et al., 1987; Griffiths and Fink, 1992), and, for intrusions, the host sediment character (Busby-Spera and White, 1987). In most cases, both lava flows and syn-volcanic intrusions include varying proportions and arrangements of *coherent* facies and *autoclastic* facies. The coherent facies consists of solidified lava or magma and is characterized primarily by evenly porphyritic or aphyric

texture, with glassy, cryptocrystalline or aphanitic groundmass. Non-explosive autoclastic processes of autobrecciation and quench fragmentation generate significant volumes of fragmented lava as normal by-products of effusive eruptions, regardless of composition or setting. The same processes may cause brecciation of intrusions emplaced into wet sediment. Thus, the autoclastic facies comprise, for lavas, autobreccia and/or hyaloclastite and, for syn-volcanic intrusions, intrusive autobreccia, intrusive hyaloclastite and peperite.

Syn-volcanic intrusions and intrusive complexes are an important product of magmatism in subaqueous sedimentary basins. Magmas of all compositions can be emplaced as syn-volcanic intrusions. They can be coarsely porphyritic or aphyric, with aphanitic, cryptocrystalline or partly glassy groundmass, and range in vesicularity from non-vesicular to partly pumiceous. Hanson (1991) described extensive, thick, andesitic and rhyolitic intrusions and associated intrusive breccia in a Devonian arc sequence in California. Drill core retrieved from the Gulf of California (Einsele, 1986), the Juan de Fuca Ridge (ODP Leg 139, 1992) and the Japan Sea (Thy, 1992) revealed the presence of multiple basaltic sills in deep marine sediments. The sill complex discovered at the Juan de Fuca Ridge is adjacent to a 95 m-thick massive sulfide deposit. At Hellyer, in the Mount Read Volcanics, western Tasmania, basaltic sheets above the massive sulfide deposit were, in many cases, emplaced as sills into unconsolidated mudstone (McPhie and Allen, 1992; Waters and Wallace, 1992). Lower in the sequence at Hellyer, and elsewhere in the Mount Read Volcanics, syn-volcanic intrusions of intermediate and silicic composition are common but difficult to recognize and easily mistaken for lava flows. In this part, important lithofacies characteristics of lavas and syn-volcanic intrusions are reviewed, with emphasis on related autoclastic deposits, internal structures and facies geometry. Lithofacies information is obtained from map-, drill-section- and outcrop-scale observations. Some textures evident in hand specimens of lavas and intrusions are also found in volcanoclastic deposits. Genetic interpretations should be consistent with all the available lithofacies information and not depend solely on textures evident in hand specimens or thin-sections.

Autobreccia (10)

Autobrecciation involves the non-explosive fragmentation of flowing lava. Parts of lava flows that are cooler, more viscous, or subject to locally higher strain rates than the rest respond to stress in a brittle fashion. The process commonly affects the outer

surfaces (top, base, sides) of lava flows and generates a layer of rigid blocks, plates and spines. The blocks can be fused together or else remain loose, and are easily dislodged by continuing movement of the flow. The final result is a lava flow comprising a coherent interior enclosed by a carapace and floor of *autobreccia*. Parts of the brecciated surface sometimes founder into the flow interior and are preserved as irregular pockets of *autobreccia* within otherwise coherent lava.

Autobrecciation is a common by-product of the effusion of subaerial lavas and is especially important in the genesis of block lavas and a'a. Autobreccias have also been identified in submarine lavas of basaltic (Ballard et al., 1979) to rhyolitic (De Rosen-Spence et al., 1980) composition. In subaqueous settings, quenching probably accompanies flowage and autobrecciation. Intrusions can also be partly autobrecciated.

Autobreccia is composed of blocky, slabby or irregularly shaped clasts of lava (10.1-3, 10.5). Flow-banded or pumiceous clasts are typical of silicic autobreccia. The aggregates are monomict, clast-supported, matrix-poor, poorly sorted, and grade into in situ jigsaw-fit lava breccia and fractured coherent lava. Flow banding in the coherent facies may be continuous into the autoclastic facies (Allen, 1988). Textural differences between autobreccia and hyaloclastite are subtle: autobreccia typically contains only very minor amounts of fine clasts (granule and finer), and blocks lack evidence of quenching, such as glassy rims cut by "tiny normal joints" (Yamagishi, 1979).

Textures characteristic of autobreccias can be significantly modified during hydrothermal alteration and deformation. Alteration affects clast margins and fractures within clasts, transforming the original clast-supported or in situ jigsaw-fit breccia into an apparent matrix-supported breccia (Allen, 1988) (Part 5). Deformation during and after alteration can further modify apparent clast shapes, size and abundance.

Talus (10)

Talus is a general term for rock fragments that accumulate at the bases of cliffs. In volcanic terranes, talus is typically associated with the steep fronts and margins of lava flows and domes, crater or caldera walls, and fault scarps (10.4, 10.6, 19.1-2). Lava-derived talus comprises mostly coarse, angular lava clasts produced by autobrecciation, quenching or gravity-driven failure of fractured parts of the lava flow or dome, and accumulates both during and following emplacement. The clasts fall, roll or slide downslope, more or less independently, and build an outward-sloping heap of loose fragments. The heaps are prone to periodic en masse resedimentation, commonly involving grain-flow processes. Talus breccia is clast-supported, matrix-poor, massive or weakly stratified and, although strictly monomict, the clasts can be texturally diverse and derived from different parts of the parent lava flow or dome. Transport distances are small, so the clasts are largely bounded by original fracture surfaces, but

corners and edges may be variably modified by abrasion. In ancient sequences, positive identification of lava-derived talus also depends on close spatial association with coherent lava or in situ autoclastic breccia of the same composition.

Hyaloclastite (11-13)

We use the term *hyaloclastite* for clastic aggregates formed by non-explosive fracturing and disintegration of quenched lavas and intrusions (cf. Rittmann, 1962; Silvestri, 1963; Pichler, 1965; Honnorez and Kirst, 1975; Yamagishi, 1987). The term is used for both unconsolidated clastic aggregates and their lithified equivalents. Fragmentation occurs in response to thermal stress, built up during rapid cooling, and stress imposed on chilled outer parts of lava flows and intrusions by continued movement of the ductile interior (Pichler, 1965; Kokelaar, 1986). Hyaloclastite forms from magmas covering the entire range of compositions from basalt to rhyolite. Current understanding of quench fragmentation processes rests primarily on studies of ancient submarine volcanic sequences, supplemented more recently by observation and sampling of hyaloclastite on modern ocean floors.

Quench fragmentation affects subaerially erupted lava that flows into water (e.g. Waters, 1960; Moore et al., 1973), lava erupted subglacially (e.g. Furnes et al., 1980; Fridleifsson et al., 1982), lava erupted subaqueously (e.g. Dimroth et al., 1978; Bergh and Sigvaldason, 1991; Kano et al., 1991) and magma intruded into unconsolidated, wet sediment (e.g. Busby-Spera and White, 1987; Kano, 1989; Hanson, 1991). Magma intruded into water- or fluid-filled cracks (Setterfield, 1987) and pyroclasts erupted into or deposited on water (Dimroth and Yamagishi, 1987; Yamagishi, 1987) can also be quench fragmented.

Quench fragmentation initially affects the outer contact surfaces of lavas and intrusions and the topmost parts of feeder dykes. Quenching produces fractures that vary in shape and in the depth to which they penetrate. Clasts are formed in situ, by the intersection of such fractures and by the spalling of quenched glass, and range widely in size from less than one millimeter to tens of centimeters. The clasts in *in situ* *hyaloclastite* fit more or less neatly together (jigsaw-fit texture) and remain where they were formed (11.1-7). *Resedimented hyaloclastite* shows evidence of transport of the clasts from the site of formation, such as bedding, mixing of clasts from texturally different parts of flows, and absence of jigsaw-fit texture (11.8). *Intrusive hyaloclastite* (also known as *peperitic hyaloclastite*) forms from parts of intrusions that are fragmented by quenching on contact with wet, unconsolidated host sediments (14.1).

In situ hyaloclastite may be limited to narrow selvages at the margins of lava sheets or pillow lobes, may form thick envelopes around lobes or pods of coherent lava (Fig. 19; 13.5), or may be the fragmented equivalent of entire lava masses, with only the feeder dykes

remaining unfragmented (Fig. 20; 13.7). This hyaloclastite is unstratified, strictly monomict, and characterized by jigsaw-fit of clasts (11.6-7), gradational contacts with coherent lava (11.2-3, 11.5), and polyhedral blocky or splintery clasts bounded by curvilinear surfaces (11.4, 12.1). Clasts are (or were) entirely or partly glassy and can be vesicular or non-vesicular. In many examples of silicic and andesitic hyaloclastite the glass is perlitic (12.5), and flow foliations in the parent lava can sometimes be traced continuously from clast to clast in adjacent in situ hyaloclastite (Fig. 21; 11.2-3, 11.5).

In situ hyaloclastite may be disturbed by continued movement of the more ductile interior lava, by flowage over steep slopes or by intrusions of magma into the hyaloclastite pile or by seismic activity. Disturbance produces results that vary from slight modification of the jigsaw-fit fabric by rotation and separation of clasts to wholesale gravitational collapse and resedimentation. Mass-flow resedimentation of hyaloclastite by grain-flow or density-modified grain-flow processes (Part 4) generates bedded monomict resedimented hyaloclastite breccia. Separate beds can be ungraded or graded (normal or reverse) and have appreciable primary dips. Some resedimented hyaloclastite sequences display a lateral decrease in grain size with distance from the source (e.g. Dimroth et al., 1978). Although the jigsaw-fit fabric is lost, clasts in resedimented hyaloclastite usually retain shapes characteristic of quench

fragmentation. Complex gradational relationships may exist between resedimented hyaloclastite, in situ hyaloclastite, coherent lava and feeder dykes, especially close to the source.

Intrusive hyaloclastite is typically a texturally complex mixture of clasts derived from the intrusion and matrix derived from the host sediment. Clasts that initially show jigsaw-fit texture can be progressively rotated and separated by narrow seams of host sediment, or else be more widely dispersed in the sediment matrix. However, intrusive hyaloclastite is essentially in situ, and only in exceptional circumstances becomes involved in resedimentation.

On the basis of field studies of submarine volcanic sequences of southwest Hokkaido, Yamagishi (1979, 1987) recognized two types of hyaloclastite with contrasting clast morphologies, interpreted to reflect differing magma viscosity at the time of fragmentation. Hyaloclastite (A) is derived from relatively low viscosity magma (basalt, basaltic andesite), occurs in close association with pillow lavas, and comprises massive, monomict breccia composed of pillow fragments and isolated pillows dispersed in a finer matrix (*pillow fragment breccia*) (15.4, 17.1). The matrix consists of millimeter- to centimeter-sized, glassy, splintery or blocky particles with curvilinear surfaces, produced by spalling of the quenched rims of disintegrating pillows. Similar hyaloclastite-pillow lava

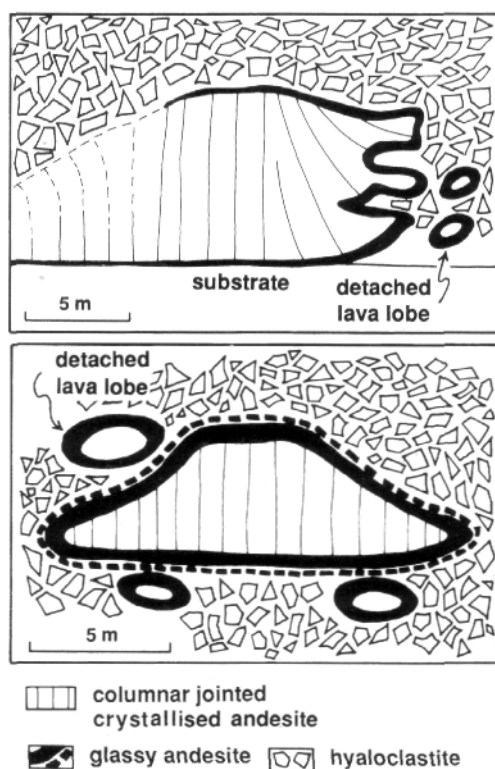


Fig. 19 Submarine andesitic lava and hyaloclastite. Lobes of coherent andesite are enveloped by cogenetic in situ hyaloclastite. Margins of the lobes and the hyaloclastite are glassy, whereas the lobe interiors are crystallized and columnar jointed. Modified from Yamagishi (1991).

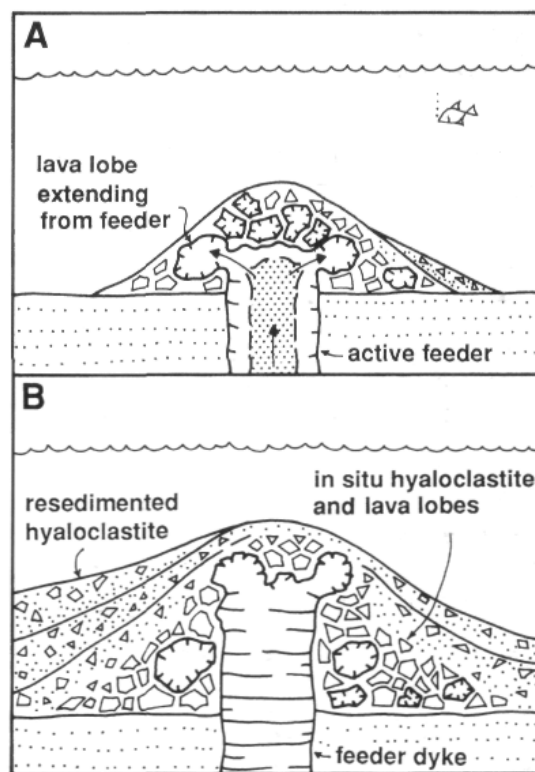


Fig. 20 In situ and resedimented hyaloclastite, and feeder dyke. (A) Lava emerging from the feeder dyke advances a short distance before being quenched. (B) The growing hyaloclastite pile is intruded by its feeder dyke. Unstable in situ hyaloclastite is resedimented downslope. Modified from Yamagishi (1987).

associations occur in other mafic submarine volcanic sequences (Carlisle, 1963; Dimroth et al., 1978; Staudigel and Schmincke, 1984). In addition to particles spalled from pillow rims, the matrix of "isolated pillow breccia" (Carlisle, 1963; Dimroth et al., 1978) also includes glassy globules that represent quenched lava droplets, possibly generated during phases of more vigorous effusion.

A distinctive variety of hyaloclastite (A) is associated with apophyseal-type feeder dykes (Yamagishi, 1987; 1991) and composed of *concentric pillows* (13.3-4). Concentric pillows are elliptical or spherical lava clasts up to a few tens of centimeters across, characterized by internal, roughly concentric joints. They have quenched glassy margins but lack the surface features of true pillows, and contain large (millimeter to centimeter), sparse, randomly distributed vesicles. Concentric pillows are thought to be produced by quenching and disintegration of tongues of lava extending outward from feeder dykes. The rounded shape is primary and mainly controlled by curved quench fractures responsible for disintegration of the lava tongues.

Hyaloclastite (B) is associated with viscous magmas (silicic and some intermediate compositions) that form massive lava sheets or detached pods and lobes, and has gradational contacts with jointed feeder dykes. First-order fractures penetrate the hot interior of emerging lava, causing further quenching, joint formation and fragmentation that progress inward (Yamagishi, 1987). Intersecting, curvilinear first-order quench fractures define polyhedral blocks, or pseudo-pillows (Watanabe and Katsui, 1976; Yamagishi, 1987) (9.6, 17.7); these may be intact, or else comprise groups of jigsaw-fit clasts (*angular fragment breccia*). "Tiny normal joints" commonly occur along the outer surfaces of pseudo-pillows (Fig. 18). No true pillow lobes are present. The hyaloclastite carapace of a growing lava flow or dome can be distended by continued advance of the plastic interior, allowing deeper penetration of water and further quenching. The formation of this type of hyaloclastite, thus, is closely connected with the process of autobrecciation (Pichler, 1965; Kano et al., 1991). Some in situ silicic hyaloclastite displays a clast-in-matrix texture, because the degree of fragmentation is quite variable: the matrix is more thoroughly fragmented, finer hyaloclastite surrounding less fragmented areas that appear to be clasts (11.2, 11.5). In detail, the clasts have gradational boundaries with the matrix, and the entire mass exhibits jigsaw-fit of constituent particles.

Hyaloclastite is a valuable indicator of the emplacement of lava into subaqueous settings and/or the intrusion of magma into wet sediment. However, hyaloclastite can be deposited in any water depth, and in fresh water or in the sea. Shallow-water hyaloclastite may be accompanied by resedimented or primary pyroclastic deposits, and may construct foreset-bedded sequences where subaerial lava flows meet the shore. Deep-water hyaloclastite is typically associated with massive or pillow lava, high-level intrusions, peperite and mass-

flow resedimented pyroclast-rich deposits. The character of enclosing sedimentary facies associations is critically important in constraining the depositional setting of ancient hyaloclastite sequences.

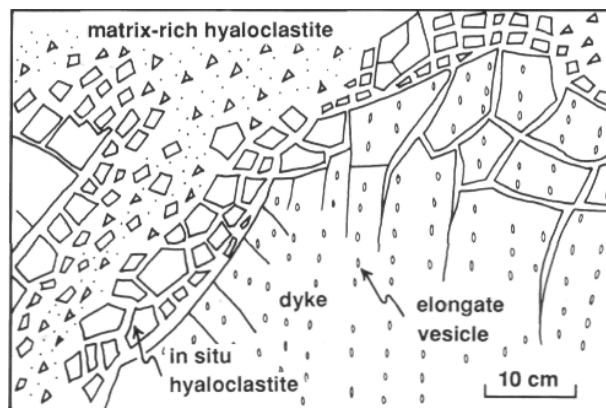


Fig. 21 Detail of the margin of a quench fragmented andesite dyke. Elongate vesicles define a flow foliation in the dyke that can be traced part way into the enveloping in situ hyaloclastite. Matrix-poor, in situ hyaloclastite at the margin of the dyke passes gradationally outward to matrix-rich hyaloclastite. Modified from Yamagishi (1991).

Facies associations comprising in situ hyaloclastite, resedimented hyaloclastite and coherent lava can amount to significant thicknesses and volumes. Basaltic hyaloclastite is a major component of ancient and modern seamount sequences (Staudigel and Schmincke, 1984; Smith and Batiza, 1989) and, at least, locally forms layers tens of metres thick in Layer 2 of oceanic crust (Schmincke et al., 1978). Sub-aqueous or subglacial silicic lava piles typically include a substantial, in some cases dominant proportion of hyaloclastite (Furnes et al., 1980; De Rosen-Spence et al., 1980; Kano et al., 1991; Pichler, 1965). For example, the island of Ponza, Italy, is principally composed of subaqueous rhyolitic to rhyodacitic hyaloclastite and feeder dykes. It is about 8 km long and 0.5–1.5 km wide. Subaerially exposed sections are over 100m thick and there is probably another 100 m or more concealed below sea level. Many of the textural and facies relationships characteristic of silicic hyaloclastite are displayed at Ponza (Pichler, 1965; Carmassi et al., 1983) (11).

Hyaloclastite is a genetic, interpretive term and should be reserved for cases where emplacement and fragmentation processes have been established. Other, more general but still genetic terms may be used instead. For example, *autoclastic breccia* caters for cases where either autobrecciation or quench fragmentation or both have operated, and *hydroclastic breccia* (Hanson, 1991) includes deposits from both explosive and non-explosive magma-water interactions. It is advisable to use descriptive nomenclature initially. Descriptive terms for aggregates that are eventually interpreted to be a variety of hyaloclastite combine information on clast composition, clast shape, clast size, and fabric; for example, basaltic pillow fragment

breccia; bedded basaltic granule breccia; poorly sorted dacitic breccia; rhyolitic jigsaw-fit breccia.

The abundance of glass and fractures, and the water-saturated setting that characterize hyaloclastite formation combine to promote its alteration. Modification of clast shapes and packing results from alteration concentrated along fractures and has the effect of converting the original jigsaw-fit texture of in situ hyaloclastite to an apparent matrix-supported fabric (42.2-4, 43.1-2; Part 5). Variable devitrification and alteration of glassy clasts can transform a strictly monomict aggregate into an apparent polymict aggregate.

Peperite (14)

Peperite is a rock generated by mixing of coherent lava or magma with unconsolidated wet sediment (Fisher, 1960; Williams and McBirney, 1979), and characterized by a clastic texture in which either component may form the matrix (14). *Peperite* occurs at the contacts between intrusions and wet sediments (Hanson and Schweickert, 1982; Hanson and Wilson, 1993), and along basal contacts of lava flows that override or burrow into unconsolidated sediments (Schmincke, 1967; Bull and Cas, 1989). Contacts are commonly complex in detail, involving intricate interpenetration between the intrusion or lava flow and the sediment, and mixed contacts can occur together with sharp, planar, unmixed contacts. Magmas involved in *peperite* formation range from basaltic to rhyolitic in composition, and from aphanitic to strongly porphyritic textural types. Sediments involved in *peperite* are also texturally diverse, ranging widely in grain size and in composition. In some cases, the host sediments are volcanoclastic deposits genetically related to the magmatism responsible for the intrusions.

The presence of pore water and the unconsolidated nature of the host sediment have important effects on processes occurring at magma-wet sediment contacts. Expansion of intensely heated pore fluid can initiate stationary fluidization of adjacent sediment, resulting in entrainment of sediment particles away from the contact. If pore fluid is flashed to steam, it can expand explosively. Both processes profoundly disrupt the coherence of the sediments adjacent to the contact and promote rapid, unconfined, and irregular penetration by magma (Kokelaar, 1982; 1986). Bedding in the sediments is commonly destroyed or else broken up and contorted. Parts of the magma may founder into the sediment and be partially detached or completely separated. The magma can also be disrupted by a combination of quench fragmentation on contact with the wet sediments and shattering by steam explosions (Wohletz, 1986; Kokelaar, 1982).

Busby-Spera and White (1987) identified two textural types of *peperite*: in *blocky peperite*, the clasts derived from the magma have sharply angular, blocky shapes and commonly exhibit jigsaw-fit texture (14.1), whereas in *globular (fluidal) peperite*, clasts derived from the

magma are lensoidal, bulbous or lobate (14.4). The textural differences between globular and blocky *peperite* were considered by Busby-Spera and White (1987) to be strongly influenced by the host sediment character. Globular clasts are thought to form in cases where a water-vapour film is established and maintained at the interface of the magma with the sediment. The vapour film insulates the magma from direct contact with the wet sediment, so both quench fragmentation of the magma and steam explosions are suppressed (Kokelaar, 1982). Furthermore, sediment in the vicinity of the vapour film is transported laterally along the contact zone, ultimately resulting in bulk displacement of the sediment and concomitant penetration by magma. Globular *peperite* is more likely to develop if the host sediments are fine grained, well sorted and loosely packed, because these are more permissive to fluid flow (either steam or hot pore water) and more easily fluidized.

Poorly sorted, coarse-grained sediments, however, are associated with blocky *peperite*. In these, the greater permeability of the host sediment interferes with development of a vapour film and, in any case, only a small part of the sediment size range is amenable to fluidization. In the absence of an insulating vapour film, magma-sediment interaction is dominated by quenching and phreatomagmatic fragmentation of the magma, accompanied by the steam-driven mixing and dispersal of clasts. *Peperite* in which magma fragmentation is largely the result of quenching is a variety of hyaloclastite (intrusive hyaloclastite or *peperitic hyaloclastite*). Thus, any one magma or lava body can be surrounded by different types of *peperite* that reflect changes in interaction processes controlled by natural variations in the host sediment properties (especially grain size, porosity and permeability).

The mechanisms of *peperite* formation are also controlled by the external confining pressure. For sills, the confining pressure is exerted by the overlying sediments and, in cases where the sediments are subaqueous, by the water column above as well. The confining pressure along bases of lava flows depends on the thickness of the flow and, for subaqueous flows, the depth of the water column. If the confining pressure exceeds the critical pressure of water (about 312 bars for sea water, 221 bars for pure water — Kokelaar, 1982), the degree of expansion of heated pore fluid is impeded, steam explosions are suppressed and fluidization may be inhibited. On the other hand, for high-level sills emplaced into relatively shallow-water sediments, the low confining pressure can allow explosive vaporization of pore fluid sufficiently disruptive to cause breaching of the sediment-magma interface above and "eruption" of the sediment-magma-steam mixture (White and Busby-Spera, 1987). Local "rootless" phreatomagmatic eruptions that break through lava flows are also generated by explosive vaporization of trapped pore fluid.

Peperite is an important component of mixed sedimentary-volcanic sequences, especially those in

subaqueous settings (e.g. Snyder and Fraser, 1963a; Brooks et al., 1982; Hanson and Schweickert, 1982; Kokelaar et al., 1984; White and Busby-Spera, 1987; Branney and Suthren, 1988; Kano, 1989; Hanson, 1991; Hanson and Wilson, 1993). In these, rising magma encounters substantial thicknesses of wet unconsolidated sediment and commonly forms sills or other irregular intrusive feeders with peperite borders. The presence of peperite along top and side contacts of sills and cryptodomes distinguishes them from extrusive lava flows and domes (Allen, 1992) (Fig. 22). Intrusions associated with peperite are essentially syn-sedimentary or syn-volcanic and should be distinguished from significantly later intrusions that invade solid host rock. Correct identification of peperite depends on well-constrained lithofacies and on details of the fabric and clast shapes. Peperite occurs in close association with coherent facies of lava flows or high-level intrusions and can be clast- or matrix-supported. In cases where the host is sandstone or finer, clasts derived from the magma are readily identified, whereas in peperite developed in polymict volcanic lithic breccia, the magma-derived clasts can be inconspicuous and difficult to distinguish from non-juvenile, volcanic lithic fragments. The sediment component of peperite is typically massive, or else bedding is highly contorted, and there is a gradation into or sharp contact with adjacent undisturbed sedimentary sequences. The sediment between the igneous clasts can be indurated and/or vesicular. Clasts derived from the magma or lava have distinctive fluidal, ragged or blocky shapes, and may have quenched glassy margins. Peperitic breccia is unstratified, ungraded and commonly poorly sorted.

Clast-forming processes that accompany interaction between magma, water and wet sediment may involve quenching, autobrecciation, steam explosions or combinations of these processes. In cases where a detailed interpretation is impossible, the general term *hydroclastic* (Hanson, 1991) is useful. This refers to clastic aggregates generated by magma-water interaction, whether explosive or non-explosive, and includes both intrusive and extrusive situations. Initially, purely descriptive nomenclature that identifies the two components (sedimentary host and the intrusion or lava) should be used for suspected peperites; for example, mudstone-matrix basalt breccia, chaotic sandstone-andesite breccia.

Pillow lavas (15-17)

Direct observations of modern ocean floors confirm the characteristic association between pillowed lava flows and subaqueous settings (Ballard and Moore, 1977; Ballard et al., 1979; Wells et al., 1979; Lonsdale and Batiza, 1980). The roughly elliptical, pillow-like shapes that characterize two-dimensional exposures of pillow lava are in fact cross-sections through interconnected tubes and lobes of lava (15, 16, 17). Only a small portion of the pillows in pillow lava are actually separate and self-contained (Moore, 1975). Pillow lobes expand and advance by stretching or rupture of quenched crust (Moore, 1975; Yamagishi, 1985;

Walker, 1992). When rupture occurs, the edges of the rupture are separated by means of symmetric or asymmetric spreading of molten lava (Fig. 23). Walker (1992) suggested that pillow lobe expansion mechanisms are influenced by lava viscosity. In relatively low viscosity lava, pillows expand mainly by stretching and have smooth surfaces with unbroken crusts. Crust rupture and spreading operate in higher viscosity lavas, and pillow surfaces are uneven, with corrugations and fault slivers. Penetration of water along cooling joints which cut the crust may simultaneously chill its inner boundary. Successive resupply of molten lava to the lobe leads to the formation of multiple-crust structure (Yamagishi, 1985) (16.2).

Pillow lobes display a wide variety of primary surface features, including ropy wrinkles, corrugations, spreading cracks, contraction cracks and tensional cracks (Moore, 1975; Yamagishi, 1985; 1987) (Fig. 23). Concentric and/or radial arrangements of textures are characteristic of pillow lobe cross-sections (Yamagishi et al., 1989; Walker, 1992). Equant vesicles vary in size and abundance concentrically, whereas pipe vesicles tend to be radial from the centre or are restricted to the lower parts of pillows in pillowed flows (17.2), at least in those emplaced on gently dipping substrates. Pipe vesicles are apparently most uncommon in pillows emplaced on slopes. Vesicles in the pillow centre are generally larger, less abundant and more spherical than those at the pillow margin. Fridleifsson et al. (1982) suggested that multiple concentric vesiculated zones are attributable to a sudden decrease in gas pressure within a pillow, as the surface crust breaks and a new pillow is formed. The rims of pillows show the effect of quenching, and are commonly glassy and intricately fractured (Yamagishi, 1987; 1991; Kawachi and Pringle, 1988). In basalts, the quenched rims (*rinds*) comprise zones of sideromelane, tachylite and tachylitic basalt that have a total thickness of 3-4 cm (Kawachi and Pringle, 1988) (15.7, 16.1). The interiors of pillows may exhibit distinct radial columnar (9.4, 15.7) or tortoise shell joints (17.1) which strongly influence the shape of fragments generated when pillow lobes disintegrate. Somewhat less well-developed concentric joints can occur together with radial columnar joints.

In some pillowed lava flows, pillow lobes are packed closely together, and successively emplaced lobes accommodate to the shapes of spaces between subjacent lobes. The resulting asymmetry in shape provides a reliable indication of the younging direction (15.5, 17.2, 17.5). In cases where the packing is more open, the inter-pillow spaces are eventually filled with hyaloclastite principally derived from spalled glassy rinds, or with other sediment. In favorable exposures, it may be possible to determine progradation directions of pillow lobes. The best indication is the sense of asymmetry of re-entrants in lobe outlines, which mark the positions of constrictions between successive segments of pillow lobes (Hargreaves and Ayres, 1979; Yamagishi, 1985). A systematic upward decrease in pillow lobe diameter in a single pillowed lava flow has

been interpreted to indicate waning discharge rates during emplacement (Dimroth et al., 1978; Staudigel and Schmincke, 1984).

Pillows are diagnostic of the subaqueous emplacement of lavas, especially those of basaltic composition. The emplacement setting, however, is not necessarily the same as the eruption setting. Subaerially erupted lava flows, especially tube-fed, basaltic pahoehoe flows, commonly reach coastlines several to tens of kilometers from source (Moore et al., 1973; Tribble, 1991). Subaerial lava flows that enter water can continue to advance, building a *lava delta*, the foresets of which are composed of dispersed, elongate pillow lobes and hyaloclastite with appreciable primary dips (Jones and Nelson, 1970). Pillows can be useful in distinguishing "relatively deep" from "relatively shallow" water depths. For example, vesicle size and abundance in pillow lobes may be used to interpret relative water depth of emplacement of pillowed flows (Moore, 1965; Jones, 1969; Moore and Schilling, 1973; Yamagishi et al., 1989; Dolozi and Ayres, 1991). In pillow lava sequences comprising more or less consistent compositions, including original volatile contents, larger and more abundant vesicles are expected to occur in pillows emplaced at shallower water depths. Kawachi and Pringle (1988) considered the presence of multiple-rind structure (16.1) at the margins of pillows to be a feature limited to flows emplaced in shallow water (less than 1-2 km, depending on the initial dissolved H₂O and CO₂). Multiple-rind structure is thought to form by the implosion and rupture of the pillow skin, processes which are probably limited to low-pressure environments (that is, relatively shallow water). The

absence of multiple-rind structure, is not, however, indicative of emplacement in relatively deep water. [Note that multiple-crust structure (Yamagishi, 1985) is distinct from multiple-rind structure and has no recognized significance with regard to water depth). Finally, although pillowed lava flows are good indicators of subaqueous emplacement, not all subaqueous lava flows are pillowed.

Ancient examples of subaqueous lava flows of compositions other than basalt (intermediate and silicic) are also organized into pillow lobes and pods (e.g. andesite — Cousineau and Dimroth, 1982; Yamagishi, 1985; 1987; 1991; rhyodacite — Bevins and Roach, 1979; rhyolite — Kano et al., 1991; trachyte-trachyandesite — Yamagishi and Goto, 1991). Studies of ancient submarine volcanic sequences show that pillow lobes also form when magma intrudes or invades water-saturated hyaloclastite or sediments (Fig. 24). Intrusive examples range from basaltic to silicic in magma composition (e.g. basalt, basaltic andesite — Kano, 1991; Snyder and Fraser, 1963b; Yamagishi, 1987; andesite, dacite — Snyder and Fraser, 1963a; Hanson 1991; silicic — Hanson, 1991). Distinguishing pillowed intrusions from extrusive pillow lava flows rests on careful examination of the top contacts and on the character of the inter-pillow sediment. Peperite sometimes occurs along the upper contacts of pillowed intrusions but does not occur above pillowed flows. The sediment in contact with pillowed intrusions is usually locally indurated or altered, and any pre-existing bedding is disturbed or else destroyed. Irregular enclaves of host sediment can be completely detached and incorporated deep into the interior parts of pillowed

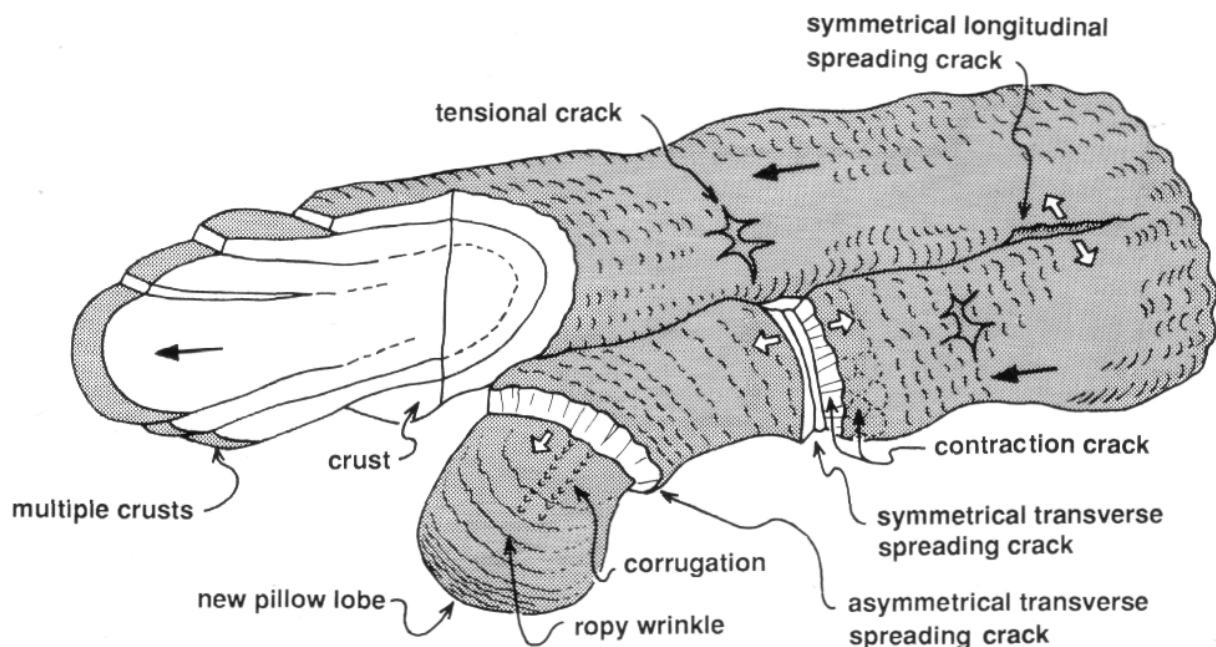


Fig. 23 Characteristic surface structures of pillow lobes and model for pillow growth. Multiple crusts form at the end of the pillow toe by repeated surges of liquid lava. Two pillow lobes diverge from the original single pillow lobe by formation of a symmetrical longitudinal spreading crack, and each pillow lobe advances from transverse spreading cracks. Open and closed arrows indicate spreading and flow direction respectively. Modified from Yamagishi (1985).

intrusions. In contrast, sediment that occurs between pillows at the top of pillow lava flows is usually bedded, because it either settles from the water column or else is washed in by currents, and is no more indurated or altered than adjacent parts of the enclosing sequence.

Subaqueous basaltic lava flows

The best documented features of subaqueous basaltic lavas are pillows (Carlisle, 1963; Jones, 1969; Moore, 1975; Ballard and Moore, 1977; Dimroth et al., 1978; Ballard et al., 1979; Lonsdale and Batiza, 1980; Staudigel and Schmincke, 1984; Yamagishi, 1985; 1987; 1991; Yamagishi et al., 1989; Tribble, 1991; Walker, 1992) (Fig. 23; **15**, **16**, **17**). Basaltic lavas in modern oceans also exhibit other flow morphologies: thick (at least several metres) massive tabular flows, thin (<1 m) sheet flows, lobate flows, block lavas, and flows with surface features (buckles, folds, coils) similar to those of subaerial pahoehoe (Lonsdale, 1977; Basaltic Volcanism Study Project, 1981). Tube systems and channels identified in lavas of the East Pacific Rise (Fornari, 1986) are apparently similar to their subaerial counterparts. Tumuli and other structures due to lava flow inflation, that are common in subaerial pahoehoe lava fields, have also been identified in submarine basalt lava fields; for example, at the summit of Axial Volcano and in the axial valley of the Juan de Fuca Ridge (Applegate and Embley, 1992).

Subaqueous basaltic lava sequences can include significant volumes of lava-derived clastic aggregates that are mainly produced by quench fragmentation and

gravitational collapse. Spaces between pillows are commonly occupied by granular hyaloclastite generated by spalling of the brittle glassy pillow rind, and large amounts of pillow fragment breccia can be formed by disintegration of pillow lobes (Carlisle, 1963; Dewit and Stern, 1978; Staudigel and Schmincke, 1984; Yamagishi, 1987; 1991). Some examples of basaltic hyaloclastite retrieved from seamounts on the East Pacific Rise occur in thin, sheet-like, graded beds (Smith and Batiza, 1989). Talus breccia accumulates adjacent to fault scarps in submarine basalt sequences and within lava tubes that have collapsed. Larger scale gravitational collapse of the flanks of pillow cones and seamounts also produces fragmental deposits, but their internal textures and structures are poorly known.

In both ancient and modern submarine basaltic sequences, some deposits include fluidally shaped clasts similar to subaerial bombs and spatter, and thought to be generated by lava fountains akin to subaerial Hawaiian- or Strombolian-style eruptions. Such lava fountains are probably restricted to relatively shallow-water settings (Staudigel and Schmincke, 1984; Dimroth and Yamagishi, 1987; Dolozi and Ayres, 1991) or, in deeper water, to brief periods of exceptionally vigorous discharge (Smith and Batiza, 1989). In some ancient sequences of subaqueous basaltic lava flows, interpreted proximal sections are dominated by massive lava flows, whereas in more distal sections, pillow lava and pillow fragment breccia predominate (Dimroth et al., 1978; Waters and Wallace, 1992) (Fig. 25).

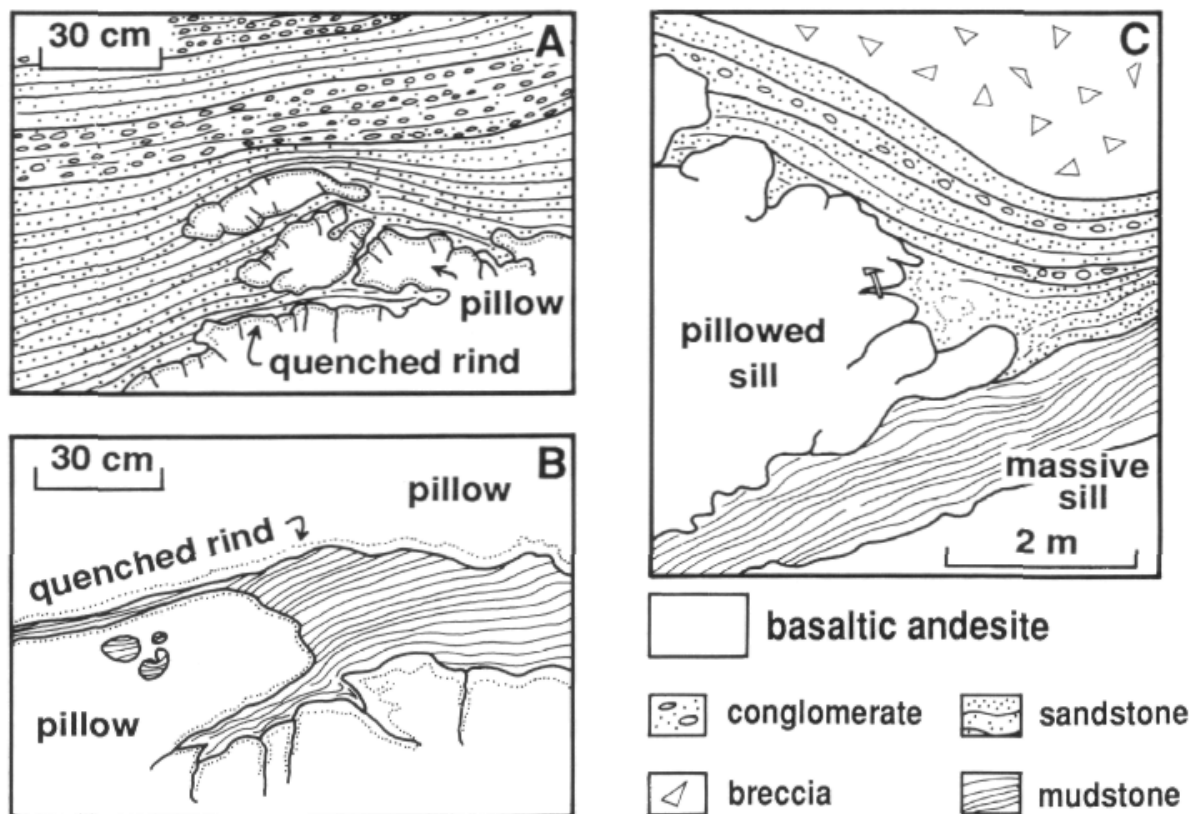


Fig. 24 Details of the top (A), base (B) and tip (C) of a single, 5 m thick, pillowed, basaltic andesite sill that intruded wet, unconsolidated sediments, Josoji Formation, Miocene, Japan. Modified from Kano (1991).

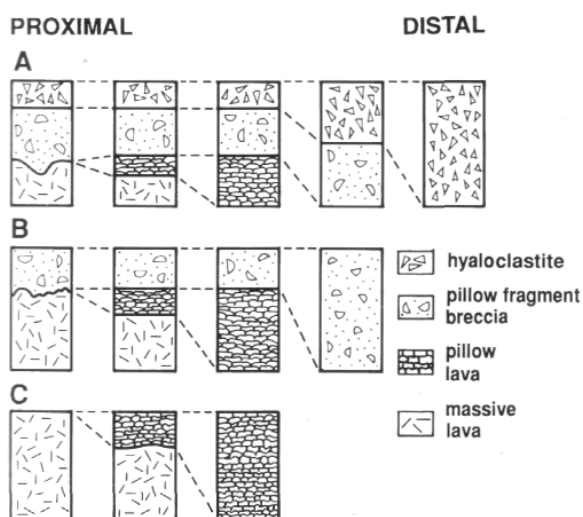


Fig. 25 Examples of proximal to distal variations in facies associations found in subaqueous basaltic and andesitic lava flows. The changes occur over lateral distances that measure tens of meters to a few kilometers. Modified from Dimroth et al. (1978).

Subaqueous silicic lava flows, domes and syn-volcanic intrusions

In subaqueous settings, magmas may be extruded as lava flows and domes, or else form sills, dykes and intrusive to partly extrusive cryptodomes. Subaqueous eruption settings are also special, because of the importance of quench fragmentation on contact with water or wet sediment. Some subaqueous effusive eruptions generate voluminous hyaloclastite, with only feeder dykes in the interior remaining unfragmented. Contact relationships and the distribution of coherent lava, peperite, hyaloclastite and resedimented hyaloclastite are the bases for determining the mode of emplacement. The upper contact relationships are critical because basal contacts of intrusions and surface flows can be similar.

Subaqueous silicic lava flows and extrusive domes

Subaqueous silicic lava flows and extrusive domes display a similar assemblage of internal textures. However, domes typically include remnants of feeder dykes and are less laterally extensive (Fig. 26). The coherent interiors of lava flows and extrusive domes are characterized by evenly porphyritic or aphanitic textures and can be massive and/or flow banded. Internal flow banding in lava flows is commonly subparallel to the base and top contacts and, at the sides, is oblique to bedding. The coherent core of lava flows may be overlain by a carapace of in situ hyaloclastite. Flow banding in the coherent cores of lava domes mirrors the outer contacts but can steepen abruptly close to the overlying carapace of hyaloclastite (Pichler, 1965). Polygenetic dome complexes are characterized by repeated alternations and gradations between hyaloclastite and intervals of coherent lava, and may involve varying compositions (Allen, 1992). Mass-flow

redeposition of in situ hyaloclastite, in response to oversteepening of flow or dome surfaces, generates stratified resedimented hyaloclastite at flow margins and along the tops and flanks of domes.

In many cases, parts of lava flows and domes in direct contact with wet sediment mix with it, producing texturally complex lava-sediment breccia (peperite). This is common along lower contacts of lava flows, at lower and side contacts of domes, and at all contacts of locally burrowing parts of lava flows. Any original bedding in the sediments involved in mixed contacts with lava is commonly destroyed, due to expansion and movement of heated pore fluid. Sediments in the contact zone can be prematurely dewatered and indurated. Lava flows and domes, especially those of silicic composition, are constructional and create topography that influences the distribution, facies and geometry of contemporaneous and succeeding volcanic or sedimentary units.

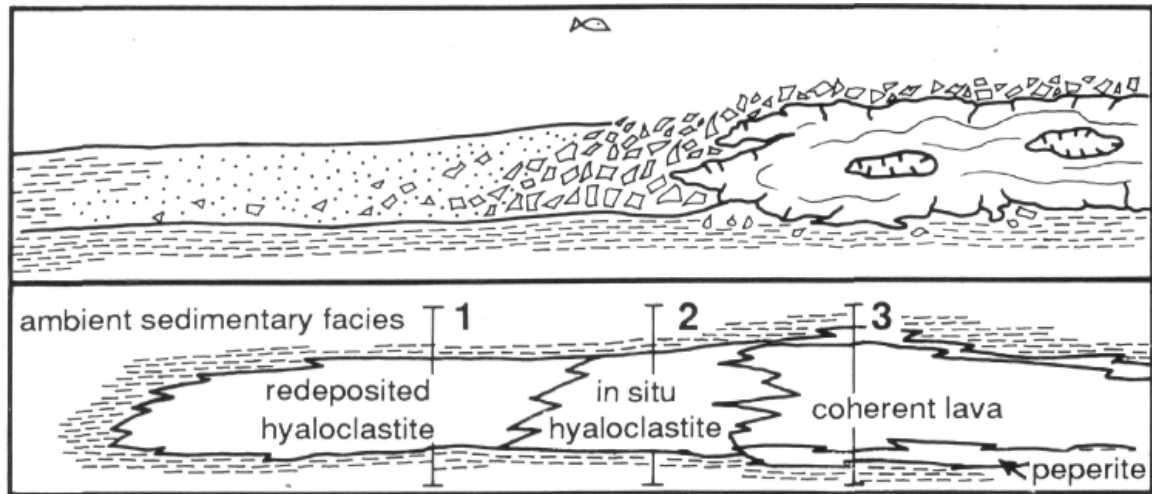
In addition to massive lava flows and domes, subaqueous silicic lavas form lobes, pods and pillow-like bodies associated with hyaloclastite. These features occur in subaqueously emplaced flows from the Canadian Archean and in subglacial Quaternary rhyolites in Iceland (De Rosen-Spence et al., 1980; Furnes et al., 1980). An Ordovician rhyodacitic pillow lava and pillow fragment breccia have been described by Bevins and Roach (1979). Rhyolite lava in the Miocene Ushikiri Formation, SW Japan, was erupted in water 200-1000 m deep (Kano et al., 1991). The total thickness of rhyolite is about 600 m, in which three lava flow units have been recognized. Each unit is composed of large (1-15 m across), pillow-like lobes of lava (Fig. 27), enclosed by masses of angular fragment breccia (in situ hyaloclastite) and partly overlain by stratified volcanic breccia (resedimented hyaloclastite — Fig. 28). Small-volume rhyolitic extrusions in the Miocene Green Tuff Belt, Japan, and in the Archean Abitibi Belt, Canada, comprise lava lobes and pods propagating from master feeder dykes and enclosed in hyaloclastite (Yamagishi and Dimroth, 1985; Yamagishi, 1987). Lava lobes are up to tens of metres across and internally texturally zoned; there is a coherent crystalline core with a flow-banded perlitic obsidian rim, enveloped by glassy in situ hyaloclastite (Yamagishi and Dimroth, 1985; Yamagishi, 1987; 1991; Kano et al., 1991) (Fig. 27). Vesicles are concentrated just within the outer glassy rim and are often aligned parallel to the flow banding in the lobes. Lobe boundaries can be sharp or gradational into the enclosing hyaloclastite.

In general, subaqueous silicic lava flows and domes do not extend far from source and are a good indication of proximity to a vent (within a few kilometers for flows, and within hundreds of metres for domes). Some ancient subaqueous silicic flows are evidently more extensive. For example, Devonian dacites in Australia have lateral dimensions up to 80 km (Cas, 1978), and Archean rhyolites in Canada extend up to 10 km from source (De Rosen-Spence et al., 1980). Cas (1978) suggested that flows erupted in a deep-water

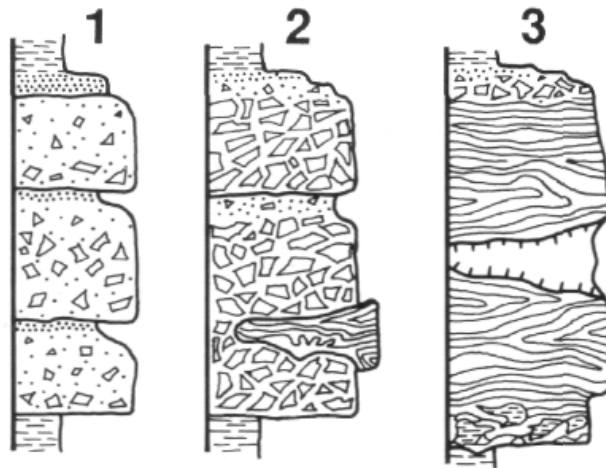
environment would retain volatiles due to the high confining pressure imposed by the water column and, in consequence, might have lower viscosity and greater

mobility than subaerial flows of equivalent compositions.

LAVA FLOWS



SECTIONS



LAVA DOMES

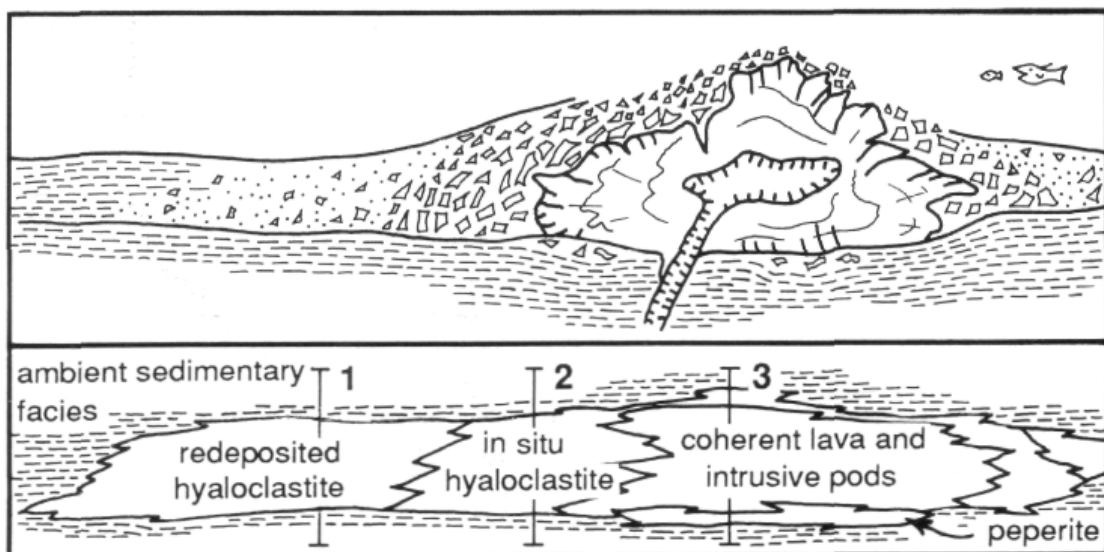


Fig. 26 Character and arrangement of contemporaneous volcanic facies that develop in association with the emplacement of submarine lava flows (top) and domes (bottom). On each volcanic facies diagram, (1), (2), (3) mark the sites of sections depicted by graphic logs in the centre diagram. Each section samples genetically related facies that differ markedly in character, texture and internal organization. Coherent lava in one section may be the direct correlate of bedded volcanoclastic breccia in an adjacent section.

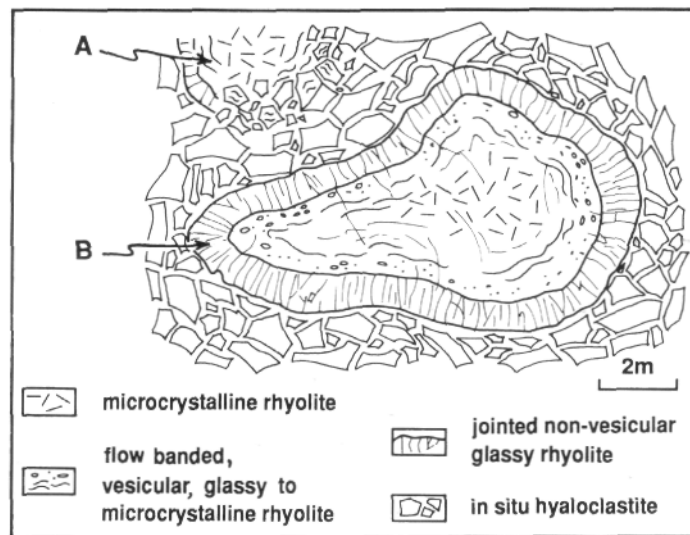


Fig. 27 Cross-section through remnants of a rhyolite lava lobe grading into in situ hyaloclastite (A), and a well-preserved, texturally zoned, lava lobe (B) in sharp contact with the enveloping hyaloclastite. Modified from Kano et al. (1991).

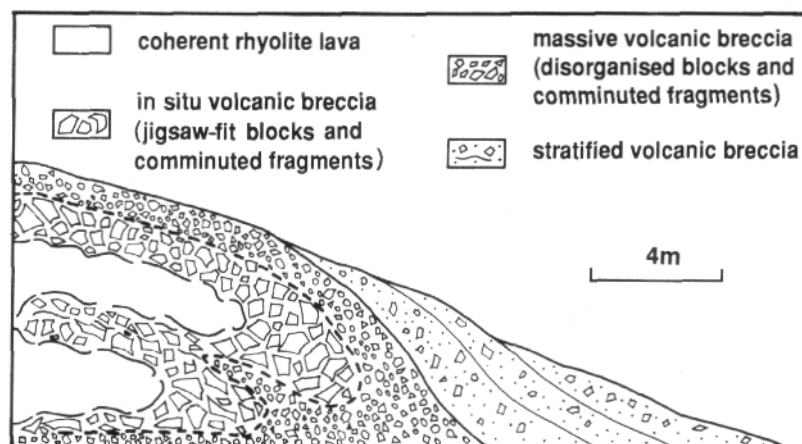


Fig. 28—Schematic volcanic fades associated with subaqueous emplacement of rhyolite lava; Miocene, Ushikiri Formation, Japan. Modified from Kano et al. (1991).

In ancient volcanic sequences, the best criterion for establishing a subaqueous setting for silicic lava flows and domes is the close spatial association of coherent lava, in situ hyaloclastite and resedimented hyaloclastite. Another constraint is the presence of lobes, pods and pillow-like masses of coherent lava. In most cases, the character of associated sedimentary facies is of prime importance in determining the setting.

Subaqueous partly extrusive cryptodomes

Cryptodomes are high-level intrusions that cause up-doming of the overlying sediments or rocks (Minakami et al., 1951). Partly extrusive cryptodomes locally break through the cover and emerge at the surface. Cryptodomes mostly involve intermediate or silicic composition magmas, and their emplacement appears to be especially favored in subaqueous, mixed sedimentary-volcanic settings. In these settings, the water column contributes to the confining pressure, allowing the magma to rise to very high levels, where it is likely to encounter a substantial interval of "weak", poorly consolidated, less dense sediments. Because

partly extrusive cryptodomes are largely subsurface, the best descriptions come from dissected ancient examples (Allen, 1992). They exhibit the characteristics of both high-level intrusions and extrusive domes (Fig. 29). The coherent core of a cryptodome passes gradationally outward into in situ hyaloclastite that is overlain locally by stratified, mass-flow resedimented hyaloclastite generated during emergence of the dome. Resedimented hyaloclastite transported farthest from the emergent portions of the dome is intercalated with other contemporaneous sedimentary or volcanic deposits. In situ hyaloclastite and peperite commonly develop along the intrusive margins of the dome and separate the coherent interior from the intruded host sequence. Dome emplacement can be responsible for local deformation of any bedding present in the host sequence. In cases involving poorly consolidated host sediments, heterogeneous compaction around the rigid dome may also cause irregularities in bedding nearby (Baldwin, 1971).

Subaqueous syn-volcanic sills and dykes

In ancient volcanic terranes, it is useful to make a distinction between sills and dykes that are essentially coeval with the enclosing sequence and those that significantly post-date the enclosing sequence. Especially in subaqueous settings, a significant proportion of the magmatism may in fact comprise syn-volcanic, high-level intrusions rather than surface lava flows. Magma movement towards the surface is influenced by its density and hydrostatic pressure compared with the density of the enclosing rocks (or sediments) and the lithostatic pressure they exert. Magma that is denser than the host is more likely to remain subsurface and be intruded as sills than erupted (McBirney, 1963; Walker, 1989a). This condition is commonly met in subaqueous settings where rising magma encounters unconsolidated sediments that have accumulated to substantial thicknesses. Host sequences to syn-volcanic sills and dykes consist of ambient basin sediments, volcanic deposits and other co-genetic sills and dykes.

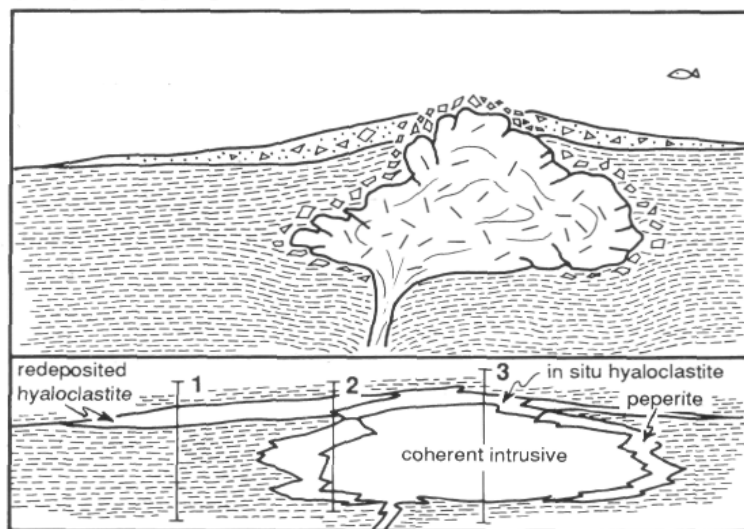
Identification of syn-volcanic or syn-sedimentary sills usually depends on the upper contact relationships, especially evidence indicating that the host sequence was unconsolidated or poorly consolidated when intruded (Fig. 30). Important features include the presence of tongues or lobes projecting upward from the sill into the host, the development of peperite along the upper margin, induration of the host, destruction or disturbance of bedding in sediments at the contact, and the presence of contacts that are locally discordant to adjacent bedding (Kokelaar, 1982; Branney and Suthren, 1988; McPhie, 1993). A chilled margin may occur along upper surfaces of both sills and surface lava flows and is not diagnostic of the mode of emplacement. Along the lower contacts of sills, textures can develop that are similar to those along the upper contact or along the bases of lava flows.

Syn-volcanic dykes are, in most cases, actually feeders to lava flows and domes, to piles of in situ and resedimented hyaloclastite (Fig. 20), or to syn-volcanic sills. Contacts of syn-volcanic dykes show the effects of quenching in the near-surface, water-saturated environment, and of interaction with the poorly consolidated host sequence. Yamagishi (1987, 1991) has recognized different types of feeder dykes distinguished by the character of their margins and of associated hyaloclastite. The margins of *apophyseal-type* feeder dykes consist of bulbous or finger-like protrusions which extend into the host and break up into concentric pillow fragments (13.3). The margins of *massive-type* feeder dykes are very closely jointed and grade outward to angular fragment breccia and peperite (13.7).

Volcaniclastic deposits associated with silicic lava dome eruptions in shallow water (18)

Silicic lava dome eruptions at vents in shallow water typically involve complex combinations of phreatomagmatic, explosive magmatic and effusive activity, complicated further by syn-eruptive mass-flow resedimentation and reworking. Volcaniclastic deposits formed in this setting can be mixtures of quench-fragmented juvenile clasts and pyroclasts, and show evidence of heat retention in spite of subaqueous deposition (e.g. Tamura et al., 1991). Sustained eruptive activity may lead to subaerial emergence of the volcanic pile, followed by cycles of growth and collapse of the edifice. In many cases, only a remnant of volcanic structure survives, and significant amounts of the volcanic products are reworked, eroded and resedimented, contributing Volcaniclastic debris to neighboring deeper water settings. The final record of dome-related, shallow-water volcanism is thus expected to include a wide range of volcanic facies and marked variations in facies geometry, especially in proximal sequences.

CRYPTODOME



SECTIONS :

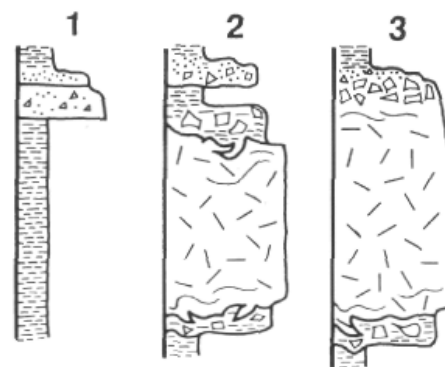


Fig. 29 Character and arrangement of volcanic facies that develop in association with the emplacement of partly extrusive cryptodomes (top). (1), (2), (3) mark the sites of sections depicted in the graphic logs (right).

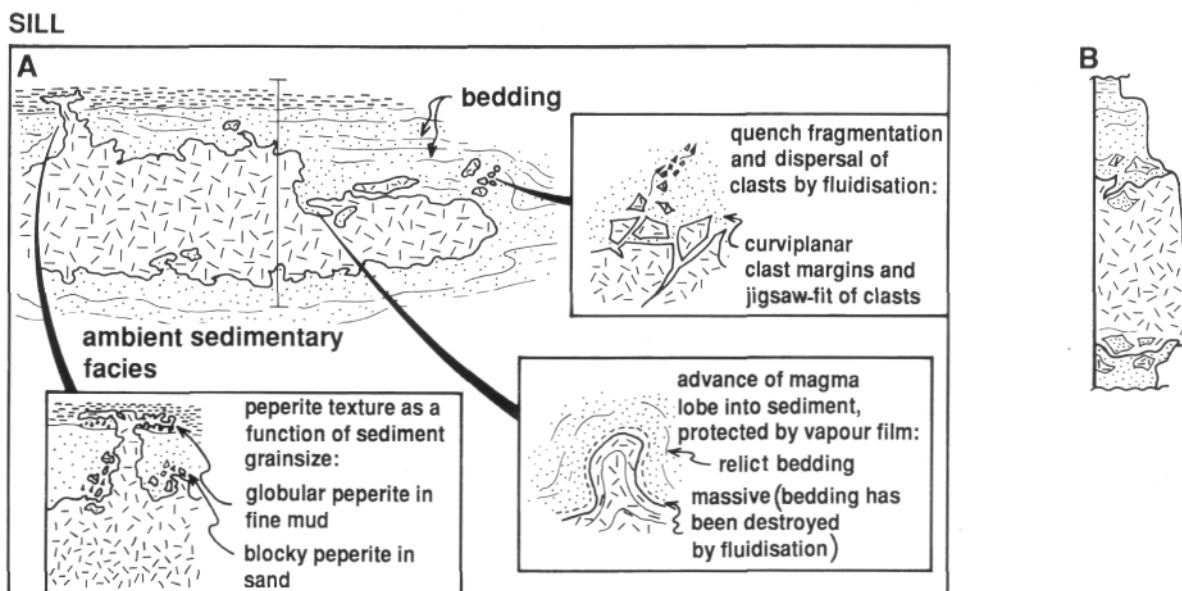


Fig. 30 (A) The character and distribution of facies that develop during the emplacement of syn-sedimentary sills, and the processes involved in peperite formation. (B) Graphic log of a section through the sill and host sediment.

A modern example of this style of activity is provided by the 1953-57 eruptions of Tulumán, a rhyolitic volcano in the Bismarck Sea, Papua New Guinea (Reynolds and Best, 1976; Reynolds et al., 1980). Effusion of lava began at a vent in about 130 m water depth and was followed by explosive eruptions, which built several small, partly emergent pumice cones. During the initial effusive stage, spectacular explosions were triggered by interaction of water with large (several meters across), floating, hot, pumiceous rhyolite masses spalled from the sea-floor lava.

Tulumán has been used as an analogue for part of the volcanoclastic sequence in the Devonian Bunga Beds, Australia (Cas et al., 1990) (18). Coherent rhyolite, monomict in situ rhyolite breccia and rhyolite-sediment megabreccia (18.2-4) at the base of the sequence record emplacement of a rhyolite dome into wet, unconsolidated sea-floor sediments (18.1) and accompanying quench fragmentation, auto-brecciation and resedimentation. Massive, rhyolitic pumice-rich breccia (18.5-6) and stratified, crystal-rich to crystal-poor, pumiceous sandstone and siltstone (18.7) above indicate the onset of pyroclastic eruptions. Settling of the pyroclasts through the water column resulted in efficient sorting according to density (hydraulic sorting) during eruption and transport, and stratification developed in response to rapidly repeated explosions and/or water turbulence. Pumiceous debris-flow deposits and turbidites elsewhere in the sequence were produced by downslope slumping and mass-flow resedimentation events during and after the pyroclastic eruptions. Cas et al. (1990) suggested that shoaling of the dome permitted the change from effusive to explosive activity, reflecting the control exerted by the confining pressure of the water column on eruption style.

CASE STUDY: Partly extrusive, submarine, dacite cryptodome, Sock Creek South, western Tasmania

Part of the Mount Read Volcanics intersected in Sock Creek South diamond drill holes (SCS-2, SCS-3) provides an example of the facies and facies geometry associated with a small, submarine, dacitic, partly extrusive cryptodome. The interpretation is based on the clast shapes and textures that constrain the fragmentation processes of the various clastic facies in the sequence, the character of contacts between coherent and autoclastic facies, and the emplacement setting indicated mainly by the associated sedimentary facies.

A very thick unit of massive to weakly graded, tube pumice- and lithic-rich breccia is present at the base of both drill holes (Fig. 31; 33.1-2). The section above comprises coherent dacite and dacite breccia, interbedded with and overlain by laminated, pyritic, black mudstone and graded, medium to thick beds of volcanoclastic sandstone. On the graphic logs, intervals of dacite and dacite breccia that have distinctive textures or structures can be easily identified (Fig. 31A-E) and provide the framework for genetic interpretation (Fig. 32).

In SCS-2, laminated mudstone is overlain by facies (A) that consists of monomict, jigsaw-fit dacite breccia (in situ hyaloclastite), the lowermost part of which locally has mudstone matrix (intrusive hyaloclastite). At the top of facies (A) is a sharp upper contact with massive, faintly to strongly flow-banded dacite (8.7) and monomict, jigsaw-fit dacite breccia (12.6), which are grouped together in facies (B) (coherent dacite and in situ hyaloclastite). Above the topmost in situ hyaloclastite interval of facies (B) are massive, matrix-to clast-supported, monomict dacite breccia and stratified crystal- and lithic-rich volcanoclastic sandstone

of facies (C) (mass-flow resedimented hyaloclastite). Clasts in the breccia of facies (C) are angular, and some have curvilinear margins; many show zoning defined by altered pink (chilled ?) rims and green cores, or are flow banded.

Drill hole SCS-3 is located 165 m southwest of SCS-2. The correlative section comprises dacite breccia intervals interbedded with laminated mudstone and graded bedded sandstone (Fig. 31). Facies (D) consists of massive, mudstone-matrix-supported volcanic lithic breccia in poorly defined beds separated by laminated mudstone. The breccia is polymict but dominated by ragged, angular dacite lava clasts. Facies (E) is composed of massive, mudstone-matrix dacite breccia (peperite), gradationally overlain by monomict, jigsaw-fit dacite breccia (in situ hyaloclastite). The thickest interval of facies (E) has sharp upper and lower contacts with massive volcanoclastic sandstone.

The intercalated and overlying sedimentary facies (laminated black mudstone and graded bedded sandstone) suggest that the original depositional setting was below-wave-base, relatively deep submarine. Facies (A) in SCS-2 is interpreted to represent the quench-fragmented, partly peperitic margin of a coherent dacite dome and associated hyaloclastite (B) emplaced into unconsolidated mud (Fig. 32). The top of the dacite, however, was emergent and overlain by resedimented hyaloclastite (C) derived from adjacent unstable parts of the active dome, or else from a coeval, active dome nearby. Facies (E) in SCS-3 is totally intrusive and may be a small dacite lobe, closely related to but separate from the larger dacite cryptodome. The resedimented hyaloclastite in SCS-3 (D) is partly dacite-dome derived but also includes clasts contributed from other sources.

Subaerial silicic lava flows and domes (19, 20)

Subaerial silicic lavas are commonly found as thick (several tens to more than a hundred metres), short (less than a few kilometers), small-volume (less than one cubic kilometer) flows and domes (19.1). However, in some cases, single lava flows and the coalesced products of eruptions from adjacent vents are far more voluminous. Young (< 155 ka) high-silica rhyolite lava flows that infill Yellowstone caldera have maximum outflow dimensions of 25-32 km, cover 275-350 km² and amount to 30-60 km³ each (Christiansen and Hildreth, 1989). The Quaternary Chao dacite lava flow in northern Chile extends 14.5 km from source and has a volume of 26 km³ (Guest and Sanchez, 1969; De Silva and Francis, 1991) (19.4). Other examples of voluminous (10-200 km³) and extensive rhyolite lava flows occur in Idaho (Miocene — Bonnicksen and Kauffman, 1987; Manley, 1992), Mexico (Miocene — Hausback, 1987), West Texas (Tertiary — Henry et al., 1988; Henry et al., 1990), North America (Proterozoic — Green and Fitz, 1993) and eastern Australia (Devonian — Dadd, 1992). The viscosity, rate of cooling, volume erupted and substrate gradient all influence the final shape and dimensions of silicic lava

flows. Cooling of the interior of thick silicic lavas (100-300 m) is very slow, so providing sufficient volume is erupted, flowage can continue for decades and produce extensive, thick flows (Manley, 1992).

Silicic lava flows advance by means of laminar shear. Many of the internal textures and structures preserved in lava flows, such as flow banding, axes of flow folds, aligned elongate phenocrysts and stretched vesicles, reflect the combination of high viscosity and laminar shear (Fink and Pollard, 1983). These flowage-related internal structures are overprinted by cooling joints. Cross-sectional profiles of unconfined, subaerial silicic lava flows and domes are characterized by flat or very gently sloping top surfaces, steep sides and steep flow fronts (Fig. 33). Upper parts of domes and lava flows exhibit steep flow foliations and ramp structures, some of which have surface expression as ridges. Near the basal contacts and flow fronts, foliations are shallowly dipping (Christiansen and Lipman, 1966; Duffield and Dalrymple, 1990; Fink, 1983). Local deviations from the general pattern are very common. Interpreting internal structures of domes or the attitudes of lava flow contacts from measurements of flow banding in ancient examples thus requires considerable care.

In addition to variation in flow-foliation attitude, the interiors of subaerial silicic lava flows and domes display diverse textures, involving the distribution of coherent versus autoclastic facies, variations in vesicle size and abundance, and the effects of devitrification, crystallization and hydration (Fig. 33). Development of these textures reflects the interplay of pre-eruption conditions (composition, especially volatile and phenocryst content), processes that operate during extrusion (vesiculation, autobrecciation, crystallization and devitrification), and post-emplacement changes (further crystallization and devitrification, hydration and joint development).

The distribution of coherent and autoclastic facies in silicic lava flows is strongly controlled by the lava rheology. The rheology of rhyolitic lavas depends on strain rate, temperature and volatile contents (Fink, 1983). Flowage occurs when the applied shear stress exceeds the yield strength. Brittle failure occurs if the applied shear stress exceeds the tensile strength. Both yield strength and tensile strength are thought to decrease with increasing temperature (Fink and Manley, 1987). Numerical models of temperature profiles through active lava flows show minima at the base and top surface, with increases to near-eruption temperatures in the centre (Fink, 1983; Manley, 1992). Thus, the hot interior of the lava is able to deform and flow between rigid, non-deforming cooler layers at the top and base. Movement of the flow interior causes fragmentation of the rigid top and base, so that silicic lava flows and domes typically have an upper, basal and marginal breccia composed of lava blocks in granular matrix (autobreccia). Spatial and temporal changes in rheology within the flow can produce brittly fractured zones that are encased in and healed by ductile coherent lava.

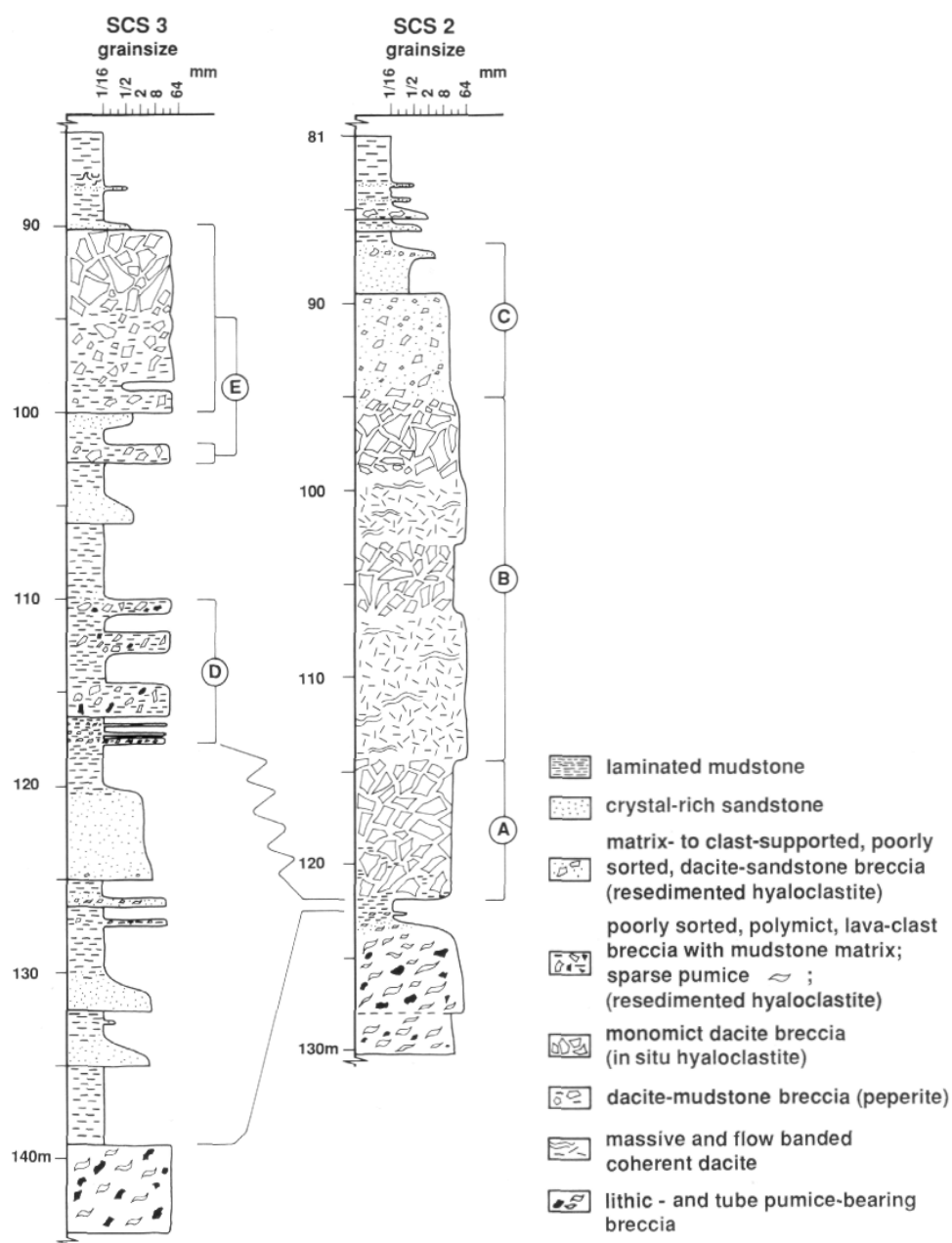


Fig. 31 Graphic lithological logs for parts of two nearby drill holes, DDH SCS2 and DDH SCS3, Sock Creek South, Mount Read Volcanics, Tasmania.

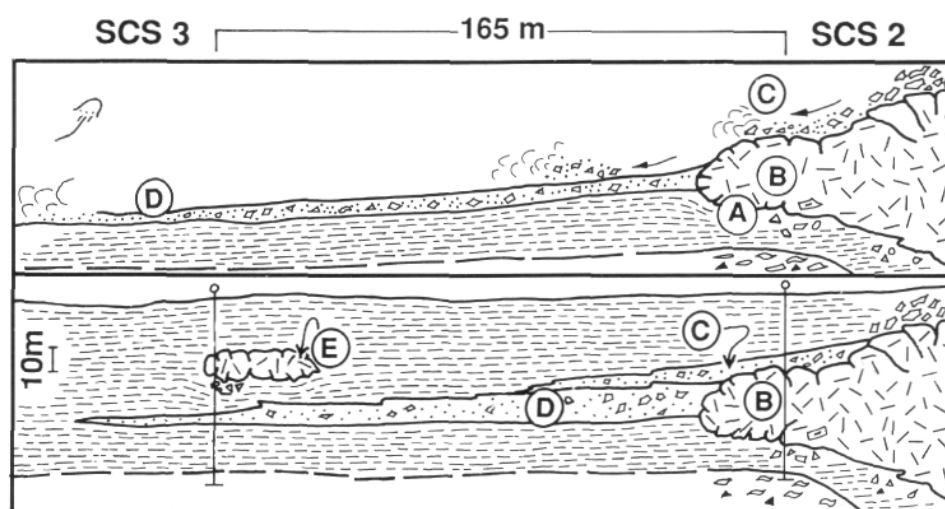


Fig. 32 Interpretation of correlations between sections through the submarine, dacitic volcanics intersected in DDH SCS2 and DDH SCS3, Sock Creek South, Mount Read Volcanics, Tasmania (Fig. 31).

Rhyolitic lavas also show a great deal of internal variation in vesicle size and abundance. A simple case, illustrated by Little Glass Mountain in California (Fink, 1980; 1983), comprises a basal breccia of pumiceous rhyolite lava, overlain by coarsely vesicular pumice, dense (non-vesicular) obsidian, finely vesicular pumice and, finally, an upper layer of breccia (Fig. 33; 20). Sections through other rhyolite flows and domes include layers of the same textures but in various arrangements, some of which are considerably more complex (Swanson et al., 1989; Fink and Manley, 1987). The internal stratigraphy in part reflects pre-existing volatile gradients in the magma source, as well as processes operating immediately prior to and during extrusion (especially crystallization, volatile exsolution, volatile redistribution and vesicle growth) (Eichelberger et al., 1986; Friedman, 1989; Swanson et al., 1989; Fink et al., 1992). Temperature increase in response to shear stress in the moving flow ("thermal feedback" — Nelson, 1981) may be another process by which silicic lava flows can become locally coarsely vesicular. The different textural types have different densities and rheological properties; for example, coarsely vesicular pumice is less dense and more viscous than obsidian. Local complexities in the distribution of textures can develop if basal, less dense, coarsely vesicular pumice layers form diapirs that penetrate up through and deform overlying layers. Also, shearing at the boundaries between layers causes local mixing and interleaving of

different textural types (Fink, 1983).

Textural heterogeneity in silicic lava flows and domes also arises as a result of devitrification and hydration. Substantial parts of lava flows, especially the outer parts, cool rapidly to glass, in which there may be abundant, very small quench crystallites. Thus, the outermost pumiceous layers, breccia derived from them, and obsidian all consist of glass. The coolest glassy parts of the lava flow do not devitrify further, although the glass may be subsequently hydrated, forming perlite (5), or else altered and recrystallized. The lava flow interior cools more slowly, resulting in one or more zones of spherulitic obsidian around a core of crystallized rhyolite in which spherulitic, micropoikilitic and granophyric textures occur (Fig. 33, 34). High-temperature devitrification clearly begins before flowage ceases because, in some silicic lavas, flow laminae are deformed around early-formed lithophysae (8.2) and basal autobreccias contain spherulitic clasts (Bonnichsen and Kauffman, 1987; Manley, 1992). Some single flows also exhibit heterogeneity defined by variation in the sizes, proportions and types of phenocrysts present, microlite abundance, glass colour and glass chemistry (eg. Sampson, 1987; Swanson et al., 1989; Gibson and Naney, 1992); these are evidently mixtures of two or more magma compositions.

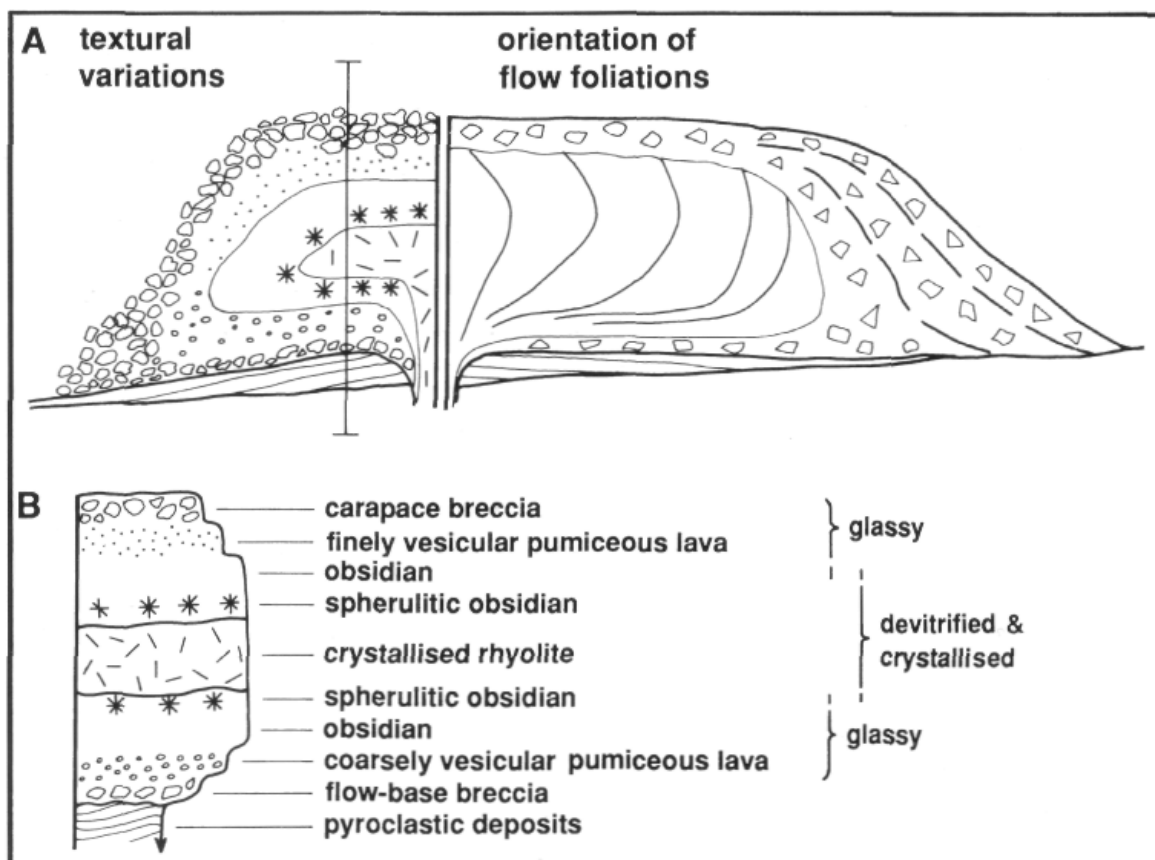


Fig. 33 (A) Schematic cross-section through a subaerial silicic lava flow. The left side shows the internal textural variations arising from vesiculation, devitrification and flow fragmentation. The right side shows the orientations of internal flow foliations, and crude layering in flow margin talus breccia. (B) Vertical section through the flow at the position indicated in (A), showing the major textural zones. Modified from Fink and Manley (1987) and Duffield and Dalrymple (1990).

Subaerial silicic domes and lava flows commonly occur in association with co-magmatic pumice and ash deposits produced by explosive eruptions (Newhall and Melson, 1983; Heiken and Wohletz, 1987; Swanson et al., 1987; Moore et al., 1981). In many cases, explosive eruptions precede lava effusion, a sequence that reflects pre-existing volatile gradients and degassing behaviour of the source magma (Eichelberger and Westrich, 1981; Swanson et al., 1989). However, explosive activity is just as likely during and immediately following dome growth and lava outflow, as a result of continued increases in internal gas pressure in vesicular zones, attendant upon cooling and crystallization of the lava, and/or local interaction with surface water (Heiken and Wohletz, 1987; Fink et al., 1992). Deposits from explosive eruptions that accompany and partly destroy domes and lava flows contain juvenile clasts that display a range in vesicularity and crystallinity as wide as that in the parent lava, with the possible addition of fresh pumice or dense lava clasts and accidental lithic fragments.

Silicic lava flows and domes are also associated with clastic deposits generated by gravitational collapse. These deposits include aprons of talus breccia (10.4, 19.1) that accumulate at steep lava flow fronts and dome margins during and after emplacement, and block and ash flow deposits (21.1-2) generated during growth of domes and lava flows on steep slopes. Studies of gravitational collapse of actively-growing dacite domes at Unzen, Japan, and Mount St Helens, Washington, show that hot, spalled lava blocks disintegrate spontaneously on release from the domes, as a result of thermal stress, decompression and rapid exsolution of volatiles (Mellors et al., 1988; Sato et al., 1992; Yamamoto et al., 1993), and generate block and ash flows.

The textures and structures outlined above are all integral parts of modern subaerial silicic lava flows and domes, and should be anticipated and searched for in their ancient counterparts. However, the autobreccia carapace and surface structures have low preservation potential, and glass is likely to be replaced by fine-grained quartz, feldspar, zeolites or phyllosilicates. As a result, ancient silicic lavas tend to be dominated by coherent, poorly or non-vesicular, and spherulitic, micropoikilitic or granophyric textural facies.

Subaerial basaltic lava flows (19)

Subaerial basaltic lavas commonly exhibit either of two flow types: *a'a* or *pahoehoe* (Macdonald, 1953; 1972; Wentworth and Macdonald, 1953; Rowland and Walker, 1990) (19.7). Many of the differences in surface and internal textures between the two reflect differences in lava viscosity and volumetric flow rate (the volume erupted divided by the eruption duration). A'a formation is correlated with high volumetric flow rates and flowage in open channels from which heat loss is rapid, resulting in relatively high viscosity (Rowland and Walker, 1990). A'a lava flows consist of a massive interior encased in scoriaceous and spinose lava

fragments, generally known as *clinker* (Fig. 34). Levees composed of clinker develop along the margins of a'a flows and create channels between which the central, hotter and less viscous lava is constrained to flow (Sparks et al., 1976). On average, a'a flows are thicker than pahoehoe flows and have irregularly distributed, large vesicles that are deformed during flowage.

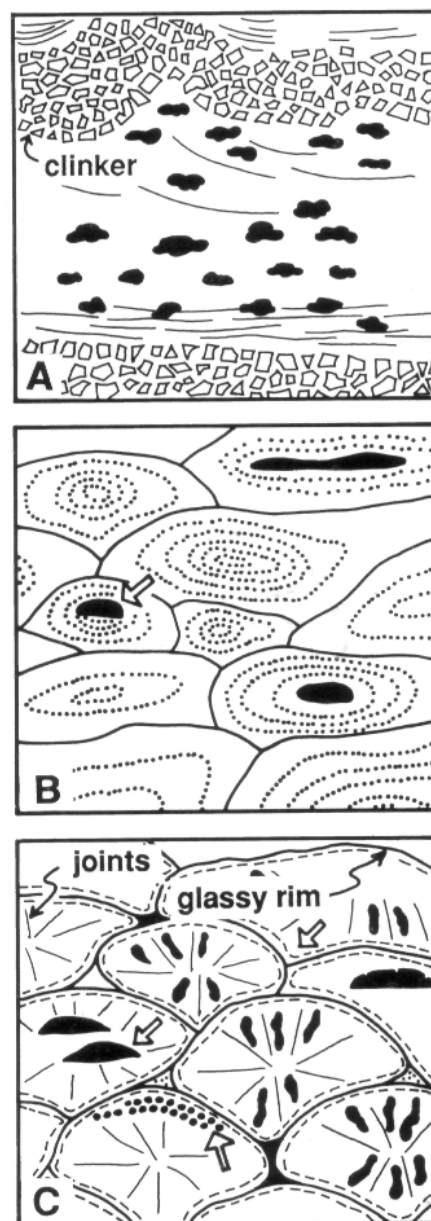


Fig. 34

Pahoehoe forms at low volumetric flow rates and flowage in tubes from which heat loss is minimal, allowing maintenance of relatively low viscosity. Pahoehoe flows may change to a'a with distance from source, in response to cooling-induced viscosity increases or if subject to high rates of shear strain; for example, as a result of flowing over steep slopes (Peterson and Tilling, 1980). Pahoehoe lava is

characterized by smooth, lobate surfaces that may be buckled and folded into intricate ropy patterns (Fink and Fletcher, 1978), and flows usually comprise many small flow units (Rowland and Walker, 1990). Single flow units can be very thin (< 20 cm). They often have a glassy crust and contain large, formerly gas-filled cavities (*shellypahoehoe*), or else are relatively dense and vesicle-poor. Pahoehoe lavas sometimes construct tunnels or tubes through which lava can flow great distances because cooling is minimized (Fig. 35). The tunnels form when levees either side of lava channels meet, due to gradual accretion, or when the top of a lava stream cools and forms a solid crust beneath which fluid lava continues to flow (Macdonald, 1972; Basaltic Volcanism Study Project, 1981; Swanson, 1973).

The abundance, size, distribution and shape of vesicles in solidified pahoehoe are partly inherited from vesicularity at the time of eruption, and are modified by coalescence and escape of bubbles during outflow (Walker, 1989b; Wilmoth and Walker, 1993). *S-type* (spongy) pahoehoe has abundant spherical vesicles and most closely reflects the vesicle population at the time of eruption (19.6). *P-type* (pipe vesicle-bearing) pahoehoe has lower porosity, reflecting greater loss of gas before cooling. *Toothpaste lava* (Rowland and Walker, 1987; 1988) is a transitional lava type between pahoehoe and a'a, and develops in cases where both degassing and cooling are advanced.

Tumuli are mounds or whale-back ridges, 1-10 m high, that are common on subaerial pahoehoe lava flow fields. They are more or less polygonal in plan and cut by axial or radial clefts. Walker (1991) suggested that tumuli form by uptilting of rigid plates of vesicular lava crust above more dense, fluid lava injected beneath. Related features, lava rises and lava-rise pits, were also described by Walker (1991).

Compared with silicic lavas, subaerial basaltic lavas have low viscosity and form extensive (up to several tens of kilometers), thin (less than a few tens of meters) sheets. Amongst the most extensive and voluminous known are those in continental flood basalt provinces (Walker, 1970; Williams and McBirney, 1979; Swanson et al., 1975). Single basalt flows apparently cover thousands of square kilometres and involve volumes greater than 1000 km³.

Andesitic lavas (19)

Andesitic lavas have properties intermediate between those of silicic and basaltic lavas. They can flow several kilometers from source but also commonly form domes and short, thick flows. Walker (1973b) reported the median length of 147 andesites and dacites to be 1.2 km, and 99 basaltic andesites had a median length of 3.2 km. Thicknesses range from several tens of meters up to a few hundred metres, and substantial parts are

fragmented due to autobrecciation (Fig. 36A; 19.5). The dense interiors of andesitic flows may display columnar or prismatic joints perpendicular to cooling surfaces, or platy joints parallel to flow direction (Fig. 36B). Many historic examples of andesitic and dacitic dome-building eruptions involved brief explosive activity (Newhall and Melson, 1983). Aprons of talus breccia accumulate at steep lava flow fronts and dome margins due to gravitational collapse during and after emplacement.

Submarine basaltic andesite and andesitic lava flows in Tertiary sequences of Japan and New Zealand exhibit many features in common with submarine basaltic lavas, including pillows, lobes, and related autoclastic deposits (Yamagishi, 1985; 1987; 1991) (9.3, 16, 17.6). Some of the andesitic lava flows are massive (sheet flows), with columnar jointing, glassy margins and outward gradation into surrounding in situ hyaloclastite (Yamagishi, 1991) (Fig. 19).

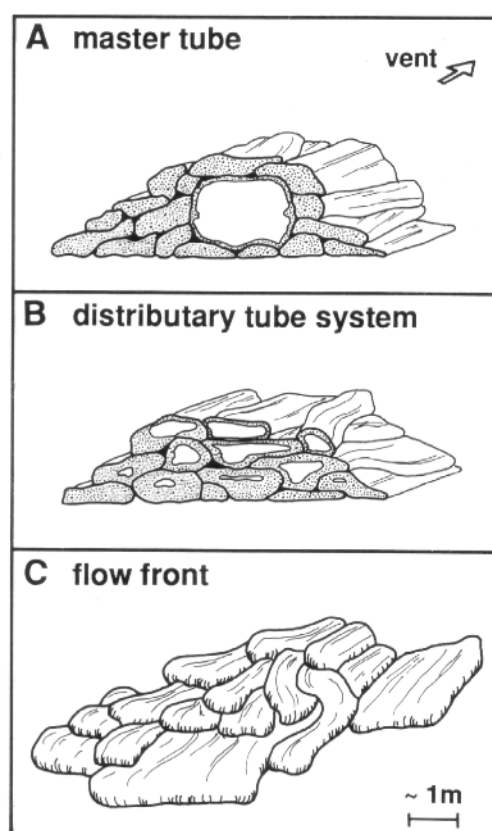


Fig. 35 Tube system in a pahoehoe lava flow. Master tubes (A) form by coalescence of several adjacent smaller tubes or by roofing-over of open channels. Master tubes deliver lava to the distal parts of flows, where there is a system of small distributary tubes (B). At the flow front, the lava emerges in several small single flow unit tubes (C). Single flow unit tubes have cross-section areas of about 1 m². Modified from Rowland and Walker (1990).

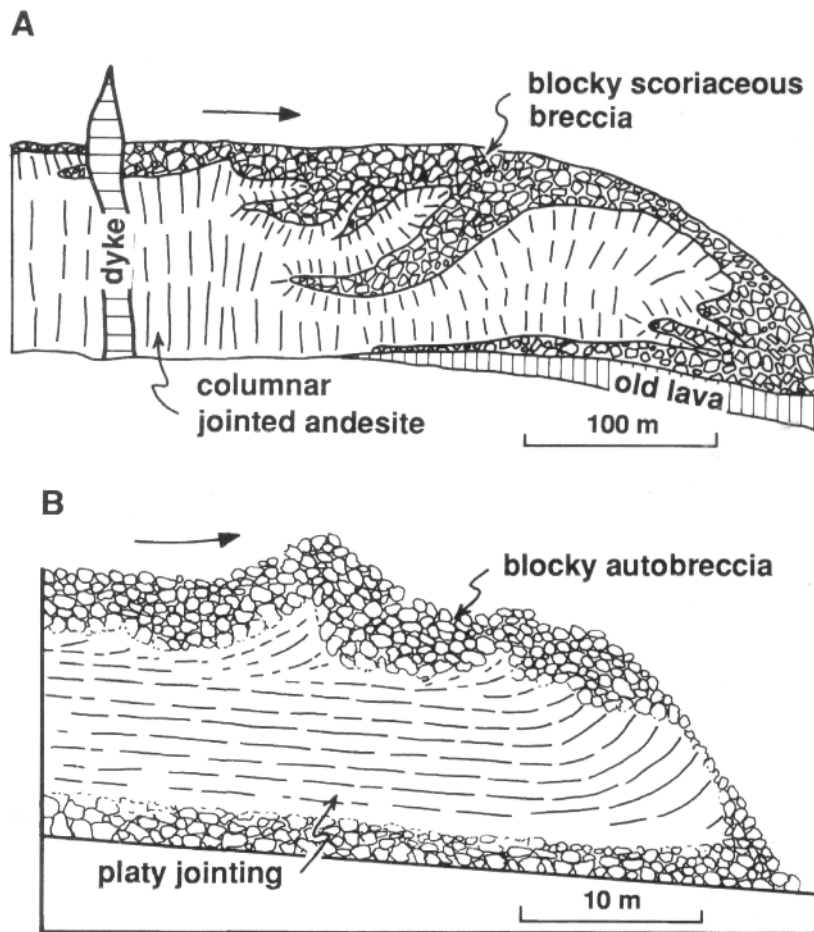


Fig. 36 Jointing and breccia associated with subaerial andesitic and dacitic lava flows. (A) At the front of a flow, the massive columnar jointed interior is enveloped in blocky scoriaceous autoclastic breccia and talus. (B) Platy jointing is parallel to the base in the interior and lower parts of the flow, but steepens at the top and the margins. Massive lava in the interior is enveloped by blocky autobreccia. Arrows indicate the flow direction. Modified from Huppert et al. (1982) and Macdonald (1972).

Plate 10 — Autoclastic breccia and talus



1. Deformed and altered, rhyolitic autoclastic breccia

Clasts in this rhyolitic autoclastic breccia are blocky and flow banded. Flow banding in adjacent clasts has different orientations. The clasts are closely packed and there is a paucity of fine matrix. These features are typical of autoclastic breccia.

Mount Read Volcanics, Cambrian; Mount Read, western Tasmania.



2. Subaerial rhyolitic autoclastic breccia

This autoclastic breccia occurs at the margin of a subaerial rhyolite dome. Matrix comprising more finely fragmented rhyolite separates blocky and slabby, flow-banded clasts of the same composition.

Boyd Volcanic Complex, Late Devonian; Eden, New South Wales.



3. Strongly altered autoclastic breccia

All the clasts in this autoclastic breccia are feldspar- and quartz-phyric rhyolite. However, the clasts have been variably silicified, chloritized and K-feldspar altered, resulting in an apparently polymict clast assemblage. Phenocrysts in silicified clasts have been recrystallized and are barely distinguishable from the groundmass. In adjacent chloritically altered clasts, the relict feldspar phenocrysts maintain their original shape, size and distribution. Many clasts are flow banded and most are blocky but lack the curvilinear outlines that are characteristic of clasts in hyaloclastite. These textural features are consistent with interpretation as an autoclastic breccia.

Mount Read Volcanics, Cambrian; specimen 42571, Chester mine area, western Tasmania.



4. Talus associated with a dacite lava dome

Coarse talus deposits are actively accumulating on the flanks of the dacite lava dome in the amphitheatre of Mount St Helens. Blocks liberated during growth of the dome tumble, bounce and roll downslope under the influence of gravity, commonly breaking up on the way. The unstructured rubble comprises a framework of angular dacite lava blocks up to tens of metres across, and minor granular matrix mainly derived from attrition of the larger blocks. Note person for scale (encircled).

Mount St Helens dacite lava dome, AD 1986; Washington, USA.



5. Subaerial andesitic autoclastic breccia

The interior of this 4 m thick andesite lava flow is coherent and enveloped by autoclastic breccia composed of annealed, spinose, twisted, scoriaceous clasts ("clinker"). The contact between brecciated and coherent andesite is highly irregular, and autoclastic brecciated clasts (C) occur locally within massive coherent lava. Clasts in the autoclastic breccia are red as a result of thermal oxidation, a process that is usually confined to subaerial environments.

Whakapapa Formation, <15ka; Ruapehu volcano, New Zealand.



6. Talus associated with a basaltic andesite lava flow

A. Incandescent lava blocks cascade down the talus slope at the front of the 1981 basaltic andesite blocky lava flow on Arenal volcano. Lava blocks are spalled from an advancing lava lobe (L), and roll or bounce downslope, disintegrating further while in transit. Width of field of view is about 30 m.

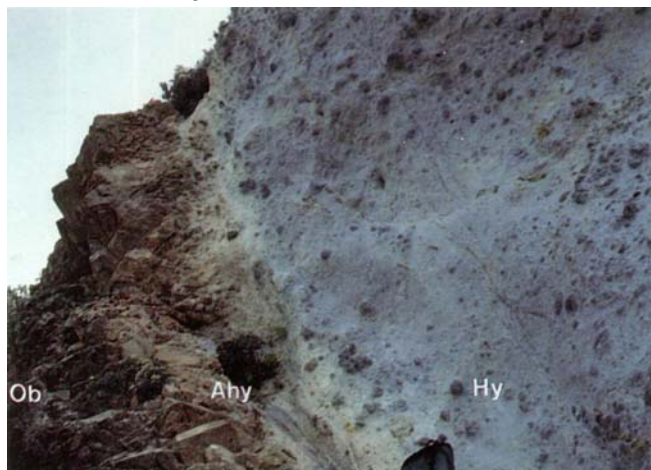
Basaltic andesite lava flow, Arenal volcano, AD 1981; Costa Rica.



B. Clasts in the talus apron at the front of the active blocky lava flow are partly formed by autoclastic brecciation but during transport, clast shapes are modified by abrasion and new fragments are created when large blocks bounce downslope and collide.

Basaltic andesite lava flow, Arenal volcano, AD 1981; Costa Rica.

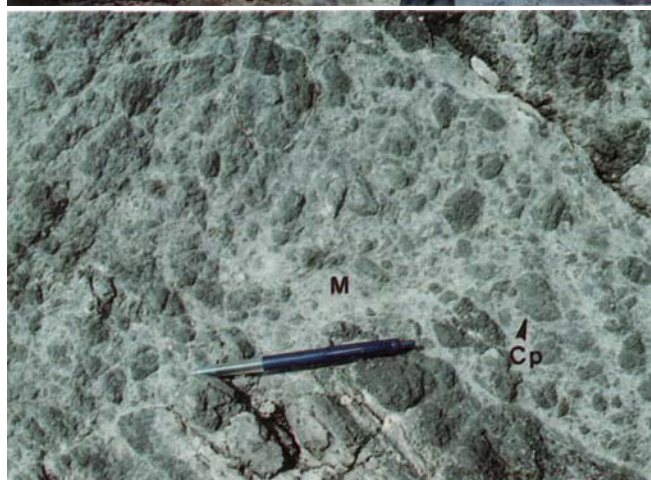
Plate 11 — Hyaloclastite



1. Feeder dyke-hyaloclastite in rhyolite

This exposure shows the gradational contact between dark grey, coherent obsidian (**Ob**) in a feeder dyke and adjacent matrix-rich, in situ hyaloclastite (**Hy**) in rhyolitic lava erupted on the sea floor. The transition zone consists of altered, tan, in situ hyaloclastite (**Ahy**). The matrix-rich hyaloclastite is unaltered and composed of dark grey rhyolite blocks embedded in white, sand-sized hyaloclastite matrix. Rucksack foreground for scale.

Rhyolite, Pleistocene; Chiaia di Luna, Ponza, Italy.



2. In situ rhyolitic hyaloclastite

There is a gradation from comparatively coherent, flow-banded lava (below the pen) into matrix-rich in situ hyaloclastite. Clasts in the hyaloclastite have curvilinear margins (**Cp**) and groups of clasts display jigsaw-fit texture (dashed line). The granular matrix (**M**) is composed of glassy particles and phenocryst fragments derived from thorough quench fragmentation of the lava.

Glassy rhyolite, Pleistocene; Cala del Gaetano, Ponza, Italy.



3. In situ rhyolitic hyaloclastite

A brecciated lobe of flow-banded rhyolite comprises jigsaw-fit to slightly rotated blocks of dark grey lava separated by narrow seams of finer matrix. The lobe has sharp contacts with enclosing pale grey, matrix-rich in situ hyaloclastite (**Hy**). Autobrecciation and quench fragmentation probably operated together during disintegration of the lobe. It may represent a pulse of lava emplaced into cogenetic, freshly formed in situ hyaloclastite.

Glassy rhyolite, Pleistocene; Cala del Gaetano, Ponza, Italy.



4. In situ andesitic hyaloclastite

This monomict andesitic breccia shows the clast shapes and jigsaw-fit texture typical of in situ hyaloclastite. White, silicic pumiceous sandstone that fills the spaces between the andesite clasts filtered down from overlying pumiceous volcanoclastic deposits.

Matsuzaki Volcanics, Late Miocene—Pliocene; Matsuzaki, Izu Peninsula, Honshu, Japan.



5. Coherent dacite-in situ hyaloclastite transition

Within this exposure there is a clear gradation from comparatively coherent, flow-banded, hornblende-phyric dacite (**D**) into matrix-poor in situ hyaloclastite (**Hy**) that in turn grades into matrix-rich hyaloclastite (**Mh**).

Green Tuff Belt, Late Miocene; Kariba, Hokkaido, Japan.



6. In situ dacitic hyaloclastite

This example of blocky, matrix-poor, in situ hyaloclastite in hornblende-phyric dacite shows characteristic jigsaw-fit texture. The clasts have curvilinear fracture surfaces, typical of quench fragmentation of coherent glass.

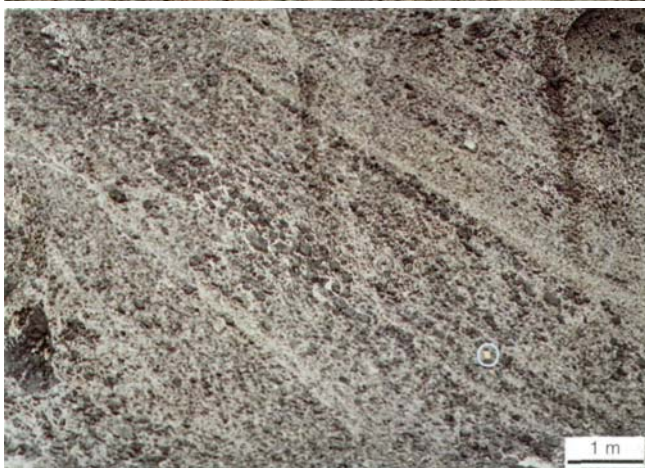
Green Tuff Belt, Late Miocene; Shiroya, Hokkaido, Japan.



7. In situ dacitic hyaloclastite

The hornblende-phyric dacite blocks and centimeter-sized clasts in this moderately matrix-rich in situ hyaloclastite are separated by a finely comminuted matrix of the same composition. Jigsaw-fit texture, indicative of in situ fragmentation, is well developed.

Green Tuff Belt, Late Miocene; Shiroya, Hokkaido, Japan.



8. Resedimented andesitic hyaloclastite

Clasts in this thickly bedded, andesitic breccia were formed by quench fragmentation. The beds have a lenticular geometry, relatively steep primary dip, and exhibit reverse grading. The section is typical of resedimented hyaloclastite generated by grain-flow redeposition and avalanching on the flanks of a submarine lava-hyaloclastite pile. Notebook, encircled, for scale.

Green Tuff Belt, Late Miocene; Kabuto Cape, Shakotan Peninsula, Hokkaido, Japan.

Plate 12 — Hyaloclastite



1. In situ andesitic hyaloclastite

In this example of in situ hyaloclastite, blocky hornblende-phyric andesite clasts (**C**) are separated by small amounts of millimeter to sub-millimeter-sized granular matrix (**Mx**) of the same composition, including splinters of andesite and sporadically distributed hornblende crystal fragments. Groups of clasts and splintery fragments in the matrix display jigsaw-fit texture.

Mount Read Volcanics, Cambrian; Anthony Road, western Tasmania.



2. Altered andesitic hyaloclastite

Part of the outcrop shown in 12.1 is affected by chloritic alteration. As a result, the boundaries between clasts (**C**) and matrix (**Mx**) have been modified and there is a distinct lenticular fabric. However, some clasts still have curviplanar outlines and jigsaw-fit texture is locally preserved.

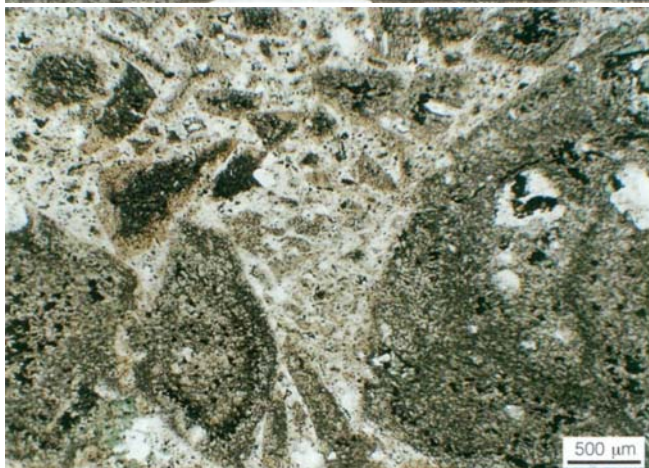
Mount Read Volcanics, Cambrian; Anthony Road, western Tasmania.



3. Andesitic hyaloclastite

Parts of the andesitic hyaloclastite outcrop shown in 12.1 are relatively matrix-rich. The larger clasts are evenly feldspar-and hornblende-phyric and have curviplanar margins. The matrix includes splinters of andesite and scattered crystal fragments. Jigsaw-fit texture is most clearly displayed by clasts intermediate in size between the largest clasts and the matrix granules but is otherwise not easy to recognize because matrix is abundant.

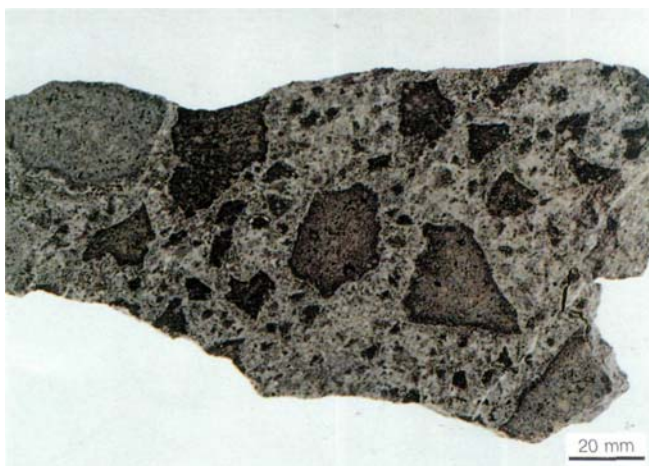
Mount Read Volcanics, Cambrian; Anthony Road, western Tasmania.



4. In situ andesitic hyaloclastite in thin-section

Equant to cuneiform andesite clasts are closely packed in a recrystallized matrix that contains scattered crystal fragments. The clasts comprise chloritized feldspar and pyroxene phenocrysts in a groundmass of fine-grained feldspar and pyroxene. Fragment margins are curviplanar and jigsaw-fit between groups of clasts is common. The margins of the clasts are more chloritic (formerly more glassy?) than the interiors. Plane polarised light.

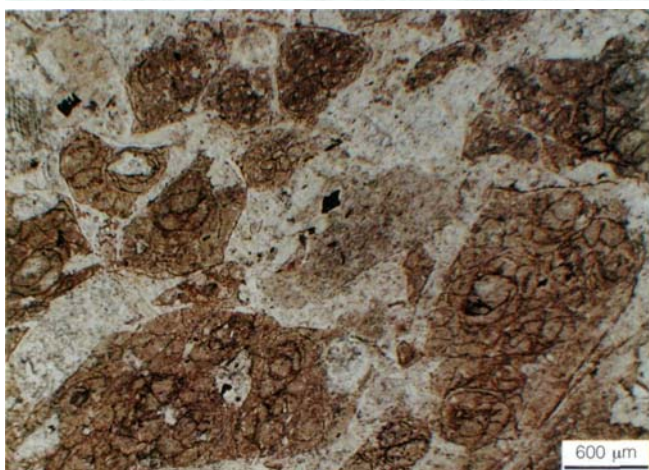
Mount Read Volcanics, Cambrian; specimen 74108, Burns Peak, western Tasmania.



5. Perlitic in situ andesitic hyaloclastite

A. Between the well-defined, dark rimmed, blocky and splintery, feldspar-phyric, perlitic andesite clasts are closely packed, finer (millimeter to centimeter), pale clasts of identical material. In detail, the boundaries of the larger clasts are gradational into granules in the matrix. The clast-in-matrix texture develops as a result of variable in situ fragmentation. More thoroughly fragmented andesite forms the matrix surrounding intact larger clasts.

Mount Read Volcanics, Cambrian; specimen FPS1, Hellyer mine, western Tasmania.



B. In thin-section, the groundmass of the larger clasts and the granules have well-developed classical perlitic fractures and, although formerly glassy, are now largely sericite. The clasts and granules locally display jigsaw-fit texture and are separated by patches of recrystallized feldspar, sericite and carbonate that contain sparse crystal fragments. Plane polarised light.

Mount Read Volcanics, Cambrian; specimen FPS1, Hellyer mine, western Tasmania.



6. Dacitic hyaloclastite

The mismatch of flow banding orientation in adjacent, variably altered, feldspar-phyric dacite clasts indicates that they have been rotated, and suggests that both autobrecciation and quench fragmentation have operated.

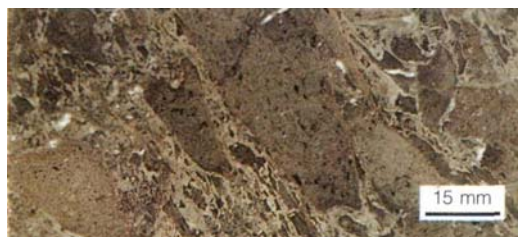
Mount Read Volcanics, Cambrian; DDH SCS2 (103.1 m), Sock Creek, western Tasmania.



7. Dacitic hyaloclastite

In situ quench fragmentation of this finely feldspar-phyric dacite is indicated by the well-developed jigsaw-fit texture, and closely packed, blocky to cuneiform clast shapes.

Mount Read Volcanics, Cambrian; DDH HPI (662.6m), High Point, western Tasmania.



8. Basaltic hyaloclastite

A. Pale to dark green, blocky and splintery clasts of amygdaloidal basalt are separated by fine-grained, more sericitic and partly recrystallized matrix, and display jigsaw-fit texture.

Mount Read Volcanics, Cambrian; DDH MAC 19 (523.5 m), Hellyer mine, western Tasmania.



B. Blocky amygdaloidal basalt clasts in this breccia have the curviplanar outlines and jigsaw-fit texture that are characteristic of in situ quench fragments.

Mount Read Volcanics, Cambrian; DDH MAC 19 (540.2 m), Hellyer mine, western Tasmania.

Plate 13 — Hyaloclastite varieties and feeder dykes



1. Trachytic hyaloclastite with quenched lava "rags"

The large, ragged and blocky shaped clasts in this breccia have complete, formerly glassy, chilled margins. The smaller clasts are fragments derived from disintegration of the larger clasts. Both consist of aphanitic, finely vesicular trachyte. Although quenched, the large ragged clasts have not necessarily been formed by quench fragmentation — their shapes suggest formation by tearing apart of lava, perhaps during mild, subaqueous fountaining, prior to quenching (cf. water-chilled bombs).

Trachytic hyaloclastite, Middle Miocene; Porto Santo, Madeira Archipelago.



2. Altered andesitic(?) hyaloclastite

The prominent pale, irregular shapes are carbonate-altered cores of blocky clasts in hyaloclastite breccia. The margins of the blocky clasts are chloritically altered and dark green, as are clasts in the apparent matrix. The true clast outlines are in fact very subtle and much less obvious than the colour contrasts caused by alteration.

Mount Read Volcanics, Cambrian; Newton Dam Spillway, western Tasmania.



3. Andesitic feeder dyke and incipient concentric pillow

This outcrop shows an apophysis extending from a feeder dyke (D), cut by overlapping curved joints (arrow) and surrounded by in situ hyaloclastite (H). Disintegration of the stems of such apophyses generates large clasts with round shapes and concentric joints (concentric pillows; 13.4).

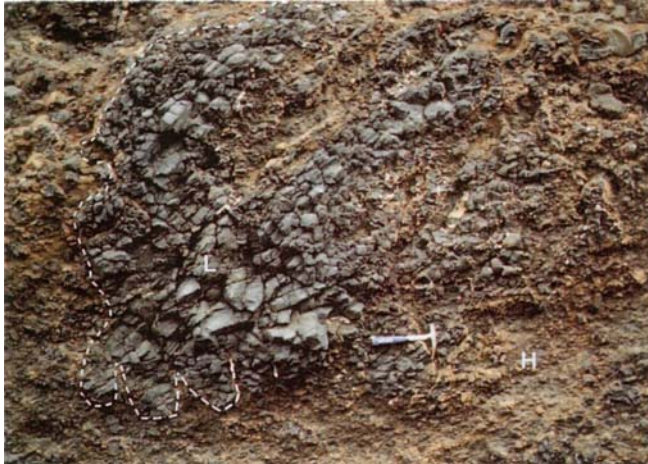
Andesite, Miocene; Cape Notoro, Hokkaido, Japan.



4. Andesitic hyaloclastite: concentric pillow breccia

Concentric pillow breccia is a distinctive variety of hyaloclastite formed by disintegration of finger-like lava apophyses along overlapping concentric joints (13.3). The larger clasts have rounded, pillow-like shapes and concentric joints, hence the term "concentric pillow breccia" (Yamagishi, 1987).

Yoshida Formation, ~3 Ma; Senjojiki, Izu Peninsula, Honshu, Japan.



5. Submarine lava lobe enclosed by in situ hyaloclastite

This outcrop shows an andesite lava lobe (**L**) surrounded by in situ hyaloclastite (**H**). The lobe is dissected into polyhedral joint blocks and locally has finger-like apophyses (outlined) extending into the hyaloclastite. Within the hyaloclastite, groups of clasts with jigsaw-fit texture are enclosed by areas where clast rotation and separation are evident.

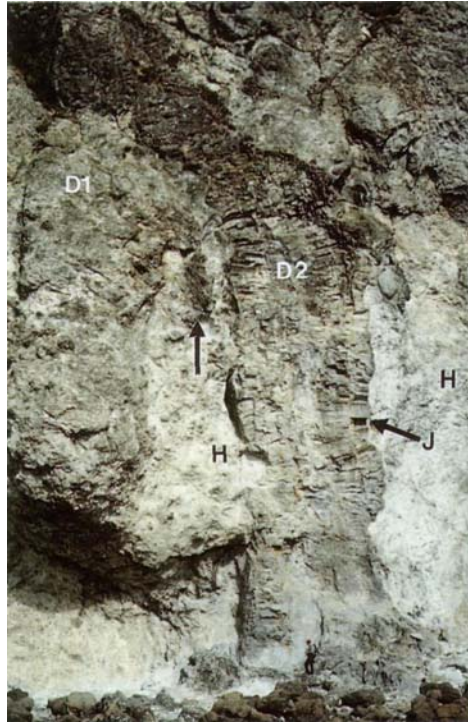
Andesite, Neogene; Rebun Island, Hokkaido, Japan.



6. Andesitic feeder dyke

The 2-4 m wide, dark grey, andesitic dyke here intrudes white, bedded pumiceous sandstone and conglomerate. Adjacent to the dyke, the host sandstone is slightly indurated and bedding is destroyed. The margins of the dyke are black and glassy, and locally protrude into the sandstone. Joint patterns within the dyke suggest it has a complex shape in three dimensions. The irregular shape of the dyke implies that it was intruded when the host sandstone was only poorly consolidated.

Ishiki Formation, ~3 Ma; Senjojiki, Izu Peninsula, Honshu, Japan.



7. Feeder dyke to andesitic hyaloclastite

A vertical andesite feeder dyke (**D2**) intrudes earlier dykes and related hyaloclastite. The dyke has a massive core, marginal columnar cooling joints (**J**), and undulating bulbous margins. It is about 10m wide at the base, but thickness varies over the exposed length. An earlier, less coherent dyke (**D1**) has an irregular shape; tongues and apophyses (arrow) propagate into adjacent in situ hyaloclastite (**H**).

Yakumo Formation, Late Miocene; Moiwa, Shakotan Peninsula, Hokkaido, Japan.

Plate 14 — Peperite (intrusive hyaloclastite)



1. Rhyolite-siltstone peperite

This example of blocky peperite occurs at the base of a rhyolitic intrusion where it is in contact with siltstone. The blocks and splinters of rhyolite (**R**) are separated by pale grey, massive siltstone. Rhyolite clasts have curvilinear margins (**C**) and in places, groups of clasts display jigsaw-fit texture.

Bedded Pyroclastic Formation, Ordovician; Llanberis Pass, Snowdonia, northern Wales, UK.



2. Dacite-siltstone peperite

The contact between feldspar-phyric dacite (**P**) and siltstone (**S**) comprises of zone of intricate mixing between the two. There is a clear transition from dacite that contains thin lenses and seams of siltstone (arrow) below the contact, to siltstone that contains rags and elongate blobs of dacite above the contact.

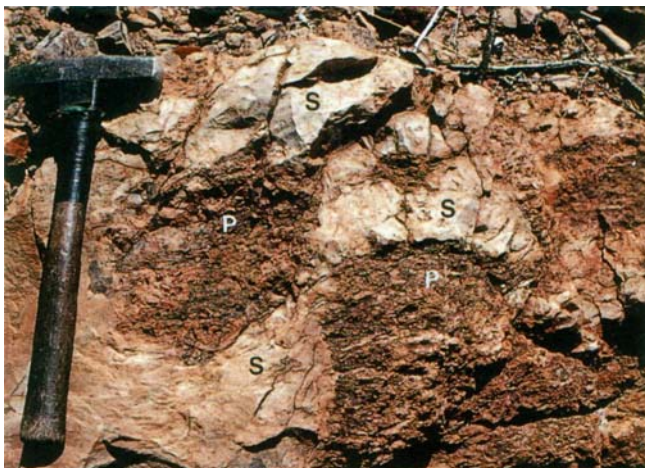
Berserker Beds, Early Permian; Mount Chalmers, Queensland.



3. Rhyolite-pumice breccia peperite

Recognition of peperite is sometimes especially challenging. The magmatic component in this example is represented by the flow-banded, blocky, feldspar-phyric rhyolite clasts (**C**). The rhyolite intruded and mixed with pumiceous breccia and sandstone (**Pb**) that now forms a matrix between the rhyolite clasts. The rhyolite-pumice breccia peperite has gradational contacts with in situ rhyolitic breccia and coherent rhyolite.

Mount Read Volcanics, Cambrian; DDH 102R (22-32 m), Rosebery mine, western Tasmania.



4. Porphyritic rhyolite-fine sandstone peperite

Pillow-like masses of quartz- and feldspar-phyric rhyolite (**P**) occur within massive fine sandstone (**S**), along the top contact of an extensive, thick sill. The sandstone is indurated and has a subconchoidal fracture. The bulbous shapes of the porphyritic rhyolite clasts are typical of globular peperite described by Busby-Spera and White (1987).

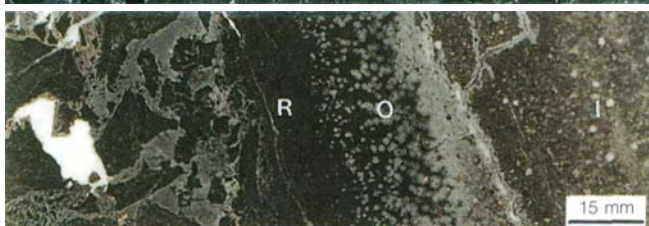
Tennant Creek porphyry, Early Proterozoic; Tennant Creek, Northern Territory.



5. Basalt-mudstone peperite in pillow basalt

This photograph shows a cross-section through a basaltic pillow from which the outer, dark grey, chilled margin has partly spalled (arrow). The matrix between the spalled pillow fragments is grey, massive, siliceous mudstone that was probably unconsolidated when the basalt was emplaced.

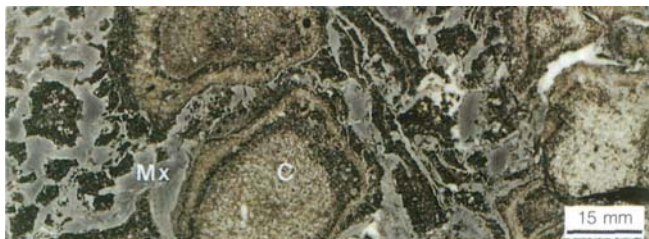
Mount Read Volcanics, Cambrian; Hellyer mine, western Tasmania.



6. Basalt-siliceous mudstone peperite

Textural zones at the margin of a basaltic pillow consist of: the pale grey interior (I), a zone of ovoid carbonate alteration spots (O) and the chloritic rim (R). The spots may be altered varioles (radial pyroxene and feldspar microlites).

Mount Read Volcanics, Cambrian; DDH HL52 (148.2 m), Hellyer mine, western Tasmania.



7. Basalt-siliceous mudstone peperite

Vesicular, pale green to dark grey, chloritized basalt clasts (C) are separated by grey massive, siliceous mudstone (Mx). The basalt clasts have quenched rims and curvilinear outlines.

Mount Read Volcanics, Cambrian; DDH HL53 (116.95 m), Hellyer mine, western Tasmania.



8. Altered basalt(?) -siliceous siltstone peperite

Blocky clasts of amygdaloidal, porphyritic, altered basalt(?) display jigsaw-fit texture (J). The clasts are separated by grey siltstone and some also contain ovoid siltstone inclusions (S).

Mount Read Volcanics, Cambrian; DDH HL629 (570.9 m) Hellyer mine, western Tasmania.



9. Altered basalt(?) -siliceous siltstone peperite

The distribution of dark grey basalt(?) clasts varies from jigsaw-fit clusters, to clasts dispersed in pale grey, siliceous siltstone matrix. Adjacent to the clasts, the colour of the siltstone becomes paler, possibly reflecting induration.

Mount Read Volcanics, Cambrian; DDH MCH1 (380 m), Mount Charter, western Tasmania.

Plate 15 — Pillowed lava flows and pillows



1. Andesitic pillow lobes

This cliff section is roughly parallel to the elongation direction of interconnected lobes in an andesitic pillowed lava flow. Some lobes display corrugations, constrictions (arrow), and ropy wrinkled surfaces. The lobes are closely packed and moulded along mutual contacts.

Collins Bay pillow lava flow, Nihotupu Formation, Miocene; Collins Bay, Muriwai, New Zealand.



2. Basaltic pillow lobes

These pillow lobes display surface features which include ropy wrinkles (**W**) and tortoise shell contraction cracks. One of the pillow lobes has a large circular hollow (**H**) in the centre that extends along the length of the lobe. This formed when lava drained from the lobe and was not replenished.

Slaughter Bluff Volcanic Breccia, Tertiary; Cape Grim, northwestern Tasmania.



3. Spreading cracks on a basaltic pillow

Three intersecting graben-like spreading cracks on the surface of this pillow have generated new flow-wrinkled crust in the suture (arrow). Tensional cracks (**t**) cut the old, and locally also the new crust. Spreading cracks form in the chilled surface crust during resupply of lava or the expansion of volatiles in the pillow interior (Yamagishi, 1987; 1991). Segments of crust between the tensional cracks have ropy wrinkled surfaces (**W**) and are cut by short (2-3 cm) contraction cracks which propagate towards the interior. Scale card is 15 cm long.

Slaughter Bluff Volcanic Breccia, Tertiary; Cape Grim, northwestern Tasmania.



4. Hollow, layered pillow lobe

An isolated, hollow, layered, pillow lobe (in section) occurs within clast-supported pillow fragment breccia. Within the pillow lobe, a large sediment-filled cavity (**C**) is separated from a lower cavity (**c**) by a thin shelf. An interruption in the supply of lava allowed partial draining of the lobe to the level of the shelf. Water that entered the cavity chilled the fluid lava. Further partial draining of lava below the shelf generated the lower cavity. Pillow lava shelves are initially horizontal (Ballard and Moore, 1977). This example is at an angle to bedding in the host breccia, suggesting that the pillow lobe is actually a large detached pillow lobe fragment and not in situ.

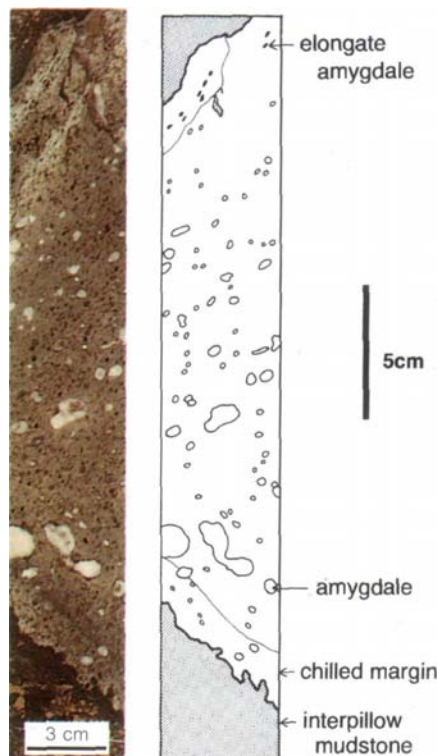
Slaughter Bluff Volcanic Breccia, Tertiary; Cape Grim, northwestern Tasmania.



5. Basaltic pillow lava

The adit to Hellyer mine exposes cross-sections through closely packed pillows that each show accommodation (arrow) to underlying pillows. The pillows have distinctly darker, chilled rims and massive interiors. Pillow lava of the Hellyer Basalt overlies the Hellyer massive sulfide deposit, and occurs near the base of and within thick pyritic mudstone (Que River Shale). It was both erupted and emplaced in a relatively deep, submarine environment.

Mount Read Volcanics, Cambrian; Hellyer mine adit, western Tasmania.



6. Basaltic pillow in drill core

The presence of abundant interpillow mudstone aids the recognition of pillow boundaries in this section of drill core. Pillow margins are chilled and pale green. Intricate interpenetration of mudstone and basalt occurs along the margin, indicating extrusion of the basalt into wet, unconsolidated sediment. At the pillow boundaries chlorite- and chlorite-carbonate-filled vesicles are small and elongate parallel to the pillow margins. In the centre, they are larger, less abundant and more equant in shape. In cases where there is no interpillow sediment and the pillows are close-packed, their boundaries are marked by subtle changes in vesicle shape, size and abundance, and by textural or colour changes that reflect chilling. The orange-colored material in the mudstone is pyrite.

Mount Read Volcanics, Cambrian; DDH HL45 (325.5 m), Hellyer mine, western Tasmania.



7. Basaltic pillow lava

This C-shaped pillow lobe segment exhibits a black, glassy chilled rind which is locally flow wrinkled. In cross-section, the pillow lobe displays radial columnar joints (C) that are coated with iron oxides and carbonate. An asymmetric transverse spreading crack (arrow) encircles the lobe.

Pillow retrieved from a Holocene(?) basaltic flow on the floor of the Manus Basin (2400 m below sea level), Papua New Guinea.

Plate 16 — Rinds and crusts on pillow lobes

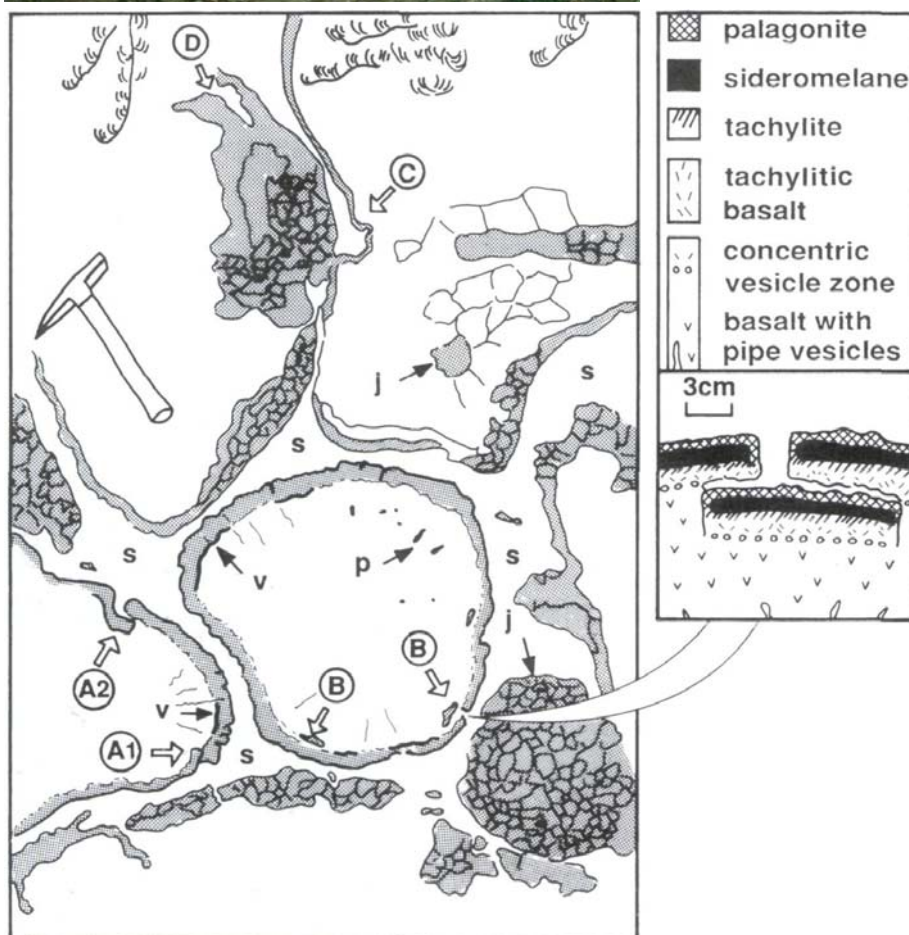


1. Multiple-rind structure in basaltic pillow lava

Some pillows in this outcrop show multiple-rind structure, considered to indicate emplacement in relatively shallow water (Kawachi and Pringle, 1988). The rinds of the pillows comprise an outer, black sideromelane layer that is partly altered to palagonite and which passes gradationally into dark grey tachylite and tachylitic basalt. The multiple-rind structure consists of: (A1, A2) one side of a broken rind thrust over its counterpart; (B) overlapping detached rinds; or (C) the inward buckling of a rind. Overlapping rinds are in direct contact (A1), or else separated by interpillow sediment (A2). The much larger area of overlapping rinds at (D) may have been formed by pulses in growth of the pillow lobe.

The interpillow sediment (S) is a mixture of shell fragments, calcareous ooze and sideromelane particles. A concentric zone of calcite filled vesicles (v) occurs near the inner rind boundary of the pillow rinds. Radial pipe vesicles (p), some filled with calcite, are distributed in a narrow zone inside the concentric vesicle zone. Subrounded vesicles are scattered in the pillow core; many are filled with calcite. Radial columnar joints dissect the pillow surface (j) and extend inward to the pillow

Waiareka Volcanics, Eocene; Boatmans Harbour, Oamaru, New Zealand

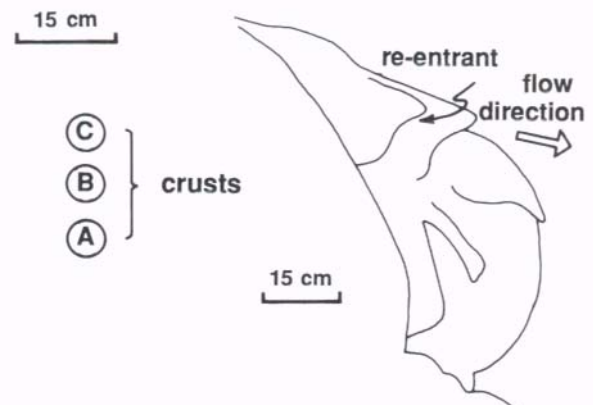
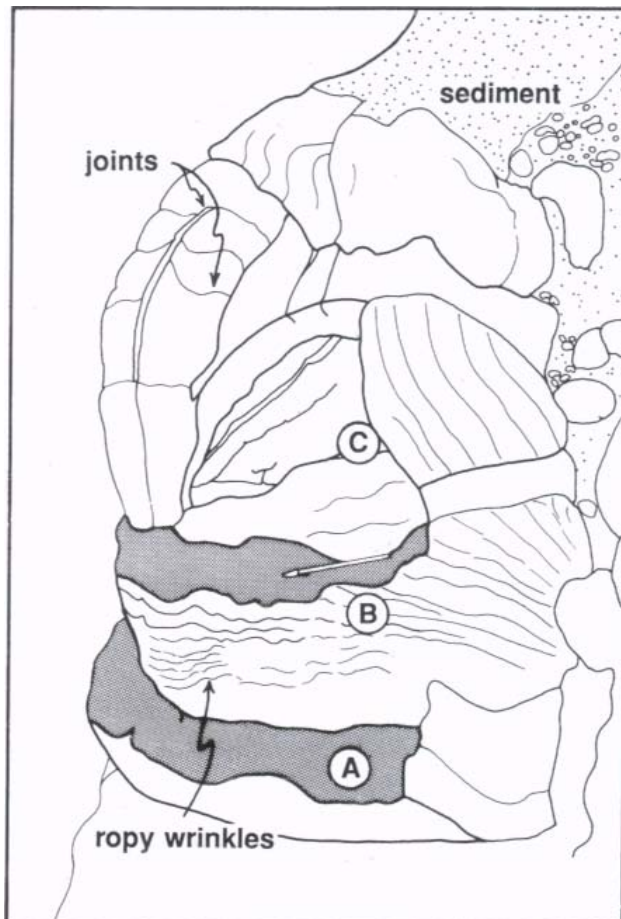




2. Multiple crusts on an andesitic pillow lobe

A "window" through the bulbous front of a pillow lobe exposes details of multiple crusts. These crusts (A, B, C) are up to about 10 cm thick and cut by evenly spaced joints (J). Their outer surfaces display ropy wrinkles (W). The lower sketch shows the multiple crusts in a side view (from the left) of the pillow lobe in the photograph. Crusts can be traced a few tens of centimeters laterally to their source which is marked by small transverse scarps (re-entrant). The sense of asymmetry of the re-entrants indicates the propagation direction of the pillow lobe.

Collins Bay pillowed lava flow, Nihotupu Formation, Miocene; Collins Bay, New Zealand.





1. Basaltic pillow fragment breccia

The clast assemblage in this breccia is typical of pillow fragment breccia, and comprises large sections of broken pillow lobes, joint-bounded blocks and granules spalled from glassy pillow rinds. The pillow breccia is clast-supported, faintly very thickly bedded, and although monomict, it includes a mixture of clasts derived from different parts of pillow lobes. Isolated pillow lobes (**P**) in the breccia have conspicuous tensional cracks (**T**) and transverse spreading cracks (**S**). They may be large pillow lobe fragments or in situ cogenetic pillow lobes. Interconnected cogenetic pillow lobes are evident elsewhere in the section.

Slaughter Bluff Volcanic Breccia, Tertiary; Valley Bay, northwestern Tasmania.



2. Pipe vesicles in basaltic pillow lava

The asymmetric shape of these pillows indicates the local younging direction. Pipe vesicles (**P**), up to 150 mm in length, are radially distributed along the bases and sides of the pillows, inside the formerly glassy pillow rinds (**R**). A wide zone with both round and pipe vesicles (**V**) occurs at the tops of the pillows. Highly vesicular zones are typically located at the uppermost margins of pillows and can be a useful indicator of stratigraphic younging.

Boucher Brook Formation, Ordovician; northern New Brunswick, Canada.



3. Pillowed lava flow emplaced on shallow-water sediments

Basaltic pillow lava here overlies white, thinly bedded, poorly consolidated volcaniclastic sandstone. Some pillow lobes at the base have penetrated as much as 0.5 m down into the sandstone and in cross-section appear to be isolated within it. Above the base, the pillow lobes are closely packed and very little sandstone matrix occurs. Field relationships show that this pillowed lava flow was erupted subaerially and transgressed a shoreline.

Roque Nublo Group, Pliocene; Barranco de Tamaraceite, Gran Canaria, Canary Islands.



4. Amoeboid pillow with tortoise shell joints

Secondary carbonate and pale volcaniclastic sandstone clearly outline the amoeboid cross-section shape of this basaltic pillow. Carbonate also fills tortoise shell joints and scattered amygdales within the pillow. Intercalated fossiliferous sandstone elsewhere in the sequence suggests emplacement in water shallower than 100 m.

Basaltic pillow lava, Middle Miocene; Zimbralinho, Porto Santo, Madeira Archipelago.



5. Closely packed trachyandesite pillow lobes

Relatively large diameter (0.5-2.5 m), closely packed pillows are exposed here in cross-section. The lower surfaces of the pillows fit neatly into the shape of pillows below, and in ancient close-packed pillow lava, the asymmetry in shape can be used to interpret younging direction. The large size of the pillows may indicate relatively low lava viscosity, related to high eruption temperature and/or alkali-rich composition (Yamagishi and Goto, 1991).

Abashiri Formation, 6.8Ma; Misaki Quarry, Hokkaido, Japan.



6. Feeder tube in a submarine andesitic lava flow

A steep sided feeder tube (**F**) is surrounded by a mass of closely packed pillow lobes (**P**). Columnar cooling joints radiate outward from the centre of the lava tube. The feeder tube delivered molten lava to the advancing flow front and also fed small pillow lava lobes that propagated through fissures in its outer margin. The flow is about 25 m thick.

Maori Bay pillowed lava flow, Miocene; Maori Bay, Muriwai, New Zealand.



7. Basaltic andesite pseudo-pillows

The pattern of joints displayed in this outcrop of coherent basaltic andesite defines large blocks termed "pseudo-pillows". Each pseudo-pillow (**1**, **2**, **3**) is outlined by curvilinear joints along which there are "tiny normal joints" (arrow) and tortoise shell joints occur in the interior. Pseudo-pillows develop in response to contraction during rapid cooling and although chilled, the joint surfaces are not glassy. Disintegration of pseudo-pillows generates hyaloclastite composed of polyhedral blocks (angular fragment breccia).

Oshinkoshin basaltic andesite dyke, Pliocene; Oshinkoshin waterfall, Shiretoko Peninsula, Hokkaido, Japan.

Plate 18 — Products of silicic lava dome eruptions in shallow water: Bunga Beds, New South Wales



1. Associated sedimentary facies: mudstone and turbidites

The rhyolitic coherent and volcanoclastic deposits of the Bunga Beds are associated with interbedded black, pyritic mudstone and coarse, mass-flow emplaced sandstone and breccia. The dominant lithofacies characteristics (planar, even, continuous, internally massive or graded bedding) are consistent with deposition from suspension and turbidity currents, and constrain the initial setting of the rhyolitic volcanism as subaqueous, below wave base and relatively quiet (Cas et al., 1990).

Basin centre facies sandstone turbidites and black mudstone, Bunga Beds, Late Devonian; Aragunnu Bay, New South Wales.



2. Rhyolite-black mudstone contact relationships

Rhyolitic magmatism in the Bunga Beds included partly extrusive cryptodomes and isolated intrusions (Cas et al., 1990). Contact relationships such as that illustrated here suggest that the enclosing sediments were poorly consolidated at the time of intrusion. The black mudstone is highly disturbed adjacent to the rhyolite and penetrates along fractures. The rhyolite shows well-developed polyhedral jointing as a result of rapid cooling and contraction.

Rhyolite type 2, Bunga Beds, Late Devonian; Aragunnu Bay, New South Wales.



3. Intrusive hyaloclastite breccia (peperite)

Breccia at the margins of the rhyolitic cryptodome consists of pale, quartz- and feldspar-phyric rhyolite clasts, locally with jigsaw-fit texture, separated by narrow bands and seams of mudstone. The breccia is interpreted to be the product of auto- and quench-brecciation of cryptodome rhyolite that came in contact with wet, unconsolidated mud during shallow intrusion (Cas et al., 1990).

Facies 1, Bunga Beds, Late Devonian; Aragunnu Bay, New South Wales.



4. Rhyolite-siltstone megabreccia

Megabreccia above the intrusive hyaloclastite (18.3) consists of angular rhyolite clasts (**R**) up to 4 m and black siltstone clasts up to 2 m across, with a matrix (**M**) of massive black siltstone and millimetre-centimetre rhyolite fragments. The megabreccia is considered to be a debris-flow deposit comprising a mixture of rhyolite and sea-floor sediment dislodged during growth of the subjacent rhyolite dome (Cas et al., 1990).

Facies 2, Bunga Beds, Late Devonian, Aragunnu Bay, New South Wales.



5. Rhyolitic pumice- and crystal-rich breccia

Gradationally above the megabreccia (18.4) is a 1 m thick, massive to graded breccia bed comprising ragged pale green rhyolitic pumice clasts (**P**), minor black siltstone and abundant crystal fragments. The breccia is a submarine mass-flow deposit and the juvenile clasts are thought to be pyroclastic in origin, indicating the onset of explosive activity (Cas et al., 1990).

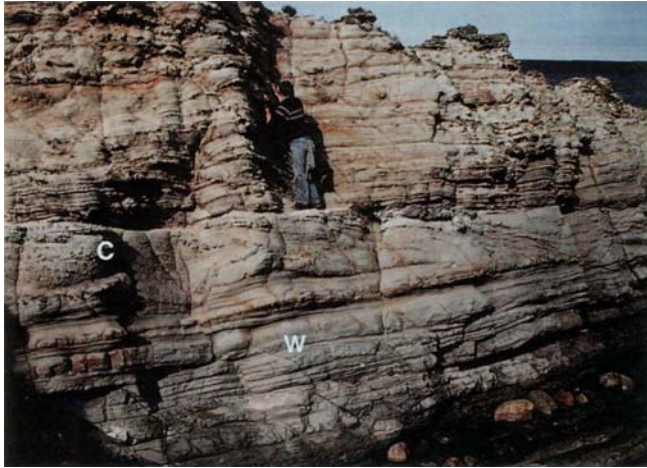
Facies 3, Bunga Beds, Late Devonian; Aragunnu Bay, New South Wales.



6. Rhyolitic pumice- and crystal-rich breccia in polished slab

The rhyolitic pumice clasts (pale green) are generally <5 cm, evenly feldspar- and quartz-phyric and in thin-section show relict fibrous tube vesicle textures. The crystal-rich matrix comprises coarse sand-size, angular, volcanic quartz and feldspar crystals and crystal fragments, pumice granules and minor non-volcanic lithic particles.

Facies 3, Bunga Beds, Late Devonian; Aragunnu Bay, New South Wales.



7. Crystal-rich and crystal-poor volcaniclastic sandstone

Above the rhyolitic pumice- and crystal-rich breccia (18.5, 18.6) is diffusely stratified, crystal-rich (lower) and crystal-poor (upper) sandstone. The lower part shows wavy bedding (W) and cross bedding (C). The two facies are interpreted to be water-settled, pyroclast-rich deposits from shallow subaqueous explosive eruptions that followed dome effusion (Cas et al., 1990). Their contrasting compositions (crystal-rich versus crystal-poor) and grain size (coarse versus fine) reflect efficient hydraulic sorting of particles during settling through the water column.

Facies 4 and 5, Bunga Beds, Late Devonian; Aragunnu Bay, New South Wales.

Plate 19 — Subaerial lava flows and domes



1. Subaerial rhyolitic lava dome

The diameter of the rhyolitic lava dome shown here is 380 m, and it is 65 m high. A carapace of autobreccia covers the flat top and an apron of talus breccia (T) has accumulated around the steep margins. The dome is partly encircled by a ring of pumice deposits (C) erupted immediately prior to dome extrusion.

Novarupta lava dome, about 80 a; Valley of Ten Thousand Smokes, Alaska, USA.



2. Subaerial rhyolitic obsidian lava flow

A cliff-section through the margin of a rhyolitic lava flow reveals large, regular columnar joints (J) at the base, and tightly contorted flow layering (F) near the top. The flow foliation is defined by trains of spherulites. The rhyolite is devoid of phenocrysts indicating eruption at a temperature above the liquidus and all but the interior was quenched to glass (obsidian). The top of the flow is pumiceous. Talus at the foot of the cliff comprises angular boulders and hides the basal contact.

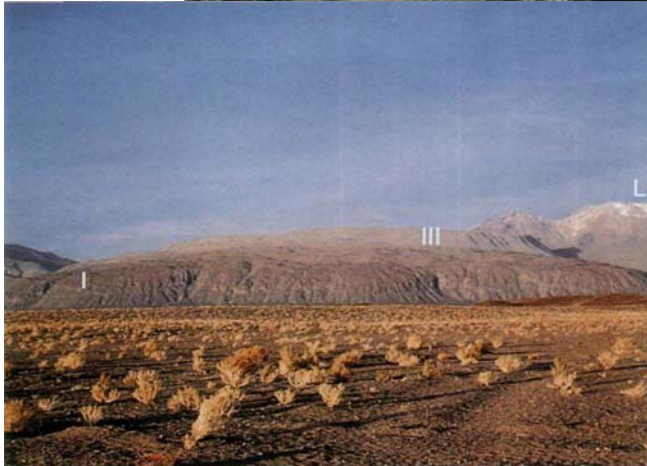
Obsidian Cliff rhyolite flow, 0.18 Ma; Yellowstone National Park, Wyoming, USA.



3. Subaerial basaltic lava flows

More than twelve 1-3 m thick, subaerial, basaltic lava flows are exposed in this cliff section. The flow interiors are massive whereas top and basal parts comprise red-brown scoriaceous breccia. Very thin fallout ash layers occur between some flows. The upper part of the thickest fallout ash deposit (arrow) has been thermally oxidized (red) close to the contact with the overlying lava.

Subaerial basaltic lavas, Late Miocene; Porto da Morena, Porto Santo, Madeira Archipelago.



4. Voluminous subaerial dacitic lava flow

In the distance is the 350-400 m high flow front of the 14.5 km long Chao dacitic lava flow. The flow comprises three lobes, two of which are visible (Chao I and Chao III; De Silva and Francis, 1991). The Chao lava has a large volume (about 26 km³) and long outflow distance. The flow occupies the saddle between two composite andesitic volcanoes, Paniri to the north and Leon (L) to the south.

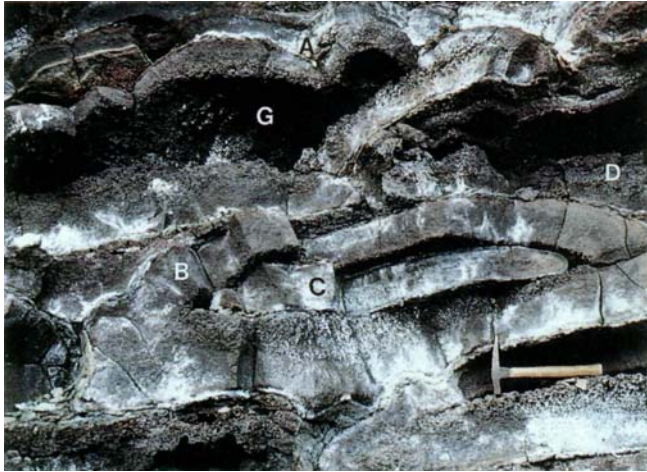
Chao lava, >100 ka; northern Chile.



5. Subaerial andesitic lava flow

This photograph shows the extremely rough, irregular surface of a subaerial andesitic lava flow. The top of the flow comprises blocks and spires up to several metres across characterized by scoriaceous and spinose surface textures. The interior of the flow consists of massive, coherent, evenly porphyritic andesite that is cut by smoothly curving cooling joints.

Oni-Oshidashi Lava, erupted AD 1783; Asama volcano, Honshu, Japan.



6. Subaerial basaltic pahoehoe lava in cross-section

The upper unit (A) in this stack of spongy pahoehoe lava flow units shows an inward increase in vesicle size, and has a medial gas blister (G) lined by disrupted vesicles. The gas blister formed when large, closely spaced vesicles near the centre of the unit coalesced, parting the floor and roof. Flow unit (B) also had a median gas blister but it has been filled by a younger lava tongue (C). Lava in the floor and roof of flow unit (D) displays concentric layers of differing vesicle size and abundance. These result from shearing during intermittent periods of flowage after the lava has begun to cool. Spongy pahoehoe develops as a result of vesicle growth, mostly by coalescence, in static lava (Walker, 1989b).

Mauna Iki pit crater, Holocene; Kilauea volcano, Hawaii, USA.



7. Subaerial basaltic a'a and pahoehoe lava flows

Surface features of subaerial a'a (left) and pahoehoe (right) lava flow types contrast markedly. The a'a flow surface is a mass of spinose, twisted blocks, some of which are loose and easily dislodged. In contrast, the pahoehoe flow has a smooth, lobate surface of shiny glassy lava folded into ropy patterns.

Lava flows from the AD 1969-74 eruption of Mauna Ulu; Chain of Craters Road, Kilauea volcano, Hawaii, USA.

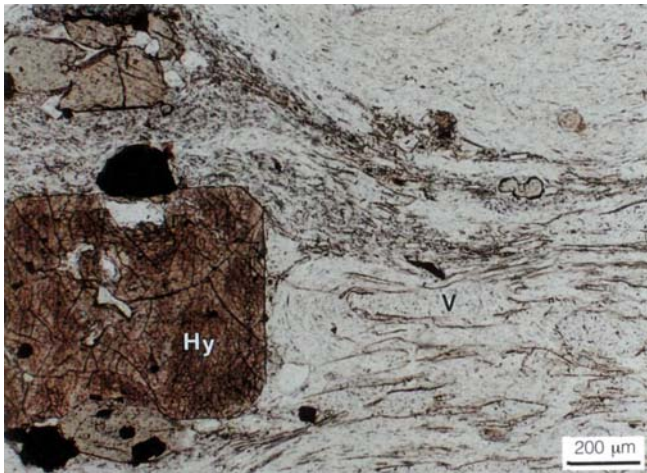
Plate 20 — Textures in glassy, subaerial rhyolitic lava



1. Finely vesicular pumiceous rhyolite

A. Pale grey, glassy, finely vesicular pumice forms a carapace about 10 m thick that covers much of the Little Glass Mountain rhyolite lava flow. Vesicles make up around 30% by volume and are generally elongate, occasionally spherical and largely less than 1 mm in diameter. Subtle flow banding is defined by variations in vesicle size and abundance.

Little Glass Mountain rhyolite flow, 1100 a; Medicine Lake Highland volcano, California, USA.



B. In thin-section, the flow banding is also defined by variations in the abundance of microlites. Vesicles (**V**) and microlites wrap around euhedral plagioclase and hypersthene (**Hy**) phenocrysts. Plane polarized light.

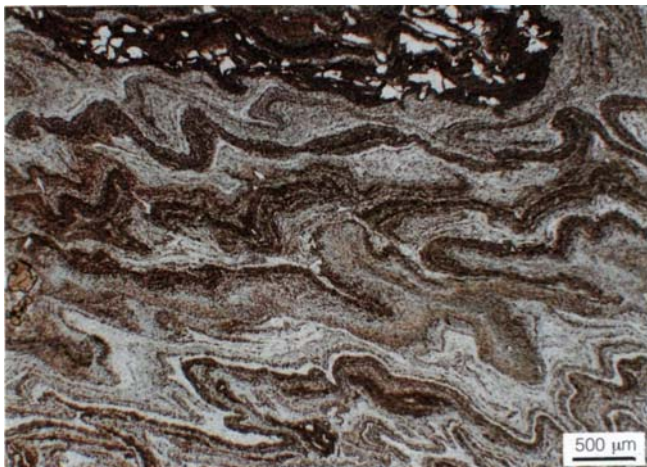
Little Glass Mountain rhyolite flow, 1100 a; Medicine Lake Highland volcano, California, USA.



2. Flow-banded obsidian

A. Black, dense, rhyolitic obsidian forms layers up to 15 m thick in the interior of the Little Glass Mountain lava flow. Obsidian overlies and is interlayered with coarsely vesicular pumice. Much of the obsidian is flow banded on a scale of microns to several centimeters, and flow folds are common. Flow banding is defined by grey, finely vesicular pumice and black, delicately flow-laminated obsidian. Pumiceous bands contain around 15% vesicles in microlite-rich glass.

Little Glass Mountain rhyolite flow, 1100 a; Medicine Lake Highland volcano, California, USA.



B. In thin-section, intricate banding in the dense obsidian is defined by varying concentrations of feldspar microlites. Microlites (12-75 μm) share a common alignment within each layer, although they are not always parallel to the boundaries of the layer. Plane polarized light.

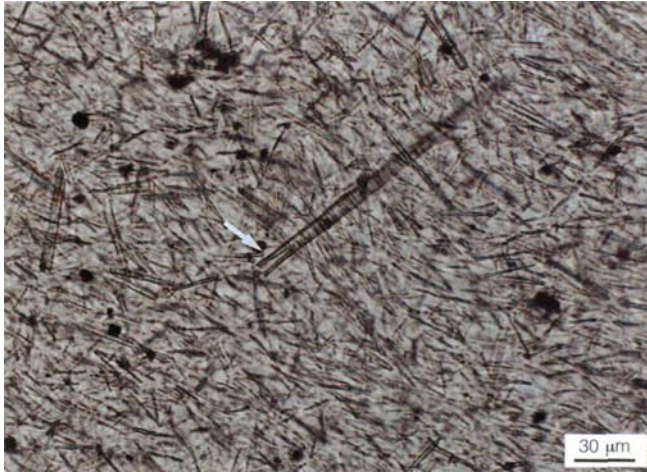
Little Glass Mountain rhyolite flow, 1100 a; Medicine Lake Highland volcano, California, USA.



3. Dense obsidian

A. Dense, dark grey obsidian contains sparse, fine, evenly distributed phenocrysts (< 1 mm) set in a glassy groundmass and has a distinctive conchoidal fracture.

Little Glass Mountain rhyolite flow, 1100 a; Medicine Lake Highland volcano, California, USA.



B. Thin-sections show that the glass contains abundant feldspar microlites ranging from 12 μm to 75 μm in length. Although the hand specimen appears unfoliated, microlites are weakly to moderately aligned and some are deflected around phenocrysts. The microlites exhibit morphologies typical of rapid growth in response to large degrees of undercooling, such as swallow-tail terminations (arrow). Plane polarized light.

Little Glass Mountain rhyolite flow, 1100 a; Medicine Lake Highland volcano, California, USA,

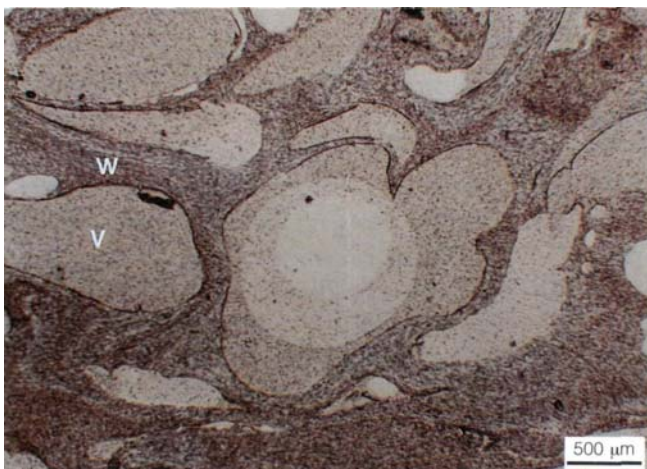
4. Coarsely vesicular pumiceous rhyolite

A. A layer of coarsely vesicular pumiceous lava several metres thick occurs sandwiched within dense obsidian in the Little Glass Mountain rhyolite lava flow. The contact is transitional from coarse pumice, to a mixture of pumice and obsidian, to obsidian with pumiceous inclusions (20.2) and finally to dense obsidian (20.3). Vesicles in the coarse pumice exceed 50% by volume, are ovoid to tabular in shape, and range from less than 1 mm to 2 cm in diameter. Variation in the size, shape and abundance of vesicles defines flow bands (F) in the hand specimen.



Little Glass Mountain rhyolite flow, 1100 a; Medicine Lake Highland volcano, California, USA.

B. Thin-sections of the coarsely vesicular pumice show that vesicle walls (W) consist of microlite-rich glass and are sometimes folded and crinkled. Microlites are aligned parallel to each other and to the vesicle walls. Vesicles (V) are filled with mounting medium. Plane polarized light.



Little Glass Mountain rhyolite flow, 1100 a; Medicine Lake Highland volcano, California, USA.

Part 4. Pyroclastic, resedimented volcanoclastic and volcanogenic sedimentary deposits

Active volcanic terranes, whether subaerial or subaqueous, combine primary volcanic and sedimentary processes, both of which have the potential to generate diverse volcanoclastic deposits. Primary volcanoclastic deposits involve volcanic processes of clast formation, transport and deposition. Clasts that are generated and initially deposited by primary volcanic processes may be rapidly resedimented, or subsequently eroded and reworked by non-volcanic surface processes, and incorporated in a variety of resedimented and volcanogenic sedimentary deposits.

Studies of volcanoclastic deposits, therefore, require information on:

- (1) the clast-forming processes;
- (2) the clast transport and depositional processes;
- (3) post-emplacement syn-volcanic processes (welding, high-temperature devitrification, hydration, vapour-phase crystallisation, diagenetic and hydrothermal alteration).

Clast type, shape, composition and texture help constrain the clast-forming processes, whereas lithofacies character (bedforms, geometry, structures, internal organisation, nature of contacts, relationships to enclosing units) helps constrain the clast transport and depositional processes. Textural evidence of hot emplacement (welding, thermal oxidation, columnar jointing, baked contacts, vapour-phase crystallisation, degassing structures) is especially important in recognition of some primary volcanoclastic deposits.

Correct information on these facets is extremely powerful, and can be used to:

- (1) distinguish among the different genetic categories of volcanoclastic deposits;
 - (2) constrain the depositional setting (subaerial versus shallow subaqueous versus deep subaqueous);
 - (3) assess the proximity of the deposits relative to the source of volcanic components;
- establish the character, composition and setting of the volcanic source.

These should be the aims of textural interpretation of volcanoclastic deposits, even though in reality, especially in the exploration context, limited time, poor exposure and poor preservation of original textures interfere and greatly restrict the yield.

Genetic classification of volcanoclastic deposits

Volcanoclastic deposits are classified on the basis of clast-forming processes *and* transport and depositional processes. The principal genetic categories are (Fig. 1): *Autoclastic* — primary volcanoclastic deposits made of particles (autoclasts) generated by in situ, non-explosive

fragmentation of lava or magma (autobrecciation and quench fragmentation (Part 3);

Pyroclastic — primary volcanoclastic deposits made of particles (pyroclasts) generated by explosive eruptions and deposited by primary volcanic processes (fallout, flow, surge); *Resedimented syn-eruptive volcanoclastic* — volcanoclastic deposits from rapid resedimentation of texturally unmodified, freshly erupted pyroclastic or autoclastic particles;

Volcanogenic sedimentary — volcanoclastic aggregates containing particles derived by erosion of pre-existing volcanic deposits and that were subject to significant reworking prior to final deposition, and/or that were redeposited long after eruption.

This part concentrates on pyroclastic deposits, resedimented syn-eruptive volcanoclastic deposits and volcanogenic sedimentary deposits. The principal components in these volcanoclastic deposits are juvenile magmatic clasts that range in vesicularity from highly vesicular pumice and scoria to variably vesicular lava bombs and blocks, glass shards, free crystals and crystal fragments, lithic fragments and accretionary lapilli (Part 2). Non-volcanic components, such as biogenic and epiclastic sedimentary particles, can be significant, especially in volcanogenic sedimentary deposits.

Explosive eruptions and pyroclastic deposits

Explosive eruptions involve the rapid release and decompression of gas which results simultaneously in fragmentation and ejection of magma and/or wall rocks. The three main sorts of explosive eruptions - *explosive magmatic*, *phreatomagmatic*, and *phreatic* - differ in the source of the gas and the extent of direct involvement of magma. Phreatomagmatic and phreatic eruptions are *hydrovolcanic* phenomena, that is, they both involve steam generated from external water. All three of these explosive eruption styles are capable of generating abundant pyroclasts ranging from fine ash (< 1/16 mm) to blocks a few metres across. The pyroclasts are dispersed by:

- (1) injection into the atmosphere followed eventually by *fallout* from suspension;
- (2) ground hugging, relatively high particle concentration *pyroclastic flows*;
- (3) relatively low particle concentration *pyroclastic surges*.

Transportation is regarded as a primary volcanic process because it follows directly from eruption, and involves pyroclasts suspended or entrained in volcanic gas, even though gravity and mixing with the atmosphere play fundamental roles.

Explosive magmatic eruptions

These involve the exsolution and expansion of magmatic volatiles. Large volumes of pumice or scoria, and glass shards are generated. They are regarded as relatively "dry" eruptions because steam contributed from external water is only a minor component. The magma composition (especially volatile content) and physical properties (mainly viscosity, temperature and density), and the vent geometry control the character and behaviour of explosive magmatic eruptions (McBirney and Murase, 1970; Settle, 1978; Wilson et al., 1978; Wilson et al., 1980; Head and Wilson, 1986; Sparks, 1986; Wilson and Walker, 1987; Wilson et al., 1987; Woods, 1988). As a result, explosive magmatic eruptions of basaltic, andesitic and silicic magmas tend to exhibit characteristic styles, as described below (although there are always exceptions).

Strombolian eruptions are largely the result of intermittent bursting of large bubbles or groups of bubbles at the top of the magma column in an open conduit (Walker and Croasdale, 1972; Walker, 1973a; Self et al., 1974; Blackburn et al., 1976; L. Wilson, 1980; Houghton and Hackett, 1984). This eruption mechanism is restricted to magmas of low viscosity and low gas content, hence the typical association of basaltic magma with Strombolian activity. Fragmentation is not very efficient and only minor amounts of ash are produced. If explosions are repeated at short intervals, a convecting eruption cloud may form above the vent and widely disperse entrained fine pyroclasts. However, most pyroclasts are deposited close to the vent and build a cone of scoria lapilli, blocks and bombs.

Hawaiian eruptions involve steady rather than intermittent discharge, but are otherwise similar to Strombolian eruptions and principally confined to low viscosity basaltic magmas (Walker, 1973a; Wilson and Head, 1981). Most pyroclasts are poorly to moderately vesicular, relatively coarse, fluidal clots of magma that experience little cooling during eruption. They form spatter deposits close to the vent, or else, in sustained eruptions, may coalesce to form fountain-fed lava flows.

Vulcanian eruptions are characterised by discrete explosions repeated at intervals of a few minutes to hours and usually involve basaltic andesite and andesitic magmas (Walker and Croasdale, 1972; Walker, 1973a; Nairn and Self, 1978; Self et al. 1979; L. Wilson, 1980). Explosions result when gas confined beneath a temporary seal of degassed, congealed lava or a blockage of the conduit is suddenly released. The gas pressure increases due to exsolution of volatiles from rising fresh magma, and in some cases, steam from heated ground water is important. The explosions eject vertically directed slugs of pyroclasts and gas, and are sufficiently vigorous to generate eruption columns 5-10 km high and convecting ash plumes. Initially, the pyroclasts are dominated by fragments of the seal and by dense accessory lithic pyroclasts, both of which may be finely comminuted. Periods of continuous gas

streaming may follow and produce vesicular juvenile pyroclasts. Pyroclasts involved in repeated cycles of ejection followed by fallback into the vent ("milling") can have conspicuously rounded shapes. Pyroclasts are deposited by fallout from the eruption column and plume, and less commonly by small volume scoria and ash flows.

Plinian eruptions are characterised by very powerful release of gas and pyroclasts in high eruption columns (Walker and Croasdale, 1970; L. Wilson, 1972, 1976, 1980; Walker, 1973a, 1981a, 1981b; Sparks and Wilson, 1976; Sparks, 1986; Carey and Sparks, 1986; Carey and Sigurdsson, 1989; Woods and Bursik, 1991; Bursik et al., 1992; Sparks et al., 1992). They involve high viscosity (in most cases silicic), vesiculating magmas, capable of generating very large internal gas pressures. When fragmentation takes place, decompression of the gas generates a high-velocity jet of comminuted magma and hot gas that feeds a buoyant, convecting plume and uppermost, laterally spreading umbrella region. Observed plinian eruption columns have reached 30 km and theoretical calculations suggest a maximum limit of about 55 km. Pyroclasts generated by plinian eruptions are relatively low-density pumice lapilli and ash, that are entrained in the high-velocity jet and eventually deposited by fallout from the convecting plume and umbrella region. Intermittent or sustained collapse of plinian columns occurs if the vent widens significantly, or if the upward gas velocity decreases, or if the gas content decreases. Widespread and voluminous pyroclastic flow deposits are formed as a result of collapse of plinian-style eruption columns (Sparks et al., 1978).

Phreatomagmatic eruptions

Phreatomagmatic eruptions involve steam produced by direct interaction of the magma (or lava) with external water (Sheridan and Wohletz, 1981; Wohletz, 1983, 1986; Kokelaar, 1986). Explosions occur when superheated water flashes to steam that rapidly expands and simultaneously fragments the magma. Quench fragmentation and magmatic-volatile driven fragmentation commonly operate at the same time to varying extents. Special circumstances are required in order for phreatomagmatic eruptions to occur: (1) There must be efficient transfer of magmatic heat to the external water. Efficiency depends on how the magma and water come in contact and the magma: water mass ratio. (2) Steam generated must be able to expand. High lithostatic or hydrostatic confining pressures will preclude explosive expansion of steam. The water depth limits for steam explosivity are not well constrained, and estimates range from less than 500 m to about 2000 m (Kokelaar, 1986). Because these conditions are not always met, phreatomagmatic eruptions do not always result when hot magma comes in contact with water.

Water-magma interaction may occur intermittently or continuously during eruptions, involve magma of any composition and affect the products of otherwise "dry"

eruptions (e.g. lava flows, pyroclastic flow deposits). Phreatomagmatic eruptions are common where ground water has access to vents, such as in marshy areas or on shorelines, and where vents are submerged in shallow water. Typical activity ranges from relatively dry, rapidly repeated explosions, generating ash-laden eruption columns and laterally directed base surges (Moore, 1967; Waters and Fisher, 1971; Kokelaar, 1986), to relatively wet jetting and continuous uprush of water-pyroclast slurries (Kokelaar, 1983; Moore, 1985). Phreatoplinian eruptions involve large volumes of vesiculating rhyolitic magma affected by interaction with water (Self and Sparks, 1978; Self, 1983; Wilson and Walker, 1985; Orsi et al., 1992), in circumstances where vents are located in caldera lakes or in calderas inundated by the sea. Secondary or *rootless* phreatomagmatic explosions may also occur at sites other than the eruptive vent; for example, where lava flows or hot pyroclastic deposits are emplaced on snow or wet ground. Littoral cones composed of phreatomagmatic pyroclastic deposits can be constructed at the shoreline where lava meets the sea (Fisher, 1968).

Phreatomagmatic eruptions produce a high proportion of ash pyroclasts, and eruption columns and plumes are steam-rich. Suspended fine, moist ash commonly aggregates into small clumps or spherical accretionary lapilli, or forms a coating around larger pyroclasts. Steam condensation produces ash-laden rain that results in deposition of fine ash at the same time as coarser pyroclasts. Pyroclasts in phreatomagmatic deposits can range widely in vesicularity (Houghton and Wilson, 1989). If the magma is largely degassed at the time of interaction with water or if vesiculation is prematurely arrested by quenching, poorly vesicular, angular, juvenile pyroclasts dominate the ejected mixture. If vesiculation is advanced at the time of interaction, pumiceous or scoriaceous pyroclasts and bubble-wall shards can be abundant. Significant amounts of accessory lithic pyroclasts are also generated in each case.

Phreatic or steam eruptions

Steam-driven explosions that do not directly involve fresh magma are called phreatic. Magma may be the heat source for steam generation but does not participate further in eruptive processes. Phreatic explosions are common in active geothermal systems (e.g. Muffler et al., 1971; Nairn and Wiradirdja, 1980; Hedenquist and Henley, 1985) and in or around active vents between eruptions (e.g. Jaggar and Finch, 1924; McPhie et al., 1990). The explosions occur when subsurface, superheated water flashes to steam as a result of rapid reduction in confining pressure.

Phreatic eruptions typically emit large amounts of steam that contain only small volumes of solid ejecta. The explosions are comparatively weak and most pyroclasts are deposited close to the eruptive site by fallout. The deposits are dominated by non-juvenile lithic pyroclasts. In cases involving geothermal systems, pyroclasts are

commonly hydrothermally altered and may include hydrothermal mud or sinter fragments (Hedenquist and Henley, 1985).

Resedimented syn-eruptive volcanoclastic deposits

In studies of volcanic sequences, especially ancient sequences, the importance of distinguishing between primary volcanoclastic (pyroclastic, autoclastic) deposits and reworked volcanogenic sedimentary deposits is widely recognised. In addition, it is just as important to distinguish resedimented, essentially syn-eruptive volcanoclastic deposits from reworked, post-eruptive volcanoclastic deposits that have no genetic connection with active volcanism. Resedimented syn-eruptive pyroclastic or autoclastic deposits have immense significance in establishing the composition, setting, eruptive style and proximity of source volcanic centres, and may also be sensitive indicators of the depositional environment. The resedimented syn-eruptive category (3) is an attempt to take account of this important class of volcanoclastic deposits.

Some criteria that distinguish resedimented, syn-eruptive pyroclast-rich deposits are listed below:

1. Sedimentation units are composed of texturally unmodified pyroclasts.
2. Each sedimentation unit, and successions of such units, are compositionally uniform in containing a narrow range of pyroclast types and compositions.
3. Only non-welded clasts can be resedimented, so resedimented deposits are invariably non-welded.
4. Bedforms indicate rapid (commonly mass-flow) deposition. However, sedimentation units are different in internal organisation from primary pyroclastic depositional units.
5. Single mass-flow depositional units are typically very thick (several tens to more than 100 m), reflecting rapid influx of large volumes of pyroclastic debris and the exclusion of non-volcanic "ambient" sedimentation, as occurs only during and immediately after a major eruption.
6. The resedimented pyroclastic deposits may be associated with primary pyroclastic deposits of the same composition.

Many of the above criteria also apply in the case of resedimented hyaloclastite but the volumes, thicknesses of sedimentation units and transport distances are much smaller, and the associated primary volcanic facies are coherent lava flows or lava domes.

There are several situations in which pyroclasts are delivered more or less directly to sedimentary transport and depositional systems, bypassing initial deposition as primary pyroclastic deposits altogether, or else being briefly stored prior to redeposition. For example:

- (1) fallout of pyroclasts onto lakes, rivers, shorelines and the sea;
- (2) entry of pyroclastic flows into rivers and transformation to subacrial water-supported volcanoclastic mass flows and hyperconcentrated flows

- (lahars);
- (3) entry of subaerial pyroclastic flows into the sea or into lakes and transformation to subaqueous, water-supported volcanoclastic mass flows;
- (4) subaerial pyroclastic flows and surges flowing across and coming to rest on the surface of lakes or the sea;
- (5) explosive eruptions at subaqueous (submarine or sublacustrine) volcanoes;
- (6) rapid, essentially syn-eruptive resedimentation of pyroclastic deposits temporarily stored in shoreline environments or on the flanks of subaqueous volcanoes.

Volcanogenic sedimentary deposits

In volcanic terranes, all surface deposits - lavas, welded pyroclastic deposits, other variably welded or consolidated volcanoclastic deposits, non-volcanic rocks - are subject to chemical and physical weathering and erosion. New particles created solely by surface weathering and erosion are termed epiclasts. However, weathering and erosion of pre-existing, poorly or non-welded primary volcanoclastic deposits can simply release the original pyroclasts or autoclasts and rapidly provide large volumes of *recycled* particles. As a result, only a proportion of the particles present in volcanosedimentary systems are true epiclasts: the rest, often the vast majority, are pyroclasts or autoclasts, some freshly erupted and some liberated from poorly consolidated primary volcanoclastic deposits. All particle types are available for transport or reworking by wind, water or ice. Final deposits are commonly mixtures and, therefore, more appropriately identified as volcanogenic sedimentary, rather than epiclastic deposits.

In order to distinguish volcanogenic sedimentary from resedimented syn-eruptive volcanoclastic deposits, we add the requirement that there is evidence of significant transport or reworking prior to deposition, and/or evidence that final deposition significantly post-dated eruption. Hallmarks of transport, reworking and post-eruptive resedimentation are modification of primary clast shapes, especially rounding, admixtures of non-volcanic particles, mixtures of widely compositionally different volcanic particles, particles that show the effects of weathering or partial diagenetic alteration, and association with non-volcanic sedimentary facies.

Volcanogenic sediments are best known in subaerial volcanic terranes, where weathering and erosion are vigorously active during and following eruptions. Such terranes commonly include a wide spectrum of sedimentary environments (e.g. fluvial, alluvial, lacustrine, shoreline) and eruptions may affect sedimentation in neighbouring non-volcanic terranes, and in offshore submarine shelf and deeper water settings. In below-wave-base subaqueous settings, weathering and erosion are in general very limited. Mass wasting processes (rock falls, slides and slumps) along fault scarps and on the flanks of island volcanoes and seamounts constitute an important exception. Although

not produced in abundance in this setting, volcanogenic sediments may nevertheless be finally deposited there, if resedimented by mass flows or transported by wind from subaerial sources nearby.

Transport and deposition of volcanoclastic particles

More or less similar processes of transport and deposition operate in the formation of primary pyroclastic, resedimented syn-eruptive volcanoclastic and volcanogenic sedimentary deposits. Regardless of the clast-forming mechanism, each case essentially involves particles and interstitial fluid. Although the physical properties of volcanoclastic particles vary widely, and the interstitial fluid can be gas (volcanic gas, air, steam, or a mixture) or liquid (water, watery mud, muddy water), volcanoclastic deposits display a limited range of sedimentary structures. Volcanoclastic deposits are reviewed here firstly in terms of the depositional processes that are evident from outcrop and lithofacies information, and then in terms of textures and facies associations that help distinguish among the different genetic categories.

Transport of volcanoclastic particles from the site of initial fragmentation to depositional sites may be continuous with a primary volcanic clast-forming process, such as an explosive eruption, or involve surface sedimentary transporting agents, such as wind, water or ice, or else involve both these processes in rapid succession. In each case, there are three broad categories of clast transport processes:

Mass-flow transport — groups of clasts, or clasts plus interstitial fluid (air, water, volcanic gas) move together and interact; mass flows vary widely in rheology and particle concentration;

Traction transport — clasts are entrained in moving interstitial fluid (air, water, volcanic gas) and are free to behave independently;

Suspension transport — clasts are fully suspended in interstitial fluid (air, water, volcanic gas).

Each of these categories of transport processes produces a suite of characteristic textures and structures in the resulting deposits. Transport in each mode can be strongly influenced by the particle concentration and the properties and behaviour of the interstitial fluid (air, water, muddy water, watery mud, volcanic gas, steam, ice), or else can occur primarily in response to gravity acting directly on the particles or paniculate aggregate, regardless of the presence or character of an interstitial fluid. Particle concentration and other properties of the particle-fluid system fluctuate with time and are rarely homogeneous throughout the system, especially during deposition; therefore continuous sedimentation may involve alternation from one mode to the other, locally or temporarily. All three modes operate in subaerial and subaqueous settings, and are involved in formation of pyroclastic, resedimented syn-

GENETIC CATEGORY	DOMINANT TRANSPORT		
	Mass-flow	Traction	Suspension
primary pyroclastic deposits	• pyroclastic flows	• pyroclastic surges	• fallout • water-settled fallout
resedimented syn-eruptive volcanoclastic deposits and volcanogenic sedimentary deposits	• turbidity currents • debris flows, mud flows • grain flows • density-modified grain flows • slides, debris avalanches	• fluvial and shallow subaqueous currents • waves	• suspension associated with mass flows • hemipelagic suspension

Table 4. Mass-flow, traction and suspension transport processes that operate in the formation of pyroclastic, resedimented volcanoclastic and volcanogenic sedimentary deposits.

eruptive volcanoclastic and volcanogenic sedimentary deposits (Table 4). Common types of mass-flow, traction current and suspension transport processes and their deposits are outlined below.

Mass movement and mass-flow deposits

Mass movement of particles involves a variety of particle support processes that operate during transport: interstitial fluid turbulence, matrix strength, particle buoyancy, hindered settling, upward movement of interstitial fluid, dispersive pressure and grain collisions (Lowe, 1979, 1982; C. J. N. Wilson, 1980). These processes and flow rheology are the basis for the recognition of several ideal types of mass flows (also known as sediment gravity flows and density currents), and criteria for discrimination among their deposits are well defined but often difficult to apply in ancient sequences. Some natural deposits exhibit textural features consistent with only one of the ideal flow types but, in many cases, a precise interpretation is impossible, because the natural systems are much more complex than the classification recognises and combine a number of particle support processes simultaneously, together with being inhomogeneous and unsteady. Nevertheless, deposits from mass flows display distinctive textures and facies characteristics, the most generally applicable of which are poor sorting, being massive or graded or diffusely bedded, having sharp basal contacts and tabular bed geometry (Fig. 37).

In volcanic terranes, volcanoclastic mass flows are an important means of particle transport. Volcanoclastic mass flows can be very mobile and transport particles long distances from the site of flow initiation. Mobility reflects momentum imparted by gravity and by eruption processes, and the efficiency of clast support mechanisms during flowage. Volcanoclastic mass-flow deposits are found in both subaerial and subaqueous, volcanic and mixed volcanic-sedimentary sequences, and indicate rapid sedimentation (or resedimentation). In general, only minor textural modification of particles occurs during mass-flow transport, so particle shapes and sizes strongly reflect clast-forming processes and shape-modifying processes that operated prior to incorporation of the clasts in the mass flow. This is an important point: mass-flow

deposits tell a great deal about the character, setting and clast-forming processes at their source, and much less about where they are finally deposited. Types of mass flows associated with each of the genetic categories of volcanoclastic deposits are:

Pyroclastic — primary pyroclastic flows in which the particles are pyroclasts, and the interstitial fluid is hot volcanic gas, steam, entrained air, or a mixture of all three;

Resedimented syn-eruptive volcanoclastic — water-supported volcanoclastic mass flows (e.g. volcanoclastic turbidity currents, debris flows, mud flows, density-modified grain flows) and gravity-driven volcanoclastic mass flows (e.g. grain flows, volcanoclastic slides, debris avalanches) that occur contemporaneously with eruptions (syn-eruptive);

Volcanogenic sedimentary — water-supported and gravity-driven mass flows that are unrelated to, or much later than, eruptions (post-eruptive).

Primary pyroclastic flow deposits (21-27)

Definition and genesis

Pyroclastic flows are hot, high-concentration, ground-hugging, highly mobile, gas-particle dispersions generated by volcanic eruptions (Wright and Walker, 1981). The particles are pyroclasts formed as a result of explosive disintegration of erupting magma and wall rocks. The flows are a type of mass flow in which the continuous phase between the pyroclasts is hot gas. The gas comprises magmatic volatiles exsolved prior to and during eruption, and released from pyroclasts during flowage, ingested air, steam from incorporated snow or surface water, and gas from combustion of vegetation. Particle support mechanisms include fluidisation (upward flux of gas), buoyancy, grain collisions and hindered settling. Flow mobility is partly attributable to gravitational forces, partly to momentum inherited from eruptive processes, and partly to very efficient particle support during outflow. Pyroclastic flows are produced (Fig. 38):

(1) in association with extrusion of lava domes and lava flows; these pyroclastic flows can originate directly from hot, growing lava domes and lava flows that undergo gravitational or explosion-triggered collapse, or else be generated by vertical or laterally-directed, explosive eruption columns accompanying lava dome extrusion; the flows are called

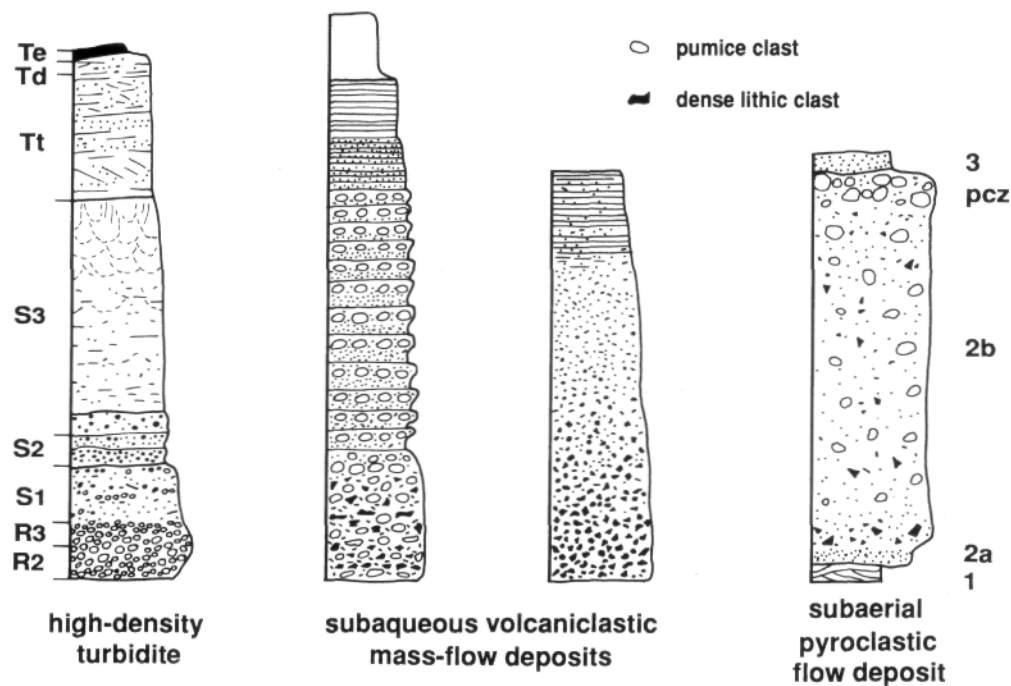


Fig. 37 Comparison of grain size variations and bedforms in deposits from subaqueous mass flows and primary pyroclastic flow deposits. Based on Lowe (1982), Yamada (1984), Fiske and Matsuda (1964) and Sparks et al. (1973). pcz, pumice concentration zone.

block and ash flows or *nuee ardentes* or *hot avalanches*, and their deposits are called *block and ash flow deposits* or *hot avalanche deposits*;

(2) by collapse of vertical explosive eruption columns; collapse may follow immediately after a single explosion or a series of closely spaced explosions, as occurs in some vulcanian eruptions that produce small volume scoria and ash flows (Nairn and Self, 1978); their deposits are called *scoria and ash flow deposits*; otherwise collapse can intermittently affect maintained, continuously streaming, plinian-style eruption columns and generate voluminous pumiceous pyroclastic flows, the deposits of which are called *ignimbrite*;

(3) directly from vents by upwelling and overflow, or low fountaining of pyroclast-gas mixtures; some pumiceous pyroclastic flows and scoria and ash flows are formed in this way.

Transport and depositional processes

It is important to recognise the difference between the active pyroclastic flow and the deposit it generates. The deposit may, or may not preserve textures and structures that can be used to interpret the character of the flow, such as flow density and rheology, particle concentration and particle support mechanisms. Deposition from pyroclastic flows is not fully understood, although two main processes appear to be important:

(1) progressive aggradation by sedimentation from the base of the active flow continuously over the entire runout extent (Fisher, 1966a; Branney and Kokelaar, 1992); in this case, the deposit is only a partial sample of the parent flow and principally records processes operating in the depositional regime at the flow base;

transport and depositional processes are analogous to those operating in high-density turbidity currents;

(2) en masse "freezing" of most of the flow at once (Wright and Walker, 1981); the deposit represents, more or less, a frozen portion of the entire flow; in this case the flow is considered to be comparable to a cohesive debris flow.

The textures, structures and dimensions of pyroclastic flow deposits vary enormously. No single model for transport and deposition is likely to adequately account for all the textural variations in the deposits, nor describe the diversity of processes. Many deposits have features consistent with progressive aggradation, but some appear to have been emplaced by very rapid freezing of the bulk of the flow. Furthermore, flows can undergo transformation in rheology during outflow (Fisher, 1983), as a result of changes in the eruption or due to topographic effects or due to inherent changes caused by deposition of particles or gas loss. Some of the textural variations in pyroclastic flow deposits also reflect whether the parent flow was steady or unsteady (Freundt and Schmincke, 1986; Branney and Kokelaar, 1992).

The concept of stratified flow (Valentine, 1987; Wilson, 1988; Branney and Kokelaar, 1992; Druitt 1992) may eventually prove important in understanding textural variations in pyroclastic flow deposits. Such flows have an internal particle concentration gradient, enabling identification of a high particle concentration depositional regime near the base, and a lower particle concentration transport regime above (Fig. 39). Particle concentration and particle support mechanisms may be different in each regime, particles may be transferred

from one regime to the other, and the two regimes may be locally or temporarily detached. Laminar flow probably operates in the basal depositional regime, whereas the transport regime above can be relatively dilute and turbulent.

Recognition of a distinction between the transport processes and depositional processes in pyroclastic flows is only just emerging. Such a distinction is well established in clastic sedimentology, and much can be learnt from that field. Water-supported systems analogous to pyroclastic flows can be readily identified and are potentially informative but should be used cautiously, because of the many, special properties of pyroclastic flows — an extremely wide range in particles sizes and densities, high temperature, high flow velocities, rapid generation and potentially large volume, and the interstitial fluid is gas.

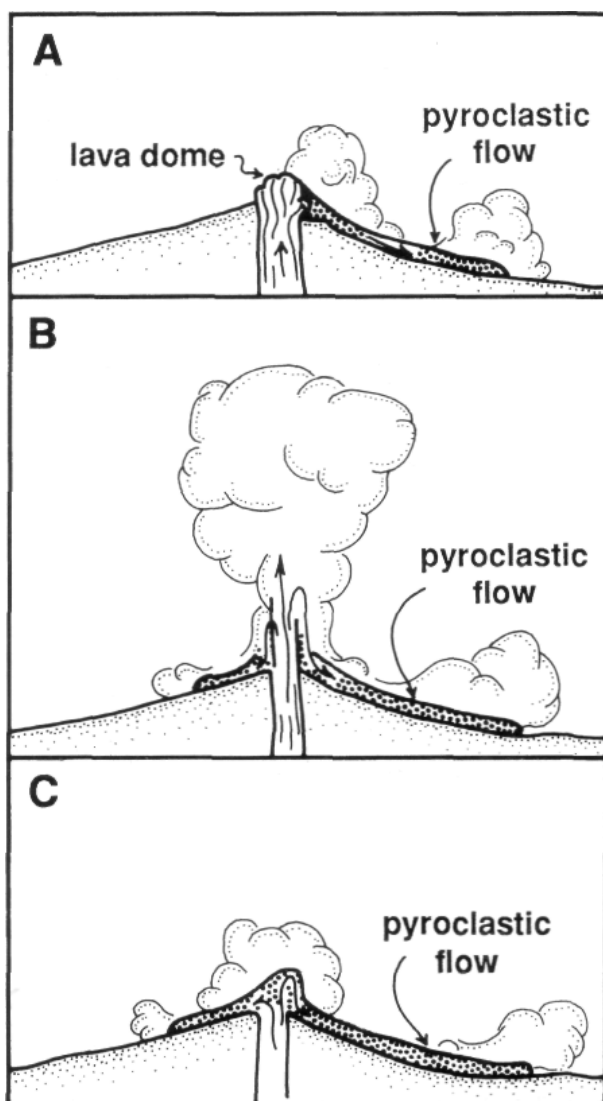


Fig. 38 Principal ways that pyroclastic flows are generated.

(A) Gravitational or explosion-triggered lava dome collapse.

(B) Collapse of an explosive eruption column.

(C) Low fountain, or overflow directly from the vent. Modified from Macdonald (1972).

Characteristics of pyroclastic flow deposits

Components

Pyroclastic flow deposits are dominated by juvenile magmatic pyroclasts derived from explosive disintegration of magma, together with cognate lithic pyroclasts, accessory lithic pyroclasts from the conduit and vent, and accidental lithic clasts collected by the flow. The juvenile components comprise pumice or scoria, other less vesicular juvenile clasts, glass shards and, in cases involving porphyritic magma, crystals and crystal fragments. Some pyroclastic flow deposits, especially those produced by phreatomagmatic eruptions, contain accretionary lapilli. Pyroclastic flows have been produced by a wide range of magma compositions, and many deposits are mixtures of two or more compositions. The most voluminous deposits are dacitic or rhyolitic whereas, in general, small volume deposits are dacitic or andesitic or uncommonly, basaltic.

Types of deposits

In simplest terms, the predominant juvenile pyroclasts in pyroclastic flow deposits reflect the character of the flow and the probable eruptive mechanism (Wright et al., 1980) (Fig- 40).

Block and ash flow deposits comprise poorly to moderately vesicular lapilli and ash (21.1-2). Juvenile lapilli are commonly blocky and angular. Ash pyroclasts consist of angular glass shards and, in cases involving porphyritic magma, crystal fragments. Juvenile lapilli may be thermally oxidised, but welding textures are very uncommon. These deposits are in most cases associated with extrusion of andesitic, dacitic or rhyolitic lava domes or lava flows, especially on composite volcanoes and in caldera environments.

Scoria and ash flow deposits are dominated by scoriaceous lapilli of andesitic or basaltic composition (21.3—4). These deposits are generated mainly by small-volume, explosive eruptions on composite volcanoes. Because relatively mafic magmas are involved, eruption temperatures and, hence also, emplacement temperatures can be high, and pyroclast viscosities are quite low, so welding may occur even in thin (< 10 m) deposits.

Ignimbrite or pumice flow deposits consist predominantly of pumiceous lapilli and blocks, and glass shards (21.5—7). Porphyritic magmas generate porphyritic pumice lapilli and ash that includes crystals and crystal fragments as well as glass shards. Most of these deposits contain at least a few percent accessory lithic pyroclasts and accidental lithic clasts. They show a wide range of welding, devitrification and vapour-phase crystallisation textures, and can be compositionally mixed or zoned. Ignimbrites most commonly involve dacitic and rhyolitic magma compositions. Relatively small-volume deposits are produced by intermittent collapse of plinian eruption

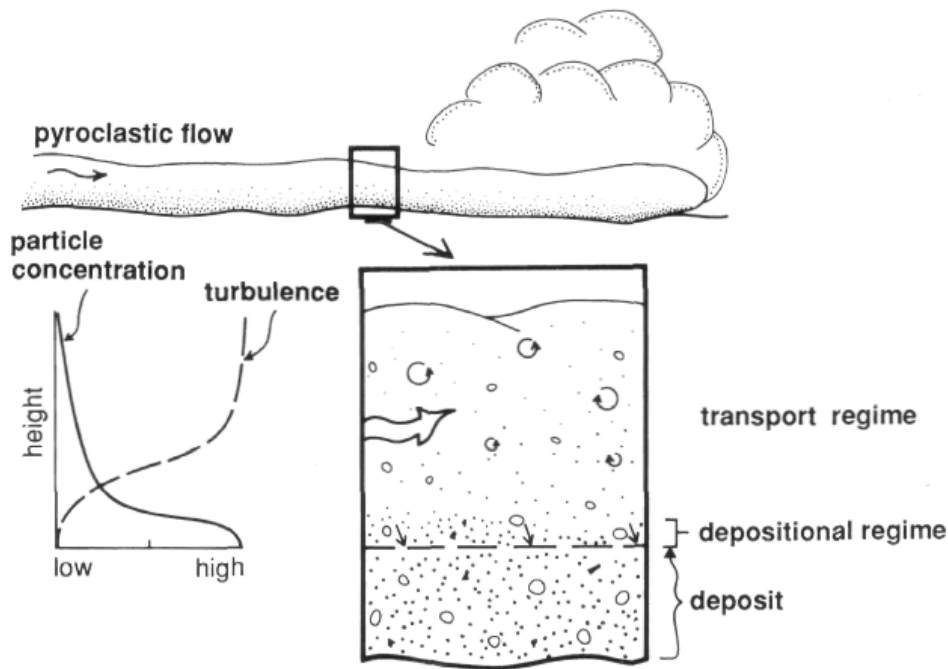


Fig. 39 Progressive aggradation of a pyroclastic deposit at the base of a stratified, steady pyroclastic flow. The graph shows a snapshot of the vertical gradients in particle concentration and turbulence above the aggradation surface. Based on Branney and Kokelaar (1992) and Druitt (1992).

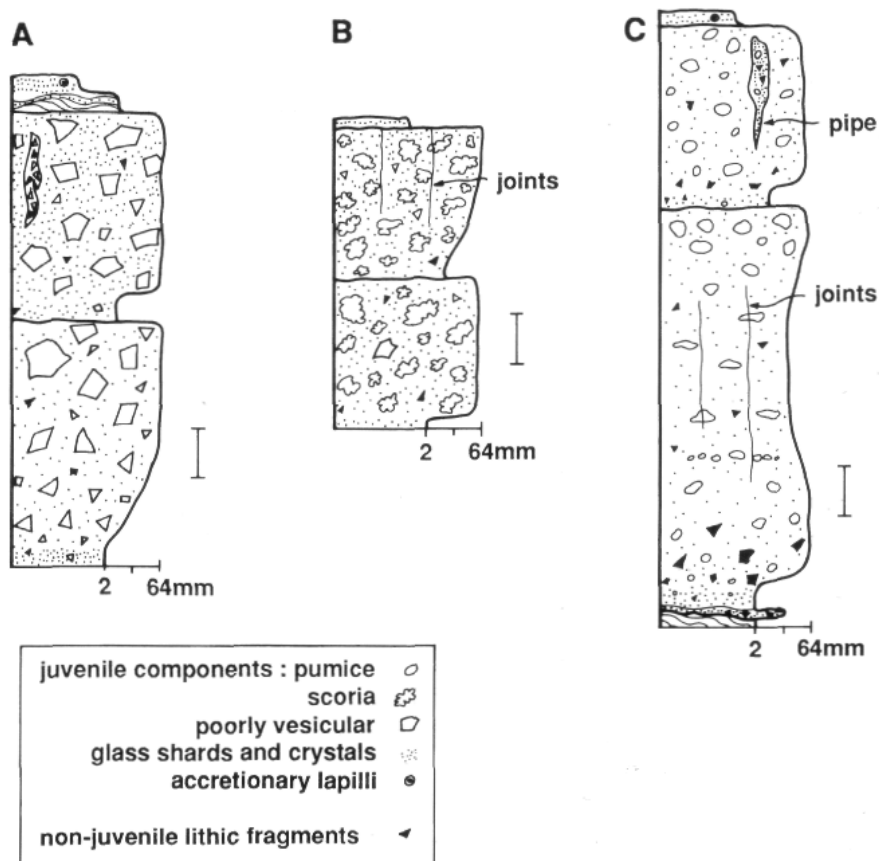


Fig. 40 Schematic graphic logs of three types of primary pyroclastic flow deposits. (A) Block and ash flow deposit, overlain by co-genetic ash cloud surge and fine grained fallout deposits. Based on Fisher and Heiken (1982). (B) Scoria and ash flow deposit. Based on Nairn and Self (1978). (C) Pumiceous pyroclastic flow deposit, or ignimbrite, underlain by co-genetic ground surge deposits and a thin ground layer, and overlain by a co-ignimbrite fine ash fallout deposit. Based on Sparks et al. (1973). The scale bars in (A) and (B) are about 1 m, and in (C) 1 to 10 m.

columns. The most voluminous examples associated with caldera formation possibly involve continuously collapsing, eruptive fountains.

Textures and internal organization of depositional units

Pyroclastic flow deposits are, in most cases, extremely poorly sorted (Sparks et al., 1973; Sparks, 1976). Lapilli and block-size pyroclasts are supported in ash matrix and may be weakly or distinctly graded. The matrix is characterized by pristine vitriclastic texture. Pipe-like and pod-shaped parts of the deposit can be significantly depleted in fine ash, due to locally vigorous gas streaming through the moving flow or through the deposit (22.5-7, 26.6-7). Elutriation of fine ash (dominantly glass shards) from moving pyroclastic flows leads to the characteristic enrichment of crystal components in the matrix relative to the original pre-eruptive phenocryst content of the source magma indicated by pumice or scoria clasts (Walker, 1972). Crystal components in the matrix of pyroclastic flow deposits are typically fragments of euhedra and, in addition to being more abundant, are finer than the euhedral phenocrysts in associated pumice or scoria clasts. Although matrix shards and crystal fragments are typically angular, larger pyroclasts can be sub-angular to rounded, reflecting abrasion during flow (21.4, 22.7).

The internal organization of deposits from pyroclastic flows is strongly controlled by the transport and depositional processes, any changes in the material supplied by the eruption, and the effects of interaction between the flow and topography. In addition, the deposits are hot when deposited. Heat retention may result in textural modification and textural zonation which overprint and, in some cases, completely mask the primary depositional facies. The most important changes are welding, high-temperature devitrification of glassy components and vapour-phase crystallization.

Depositional facies

Figure 41 shows ideal sections through pyroclastic flow depositional units (Sparks et al., 1973; Sheridan 1979). In one case (Fig. 41A), most of the deposit (Layer 2b) is relatively homogeneous and shows smooth normal grading in dense lapilli (usually lithic fragments) and reverse grading in pumice or scoria lapilli (21.5). Some deposits have a well-defined, coarse pumice or scoria clast concentration zone at the top of Layer 2b. The base of Layer 2 (Layer 2a or basal layer) may be conspicuously depleted in coarse clasts, somewhat better sorted than the rest of the deposit and reversely graded. The boundary with the overlying part of the flow unit is transitional or sharply defined. The basal layer develops in response to shearing of the deposit at the boundary between the main flow and the substrate during emplacement. In the other case (Fig. 41B; 21.7), the deposit is distinctly stratified and comprises many subdivisions that are more or less comparable to but much thinner

than the Layer 2a and Layer 2b subdivisions in Figure 41A. The contrasts in textural variations shown in these examples reflect the ends of a spectrum in dynamic processes that operate during flow emplacement.

Both these deposit types can be associated with a fine ash deposit (Layer 3) which, in most cases, comprises fallout from a dilute ash cloud accompanying the pyroclastic flow (*co-ignimbrite ash* — Sparks and Walker, 1977; Walker, 1981b). Although voluminous, this ash is usually very widely dispersed, and only in exceptional circumstances is it deposited and preserved on top of the related pyroclastic flow deposit. Layer 1 comprises deposits resulting from processes operating within or in advance of the front of the flow. It consists of *ground surge deposits* or a lithic-rich *ground layer*, produced by the early sedimentation of the densest particles from the front of the flow (Sparks and Walker, 1973; Walker et al., 1981b; Wilson and Walker, 1982).

Welding, devitrification and vapour-phase crystallization. Conservation of magmatic heat of juvenile pyroclasts is remarkably efficient in pyroclastic flow deposits, and the degree to which they undergo subsequent textural modification is a reflection of emplacement temperature and particle viscosity. The principal processes are welding, devitrification and vapour-phase crystallisation (Ross and Smith, 1961; Smith, 1960a, b; Ragan and Sheridan, 1972; Riehle, 1973). *Welding* is the sintering together and plastic deformation of hot, low viscosity, juvenile pyroclasts (principally pumice or scoria and glass shards) (Smith, 1960a) (23.1-3, 24, 25, 26.3-5, 27). Post-emplacement welding involves plastic deformation of pumice or scoria and shards, so that pore space is eliminated and the original pyroclastic aggregate is transformed to a relatively dense rock (welded ignimbrite or welded ash flow tuff or welded scoria flow deposit). Welding compaction results in an approximately bedding-parallel foliation defined by aligned flattened, lenticular pumice or scoria clasts (*fiamme*) and matrix shards (*eutaxitic* texture) (24, 28.5). The process depends on the viscosity of the pyroclasts and the lithostatic load, so the emplacement temperature, pyroclast composition and the thickness of the deposit are all important (Ragan and Sheridan, 1972; Riehle, 1973). Post-emplacement welding is faster and more complete for thicker deposits, higher emplacement temperatures and for relatively low pyroclast viscosities. Some pyroclastic flow deposits are completely welded, many are completely non-welded and others show internal zonation in the degree of welding (Fig. 42A). The welding zonation depicted in Figure 42A develops in pyroclastic flow deposits that cooled as a single unit, and constitutes a *simple cooling unit* (Smith, 1960b). *Compound cooling units* show more complex welding zonation. They comprise successions of deposits emplaced at significantly varying temperatures or separated by time intervals long enough for significant cooling to occur.

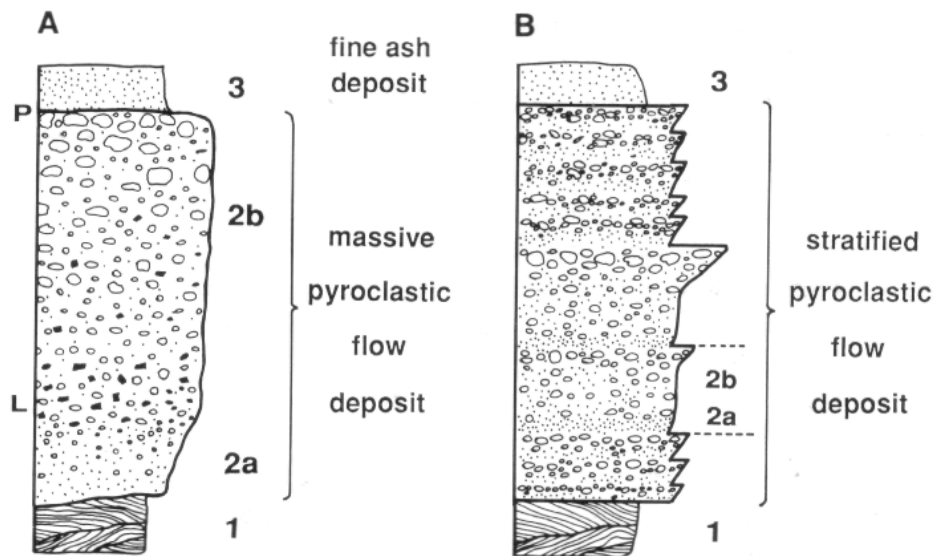


Fig. 41 Ideal sections through non-welded pyroclastic flow deposits. (A) Massive pyroclastic flow deposit. (B) Stratified pyroclastic flow deposit. P: pumice-rich part of Layer 2b; L: lithic-rich part of Layer 2b. Modified from Sparks et al. (1973) and Sheridan (1979).

In pyroclastic flows comprising especially low viscosity particles, welding begins almost the instant particles come in contact during deposition and can occur independently of loading (Mahood, 1984; Branney and Kokelaar, 1992). Even very thin (5 m) deposits of low viscosity pyroclasts can be thoroughly welded. Branney and Kokelaar (1992) use the term *agglutination* to refer to the process of almost immediate welding of pyroclasts on contact, and distinguish this process from post-emplacement welding in response to load compaction. In cases involving very low viscosities, the pyroclasts are fluidal droplets that rapidly recombine or coalesce to form a homogenous liquid. The solidified deposit has matrix textures similar to the groundmass of a coherent lava and almost completely lacks signs of a pyroclastic origin. Agglutination and coalescence are important in the formation of high-grade and extremely high-grade ignimbrites (26.3-5). Coalescence, agglutination and post-emplacement welding are gradational, continuous stages in the degree of welding (Branney and Kokelaar, 1992).

Devitrification. The juvenile pyroclasts in pyroclastic flow deposits are composed of glass or porphyritic glass when first deposited. Slowly cooled, initially glassy components of hot pyroclastic flow deposits, especially welded and partly welded deposits, may *crystallize* or *devitrify* soon after emplacement (Fig. 42B). In silicic deposits, fine-grained alkali feldspar and cristobalite (silica) crystallize from and replace the glass (Ross and Smith, 1961). High-temperature devitrification of some initially glassy, welded ignimbrites results in the formation of spherulites, lithophysae and micropoikilitic texture (23.3-4, 25). The interiors of welded zones in thick ignimbrite sheets are characterized by granophyric crystallization, and comprise a mosaic of fine quartz and feldspar grains in which vitriclastic textures are no longer preserved (Smith, 1960b) (24.3-4, 28.5).

Vapour-phase crystallization involves growth of new, typically very fine-grained minerals in pore space within non-welded pyroclastic flow deposits and partially welded zones of welded deposits, soon after emplacement (Smith, 1960b). Pyroclasts are cemented together, forming a coherent rock that is nevertheless texturally non-welded and non-compacted (23.1-2). Vapour-phase crystallization commonly occurs in vesicles of uncollapsed pumice fragments. The vesicular texture may be partly or entirely destroyed by the growth of new crystals and crystal aggregates (23.5). The gas is derived from the pyroclasts by continued exsolution of small amounts of magmatic gas, from heated ground water rising through the deposit and, possibly, also as a **by-product** of glass devitrification (Smith, 1960b). Textural and mineralogical modifications in pyroclastic flow deposits that are caused by vapour-phase crystallization can be confined to small areas surrounding gas escape pipes, or else be pervasive and affect extensive, bedding-parallel zones.

Grade

Grade is a descriptive term for the amount of welding deformation exhibited by pyroclastic flow deposits (Wright et al., 1980; Walker, 1983) and mainly reflects pyroclast viscosity during and after deposition, emplacement temperature and deposit thickness. Pyroclastic flow deposits display textures and structures indicating a spectrum in grade (Branney and Kokelaar, 1992). Extremely high-grade pyroclastic flow deposits are intensely welded throughout, and parts may be texturally indistinguishable from lava flows (*lava-like ignimbrite* — Ekren et al., 1984; Henry et al., 1988). High-grade or *rheomorphic* pyroclastic flow deposits are predominantly welded and also include intensely welded zones that show structures produced by non-particulate flowage (Schmincke and Swanson, 1967; Chapin and Lowell, 1979; Wolff and Wright,

1981). Moderate-grade pyroclastic flow deposits have welded, partially welded and non-welded zones, and

low-grade pyroclastic flow deposits are entirely non-welded.

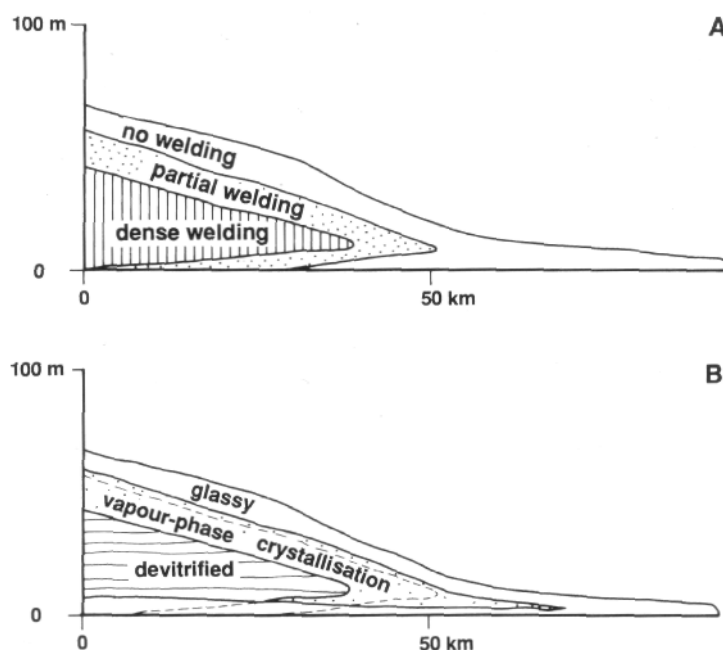


Fig. 42 Ideal lateral and vertical arrangement of welding (A) and crystallization (B) zones in a simple cooling unit of ignimbrite. The fine dashed lines in (B) mark the welding zone boundaries in (A). The devitrified zone includes spherulitic, lithophysal and granophyric crystallization. Modified from Smith (1960b).

Geometry and aspect ratio

In most cases, pyroclastic flow deposits pond in topographic depressions and are much thinner or completely absent from topographic highs (Fig. 43). They have the effect of smoothing out and in-filling topography (22.1-2). Top surfaces of ponded deposits are flat, although there may be levees at the margins and a gentle sag in the centre where compaction has been greatest.

Aspect ratio is a descriptive measure that compares deposit thickness with lateral extent (Walker et al., 1980). Low-aspect ratio pyroclastic flow deposits are very thin and widespread (e.g. 1:70 000 for the Taupo Ignimbrite, New Zealand). High-aspect ratio deposits are thick and have restricted extents (e.g. 1:400 for the Valley of Ten Thousand Smokes pyroclastic flow deposit, Alaska). Aspect ratios of deposits are interpreted to reflect the velocities of the parent pyroclastic flows and the violence or energy release associated with emplacement (Wilson and Walker, 1981; Walker et al., 1981a; Walker, 1983). Deposits with low aspect ratios are thought to form from high-velocity flows, and commonly comprise two mappable facies:

Valley-pond deposits in topographic depressions — relatively thick, internally massive or graded deposits with flat upper surfaces (22.1);

Ignimbrite veneer deposits on topographic highs — relatively thin deposits, depleted in coarse clasts and internally diffusely layered (22.7).

Deposits with high aspect ratios are thought to form

from low-velocity flows and principally comprise valley-pond facies.

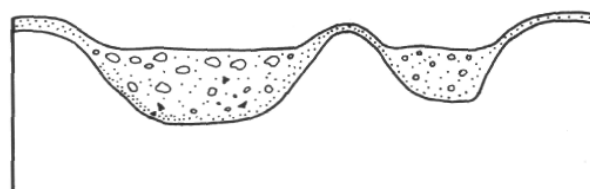


Fig. 43 Geometry of a subaerial pyroclastic flow deposit emplaced on uneven topography. The deposits infill valleys (valley pond deposits) and may also thinly drape topographic highs (ignimbrite veneer deposit, or overbank deposit). Modified from Wright et al. (1980).

Dimensions of pyroclastic flow deposits

Volumes range from less than 1 km³ (e.g. scoria and ash flow deposits from the Ngauruhoe eruption, New Zealand, in 1975 — Nairn and Self, 1978) to 3000 km³ (e.g. Fish Canyon Tuff, Colorado — Steven and Lipman, 1976). Diverse magma compositions are represented by small-volume deposits, although documented basaltic pyroclastic flow deposits are not common (e.g. Freundt and Schmincke, 1990, 1992). Large-volume pumiceous deposits (ignimbrites; >10 km³) are dominated by silicic (dacitic and rhyolitic) magma compositions.

Outflow distances range from as little as a few kilometers for small-volume block and ash flows and scoria and ash flows to several tens of kilometers for pumiceous pyroclastic flows that deposit ignimbrite sheets. The Guataquina Ignimbrite extends for 100

km from its source at Cerro Guacha in the central Andes, South America (Francis and Baker, 1978). Single ignimbrites can cover hundreds to thousands of square kilometers (e.g. 35,000 km² for the Peach Springs Tuff, USA — Glazner et al., 1986; 20 000 km² for the Taupo Ignimbrite, New Zealand — Wilson, 1985). Deposit thicknesses produced by single pyroclastic flows range from very thin (<1 m) to a few tens of metres. Composite thicknesses of deposits from sustained flows or rapid successions of flows range from several meters to hundreds of meters.

Proximal to distal textural variations

The influence of topography on thickness of pyroclastic flow deposits means that thinning does not necessarily correlate with increasing outflow distance. However, in areas of low relief, deposits thin very gradually with distance from source. Pyroclastic flows are capable of transporting large pyroclasts, especially light pumice, to the limits of their extent, and changes in pumice clast dimensions are not strongly controlled by outflow distance. The best indicator is the maximum size of vent-derived, dense accessory lithic pyroclasts, which usually decreases systematically with outflow distance. Accidental lithic clasts eroded from the substrate during flowage do not necessarily vary systematically in grain size with distance from source (Suzuki-Kamata, 1988). Very close to source, lithic pyroclasts may be present in abundance and exceptionally coarse, as a result of rapid, early deposition of the densest components in the flow (*proximal coarse lithic breccia* — Druitt and Sparks, 1982; Walker, 1985).

Compositional zonation

In addition to textural zonation inherent in the various depositional facies and zonation produced by variations in welding, devitrification and vapour-phase crystallization, many pyroclastic flow deposits show variations in the compositions of juvenile pyroclasts (e.g. the Acatlan Ignimbrite, Mexico — Wright and Walker, 1981; the Bishop Tuff, California — Hildreth, 1979; the Bandelier Ignimbrite, New Mexico — Smith and Bailey, 1966; the Valley of Ten Thousand Smokes Ignimbrite, Alaska — Hildreth, 1983; PI Ignimbrite, Gran Canaria — Freundt and Schmincke, 1992; Crater Lake pyroclastic flow deposits, Oregon — Bacon, 1983) (26.2). Compositional zonation primarily reflects heterogeneity in the composition of the magma tapped by the eruption. The variation can be subtle or conspicuous (e.g. rhyolite to basalt in PI on Gran Canaria), and involve continuous gradation or sharp discontinuities. Some examples appear to have involved mixing of discrete magma compositions immediately prior to and during eruption, and others reflect smooth compositional gradients in one source magma.

Significance of pyroclastic flow deposits

Primary pyroclastic flow deposits are especially important in helping to reconstruct the depositional

environments of enclosing sequences. Hot, gas-supported pyroclastic flows, and hence also their primary deposits, are restricted to subaerial and shallow-water settings. Extensive, voluminous, silicic ignimbrites are likely to be associated with calderas. Very thick (more than a few hundred meters), thoroughly welded and devitrified, silicic ignimbrites are commonly found in, but are not restricted to, intracaldera settings. The juvenile components of pyroclastic flow deposits provide direct information on the eruptive style and setting of source volcanoes.

The challenge is establishing a primary origin. Many deposits retain clear evidence of hot, gas-supported emplacement (welding; granophyric crystallization, spherulitic devitrification or lithophysae overprinting vitriclastic textures; perlitic fractures; gas-escape structures; columnar jointing; thermally oxidized pyroclasts; vapour-phase crystals; siliceous nodules; baking of underlying deposits) (25, 26). However, non-welded pyroclastic flow deposits can be very similar in texture and internal organization to deposits from water-supported pumiceous volcanoclastic mass flows that occur in a wide range of settings from subaerial to deep subaqueous. In ancient sequences, it may be impossible to decide whether a pyroclast-rich, texturally non-welded, mass-flow-emplaced unit was a primary pyroclastic flow deposit or a resedimented pyroclast-rich deposit. Such deposits are useful for provenance studies but, in the absence of firm evidence for primary emplacement, cannot be used to constrain the depositional environment.

Subaqueously emplaced pyroclast-rich mass-flow deposits

Pyroclast-rich mass-flow deposits that are texturally and compositionally similar to subaerial pyroclastic flow deposits (Fig. 37) occur interbedded with marine and lacustrine sedimentary rocks in many ancient volcanic sequences. Although clearly generated by explosive eruptions from either subaerial or subaqueous vents, only in special circumstances are these subaqueous deposits likely to be strictly primary. It is important to adhere to the definition of primary pyroclastic flows as being hot and gas-supported, in order to distinguish them from a variety of water-supported mass flows of pyroclastic material that may or may not be directly generated by explosive eruptions. Discrimination of deposits from flows of each type is an outstanding and challenging problem for geologists working in submarine volcanic-sedimentary sequences. Evaluating the status of any particular pyroclast-rich deposit requires careful consideration of: (1) the character and abundance of juvenile pyroclasts present; (2) independent evidence for the depositional environment; (3) evidence that the deposit was emplaced hot.

Transgression of shorelines by pyroclastic flows

A close genetic relationship between subaqueous,

pyroclast-rich mass-flow deposits and subaerially erupted pyroclastic flows is suggested by good evidence indicating that the latter frequently reach coastlines:

1. Pyroclastic flows are valley-confined and will follow drainage ultimately directed to the sea.
2. Pyroclastic flows have runout distances from a few to tens of kilometers.
3. Pyroclastic flow deposits form coastal cliffs around many modern active island volcanoes (e.g. around Krakatau, Indonesia), and seaward of hinterland volcanoes.
4. Pyroclastic flows generated in historic eruptions have reached the coast (e.g. Krakatau, 1883 — Self and Rampino, 1981; Sigurdsson et al., 1991; Mt Pelee, 1902 and 1929-1932 — Fiske, 1963; Perret, 1937).

The subsequent history of a pyroclastic flow delivered to the coast depends on:

- (1) the density of the pyroclastic flow relative to the density of water;
- (2) the temperature, velocity and volume of the pyroclastic flow; and
- (3) the gradient at the shore and offshore, and water depth.

Several conceivable outcomes were reviewed by Cas and Wright (1991). Although theoretically plausible, it is not known at present whether pyroclastic flows actually enter standing bodies of water, become submerged and continue to flow as primary, hot, gas-supported particulate flows. Sparks et al. (1980a, b) considered the case of poorly inflated, block and ash flows composed of relatively dense, juvenile pyroclasts flooding steeply-sloping shorelines. Such flows could continue underwater, maintaining gas support of pyroclasts by conversion of absorbed water to steam with only minor heat loss from the flow interior. Some of the initial flow would be dispersed by turbidity currents generated from dilute portions that mix turbulently with water (Sparks et al., 1980b). Miocene block and ash flow deposits interbedded with lacustrine sedimentary rocks in the Donzurubo Formation, Japan (Yamazaki et al., 1973) may have been emplaced in this manner. The natural remanent magnetization in these deposits indicates emplacement at about 500°C. The evidence for hot emplacement is critical; without it, flowage as water-supported, cold mass flows would be an equally valid interpretation. Under other circumstances, block and ash flows delivered to shorelines may, instead, interact with the water immediately and undergo transformation to water-supported mass flows, or else cease to flow, building a fan or delta of deposits prograding into the water.

Pyroclastic flows (and surges) that are less dense than sea water will continue to flow across the sea surface. That this actually happens is indicated by the occurrence of pyroclastic flow deposits on land masses separated from source vents by expanses of water (e.g. Koya pyroclastic flow deposits, Japan — Ui et al., 1983). Pyroclastic flow deposits generated by the 1883 eruption of Krakatau, Indonesia, are present on Sumatra, about 40 km to the

north. Deposits from this eruption also accumulated offshore from the source, forming a submarine pyroclastic apron. Sigurdsson et al. (1991) suggested that the initial, subaerial pyroclastic flows segregated into a denser basal part that entered the sea, and a more dilute upper part that traveled across the sea. The character of the submarine deposit that results when such flows come to rest on water and are eventually waterlogged, is completely unknown.

Welded ignimbrite interbedded with submarine sedimentary sequences (27, 28)

Ordovician welded ignimbrite sheets in the Capel Curig Volcanic Formation (Garth Tuff, Racks Tuff, **Lledr** Valley Tuff — Francis and Howells, 1973; Howells et al., 1979; Howells et al., 1985; Howells et al., 1991) and the lower tuff of the Pitts Head Tuff Formation (Wright and Coward, 1977; Reedman et al., 1987; Orton et al., 1990) (28.4-5) are greater than 10-80 m thick and interbedded with shallow marine sedimentary rocks. They exemplify delivery of pyroclastic flow deposits to a shallow shore and apparently simple migration of the shoreline seaward (or intracaldera lakeward), without any significant interaction between the flows and the water. In this circumstance, sufficiently hot and thick deposits will weld, just as they would on a dry substrate. The main requirements are (1) low offshore gradients and (2) water depths shallower than the thickness of the pyroclastic flow deposits. Single sedimentation units in large-volume, pumiceous pyroclastic flow deposits (ignimbrites) are typically several to a few tens of meters thick, and many deposits comprise numerous rapidly emplaced units, so at least the second condition is commonly met.

Many modern silicic calderas are partly inundated by the sea (e.g. Rabaul, Papua New Guinea; Aira, Japan; Santorini, Greece) or by lakes (e.g. Taupo, Rotorua, New Zealand; Toba, Indonesia). Marine or freshwater sediments are currently accumulating within them. All are active or else adjacent to active calderas that are potential sources of large ignimbrites. Subaerial intracaldera ignimbrites are typically very thick and show little sign of interruption during their emplacement. Thus, it is conceivable that partly or wholly submerged calderas could be filled by locally erupted pyroclastic flow deposits which, if emplaced rapidly, would bypass significant interaction with water. The intracaldera fill would be underlain and overlain by subaqueously deposited sedimentary rocks. A similar sequence would be expected for shallowly submerged calderas in which collapse is synchronous with pyroclastic eruptions and thick ignimbrite is ponded within the depression. The intracaldera facies of the Ordovician Lower Rhyolitic Tuff Formation in northern Wales is so interpreted (Howells et al., 1986, 1991) (28.1—3), as are four thick Mesozoic ignimbrites interbedded with marine sedimentary rocks at Mineral King, California (Busby-Spera, 1984, 1986; Kokelaar

and Busby, 1992). The Lower Rhyolitic Tuff Formation is thought to have been erupted from a shallow subaqueous vent and emplaced completely under water. The very thick (>500 m) intracaldera facies and the much thinner (<100 m) outflow facies are locally welded.

Non-welded, pyroclast-rich, submarine mass-flow deposits

Especially problematic are relatively thin (< 100 m), regionally widespread, pumiceous, volcaniclastic mass-flow deposits that are interbedded with marine sedimentary rocks but lack evidence of hot emplacement (e.g. the Dali Ash, Greece — Wright and Mutti, 1981; many volcaniclastic units in the Mount Read Volcanics) (Fig. 44). Possible interpretations are:

- (1) primary pyroclastic flow deposits, that is, non-welded deposits from genuine, subaqueous, hot, gas-supported, pyroclastic flows, equivalent to and laterally continuous with subaerial pyroclastic flow deposits; only where primary (hot, gas-supported) transport and continuity with subaerial pyroclastic deposits have been established can other interpretations be discounted;
- (2) subaqueously-erupted volcaniclastic deposits, that is, water-supported, volcaniclastic mass-flow deposits generated by subaqueous explosive eruptions and emplaced subaqueously;
- (3) syn-eruptive resedimented deposits, that is, coarse volcaniclastic turbidites, direct correlates of contemporaneous subaerial ignimbrites; interaction (possibly explosive) with water at or near the shoreline transformed the hot, gas-supported pyroclastic flows into water-supported volcaniclastic mass flows;
- (4) post-eruptive resedimented deposits, that is, coarse volcaniclastic turbidites generated by catastrophic slumps or slides of coastal, non-welded pyroclastic deposits, not necessarily coeval with a subaerial eruption.

Volcaniclastic mass-flow deposits thought to have been generated by subaqueous explosive eruptions (interpretation 2) are dominantly composed of pumiceous and poorly vesicular juvenile clasts, shards and crystals. Such an origin has been proposed for the Miocene Wadaira Tuff, Japan (Fiske and Matsuda, 1964) (Fig. 45). Vertical sections are characterized by a lower, very thick, massive to graded unit, overlain by a thinner unit comprising several graded beds. The lower unit is coarser grained than the upper unit, so overall the sequence is "doubly graded" (Fiske and Matsuda, 1964). It could be argued that such deposits are primary volcaniclastic deposits, fragmentation, transport and deposition being dominantly the direct results of a volcanic eruption. However, if the continuous phase during transport is water (and not gas), they are not strictly pyroclastic flow deposits as defined above. Lithofacies and textures of these deposits are similar to those found in volcaniclastic megaturbidites (Fig. 37), and the interpretation of a subaqueous eruptive source is difficult to prove. Yamada (1984) proposed a model for the proximal to distal facies variations in such subaqueous, pyroclast-rich mass-flow deposits. The principal features are distal thinning and loss of coarse dense clasts, combined with better development of bedding and grading.

It has yet to be demonstrated that subaqueous pyroclast-rich deposits generated by transformation of primary subaerial pyroclastic flows into volcaniclastic mass flows (interpretation 3), or as a result of resedimentation of subaerial non-welded pyroclastic deposits (interpretation 4), are uniquely distinguishable. Neither is it clear whether such deposits differ in any significant way from those inferred to originate directly from explosive eruptions at subaqueous vents (interpretation 2).

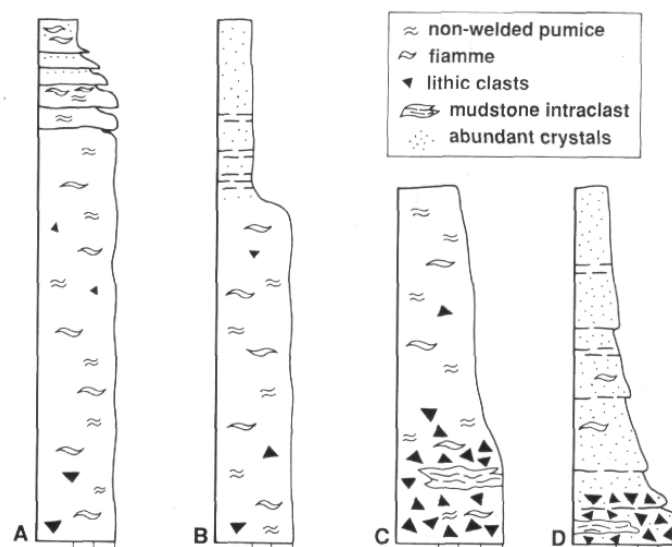


Fig. 44 Schematic graphic logs showing the internal organization of submarine, rhyolitic, pumiceous mass-flow deposits in the Mount Read Volcanics at Rosebery, western Tasmania. (A), (B) Very thick, massive-graded pumice breccia units; thicknesses range from 10 m to more than 150 m. (C) Pumice breccia with lithic fragment-rich base; thickness range is 20-70 m. (D) Volcanic lithic breccia-crystal-rich sandstone; thickness range is 2-75 m. (R. L. Allen, unpubl. data.)

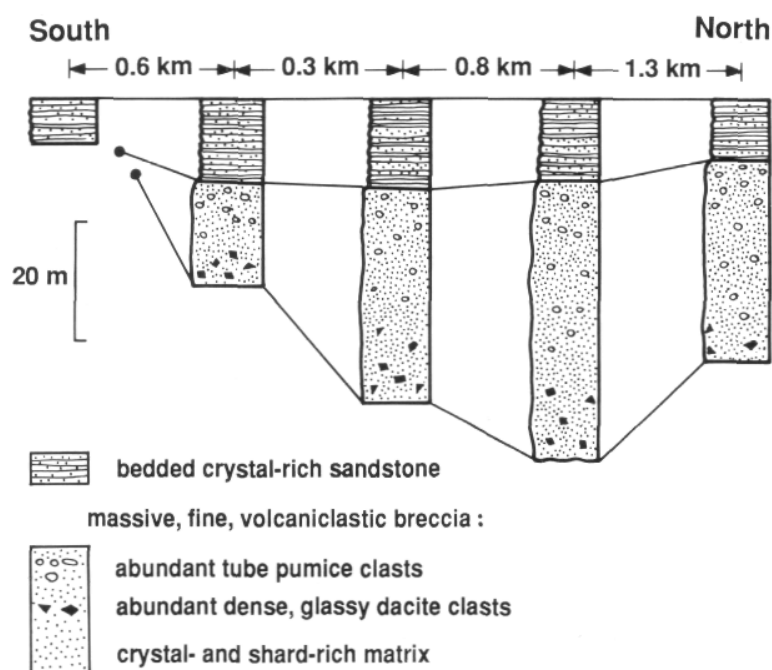


Fig. 45 Correlated sections through a Miocene, submarine volcanoclastic mass-flow deposit (Wadaira Tuff D, Honshu, Japan). The deposit is dominated by juvenile magmatic components (glassy, pumiceous and dense dacite clasts, crystals, shards) and organized into distinctive doubly graded units. It is interpreted to be syn-eruptive and generated by a submarine explosive eruption. Modified from Fiske and Matsuda (1964).

Significance

The pyroclast-rich mass-flow deposits that are common in ancient, below-wave-base, mixed volcanic-sedimentary sequences are, in most cases, volcanoclastic turbidites or debris-flow deposits. They include syn-eruptive deposits resedimented from subaerial sources, syn-eruptive deposits from shallow subaqueous explosive eruptions and post-eruptive resedimented deposits. They give information on the composition, eruption style and setting of the source volcanic terrane, and help discriminate active from inactive terranes. Although primary pyroclastic flow deposits are most common in subaerial settings, there are some well-documented ancient examples of primary deposits in shallow submarine settings (Francis and Howells, 1973; Kano, 1990) and inundated intracaldera environments (Busby-Spera, 1984, 1986; Kokelaar and Busby, 1992). Explosive eruptions capable of generating primary pyroclastic flows are restricted to vents in subaerial and relatively shallow subaqueous settings (theoretically <1000 m, McBirney, 1963). Deep subaqueous emplacement of primary pyroclastic flow deposits, whether sourced subaerially or subaqueously, has yet to be demonstrated.

Water-supported and gravity-driven volcanoclastic mass flows and their deposits

Mass flows in which particle support depends on interstitial water (or muddy water) are classified according to the dominant particle support mechanism, the flow rheology (Fig. 46), and whether laminar or turbulent (Lowe, 1979, 1982) (Fig. 47). The types of water-supported mass flows that are most important in volcanic terranes are: turbidity currents, cohesive

debris flows and density-modified grain flows. Mass flowage involving grain flows, slides, and debris avalanches is due largely to gravity acting on unstable deposits and is especially common in volcanic environments. Although none of these flow processes is strictly primary, they may be syn-eruptive and leave deposits that provide a clear record of an eruption. They are the principal means by which clasts formed in subaerial or shallow marine settings are deposited or redeposited into deep marine settings (Fig. 48).

Turbidites (29-33)

Turbidity currents are flows of cohesionless particles, in which suspended particles are supported largely by an upward component of interstitial fluid turbulence. Particles that are too dense to be suspended are instead transported by traction (as bedload and by saltation) at the base of the flow. The sediment suspension is denser than the enclosing fluid, and flowage is driven by gravity. Deposits from turbidity currents are termed *turbidites* (29). Particle concentration and grain size strongly influence the behavior of turbidity currents and the character of their deposits, and are the basis for recognition of two end-member types, high-density and low-density turbidity currents (Lowe, 1979, 1982).

Low-density turbidity currents

These are relatively dilute flows dominated by clay to medium sand-size grains that are supported by fluid turbulence (Lowe, 1982). Documented low-density turbidity currents are relatively slow moving (10-50 cm/s), and flow thicknesses range from a few metres to more than 800 m (Stow 1986).

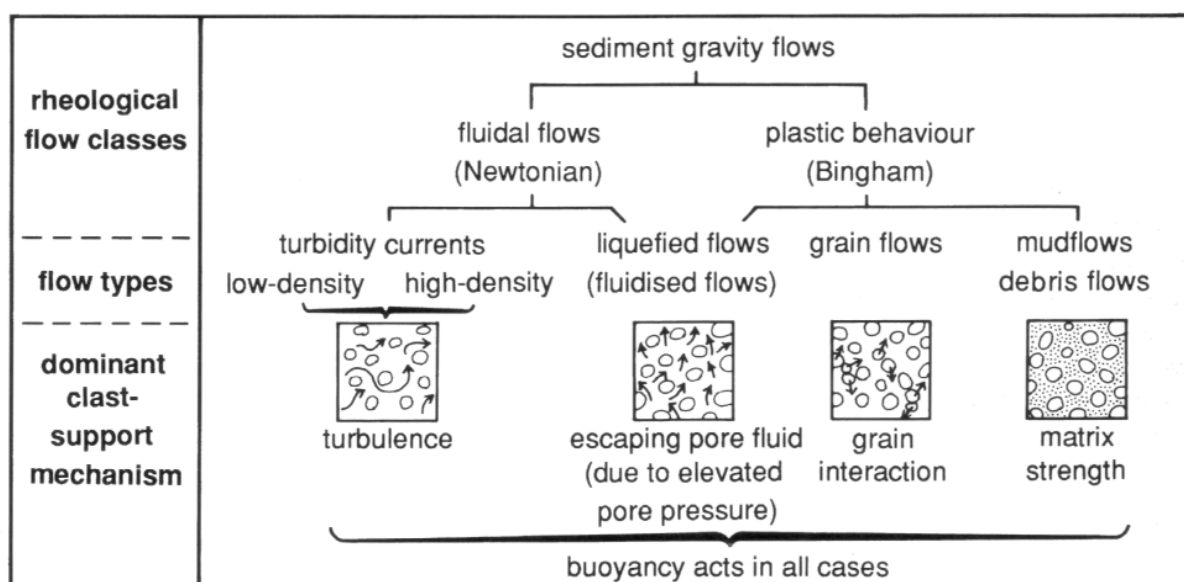


Fig. 46 Particle-support mechanisms and different end-member types of sediment gravity flows (granular mass flows) in which the interstitial fluid is water. Modified from Collinson and Thompson (1989).

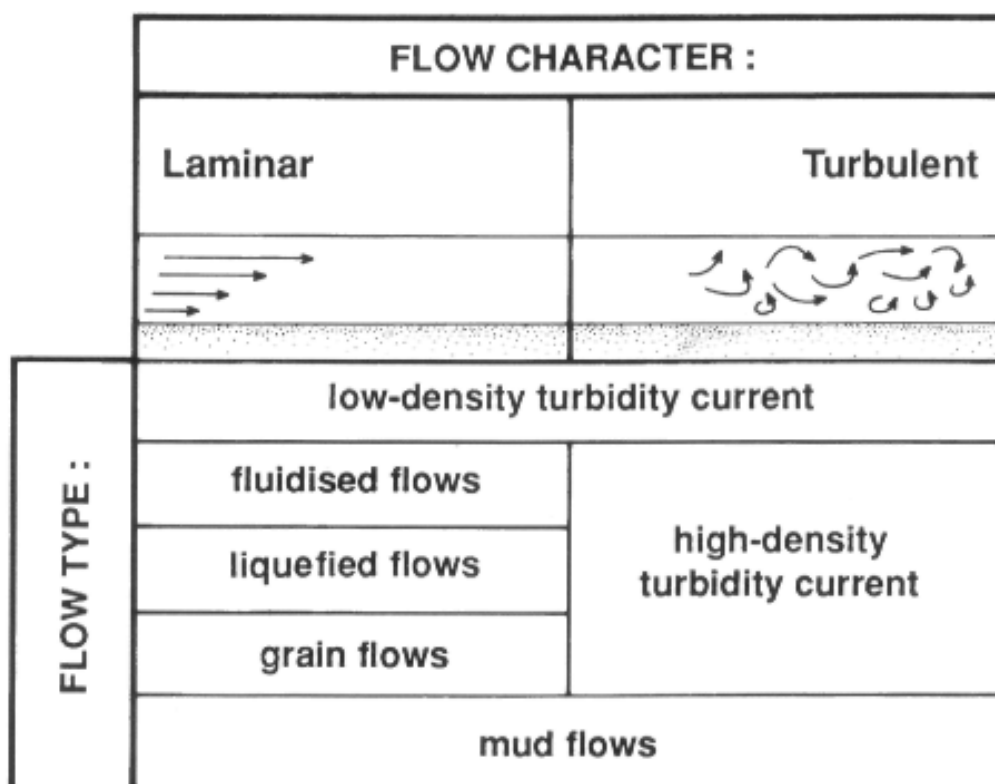


Fig. 47 Laminar versus turbulent mass-flow types (sediment gravity flows). Modified from Lowe (1979).

Deposition begins as the flows decelerate. Coarse and dense particles initially settle rapidly from suspension, forming a relatively massive to weakly graded layer, and subsequent deposition of finer particles involves both traction and suspension that generate cross-bedded and laminated layers (Fig. 49A; 29.1-2). Complete sedimentation units thus typically show a vertical sequence that reflects gradually changing depositional processes during progressive aggradation in response to flow deceleration (Bouma sequences — Bouma, 1962).

Single sedimentation units have thicknesses ranging from several centimeters to several tens of centimeters. Successive turbidity currents may be rapidly generated and deposit a stack of sedimentation units which lack the fine, suspension-settled mud layer (amalgamated turbidites). This is a common situation in near-source settings. In distal settings, sedimentation units lack the lower, massive, coarse-grained layer of the ideal sequence, and are dominated by the finer upper divisions.

Low-density turbidity currents may be generated independently, for example, by rivers discharging into the sea, or develop from subaqueous debris flows and high-density turbidity currents. They are a very important means by which sediment is transported or resedimented from shallow to deep-water settings.

High-density turbidity currents

High-density turbidity currents have greater concentrations of particles, and can transport coarser particle sizes than low-density turbidity currents. High-density turbidity currents have widths and lengths estimated to be up to tens of kilometers, and thicknesses of hundreds of meters. Recorded examples traveled at tens of kilometers per hour (e.g. 70 km/hr maximum velocity for the turbidity current generated by the Grand Banks earthquake in 1929 — Stow, 1986). Runout distances depend on sediment supply and probably reach several hundred kilometers from source.

Grain support and depositional processes in high-density turbidity currents are more complex than in low-density turbidity currents, and depend strongly on grain size and concentration (Lowe, 1982). *Sandy high-density turbidity currents* are dominated by sand-size

particles with minor granules or pebbles. Particles are supported mainly by turbulence and hindered settling. *Gravelly high-density currents* carry up to 15% pebble and cobble-size particles, together with clay to coarse sand, supported by a combination of dispersive pressure and matrix buoyant lift.

Deposition from sandy high-density turbidity currents occurs progressively from the base up, in stages that reflect increasing flow unsteadiness and decreasing flow competence (Fig. 49B; 29.3). Traction structures are generated by interaction between deposited sediment and the current. An ideal sequence comprises: a lower division of coarse sand to gravel with plane lamination and cross stratification generated by traction sedimentation (S_1); an intermediate division of reverse graded (sand to granule), horizontal, thin beds, representing traction-carpet deposits (S_2); and an upper division of grain-supported, massive or normally graded sand, commonly with water-escape structures, deposited directly and rapidly from dense suspensions (S_3) (Lowe, 1982). The residual turbulent suspension of fine sediment may be deposited above the S_{1-3} sequence as a low-density turbidite or else progress downslope, bypassing the sandy units.





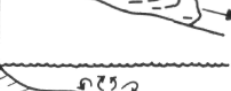


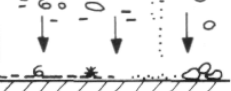
PROCESSES:	CHARACTERISTICS:	DEPOSITS:
resedimentation		
rockfall		talus deposit
slide/slump		debris avalanche deposit
debris flow		debris flow deposit
grain flow		{ grain flow fluidised flow liquefied flow } deposit
fluidised flow		
liquefied flow		
turbidity current (high/low density)		turbidite
normal bottom currents		
internal tides		normal current deposit
waves		
canyon currents		
bottom (contour currents)		contourite
surface currents and pelagic settling		
flocculation		pelagite, hemipelagite, water-settled fall deposit
pelletisation		
flotation		

Fig. 48—Summary of the principal transport and depositional processes and deposits in deep subaqueous settings. Modified from Stow (1986).

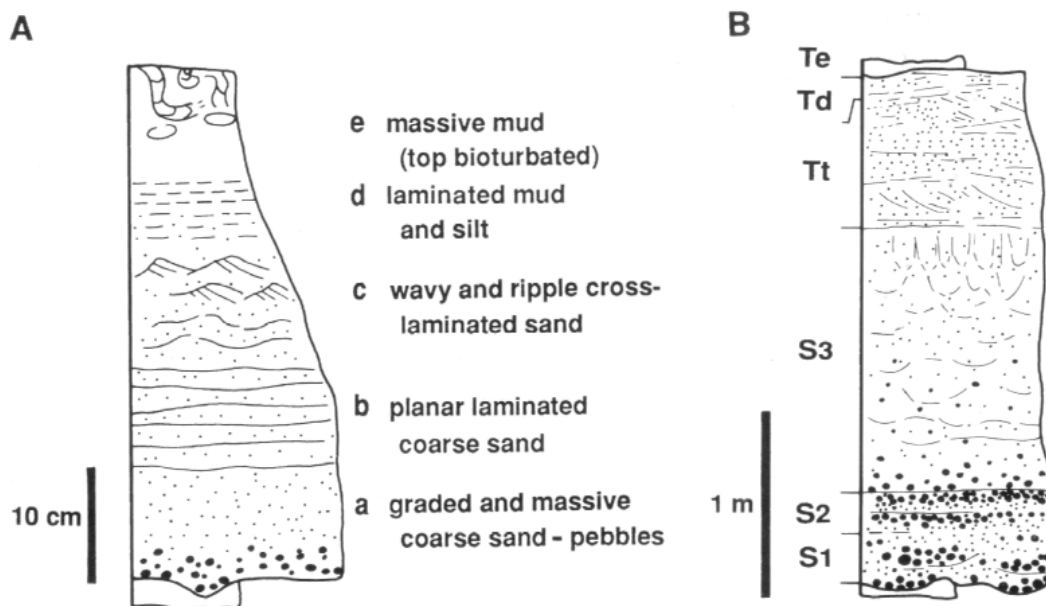


Fig. 49 Turbidity current deposits (turbidites). (A) Low-density (classical) turbidite, showing the Bouma divisions (a to e). (B) Sandy, high-density turbidite, showing deposits from the high density stage (divisions S_{1-3}) and from the residual low density stage (divisions $T_{e,d,t}$). Modified from Lowe (1982) and Stow (1986).

Coarse particles in gravelly high-density turbidity currents are probably transported in a basal, highly concentrated traction carpet and in suspension at the base of the flow. When flow velocity declines sufficiently, the traction carpet freezes and suspended clasts are sedimented very rapidly. Deposits thus have a basal, reversely graded traction carpet layer (R_2), succeeded by a normally graded suspension sedimentation layer (R_3) (Fig. 37). This process leaves a residual sandy high-density turbidity current that may rework the underlying gravel or else continue downslope and deposit independently.

Volcaniclastic turbidites

Volcaniclastic turbidity currents are responsible for resedimentation of a wide variety of unconsolidated, primary volcaniclastic and volcanogenic sedimentary deposits that are initially temporarily deposited in shallow subaqueous shelf and delta settings. In this case, they are generated by slumping of unconsolidated deposits, triggered by earthquakes, rapid loading or rapid changes in pore fluid pressure. They are also fed directly, from subaerial settings by syn-eruptive transformation of pyroclastic flows, volcanic debris avalanches, volcaniclastic debris flows and lahars that transgress shorelines, and from explosive eruptions at submerged vents. In some cases, such syn-eruptive deposits are overlain by thinner bedded volcaniclastic turbidite sequences characterized by upward thinning and fining bed thickness/grain size profiles (Bull and Cas, 1991). These subaqueous sequences develop in response to the inundation of a subaerial fluvial or deltaic system during a pyroclastic eruption. They record the gradual post-eruptive readjustment of the sedimentary transport and depositional processes by means of mass-flow resedimentation.

Deposits from volcaniclastic turbidity currents show many of the textural and structural features of their non-volcanic equivalents (29, 30, 31, 32). The principal differences arise in cases involving pumice-rich flows. The low density of pumiceous particles means that coarse pumice particles are deposited together with markedly finer, non-vesicular particles such as crystal fragments, resulting in much poorer sorting in deposits. Furthermore, pyroclastic eruptions effectively supply enormous volumes of particles instantaneously and have the potential to generate very large-scale, far-traveled turbidity currents. The term *megaturbidite* is sometimes used for deposits from voluminous volcaniclastic turbidity currents (29.4, 30). Volcaniclastic megaturbidite sedimentation units can be of the order of 100 m thick and include abundant, coarse, dense components (Fig. 44).

Significance

Turbidites, in general, are diagnostic of subaqueous, below-wave-base depositional settings, and provide a very valuable constraint on interpretations of ancient volcanic sequences. However, they do not independently discriminate lacustrine from submarine settings and cannot be used alone to give precise water depths. The components in volcaniclastic turbidites give information on the character, composition, and setting of the source volcanic terrane, and whether it was active or inactive (33). Shapes of volcanic clasts in syn-eruptive volcaniclastic turbidites strongly reflect original fragmentation processes. In post-eruptive deposits, clast shape also records the history of reworking and transport during temporary storage in subaerial or shallow-water settings, prior to final deposition below wave base.

Cohesive debris flows, volcanoclastic debris flows and their deposits (34)

Cohesive debris flows involve high-concentration, poorly sorted, sediment-water mixtures. Fine (clay-size) particles totally suspended in the water create a muddy water or watery mud cohesive slurry that has sufficient strength to support very large clasts during flowage (Lowe, 1979, 1982). Buoyancy, hindered settling and dispersive pressure probably also contribute to clast support. However, a proportion of the larger clasts may not be fully supported, and instead may roll or slide along as bedload at the flow base. Cohesive sediment-water mixtures have a yield strength which must be exceeded for flowage to occur. Once that condition is met, cohesive flows behave as viscous fluids, and flowage can be a combination of laminar and plug flow or turbulent. Deposition begins if the applied shear stress decreases below the yield strength, commonly as flows decelerate on encountering gentle slopes. Flows "freeze" en masse, or else in a piecemeal fashion progressively from free surfaces inward and downward. As a result, the deposit is reasonably similar in thickness and internal fabric to that of the parent flow (Smith and Lowe, 1991). The term *mud flow* is used both for clay-rich, cohesive debris flows with low proportions of coarse clasts, and as a synonym for cohesive debris flow.

Volcanoclastic debris flows are dominated by volcanoclastic particles and are generally poorer in clay than non-volcanic cohesive debris flows. As a result, particle support probably depends on both grain collisions and cohesion between silt-size ash particles, and deposition may involve progressive aggradation rather than en masse freezing (Smith and Lowe, 1991). Volcanoclastic debris flows have volumes ranging up to 10^7 m^3 and very long outflow distances (up to 100 km), reflecting the coincidence of abundant particles, steep unstable slopes, frequent triggering mechanisms, and water or snow in volcanic areas.

In general, debris-flow deposits are very poorly sorted, consisting of particles ranging from clay to cobble or boulder size (Fig. 50). Both clast-supported and matrix-supported fabrics occur, and most examples are non-graded, with sharp but rarely erosive lower contacts. Deposits display tabular geometry and range widely in thickness from less than 1 m to greater than 100 m. The lowermost part of some deposits directly above the basal contact comprises a thin layer lacking in coarse clasts. In volcanoclastic debris-flow deposits, clast types reflect the source volcanic edifice and, therefore, can be markedly polymict or else show a dominance of one clast type. Deposits from volcanoclastic debris flows triggered by phreatic explosions lack juvenile magmatic clasts. Juvenile magmatic clasts occur in other syn-eruptive volcanoclastic debris-flow deposits but can be both difficult to recognize and present in only very minor amounts.

Volcanoclastic debris flows are generated in both subaerial and subaqueous environments (34, 35). Volcanoclastic debris flows from subaerial sources that reach the coast can feed subaqueous debris flows or else be transformed into other subaqueous mass-flow types. The characteristic internal textures of volcanoclastic debris-flow deposits are very similar to those of some primary pyroclastic flow deposits, especially non-welded ignimbrite and block and ash flow deposits. In ancient sequences, establishing a primary origin for poorly sorted, ungraded, pyroclast-rich, monomict mass-flow deposits that lack evidence of hot emplacement can thus be very difficult. Even establishing a genuine clastic fabric can be difficult in ancient sequences, especially altered sequences. Hydrothermal alteration of coherent lava and autoclastic breccia can produce apparent matrix-supported, poorly sorted fabrics and apparent polymict clast populations that are typical of debris-flow deposits (Part 5).

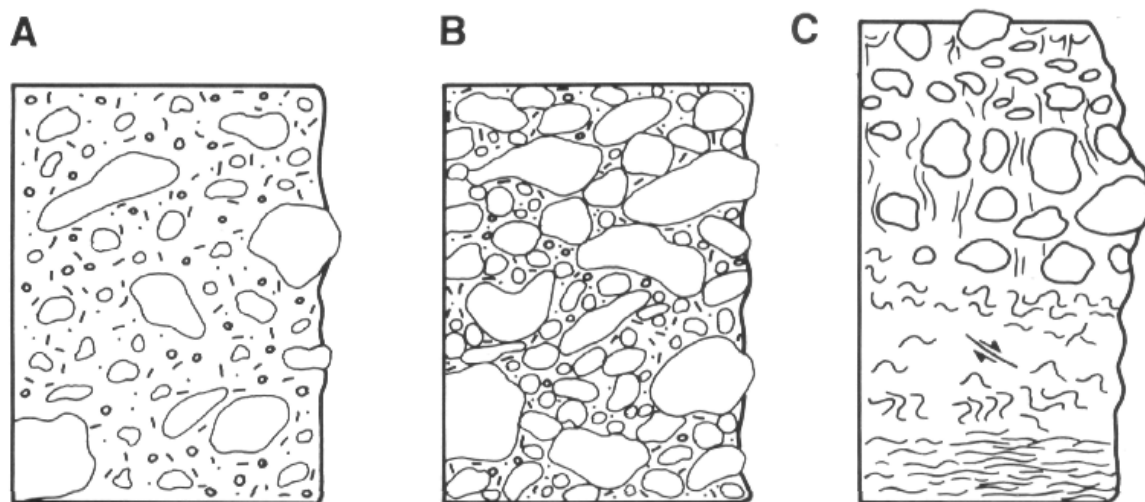


Fig. 50 Cohesive debris-flow deposits: (A) Massive, matrix-supported pebbly mudstone deposited from a debris flow in which the clasts were suspended in and supported by the matrix. (B) Massive, clast-supported muddy conglomerate deposited from a debris flow in which the clasts were not fully supported by or suspended in the matrix. (C) Matrix-supported, clast-rich muddy conglomerate that shows dewatering structures and overlies strongly deformed (middle) and sheared (basal) clast-poor zones. Modified from Lowe (1982) and Stow (1986).

Lahars (35)

Lahars are rapid water-supported flows of volcanoclastic particles generated on volcanoes (Fisher, 1984). In many cases, lahars move partly or entirely as debris flows (Smith and Lowe, 1991), and their deposits show the characteristics of debris-flow deposits outlined above (35.1-7). Other important flowage mechanisms exhibited by lahars are hyper-concentrated flow and dilute streamflow (Pierson and Scott, 1985; Smith, 1986) (35.5-7). Some lahars are generated directly by or are synchronous with volcanic eruptions, and result from, for example, an explosive eruption through a crater lake, or primary pyroclastic flows entering rivers, or interaction between freshly erupted lavas or pyroclastic deposits and snow or ice (Major and Newhall, 1989). These lahars contain hot juvenile magmatic clasts and their deposits can be texturally very similar to primary volcanoclastic deposits. In other cases, the connection with volcanic activity is indirect, and lahars are triggered by the effects of earthquakes or heavy rain on unconsolidated volcanoclastic deposits, or follow on from slope failure events that produce slides and debris avalanches (Siebert et al., 1987).

Volcanoclastic grain-flow deposits (36)

Grain flow affects cohesionless grains on steep slopes. Grains roll and slide downslope under gravity (Lowe, 1976, 1979) and, ideally, transportation is independent of the interstitial fluid (air or water). Particle collisions generate dispersive pressure that contributes to particle support during flowage. Grain flows have a frictional yield strength that must be exceeded in order for flowage to occur; thereafter, their behavior is laminar. Deposition from grain flows involves frictional freezing of the particles and restores the particulate aggregate to a more stable "angle of repose" configuration. Angle of repose for sand-size particles is about 30°-35° for subaerial settings and 18°-28° for subaqueous settings. Angle of repose is achieved by multiple grain flows cascading down steep, unstable slopes. As a result, grain-flow deposits are characterized by thin (centimeters to a few tens of centimeters), commonly lenticular beds with appreciable primary dip. The beds are typically reversely graded and clast-supported (Fig. 51A; 36.1). Foresets of subaerial and subaqueous dunes, fronts of prograding deltas, and talus aprons are common situations where grain flows operate. Volcanoclastic grain flows are important in many subaerial and shallow subaqueous volcanic environments where there is an abundant supply of loose particles and steep slopes. Primary non-welded fallout deposits on steep subaerial slopes, especially pumice or scoria lapilli fall deposits, are especially prone to downslope movement by grain-flow processes.

Lowe (1976, 1982) has interpreted some pebble and cobble conglomerate beds to be deposits from a cohesionless particulate flow type termed a *density-modified grain flow*. These involve sediment mixtures in which larger and denser clasts are buoyant in a silt-sand suspension. As a result, deposits are coarser (cobbles) and in thicker beds (>0.4 m) than normal for true grain-flow deposits. Clast-supported pebbles and cobbles

show reverse grading, reflecting the importance of dispersive pressure, and the matrix comprises poorly sorted sand- to clay-size sediment (Fig. 51B; 34.2-3). Volcanoclastic deposits from flows of this type are probably important, given the common coincidence of abundant coarse clasts and steep slopes in volcanic terranes. Reversely graded, monomict, clast-supported beds of hyaloclastite breccia, associated with subaqueous coherent lava domes and the margins of lava flows, may be resedimented hyaloclastite emplaced by grain-flow processes.

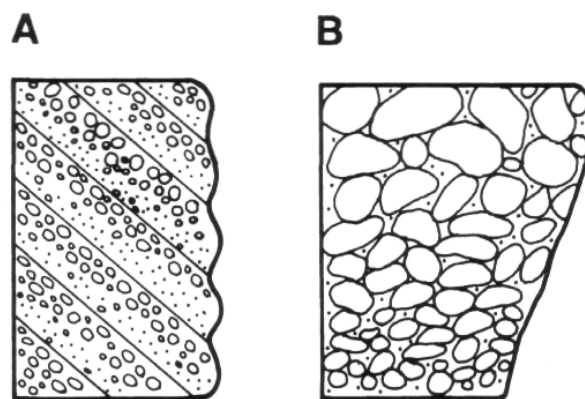


Fig. 51 Grain-flow deposits. (A) Thinly bedded grain-flow deposit with characteristic reverse grading and steep primary dip. (B) Thick, reversely graded, density-modified grain-flow deposit. Modified from Lowe (1982).

Volcanic slides, volcanic debris avalanches and their deposits (36)

Slides and debris avalanches are mass movement processes, primarily driven by gravity and not significantly influenced by or dependent on interstitial fluid. *Slides* involve the downslope, gravity-driven displacement of a coherent rock or sediment mass along a basal shear plane (Stow, 1986). Slides may be small-scale, local events or involve collapse of entire sectors of volcanoes that incorporate large volumes of rock. Slides affect subaerial, island and subaqueous volcanoes, and volcanoclastic deposits in unstable positions on steep offshore shelves and deltas. Sector collapse of Socompa volcano, northern Chile, generated slide blocks up to 2.5 km long and 400 m high, which in total constitute a minimum volume of 2.5 km³ (Francis et al., 1985) (36.4). Avalanche and several slide deposits have been recognized on the submarine flanks of Hawaiian shield volcanoes (Moore, 1964; Lipman et al., 1988).

The deposits of slides consist of relatively coherent masses of the source volcanic edifice, within which there may be evidence of internal deformation such as faults, folds and shearing. A strongly sheared contact typically separates slide blocks from the substrate. In modern settings, the source areas of slides are marked by major arcuate topographic scars (Moore, 1964).

There are very few detailed or convincing descriptions of volcanic slide deposits in ancient volcanic sequences. Intra-caldera, heterolithic megabreccia in some Tertiary subaerial caldera sequences in the western USA

(Lipman, 1976) probably include deposits from true slides. The paucity of examples is a reflection of the difficulty of recognizing these deposits, rather than their abundance. Slide blocks in ancient sequences are likely to be misinterpreted as faulted parts of otherwise in situ and intact volcanic stratigraphy.

Slides are commonly associated with *debris avalanches*, rapid, gravity-driven flows of unsorted mixtures of rock and sediment (Ui, 1983; Siebert, 1984; Siebert et al., 1987). Water or ice may be present within and between debris avalanche blocks but they do not contribute to particle support or transportation. Deposition occurs en masse by frictional freezing. Volcanic debris avalanches commonly evolve from slides initiated by sector collapse and may be synchronous with explosive eruptions, the best known recent example being that of Mount St Helens, Washington, in 1980 (Voight et al., 1981; Siebert, 1984; Siebert et al., 1987). Slope failure and initiation of volcanic debris avalanches also occur on inactive volcanoes (dormant and extinct). Although debris avalanches affect volcanic islands and totally subaqueous volcanoes, the best studied examples of volcanic debris-avalanche deposits are confined to subaerial volcanoes (e.g. Voight et al., 1981; Crandell et al., 1984; Ui and Glicken, 1986; Palmer et al., 1991). Youthful submarine debris-avalanche deposits associated with slides have been mapped on the flanks of Hawaiian volcanoes, using detailed bathymetry and GLORIA side-scan sonar imaging (Lipman et al., 1988). Volcanic debris avalanches are highly mobile and may override significant topographic features. An avalanche from Socompa volcano traveled more than 35 km from source and reached up to 250 m above its lowest point (Francis et al., 1985) (36.4-6). Velocities of 160 km/hr were calculated for a volcanic debris avalanche at Chaos Crags (Crandell et al., 1974), and the Mount St Helens debris avalanche (18 May 1980) had velocities in the range of 180-288 km/hr (Voight et al., 1981). Many avalanche deposits exceed a cubic kilometre in volume. The Socompa debris-avalanche deposit exceeds 15 km³ (Francis et al., 1985), and a 360 ka debris-avalanche deposit at Mount Shasta, California, amounts to at least 26 km³ (Crandell et al., 1984). Sundell (1983) calculated a volume of 292 km³ for a Tertiary debris-avalanche deposit in Wyoming.

Volcanic debris-avalanche deposits are characteristically non-graded and very poorly sorted, with clasts ranging in grain size from centimeters to tens of meters (36.2-3). They show small-scale variation from clast- to matrix-supported fabric, and are unstratified. Although overall the deposits are polymict, the range of compositional variation depends on the heterogeneity of the source, and small exposures can be dominated by only one clast type. In some young examples, it is possible to match material in the deposits with different parts of the volcanic edifice and subvolcanic basement (Francis et al. 1985) (36.5). Syn-eruptive volcanic debris-avalanche deposits may include a small proportion of juvenile magmatic clasts (36.6), although in many cases, these are difficult to distinguish from abundant other volcanic lithic clasts.

Two distinct facies are typically present within volcanic debris-avalanche deposits: *block facies* consists of relatively intact pieces (debris avalanche blocks) of the source volcano, whereas *mixed facies* consists of an unsorted, unstratified, thorough blend of all the rock types present in the source (Glicken, 1991). Debris avalanche blocks can be gigantic and usually measure at least several metres to tens of metres across (36.5-6). Blocks up to 500 m across occur in the Nirasaki avalanche deposit of Yatsugatake volcano, Japan (Ui, 1983). Block size commonly decreases with distance of outflow from the source. Blocks dislodged at the time of failure are fractured as a result of dilation and shattered during transport (Glicken, 1991). Blocks that comprise weaker lithologies disintegrate rapidly and contribute to mixed facies in the deposit, whereas stronger lithologies survive and form the block facies (Fig. 52). Even relatively intact blocks are usually fractured, and adjacent but separate blocks may show jigsaw-fit texture (36.3).

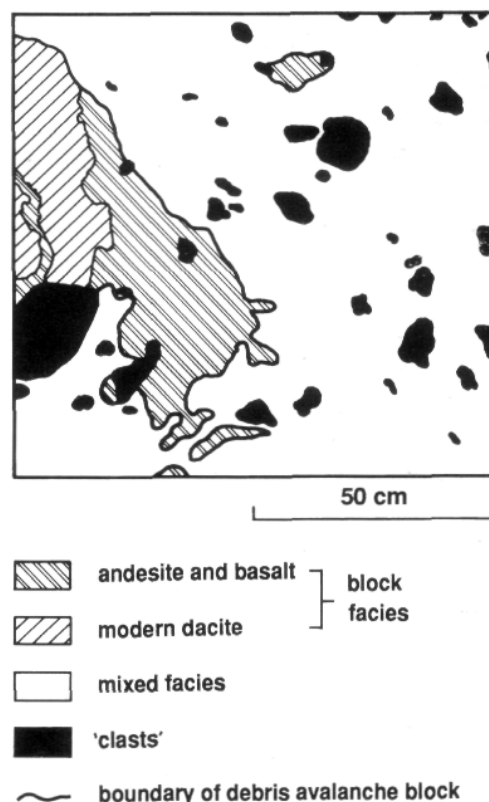


Fig. 52 Detail of the internal texture of the 1980 Mount St Helens volcanic debris-avalanche deposit, showing both debris avalanche block facies and mixed facies. Block facies consists of chunks of the source volcano transported more or less intact in the debris avalanche. Mixed facies is a thorough blend of lithologies and commonly dominated by matrix derived from poorly consolidated material and solid, separate clasts derived from break-up of blocks. Modified from Glicken (1991).

The surface morphology of debris-avalanche deposits is hummocky (36.4, 36.7), with relief ranging from metres to tens of metres, and the deposits are commonly lobate in plan, with steep margins marked by levees, reflecting appreciable yield strength (Siebert,

1984). In any one deposit, some of the hummocks consist of block facies, either a small number of blocks all of one lithology or groups of blocks of different lithologies, and other hummocks consist of only mixed facies or combinations of mixed facies and debris avalanche blocks (Glicken, 1991). Deposit thicknesses range from several metres to more than 100 m. Volcanic debris avalanches that include or incorporate large volumes of water or snow or ice may transform laterally into debris flows, and deposits from the two flow types are commonly closely associated.

Massive sulfide clast-bearing submarine volcanoclastic mass-flow deposits (37)

The importance of studies of the clast populations in mass-flow deposits is clearly demonstrated by cases where clasts derived from massive sulfide deposits are included. These are not uncommon in submarine volcanoclastic mass-flow deposits in host sequences to massive sulfide mineralization, such as the Mount Read Volcanics (37). The clasts could be derived from a massive sulfide deposit present at the source of the mass flow (e.g. Fig. 53) or collected from a massive sulfide deposit exposed somewhere along the flow path. The transport distance depends on the size of the clasts and the character of the host mass flow. High-particle concentration mass flows, such as high-density turbidity currents, cohesive debris flows and density-modified grain flows, can probably transport small clasts (up to a few cm across) for substantial distances (kilometers). Transport distances of large massive sulfide clasts (10 cm or more) are likely to be much less, but cannot be precisely established without data on the dynamic properties of the host mass flow. Some idea of the source direction can be obtained, in favourable circumstances, by systematically mapping the maximum dimensions of clasts (massive sulfide and dense lithic fragments) and the host unit thickness. Other clast types present in the mass-flow deposit, especially any juvenile magmatic clasts, help constrain the setting of the massive sulfide deposit, and may include samples of the associated alteration styles.

The implications for massive sulfide exploration are ambiguous: although the clasts provide clear evidence of the presence of a massive sulfide deposit, it may have been destroyed or dispersed by the mass-flow forming event or since eroded and, in most cases, neither the direction nor the distance to the source of the clasts can be accurately determined.

Traction transport and volcanoclastic traction current deposits

Traction refers to particulate transport of cohesionless grains entrained by fluid currents (water, air or volcanic gas). Particles roll or slide along at the base of the current (bedload transport), skip or bounce along (saltation), and intermittently go into suspension. Traction currents involving wind and water are especially important in formation of volcanogenic sedimentary deposits. Primary pyroclastic surges are

currents of volcanic gas and steam that are produced by explosive eruptions and transport pyroclasts largely by traction.

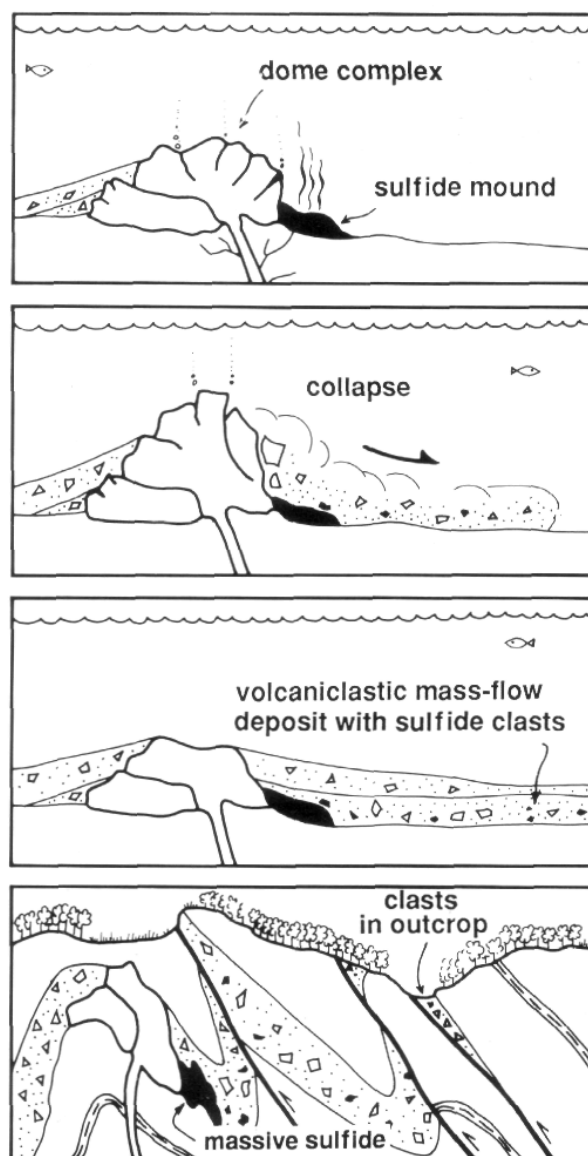


Fig. 53 Cartoon showing one interpretation of the origin of massive sulfide clasts in a submarine volcanoclastic mass-flow deposit in the Mount Read Volcanics, western Tasmania (Newton Dam Spillway). The final frame shows the outcrop where the clasts occur and a highly speculative reconstruction of the present-day subsurface structure, including the source massive sulfide deposit. (J. McPhie, unpubl. data.)

Tractional sedimentary structures (38, 40)

Sustained currents of water generate a series of tractional sedimentary structures in cohesionless particulate aggregates that reflect the mean flow velocity and the mean grain size (Allen, 1985; Collinson and Thompson, 1989) (Fig. 54). Tractional sedimentary structures are also generated by currents of air (wind) and volcanic gas (pyroclastic surges). Experiments with sediments and water currents have shown that increasing flow velocities produce a sequence of bedforms, comprising ripples, sandwaves and dunes. Internally, these bedforms consist of asymmetric cross

stratification with the foresets dipping downstream. An additional increment of current velocity has the effect of "smearing out" the dune bedforms and generates horizontal, planar bedforms, that are internally represented by horizontal, planar laminations. Plane beds constitute a transition from a relatively low-energy, low-flow regime to a higher energy, high-flow regime where antidunes develop. The underlying structure of antidunes is low-angle ($<20^\circ$), upstream-dipping cross stratification.

At peak flow velocities, the sediment load may be too high for true tractional transport to operate. Under such conditions, the system becomes a *hyperconcentrated flow*, in which other particle support processes (dispersive pressure, hindered settling, buoyancy) are important. Deposition from hyperconcentrated flows occurs very rapidly when the flows decelerate, and involves progressive base-upwards aggradation. Sand- and granule-dominated deposits show planar, thin, diffuse stratification, in which separate layers are massive or graded. Hyperconcentrated flows that carry coarser grains (pebble-size) produce normally graded, clast-supported units. Deposits from hyperconcentrated flows are similar

to those generated by subaqueous, high-density turbidity currents (Lowe, 1982; Smith, 1986; Smith and Lowe, 1991).

Hummocky cross stratification is a tractional sedimentary structure characteristic of fine to medium sand deposited in shallow subaqueous or near-shore settings (Walker, 1979; Dott and Bourgeois, 1982; Duke et al., 1991). The structure occurs both within thick sandstone units and within sandstone beds in interbedded sandstone-mudstone sequences. Sets comprise broadly convex-up (hummocks) and concave-up (swales) layers, with dips less than 12° , and are separated by low-angle truncations (Fig. 55). Layers may thicken into swales and thin over hummocks, so the structure tends to die out upward. Hummock-swale wavelengths are 1-5 m, and sets are up to about 25 cm thick. Hummocky cross stratification is thought to develop in response to vigorous and complex wave and current activity during storms and is only preserved in sediment at water depths between fair-weather and storm wave base. The structure is, thus, a very useful water depth indicator.

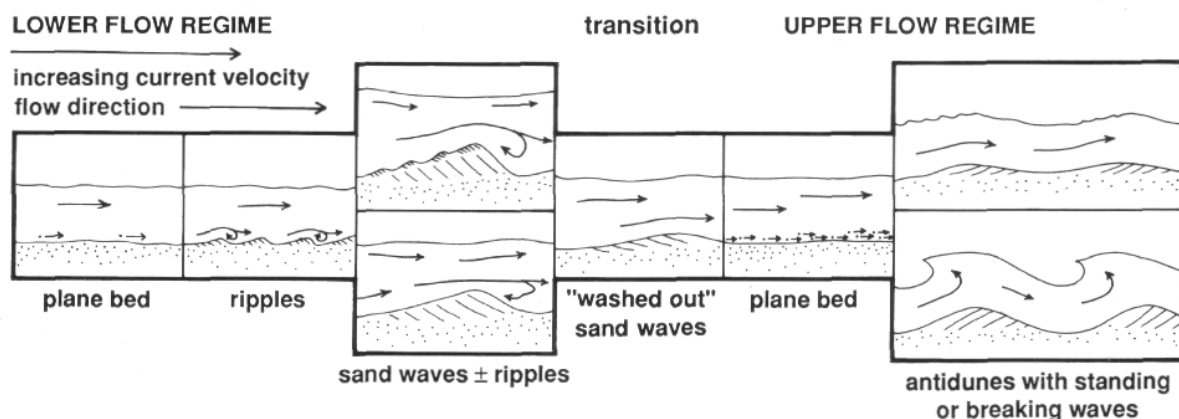


Fig. 54 Tractional sedimentary structures and bedforms formed in cohesionless sediments in response to increasing current velocity. Modified from Friedman and Sanders (1978).

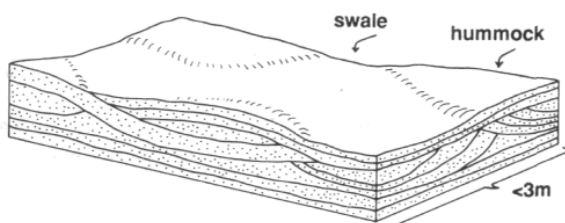


Fig. 55 Main features of hummocky cross stratification. Upward-convex hummocks alternate with upward-concave swales. Low-angle truncations between sets and shallow dips of component layers characterize the internal structure. Modified from Allen (1985).

Characteristics

Traction transport involves repeated collisions of particles until they are finally deposited, and particles,

especially coarse particles, rapidly become rounded. Because particles are carried and deposited independently, aggregates are generally well sorted. Thus, traction current deposits are characterized by the presence of tractional sedimentary structures, particles with appreciable rounding and relatively good sorting (38). However, particles rounded during traction transport may be redeposited by mass-flow processes, and are not restricted to traction current deposits.

Significance

Wind and pyroclastic surges are restricted to subaerial settings, and their deposits are, therefore, very important in constraining ancient depositional environments. Water currents capable of generating fractional sedimentary structures operate in a wide spectrum of settings but are abundant in fluvial, shoreline and above-wave-base subaqueous environments (38.1-4, 40.5-8). Hummocky cross stratification is generally

considered to be a good indicator of relatively shallow-water (above storm-wave-base), storm-affected shelf settings.

Pyroclastic surges and their deposits (38)

Pyroclastic surges are ground-hugging, dilute (low particle:gas ratio), particulate flows in which pyroclasts are carried laterally, entrained in turbulent gas (Fisher, 1979; Walker, 1981c). Pyroclastic surges are generated directly from explosive phreatomagmatic and phreatic eruptions (*base surges*), and in association with the eruption and emplacement of pyroclastic flows (*ash cloud surges* and *ground surges*). The passage of a pyroclastic surge results in deposition of a set of very thin beds or laminae, collectively termed a *bed-set*.

Base surges occur at both inundated vents and vents that are saturated with ground water (Moore, 1967; Fisher and Waters, 1970; Crowe and Fisher, 1973; Waters and Fisher, 1971; Wohletz and Sheridan, 1979). They are most commonly associated with small basaltic volcanic centers, but more silicic magmas are known to have generated base surges (e.g. Schmincke et al., 1973; Sheridan and Updike, 1975). Ground surges are pyroclastic surges that precede emplacement of pyroclastic flows (Sparks et al., 1973). Moving pyroclastic flows are invariably associated with overriding, dilute, turbulent ash clouds that may become detached and flow independently, as ash cloud surges (Fisher, 1979; Fisher and Heiken, 1982; Fisher et al., 1980). Ground surges and ash cloud surges are mainly associated with dacitic or rhyolitic, pumiceous pyroclastic flows and block and ash flows.

Characteristics

Pyroclastic surge deposits drape topographic highs and thicken slightly into topographic depressions (Fig. 56). They are usually stratified and commonly show unidirectional bedforms, such as dunes, cross bedding and chute-and-pool structures (Fig. 57). Most deposits are better sorted than pyroclastic flow deposits but less well sorted than pyroclastic fall deposits. Compared with pyroclastic flow deposits, surge deposits are significantly or strongly fines-depleted, and pyroclasts coarser than lapilli are uncommon (except as near-vent ballistic pyroclasts).

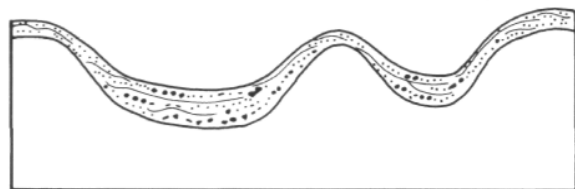


Fig. 56 Geometry of deposits from a pyroclastic surge that has traversed uneven topography. The deposits in lows are slightly thicker and coarser than those that drape highs. Beds are lenticular (cf. beds in fallout deposits). Modified from Wright et al. (1980).

Bedding is especially well developed in base surge deposits (38.5-8). Sandwave bedforms (dunes, cross bedding — Moore, 1967; Fisher and Waters, 1970;

Crowe and Fisher, 1973; Lorenz, 1973; Cole, 1991) occur near vent, and planar bedded deposits dominate at distal sites (Wohletz and Sheridan, 1979). Sets of surge sandwave beds can be separated by laterally continuous, even, thin, fine ash layers that commonly contain accretionary lapilli (*co-surge fallout ash* — Walker, 1984). Near vent, base surge deposits may be disturbed by impact craters from ballistic bombs and blocks, and there is a general decrease in grain size and thickness of deposits with distance from source. Evidence for dampness of pyroclasts during emplacement is common (e.g. accretionary lapilli, vesiculated ash, ash-coated lapilli — Lorenz, 1974; adhesion to steeply inclined surfaces — Moore, 1967). Juvenile pyroclasts may show the hallmarks of interaction with water during fragmentation, and be blocky and poorly vesiculated.

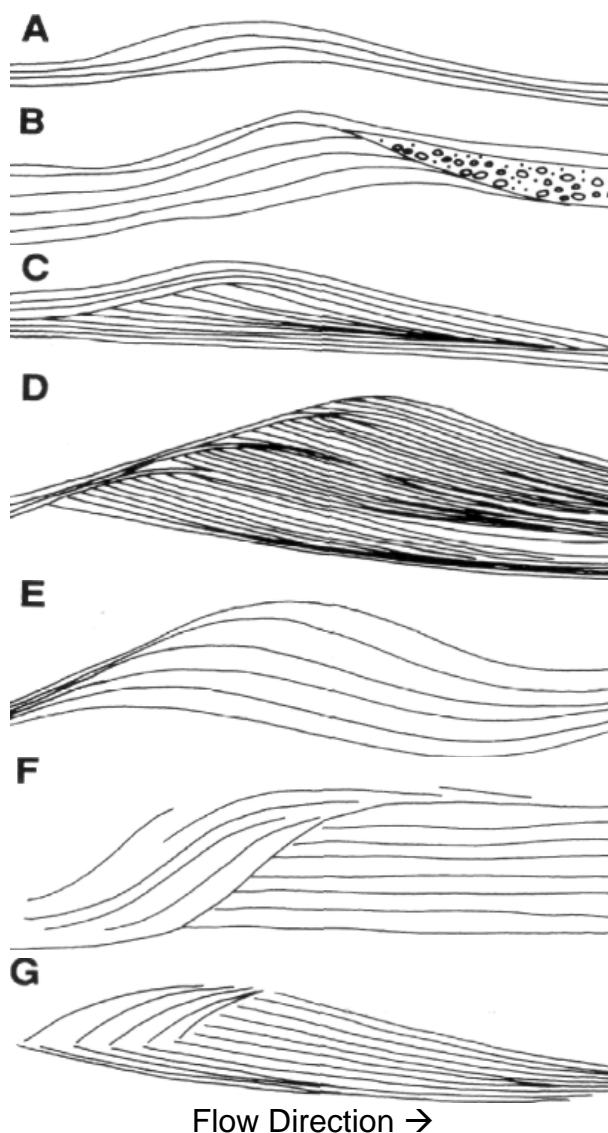


Fig. 57 Types of unidirectional sandwave bedforms and internal structures commonly found in pyroclastic surge deposits. Similar structures are developed by migrating aeolian dunes and in fluvial sediments. Progressive sandwave structures migrate downstream (e.g. D, E). Regressive sandwave structures migrate upstream (e.g. B, F, G). Some sandwave structures may be stationary (that is, show no net migration), progressive or regressive, (e.g. A, C). Modified from Cole (1991) and Wohletz and Sheridan (1979).

Ground surge deposits and ash cloud surge deposits are primarily distinguished by their stratigraphic relationships with associated pyroclastic flow deposits: ground surge deposits underlie the associated flow, whereas ash cloud surge deposits overlie, are interbedded with or occur as lateral facies equivalents of associated pyroclastic flow deposits. In both instances, the components of these deposits are closely similar to those of the associated flow, and both may show evidence for having been emplaced hot. Thickness variations with distance from source are unpredictable, except for vent-derived ground surge deposits that become thinner distally.

Distinguishing among the different genetic types of pyroclastic surge deposits is usually difficult and relies heavily on context. Pyroclastic surge deposits also have features in common with other sorts of primary pyroclastic deposits (especially bedded, fine-grained, fallout deposits), and with reworked volcanogenic sediments (McPhie, 1987; Smith and Katzman, 1991). Reworking of pyroclasts by water or wind may produce planar bedded and cross-bedded pyroclast-rich deposits that superficially resemble primary surge deposits. However, water-reworked cross-bedded pyroclast-rich deposits commonly contain appreciably rounded or abraded clasts and significant amounts of admixed epiclastic (volcanic or non-volcanic) detritus and are lacking in fine ash components. They show no systematic changes related to distance from a volcanic vent, and are also distinguishable by the context. Wind-reworked cross-bedded pyroclast-rich deposits are well-sorted, lack both the finer (ash) and coarser (lapilli) clasts usually present in surge deposits, contain admixtures of non-volcanic particles and show distribution, thickness, and palaeoflow patterns that reflect regional wind directions rather than point sources (such as volcanic vents).

Dimensions of pyroclastic surge deposits

Single, base surge-producing eruptions involve very small volumes of pyroclasts ($<0.01 \text{ km}^3$), most of which are deposited within 3-5 km of the source vent. The maximum thickness (generally $<1 \text{ m}$) of bed-sets occurs closest to source, thinning to a few centimeters distally. A series of base surge eruptions repeated in rapid succession may build up near-vent deposits several tens of metres thick and produce a total erupted volume of about 0.1 km^3 .

Ground surge and ash cloud surge deposits are typically less than 1-2 m thick, and thickness variations can be marked over short distances. Some ash cloud surge deposits thicken away from the source of the parent pyroclastic flow (Fisher, 1979). Areal extents of discrete ground surge or ash cloud surge deposits are very poorly known but, presumably, are at least as great as the extent of the associated pyroclastic flow deposits, and therefore likely to range up to hundreds of square kilometers.

Significance

Primary pyroclastic surge deposits are restricted to

subaerial depositional settings, although they can be generated from shallowly submerged vents and travel across water. Base surge deposits indicate proximity to a volcanic vent. Surge deposits thus provide narrow constraints on depositional settings of ancient volcanic sequences. However, they resemble non-primary volcanoclastic deposits, and it is therefore imperative to establish beyond doubt a primary origin.

Suspension transport and volcanoclastic suspension deposits

Suspension refers to transport of particles fully supported by buoyancy and fluid turbulence within the fluid (water, muddy water, air, volcanic gas). Whether particles are suspended within the flow or moved by traction (as bedload or by saltation) depends on their density relative to the fluid and on the velocity of the flow. Relatively rapid flows of dense fluid are able to carry coarse grains in suspension. Deposition takes place when the flows decelerate and the suspended grains settle through the fluid under the influence of gravity. Very fine particles (fine volcanic ash, clay platelets) settle only when the fluid reaches a standstill.

Explosive volcanic eruptions eject pyroclasts, which fall out from suspension in eruption columns and dilute ash clouds in the atmosphere or from suspension in water. Suspension sedimentation of fine pyroclasts also accompanies and follows the subaerial emplacement of pyroclastic flows (Layer 3 deposits) and pyroclastic surges. Subaqueous volcanoclastic mass flows are associated with dilute suspensions of fine particles that eventually settle from the water column.

Suspension sedimentation is an important depositional process in below-wave-base subaqueous settings, especially quiet, deep-water settings that occur in deep lakes and ocean basins (Fig. 48). The deposits are characteristically fine grained (mud; $<0.0625 \text{ mm}$) and may be massive or planar laminated. In these settings, suspension sediments are closely associated with subaqueous mass-flow deposits.

Differences in textures and lithofacies among the various types of subaerial pyroclastic fallout and water-settled volcanoclastic suspension deposits are subtle. Criteria for distinguishing subaerial fallout from syn-eruptive water-settled fallout deposits are still being developed (Cashman and Fiske, 1991). In ancient volcanic sequences, the presence of volcanoclastic suspension deposits does not uniquely constrain the depositional setting, nor the genetic process (primary pyroclastic, syn-eruptive resedimentation, or post-eruptive sedimentation). Correct interpretation depends on consideration of the character of enclosing facies.

Pyroclastic fall deposits (39)

Subaerial fall deposits can be generated by the entire range of explosive eruptions (magmatic, phreatomagmatic and phreatic) and by magmas of any composition. Pyroclasts ejected explosively into the

atmosphere are temporarily suspended, but eventually fall back down and accumulate to form pyroclastic fall deposits. Large, dense pyroclasts follow ballistic trajectories unaffected by wind, and fall close to the vent. Small, light pyroclasts entrained into the eruption column and plume are deposited further from the vent, the distance depending on their terminal fall velocity, the lateral expansion of the plume and wind velocity (Walker et al., 1971; Walker, 1973a; Wilson, 1972; Carey and Sparks, 1986; Wilson and Walker, 1987; Wilson et al., 1987).

Clouds of (ash) pyroclasts are also generated by elutriation from moving pyroclastic flows (Sparks et al., 1973; Walker, 1981b; Sparks and Walker, 1977; Sparks and Huang, 1980), by wholesale lofting of pyroclastic flows that become buoyant (Sparks et al., 1986) and by secondary explosions where hot pyroclastic flows interact with surface water or enter water (Walker, 1979, 1981b; Sigurdsson and Carey, 1989). During explosive eruptions that generate pyroclastic flows, the largest and most dense pyroclasts fall out around the vent, forming deposits of coarse lithic breccia (*co-ignimbrite lag-fall deposits* — Wright and Walker, 1977; Walker, 1985).

Agglutinate is a fall deposit comprising spatter (poorly vesicular, fluidal, juvenile pyroclasts) and bombs that accumulate near vents in explosive eruptions of low viscosity magma. *Agglomerates* a coarse-grained (>64 mm) pyroclastic fall deposit that contains a significant proportion of volcanic bombs and blocks, and is restricted, in general, to very proximal settings. In *welded fall deposits*, the juvenile pyroclasts are sintered together and flattened, forming a coherent rock. These fall deposits result from very rapid accumulation of pyroclasts that have low viscosity. After deposition, the hot pyroclasts deform plastically and weld, due to load compaction (Sparks and Wright, 1979; Wright, 1980). Welded fall deposits on steep slopes can subsequently flow in a non-particulate fashion and develop textures and structures similar to lavas. The requirement of the particles retaining low viscosity means that these deposits are more commonly produced by peralkaline and mafic magmas than other compositions, are usually restricted to near vent settings, and involve relatively low eruption columns, in which heat loss is minimal (Thomas and Sparks, 1992).

Characteristics

Subaerial pyroclastic fall deposits decrease systematically in grain size and thickness with increasing distance from the source vent (Walker, 1973a). At any one locality, they are characterised by even-thickness, laterally continuous, mantle bedding (Fig. 58) and relatively good sorting that reflects the density as well as the size of the pyroclasts (39). Lapilli-grade deposits are clast-supported. Beds may be internally graded (normal or inverse) according to clast density. Dense, non- or poorly vesicular, ballistic pyroclasts, in many cases, produce impact sag structures in underlying layers (38.8). Accretionary lapilli are

commonly present in ash grain size fall deposits (39.6). Juvenile pyroclasts are typically ragged or irregularly shaped. Sorting of particles according to density and size has the effect of producing layers that are dominated by one particular pyroclast type, such as pumice or scoria lapilli, crystals, or glass shards.

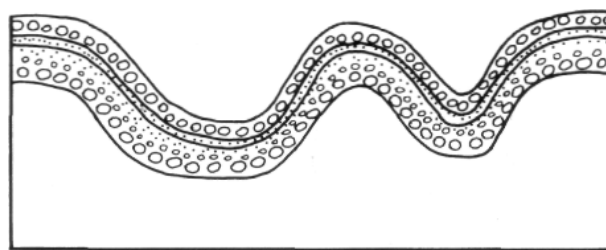


Fig. 58 Geometry of subaerial deposits generated by fallout from eruption clouds. Fallout deposits mantle underlying topography, and are relatively well sorted and bedded (cf. pyroclastic flow deposits). Modified from Wright et al. (1980).

The most voluminous fall deposits are those produced by plinian eruptions involving silicic magma and in association with the emplacement of pyroclastic flows (co-ignimbrite ashes). For example, fall deposits of the Los Chocoyas Ash amount to 150 km³ DRE (Dense Rock Equivalent; 85 ka, Guatemala — Rose et al., 1987) and those of the Oruanui Pumice Formation are estimated to be 90 km³ DRE (23 ka, New Zealand — Self, 1983). Many plinian fall deposits and deposits from other eruption styles have volumes less than a few cubic kilometres (DRE). Distal fall deposits from plinian eruptions commonly extend as thin (centimeter), fine ash layers for hundreds of kilometers from source. In general, deposits from other eruption styles are confined to within several tens of kilometers from source.

Water-settled pyroclastic fall deposits (40, 41)

The wide distribution of ash clouds generated by explosive subaerial eruptions means that in many cases, fallout occurs onto the oceans. Explosive eruption columns from totally submerged vents also release abundant pyroclasts into the oceans. Eventually all the pyroclasts will settle through the water and be deposited. However, currents and the contrasting hydrodynamic properties of different pyroclast types operate to greatly enhance sorting, and only rarely are all the pyroclasts deposited together. Denser lithic and crystal pyroclasts and hot pumice or scoria begin to sink immediately and are sorted according to their respective settling velocities (in turn dependent on particle shape and density). Cashman and Fiske (1991) found that water-settled pyroclastic aggregates are characterised by marked bimodality and pumice:lithic clast diameter ratios in the range 5:1 to 10:1, whereas subaerial fallout deposits have pumice:lithic clast diameter ratios close to 3:1. Deposition of low-density, cold pumice that floats at the surface, and fine ash, with very low settling velocity, are delayed. These components are likely to be transported by currents and widely dispersed. In some cases, fine ash and water-logged pumice are deposited

together, forming even more markedly bimodal deposits (40.3-4).

Distal water-settled ash deposits are composed of shards and crystal fragments, and are graded from coarser crystal-rich bases to finer shard-rich tops, or are massive. They typically occur in thin (centimeter to tens of centimeters) but very widespread (thousands of square kilometers) intervals within other deep subaqueous sedimentary deposits (Ninkovich et al., 1978; Ledbetter and Sparks, 1979; Sparks and Huang, 1980). Primary vitriclastic textures are commonly modified or destroyed during glass crystallization and diagenesis, and ancient, lithified, fine-grained, water-settled fall layers have a cherry or flinty appearance.

Coarser, proximal, syn-eruptive water-settled fallout deposits are parallel stratified, with beds being internally graded or massive, and bimodal, with coarser pumice clasts occurring together with finer lithic clasts and crystals (Dimroth and Yamagishi, 1987; Cashman and Fiske, 1991). Cashman and Fiske (1991) described Late Miocene volcanoclastic deposits thought in part to be proximal (2-3 km from source) water-settled fallout (41). The deposits consist of both dense and pumiceous, intermediate composition, juvenile clasts, crystals and lithic fragments. Thermoremanent magnetization studies show that juvenile andesite blocks in the base of the sequence were emplaced hot (450-500°C — Tamura et al., 1991) and fossils in enclosing sedimentary facies constrain the environment of deposition to shallow submarine (Cashman and Fiske, 1991). The combination of vesicular and hot, dense juvenile clasts suggests that the volcanoclastic deposits were related to explosive activity accompanying submarine dome extrusion.

The unit studied by Cashman and Fiske (1991) has a dense-clast-rich, poorly sorted breccia at the base, overlain gradationally by diffusely stratified to graded, pumiceous breccia and sandstone, with an interval of cross-bedded pumiceous sandstone at the top (41.1). In the graded part of the section, the grain size distribution is distinctly bimodal, and pumice:lithic clast diameter ratios are consistent with settling of a pumice-crystal-lithic clast mixture through water. However, the overall character of the enclosing unit suggests an alternative interpretation which is also consistent with the grain size distribution. The unit shows the internal organisation of deposits from a coarse, high particle concentration, volcanoclastic mass flow (cf. Lowe, 1982). The diffusely stratified-graded interval analysed by Cashman and Fiske (1991) could reflect rapid aggradation by fallout from suspension at the base of a decelerating, high particle concentration mass flow. Notwithstanding the possibility of an alternative interpretation, Cashman and Fiske (1991) have convincingly proven and quantified the characteristic bimodality and fines-depletion of water-settled pumiceous volcanoclastic aggregates.

Suspension sedimentation associated with subaqueous volcanoclastic mass flows

Turbulence accompanying subaqueous volcanoclastic mass flows produces dilute suspensions of fine volcanoclastic particles in the enclosing body of water. If quiet conditions are restored, particles eventually settle from suspension and are preserved as a layer of laminated or massive, volcanoclastic mud capping the mass-flow deposit (40.1, 40.5-6). Alternatively, the suspension may be affected by currents that delay settling and result in transport and sedimentation of the finer components separately from the parent mass-flow deposit. Thus, volcanoclastic suspension deposits associated with subaqueous mass flows may gradationally overlie the coeval parent mass-flow deposit, or else may be deposited with other non-volcanic suspension sediments such as muds or biogenic oozes. They are moderately well sorted, commonly graded, dominated by relative fine grain sizes (sand and finer), and may include a significant admixture of non-volcanic particles such as clay and biogenic particles simultaneously settled from the water column.

Sedimentation in volcanic terranes

In non-volcanic sedimentary environments, facies and facies variations are dependent on several interrelated controls (Reading, 1986): sedimentary processes of erosion, transport and deposition; grain size, volume and rate of the sediment supply; climate, especially temperature, precipitation and wind; subsidence rate and the influence of regional tectonics on sediment sources; sea level changes; biological activity; and, for biogenic and chemical sediments, the water chemistry. In active volcanic terranes, there are additional special controls on sedimentation, for example:

1. Eruptions strongly influence sedimentary processes and sediment supply.
2. Because steep slopes and earthquakes are very common, slope failure events are especially important.
3. Volcano-tectonism, in particular, faults, local rapid uplift and subsidence, causes frequent and sudden changes to sedimentation.
4. Some volcanic processes are constructional and rapidly create and modify topography and drainage.

These special volcanic controls have conspicuous effects on grain size distributions, sedimentary structures and facies architecture of resedimented and volcanogenic sedimentary deposits. *Grain size distributions* are affected because eruptions can instantly produce abundant clasts of either a very narrow or an exceptionally wide grain size range, and clasts that vary widely in shape and in density. *Sedimentary structures* are affected because aggradation rates can be abnormally high, and inhibit or modify the ordered development of sedimentary structures. Water-supported and gravity-driven volcanoclastic mass flows are common in a wide range of subaerial and subaqueous volcanic settings. Grain size grading and sorting are often weakly developed in pumice- or scoria-rich volcanogenic sedimentary deposits, because clasts

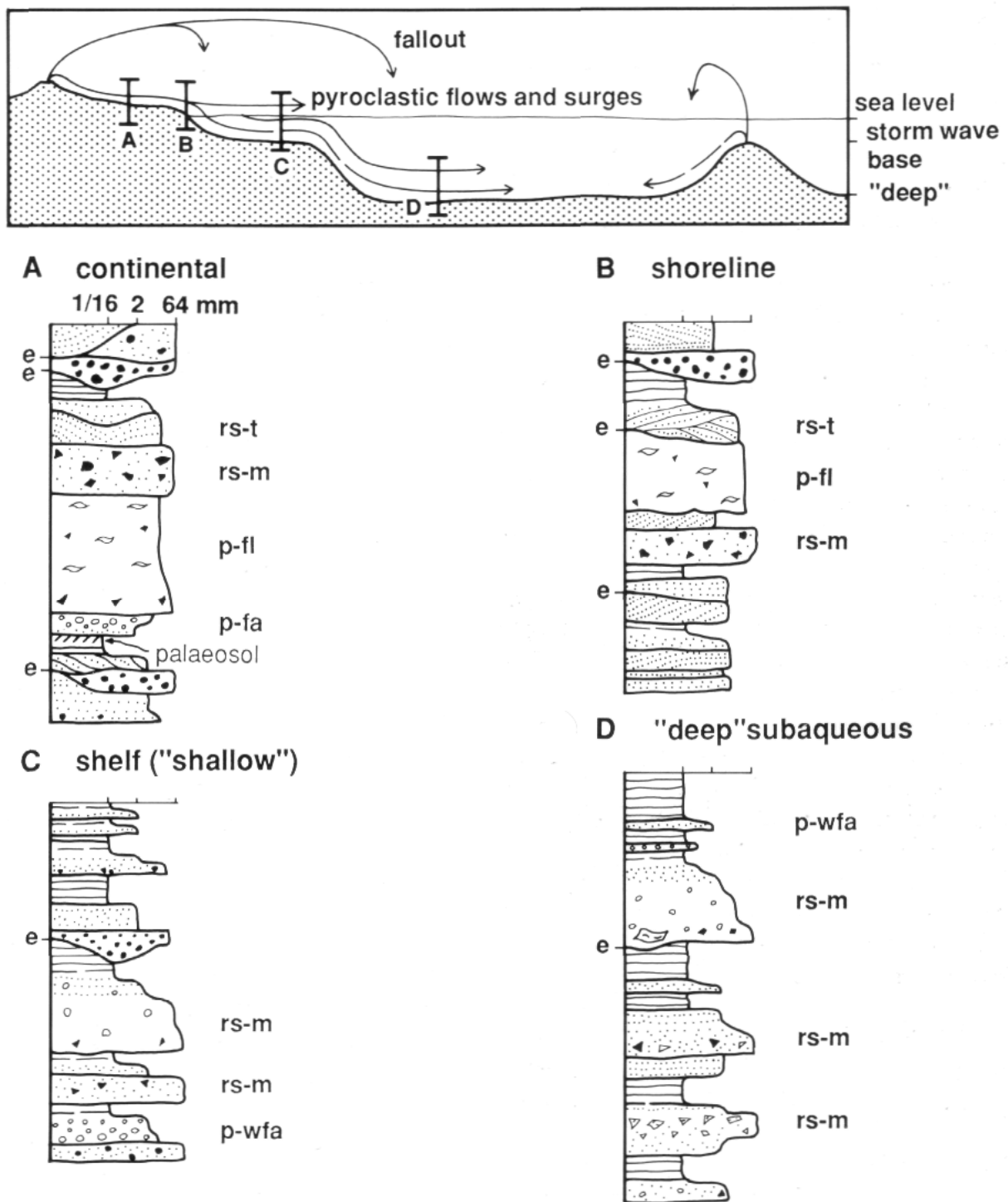


Fig. 59 Sedimentary environments and volcanogenic sedimentary facies associations near active volcanoes. The top frame gives the positions of the schematic sections A-D below. (A) Continental (fluvial and alluvial fan). (B) Shoreline. (C) Subaqueous shelf. (D) "Deep" subaqueous (lake or ocean), p - pyroclastic deposit; fl - flow; fa - fallout; wfa - water-settled fallout; rs - resedimented syn-eruptive deposit: t - traction; m - mass-flow. The grain size subdivisions in (B), (C) and (D) are the same as those shown in (A).

of pumice and scoria have much lower densities than other non-vesicular clasts of the same size. *Facies architecture* is affected because facies geometry is complex, and lateral and vertical facies changes are abrupt and difficult to predict. Erosion surfaces may be carved by primary pyroclastic flows or surges, or by volcanic events, such as steam blasts, that leave no other traces. Facies changes relate ultimately to the source

vents for eruptions, although the relationship is not necessarily simple and direct.

It is important to appreciate that current facies models for sedimentary deposits incorporate assumptions regarding the type of sediment and supply rate. The effects of volcanic events on volcanogenic sedimentary facies have been explored in the case of an active

subaerial composite volcano (Davies et al., 1978; Kuenzi et al., 1979; Vessell and Davies, 1981). However, few studies have considered facies models specifically catering for the enormous and abrupt increases in particle supply, and the abundance of large, low-density particles that are likely to accompany and follow intermediate and large-magnitude explosive silicic eruptions (Smith, 1991).

There are diverse sedimentary environments around active subaerial and subaqueous volcanoes that serve as permanent or temporary repositories of volcanoclastic particles. The different environments are characterized by broad differences in the kinds of sedimentary processes that operate. For example, traction transport and deposition dominate in most continental and shallow subaqueous settings, whereas mass flows and suspension dominate in below-wave-base, deep subaqueous settings. These contrasts have an effect on the volcanogenic sedimentary facies associations and geometry (Fig. 59). In addition to particles delivered by resedimentation and other sedimentary transport processes, all these settings may receive pyroclasts contributed directly by fallout from eruption columns and widely wind-dispersed ash clouds. Subaerial and shallow subaqueous settings in proximity to explosive volcanoes can also include primary pyroclastic flow deposits. The main sedimentary transport and depositional processes in each of five such environments are listed below.

Lakes (especially caldera lakes) (Fig. 59D) — Volcanoclastic particles are transported to lakes by rivers, in suspension or traction, by lahars and by subaerial mass flows. Offshore deposition takes place from suspension, turbidity currents and other types of subaqueous mass flows. Pyroclastic flows and surges may come to rest on the surfaces of lakes. Their deposits will comprise some components that begin to sink immediately (lithic fragments, hot pumice or scoria, crystals) and others that settle from suspension or flotation only very slowly (cold pumice or scoria, ash). Lakes in calderas and near active cones also receive slides and volcanic debris avalanches.

Alluvial environments (Fig. 59A) — Transport and deposition of volcanoclastic particles in alluvial fans and braidplains are dominated by fluvial traction currents, hyperconcentrated flows and sheet floods, and subaerial mass flows, especially cohesive debris flows and mud flows.

Shoreline environments (Fig. 59B) — This setting is of special importance for volcanoes near the coast and for island volcanoes. Deposition can occur in deltas, barrier island and lagoonal systems, and in near-offshore settings. Sedimentation from traction currents and suspension are dominant.

Offshore shelf environments (Fig. 59C) — Sedimentation takes place from tidal, storm and ocean currents in near-shore settings, and from suspension and water-supported mass flows farther offshore.

Hummocky cross stratification is a characteristic sedimentary structure displayed by storm-affected shelf sandstone deposits. As for lakes, pyroclastic flows and surges that travel across and come to rest on the sea deliver pyroclasts directly to offshore shelf sedimentation systems.

Deep ocean settings (Fig. 59D) — Sedimentation is dominated by suspension, flotation and mass flow processes. Volcanoclastic particles initially generated and deposited near subaerial, shoaling and shallowly submerged active volcanoes can ultimately reach deep ocean settings as a result of long-distance resedimentation by a variety of water-supported mass flows, or transport in suspension. Pyroclasts delivered directly to open ocean settings by primary volcanic transport processes are transported by surface currents before finally settling from suspension or flotation.

Plate 21 — Three types of pyroclastic flow deposits



1. Rhyolitic block and ash flow deposit

The very thick, poorly sorted, volcanic breccia shown here is the deposit from a block and ash flow generated during growth of a subaerial rhyolite lava dome. It comprises angular, blocky rhyolite clasts in ash matrix, and displays weak reverse grading. Although non-welded, primary transport and hot emplacement is indicated by the presence of charred and carbonised wood. The exposure is about 5.4 km from the source.

Kaharoa Pyroclastics, AD 1300; Crater Road, Tarawera, New Zealand.



2. Texture of a block and ash flow deposit

Fresh exposures of the rhyolitic block and ash flow deposit in **21.1** show characteristic poor sorting and matrix-supported fabric. The polyhedral, white rhyolite lapilli and blocks are reversely graded. Below the block and ash flow deposit are stratified ash and pumice lapilli layers from earlier cogenetic explosive eruptions. The section in the photograph is about 2 m thick.

Kaharoa Pyroclastics, AD 1300; Crater Road, Tarawera, New Zealand.



3. Andesitic scoria and ash flow deposit

These small volume, scoria and ash flow deposits (**S**) consist of vesicular andesitic blocks and lapilli, and only minor coarse ash. The deposits were emplaced on relatively steep slopes, and have well-developed surface ridges and levees. This suggests that prior to deposition the pyroclastic flows had appreciable yield strength.

Deposits from the AD 1975 eruption of Ngauruhoe; Tongariro Volcanic Centre, New Zealand.



4. Texture of a scoria and ash flow deposit

The juvenile clasts in this scoria and ash flow deposit are dark grey, scoriaceous andesite. The deposit is poorly sorted, clast-supported, unstratified and dominated by equant lapilli and blocks, with only relatively minor amounts of finer lapilli and ash matrix. Large clasts are subrounded due to abrasion during transport in the pyroclastic flow.

Agatsuma pyroclastic flow deposit, AD 1783, about 4 km from source; Asama volcano, Honshu, Japan.



5. Non-welded pumiceous rhyolitic ignimbrite

This exposure shows non-welded ignimbrite overlying an erosive surface (E) carved into underlying plinian fallout pumice lapilli deposits. **Layer 2a** of the ignimbrite is ash-rich, and depleted in coarse clasts but contains some pumice lapilli. **Layer 2b** above forms the bulk of the deposit, is very poorly sorted, and contains pumice and minor lithic lapilli supported in ash matrix. There is a slight upward increase in the maximum size of pumice lapilli. This internal stratigraphy differs from that of subaqueous volcanoclastic mass-flow deposits. However, textures within the massive lower parts of units formed by the two volcanoclastic mass-flow types can be closely similar. Hammer for scale (arrow).

Upper Bandelier Ignimbrite, 1.12 Ma; White Rock, New Mexico, USA.



6. Non-welded pumiceous rhyolitic ignimbrite

Pumiceous pyroclastic flow deposits are characteristically very poorly sorted, matrix-supported and, in many cases, un-stratified. This example comprises pinkish and cream pumice lapilli (P) and scattered black lithic fragments (L) set in crystal- and shard-rich matrix. Pumice clasts are undeformed and show no conspicuous alignment.

Bishop Tuff, 0.73 Ma; Crowley Lake Reservoir, California, USA.



7. Stratified pumiceous ignimbrite

Although, in many cases, pyroclastic flow deposits are internally massive or graded, some examples are distinctly though diffusely stratified. Here, stratification is defined by thin but laterally extensive concentrations of pumice lapilli spaced at intervals of 10-20 cm. The pumice trains are not continuous and no sharply defined bedding planes occur. The layering may be the result of stepwise aggradation at the base of an unsteady pyroclastic flow, or else be the result of syn- and post-emplacement shearing of the deposit.

Rhyolitic ignimbrite from the AD 1912 eruption of Novarupta; Valley of Ten Thousand Smokes, Alaska, USA.

Plate 22 — Geometry and components of pyroclastic flow deposits



1. Flat top surface of valley pond ignimbrite

The flat floor of this valley is underlain by rhyolitic ignimbrite sourced from a vent about 17 km away, behind the low hills in the distance. The ignimbrite is up to 100 m thick and has completely buried most of the pre-existing topography within the valley. Such flat upper surfaces and landscape-smoothing effects are common characteristics of valley pond ignimbrite.

Valley of Ten Thousand Smokes, filled with ignimbrite from the AD 1912 eruption of Novarupta, Alaska, USA.



2. Rhyolitic outflow ignimbrite sheet

Outflow ignimbrite sheets typically build very gently sloping plateaux. The well-developed prismatic joints (**J**) in this ignimbrite occur in a vapour-phase crystallised, texturally non-compacted zone. The original flat top of the ignimbrite is largely preserved between deeply incised canyons. The caldera source of the ignimbrite is at least 25 km in the distance. The canyon is about 300 m deep.

Upper Bandelier Ignimbrite, 1.12 Ma; Frijoles Canyon, Jemez Mountains, New Mexico, USA.



3. Lithic clast concentration zone in ignimbrite

Irregular pods rich in angular, dense lithic clasts sometimes occur in ignimbrites as a result of sorting processes operating during flowage. These examples occur near the base of the crystal-rich ignimbrite host and are almost conformable with the steeply dipping pumice foliation (S_0 , arrow). The matrix of the ignimbrite has well preserved, welded shards indicating hot emplacement from primary pyroclastic flows.

Bulgonunna Volcanic Group, Late Carboniferous; Burdekin River, northern Queensland.



4. Lithic- and crystal-rich, welded ignimbrite

This ignimbrite consists of angular, quartz-phyric volcanic lithic clasts (**L**), quartz- and feldspar-phyric, formerly glassy (now chlorite) fiamme (**F**) and shard- and crystal-rich matrix. Welding textures are well preserved in thin-section (**27.1B**) providing evidence that the unit was emplaced hot and is primary.

Tyndall Group, Mount Read Volcanics, Cambrian; Comstock Valley, western Tasmania.



5. Lithic segregation pipes in ignimbrite

Lithic clast-rich segregation pipes in pyroclastic flow deposits result from streaming of hot gas that preferentially removes much of the fine ash. Such structures provide clear evidence of hot emplacement. The illustrated examples occur in ignimbrite that is extremely poorly sorted and comprises rhyolitic pumice lapilli (**P**), a variety of volcanic lithic clasts (**L**) and abundant shard- and crystal-rich matrix.

Carpenter Ridge Tuff, 27.5 Ma; outflow sheet from Bachelor caldera, San Juan Mountains, Colorado, USA.



6. Accretionary lapilli in a gas-escape pipe

The vertical gas-escape pipes (arrows) shown here occur in non-welded ignimbrite and are filled with accretionary lapilli (A). The accretionary lapilli may have formed within the pipes as fine ash-laden steam-rich gas streamed through, or else they may have been scavenged from underlying accretionary lapilli-bearing fall deposits and concentrated in the gas-escape pipes.

Oruanui Ignimbrite, 26.5 ka; Tongariro River Bridge, Taupo, New Zealand.



7. Lee-side lenses of pumice lapilli in an ignimbrite veneer deposit

These lenses (L) of well rounded, clast-supported, matrix-free pumice lapilli are several metres long and mostly less than 0.5 m thick. They occur in ignimbrite deposited on the lee side of a topographic high (ignimbrite veneer deposit). The bedforms, rounding of pumice lapilli and fine ash depletion are interpreted to result from locally intense turbulence affecting high-velocity pyroclastic flows where they passed over obstacles (Walker et al. 1981a).

Taupo Ignimbrite, AD 186, 20 km from source; Tiraki Road, New Zealand

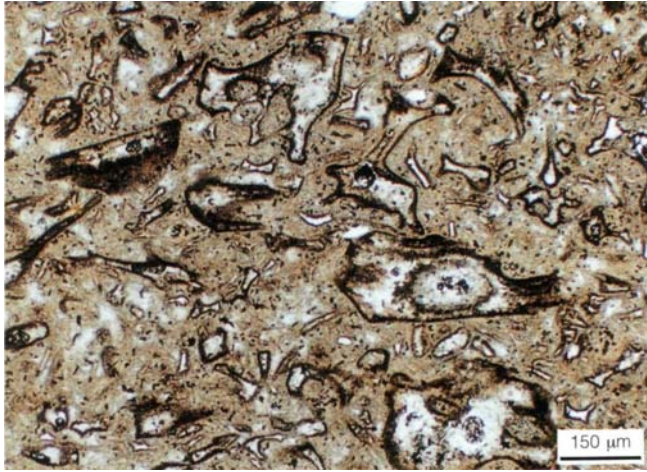
Plate 23 — Vapour-phase crystallised and slightly welded ignimbrites



1. Vapour-phase crystallised rhyolitic ignimbrite

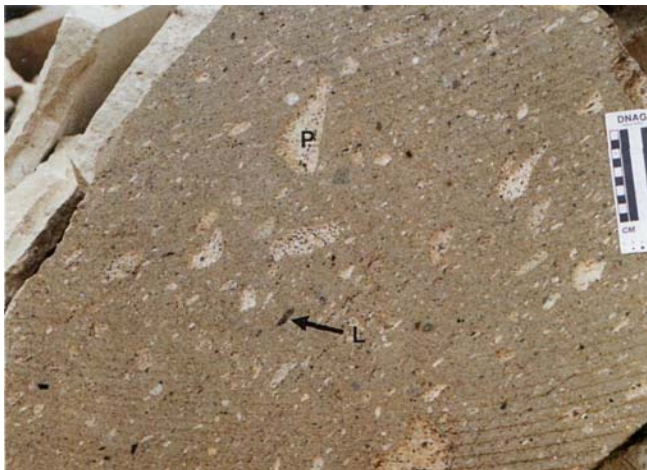
A. This ignimbrite consists of pumice lapilli (P) and volcanic lithic clasts (L) dispersed in pink, porous, crystal-bearing and glassy ash matrix. The blocky pumice lapilli have internal delicate, fibrous, tube vesicle texture. The tube vesicle alignment in separate pumice lapilli is random and is typical of non-welded tube pumice deposits. Although texturally uncompacted and non-welded, the deposit is partly lithified as a result of vapour-phase crystallisation of fine-grained, new minerals in pore spaces.

Toconao Ignimbrite, 4 Ma; specimen Ta, Toconao, northern Chile.



B. The matrix of the vapour-phase crystallised, non-welded ignimbrite shown in **23.1A** consists of uncompacted, un-deformed, cusped, rod and spike shaped, partly devitrified, bubble-wall shards. Pale brown, very fine grained, vapour-phase crystallisation minerals infill the original pore spaces in the matrix and pumice clasts. Plane polarised light.

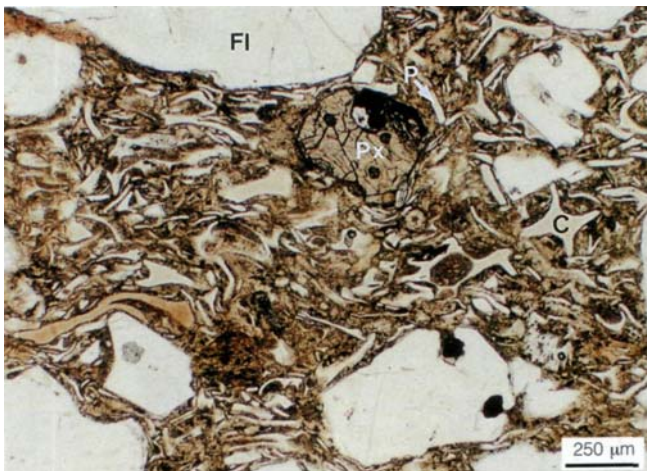
Toconao Ignimbrite, 4 Ma; specimen Ta, Toconao, northern Chile.



2. Slightly welded, glassy rhyolitic ignimbrite

A. This slab of ignimbrite shows the extremely poor sorting, and matrix-supported fabric, typical of most pyroclastic flow deposits. Pale, coarsely porphyritic pumice lapilli (**P**) and a wide variety of angular volcanic lithic lapilli (**L**) are supported in a grey ash matrix consisting of crystals, crystal fragments and glass shards. Most pumice lapilli are only slightly flattened and the ignimbrite is not strongly welded. The coherence is partly due to vapour-phase crystallisation of fine-grained silica (tridymite/cristobalite) and feldspar in the pore spaces soon after emplacement.

Ongatiti Ignimbrite, 750 ka; Hinuera Stone Quarry, Hinuera, New Zealand.



B. In thin-section, shards with cusped (**C**) and platy (**P**) shapes are evident in the matrix of the ignimbrite in **23.2A**. Although many shards retain original bubble-wall shapes, those adjacent to crystal components show the effects of slight welding and are partly deformed and compacted. Crystal components, feldspar (**F**) and pyroxene (**Px**), are moderately abundant. Pale brown, very fine ash and fine-grained vapour-phase minerals occur between the shards. Plane polarised light.

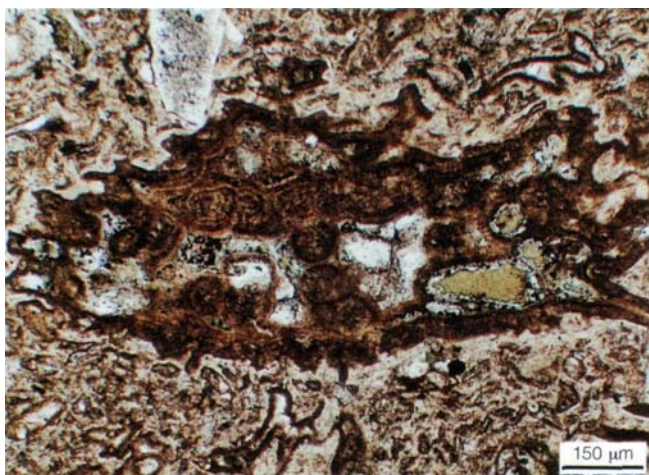
Ongatiti Ignimbrite, 750 ka; specimen CV4B, Hinuera Stone Quarry, Hinuera, New Zealand.



3. Slightly welded ignimbrite

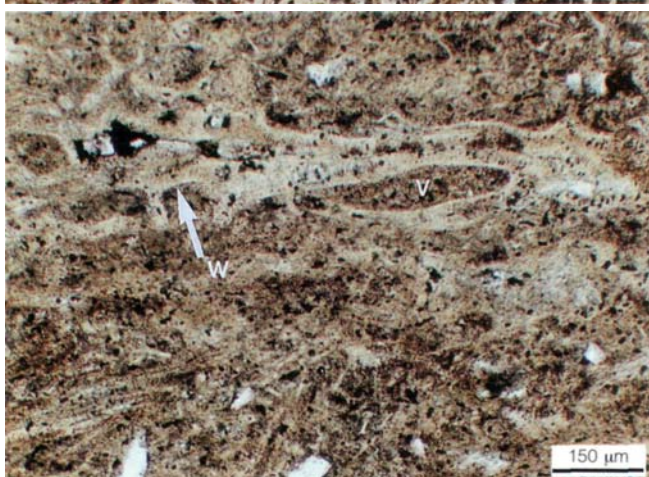
A. The conspicuous volcanoclastic texture of this ignimbrite comprises abundant crystal fragments, scattered black and grey lithic clasts, pale brown relict pumice wisps and dark brown, finer matrix. The framework components (crystals, lithic clasts, pumice wisps) are poorly sorted and matrix-supported. The relict pumice wisps define a weak foliation (parallel to the arrow).

Sapinero Mesa Tuff, 28.5 Ma; specimen SMTe-1, San Juan caldera, San Juan Mountains, Colorado, USA



B. In thin-section, the matrix of **23.3A** displays a vitriclastic texture accentuated by axiolitic devitrification of glassy components. In the centre of the field of view is a relict pumice clast in which the internal vesicular microstructure has been destroyed. The brown rims of matrix shards show axiolitic devitrification. Central parts of shards consist of a mosaic of fine grained quartz and feldspar. Plane polarised light.

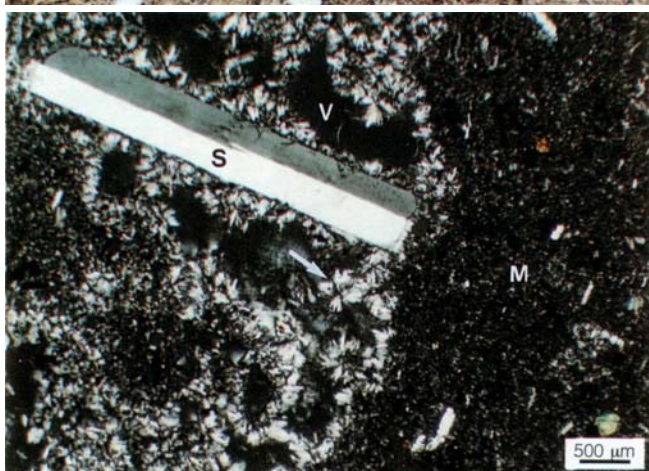
Sapinero Mesa Tuff, 28.5 Ma; specimen SMTe-1, San Juan caldera, San Juan Mountains, Colorado, USA.



4. Devitrified and slightly welded shards and pumice in thin-section

The formerly glassy shards and pumice in this ignimbrite have devitrified to axiolitically arranged fibres. Vesicle walls (**W**) and the internal vesicles (**V**) in the pumice clasts are still distinct and show the effects of slight deformation during incipient welding compaction. Plane polarised light.

Oxaya Formation, Miocene; specimen OxF, 20 km west of Parinacota, northern Chile.



5. Vapour-phase alteration of pumice lapilli in thin-section

Vapour-phase alteration of glassy pumice fragments in ignimbrite may result in total destruction of the original vesicular microstructure. Formerly glassy pumice fragments in this vapour-phase altered ignimbrite now consist of fine, radiating feldspar laths (arrow), open cavities (**V**) and unaltered sanidine (**S**) phenocrysts. The glass in the matrix (**M**) is also devitrified and no vitriclastic texture is preserved. Crossed nicols.

Campanian Ignimbrite, ~33 ka; specimen CI, Campi Flegrei, Italy.

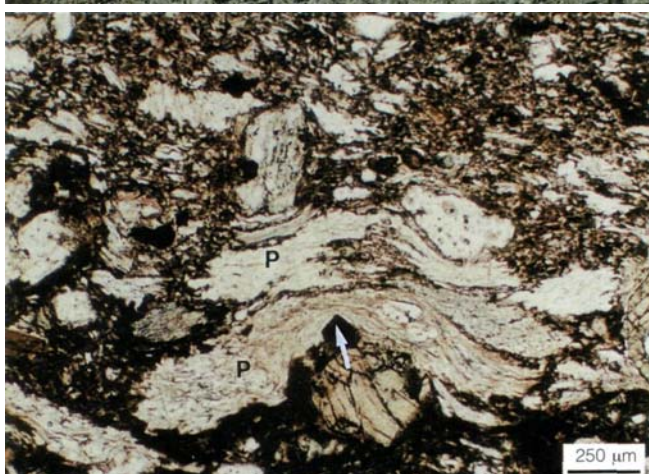
Plate 24 — Welding and granophyric crystallisation textures in ignimbrite



1. Eutaxitic texture in densely welded rhyolitic ignimbrite

A. Densely welded ignimbrite typically displays a foliation defined by aligned, flattened pumice lapilli. In this example, the pumice lapilli (**P**) have been flattened and compacted to dark grey, apparently non-vesicular obsidian lenses and are separated by pale grey matrix. The alignment of flattened welded pumice (and shards) is termed "eutaxitic texture" and is characteristic of welded, primary pyroclastic deposits.

Battleship Rock Ignimbrite, 300 ka; Jemez Road, Jemez Mountains, New Mexico, USA.



B. In thin-section, the Battleship Rock Ignimbrite (24.1A) shows strong compaction and welding of pumice lapilli (**P**) and shards, especially near the edges of crystals (arrow). Pumice lapilli display ragged terminations, internal perlitic r fractures and collapsed tube vesicles. In ancient volcanic rocks, such glassy lenses commonly devitrify, recrystallise or alter to phyllosilicates and vesicular microstructures may not be preserved. Plane polarised light.

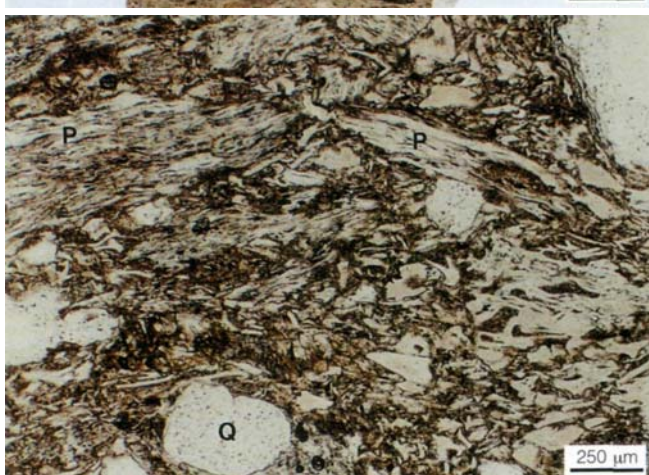
Battleship Rock Ignimbrite, 300 ka; specimen BRI, Jemez Road, Jemez Mountains, New Mexico, USA.



2. "Lenticulite" — densely welded rhyolitic ignimbrite

A. In this specimen of welded rhyolitic ignimbrite, former pumice fragments (**P**) are lenses of light and dark grey, dense glass. All the original vesicles in the pumice have collapsed during welding compaction. The aligned, flattened "lenticules" define a planar foliation that in most cases is subparallel to bedding. Also present are scattered lithic lapilli (**L**) and tan-coloured ash matrix.

Whitianga Group, Pleistocene; Owharoa Falls, Coromandel, New Zealand.



B. In thin-section, the lenticules in 24.2A are glassy wisps (**P**) in which the outlines of collapsed vesicles are nevertheless evident. The lenticules and deformed glass shards define a well-developed eutaxitic texture. Other components are quartz (**Q**), feldspar, hypersthene and biotite crystal fragments and pale brown, fine ash matrix. Plane polarised light.

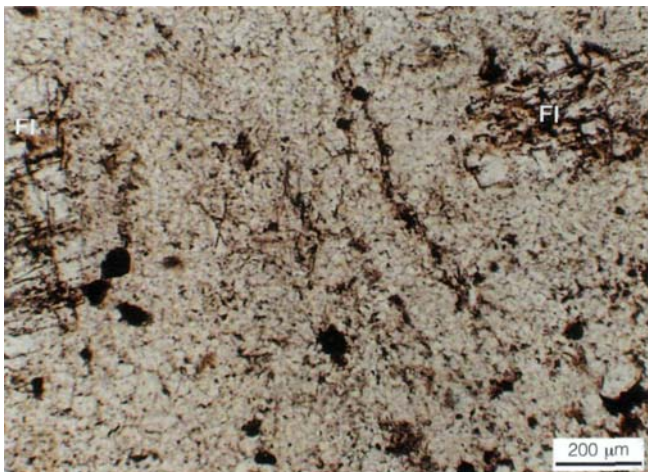
Whitianga Group, Pleistocene; specimen CV5, Owharoa Falls, Coromandel, New Zealand.



3. Granophyric crystallisation in very thick, welded, intra-caldera ignimbrite

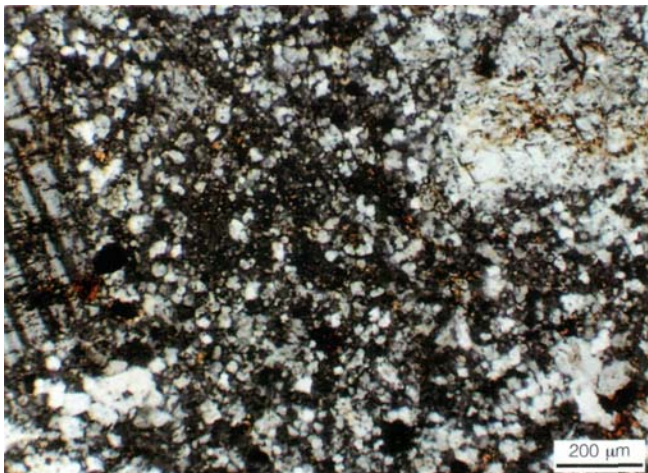
A. Pale, relict pumice fiamme define a weak foliation in this outcrop of crystal-rich, welded ignimbrite. Both the pumice lapilli and matrix glass shards are devitrified (**24.3B**, **24.3C**). The ignimbrite is at least 400 m thick and ponded within a genetically related caldera complex.

Arringunna Rhyolite, Featherbed Volcanic Complex, Early Permian; Big Watson Creek, northern Queensland.



B. Granophyric crystallisation of glass results in a mosaic of fine-grained quartz and feldspar. This example of granophyric texture occurs in the formerly glassy matrix of a densely welded ignimbrite (**24.3A**) between feldspar crystal fragments (**FI**). Granophyric crystallisation commonly completely overprints any pre-existing vitriclastic textures and other criteria must be used to distinguish a pyroclastic origin. Granophyric texture typically develops in the interior parts of very thick, welded ignimbrites that cool slowly. Plane polarised light.

Arringunna Rhyolite, Featherbed Volcanic Complex, Early Permian; specimen 87301005, Big Watson Creek, northern Queensland



C. The mosaic of fine quartz and feldspar that characterises granophyric crystallisation of glass is well displayed here under crossed nicols. The field of view is the same as in **24.3B**. Granophyric crystallisation usually overprints both pumice and matrix shards, and resembles groundmass textures in some coherent lavas and high-level intrusions. Crossed nicols.

Arringunna Rhyolite, Featherbed Volcanic Complex, Early Permian; specimen 87301005, Big Watson Creek, northern Queensland.



4. Welded rhyodacitic ignimbrite

Pale relict pumice lapilli (**P**) define a conspicuous foliation in this massive welded ignimbrite. Both the pumice clasts and the formerly glassy matrix of the ignimbrite are totally devitrified and show granophyric texture in thin-section. Only in favourable exposures is relict pumice easily recognised. Otherwise, relict pumice clasts are represented by patches in which crystal components are euhedral, and coarser and less abundant than in the enclosing matrix.

Dundee Rhyodacite, Coombadjha Volcanic Complex, Late Permian; Ooroowin Road, New South Wales.

Plate 25 — Lithophysae and spherulites in welded ignimbrite



1. Lithophysae in densely welded ignimbrite

These lithophysae (L) have central, lens to star shaped vugs which are lined by radially arranged crystal fibres. Lithophysae result from glass devitrification and begin to form early in the cooling history of primary pyroclastic deposits and lavas. In ignimbrites, they are a reliable indicator of dense welding because they only form in coherent glass, that is, in deposits that have undergone thorough welding compaction.

Carpenter Ridge Tuff, 27.5 Ma; Bachelor-caldera, San Juan Mountains, Colorado, USA.



2. Spherulites in devitrified welded ignimbrite

Dark grey spherulites (arrow) have nucleated on crystal fragments in the matrix of welded, dacitic ignimbrite. The rest of the matrix has a mottled grey and blue-grey appearance due to patchy variation in the style and grain size of devitrification. A genetic interpretation can be inferred from textural and lithofacies evidence in outcrop: broken crystals and lithic fragments indicate the rock is volcaniclastic; the presence of spherulites indicates hot emplacement and primary welding; the poorly sorted, unstratified lithofacies are consistent with welded ignimbrite (rather than welded pyroclastic fall deposits).

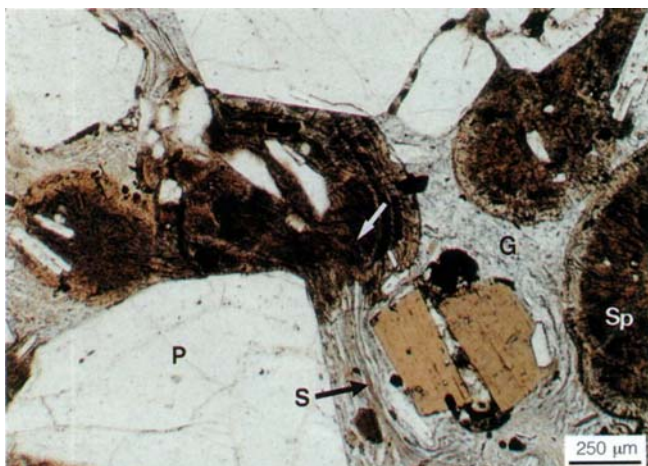
Bulgonunna Volcanic Group, Late Carboniferous; Glendon Creek, northern Queensland.



3. Crystal- and lithic-rich welded ignimbrite

A. Dominant components of this ignimbrite are feldspar, hornblende and biotite crystal fragments, glassy lenses (flattened pumice lapilli), volcanic lithic lapilli and much finer matrix. Aligned flattened pumice lapilli define a eutaxitic foliation (parallel to arrow) that is characteristic of welded ignimbrite.

Nelson Mountain Tuff, 27 Ma; specimen NMT4, San Luis caldera, San Juan Mountains, Colorado, USA.



B. A thin-section of the ignimbrite in **25.3A** shows that it is densely welded and partly spherulitically devitrified. Compacted and deformed, still glassy pumice wisps and shards (**S**) define a foliation which is deflected around plagioclase (**P**), hornblende and biotite crystals and crystal fragments. The rest of the matrix consists of glassy patches that contain clusters of crystallites (**G**), and spherulites (**Sp**) that overprint the welded shards. Remnants of the original welded vitriclastic texture are recognisable within the spherulites (arrow), especially close to their margins. Plane polarised light.

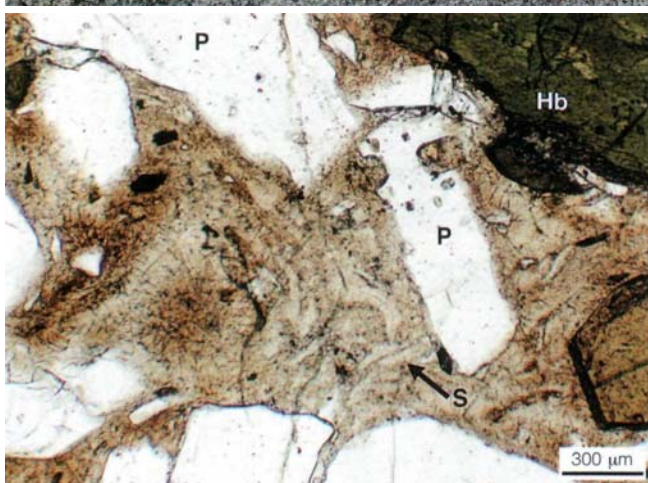
Nelson Mountain Tuff, 27 Ma; specimen NMT4, San Luis caldera, San Juan Mountains, Colorado, USA.

4. Crystal-rich devitrified welded ignimbrite

A. Crystal fragments (quartz, feldspar, hornblende, biotite) constitute more than 50 modal % of this ignimbrite. Additional components are phenocryst-rich relict pumice and even-grained possibly cognate igneous inclusions (**I**). The coarse crystal-rich texture and compact, massive character result in superficial resemblance to a coherent porphyritic intrusion.



Fish Canyon Tuff, 28 Ma; La Garita caldera, San Juan Mountains, Colorado, USA



B. In thin-section, formerly glassy shards (**S**) are evident in the matrix of the ignimbrite in **25.4A**. The shards occur between plagioclase (**P**), quartz and hornblende (**Hb**) crystal fragments and show remnants of axiolitic devitrification texture. Axiolitic devitrification develops during primary cooling and crystallisation of hot volcanic glass, and is a good indicator of primary emplacement of volcanoclastic deposits. Axiolitic devitrification of shards typically preserves and accentuates the original shard shape. Plane polarised light.

Fish Canyon Tuff, 28 Ma; specimen FCT6, La Garita caldera, San Juan Mountains, Colorado, USA.

5. Recrystallised pumice in welded ignimbrite in thin-section

Recrystallised, formerly glassy, platy and cusped matrix shards are strongly deformed at the margins of quartz and feldspar crystal fragments as a result of welding compaction. In the centre of the field of view is a compacted, recrystallised, relict pumice clast in which the internal vesicular microstructures are still discernible. Plane polarised light.



Tyndall Group, Mount Read Volcanics, Cambrian; specimen CT52, Comstock Valley, western Tasmania.

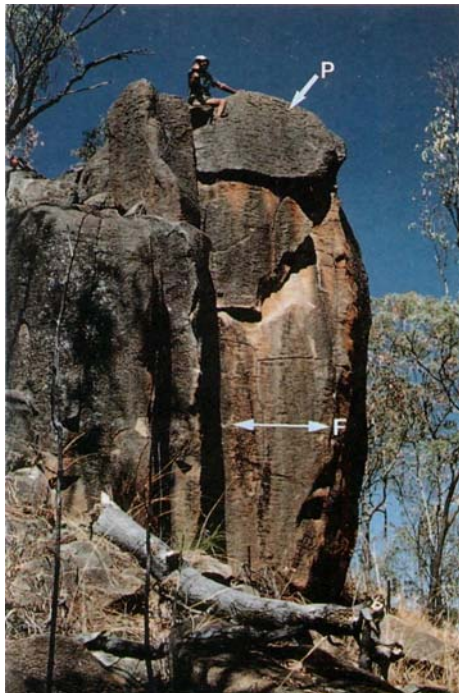


6. Altered, formerly glassy clast in welded ignimbrite in thin-section

The prominent chloritic clast in the centre of the field of view has ragged, delicately cusped margins (arrow) and contains scattered spherulites. The matrix of the ignimbrite is composed of recrystallised welded shards. The chloritic clast may have been compacted glassy pumice, or else, a glassy, dense (non-vesicular) juvenile magmatic clast (vitriclast). Plane polarised light.

Tyndall Group, Mount Read Volcanics, Cambrian; specimen CT30, Comstock Valley, western Tasmania.

Plate 26 — Heat retention in pyroclastic flow deposits and high-grade ignimbrite



1. Columnar-jointed, welded, rhyolitic ignimbrite

Wide, regular, columnar joints in this ignimbrite are perpendicular to a conspicuous foliation (**F**) defined by compacted, elongate, relict pumice lenses (**P**), some of which are up to 40 cm long. The columnar joints developed in response to contraction during cooling and imply primary emplacement. Together with the pumice foliation and massive character, the outcrop shows the typical features of very thick, welded, subaerial ignimbrite.

Arringunna Rhyolite, Featherbed Volcanic Complex, Early Permian; Convict Creek, northern Queensland.



2. Columnar-jointed, compositionally zoned ignimbrite

Compositional zonation within this ignimbrite ranges from a pale, rhyodacitic lower zone to a brown-grey, andesitic upper zone. Both zones are texturally non-welded and uncompacted. Regular columnar joints and vapour-phase crystallisation have formed in the andesitic zone and indicate somewhat hotter emplacement for it than the unjointed, unconsolidated rhyodacitic base. Although compositional zonation is a relatively common feature of small to moderate volume, Tertiary and younger ignimbrite sheets, few ancient examples have been described.

Ignimbrite from the 6845 a Mount Mazama eruption; Sand Creek, Crater Lake, Oregon, USA.



3. Flow foliation in high-grade (rheomorphic) ignimbrite

Flow foliations and flow folds can develop in high-grade (densely welded) ignimbrite that undergoes non-particulate flowage (rheomorphism) during and after deposition. These flowage features closely resemble those in coherent lavas and evidence for a pyroclastic origin may be subtle. The rapidly cooled, less welded bases of such ignimbrites are most likely to record their pyroclastic character. In this outcrop, the only suggestion of a pyroclastic origin is the abundance of angular lithic lapilli (arrow), although elsewhere vitriclastic textures are preserved in the matrix. Silicic lavas may also contain lithic inclusions, but they are typically sparse and evenly distributed.

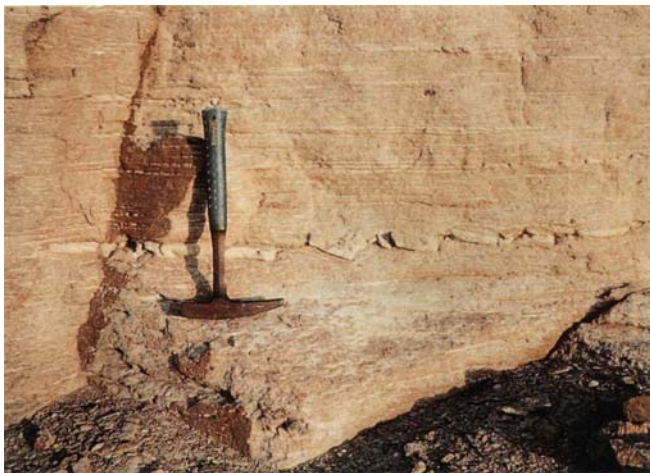
Gomez Tuff, Tertiary; Davis Mountains, southwestern Texas, USA.



4. Flow fold in high-grade ignimbrite

Non-particulate laminar flowage of high-grade (densely welded) ignimbrite has produced 1-2 cm thick flow bands that define recumbent isoclinal flow folds. Silicic lava flows commonly contain similar flow structures and thick, voluminous lavas can be as extensive as some ignimbrites. In ancient sequences, a pyroclastic origin for widespread silicic sheets may be difficult to establish beyond doubt.

Fisherman Rhyolite, Featherbed Volcanic Complex, Early Permian; Upper Combella Creek Gorge, northern Queensland.



5. Fiamme in high-grade peralkaline ignimbrite

The strong foliation in this outcrop is produced by extremely compacted, lenticular fiamme. The fiamme were formerly glassy pumice fragments but are now totally devitrified. At a late stage in the compaction, the largest fiamma in the centre of the photograph has responded in a brittle fashion to further deformation by breaking into segments, while the still ductile matrix has healed the fractures.

Ignimbrite E, Upper Mogan Formation, Miocene; Playa de Tauro, Gran Canaria, Canary Islands.



6. Gas-escape pipes in ignimbrite

Gas-escape pipes result from focussed degassing of hot pyroclastic deposits. The gas includes volatiles released from juvenile pyroclasts, steam generated by vaporisation of underlying ground water, gases from combustion of incorporated vegetation and/or air entrapped during flowage. Gas-escape pipes and other gas segregation structures indicate hot emplacement and are found in primary pyroclastic flow deposits. However, similar structures can form in syn-eruptive debris-flow and mud-flow deposits that contain hot lava blocks.

San Diego Canyon Ignimbrite B, 1.76 Ma; Valles caldera, Jemez Mountains, New Mexico, USA.



7. Degassing pipe in ignimbrite

Focussed degassing of pyroclastic flow deposits may result in alteration of the adjacent ignimbrite and encrustations of vapour-phase minerals. The brown-orange-tan zones in the non-welded ignimbrite around this gas-escape pipe reflect high-temperature mineralogical changes that accompanied degassing and the marked temperature gradient away from the pipe. The pipe is now filled with unaltered pumice lapilli and ash, washed in after activity ceased.

Ignimbrite from the AD 1912 eruption of Novarupta; Valley of Ten Thousand Smokes, Alaska, USA.

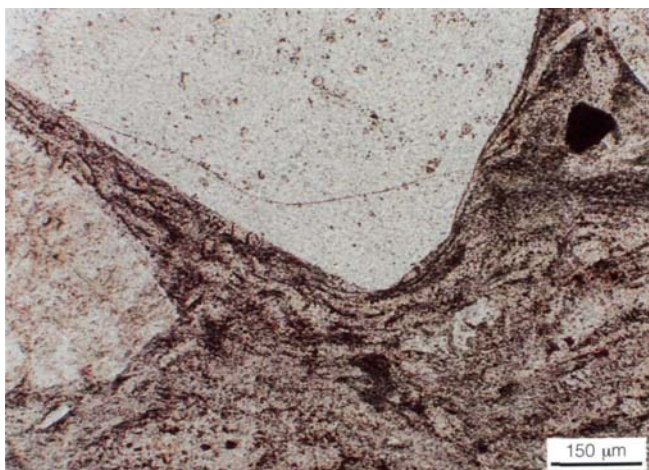
Plate 27 — Welded ignimbrite in the Mount Read Volcanics



1. Densely welded, crystal-rich ignimbrite

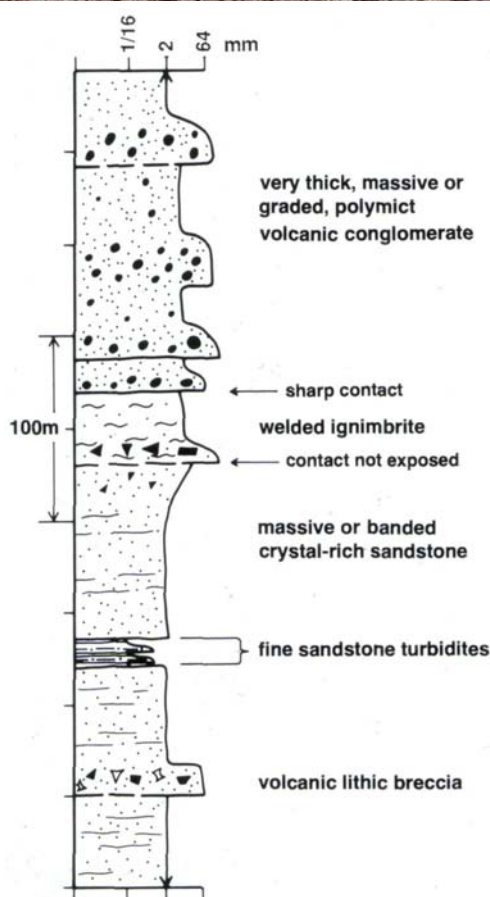
A. This hand specimen consists of abundant crystal fragments (red, altered feldspar and grey quartz) and sparse lithic clasts in fine, dark brown matrix. The sample comes from a >25 m thick, massive, poorly sorted unit within a sedimentary sequence that includes conglomerate and sandstone turbidites (27.1C).

Tyndall Group, Mount Read Volcanics, Cambrian; specimen CT52, Comstock Valley, western Tasmania.



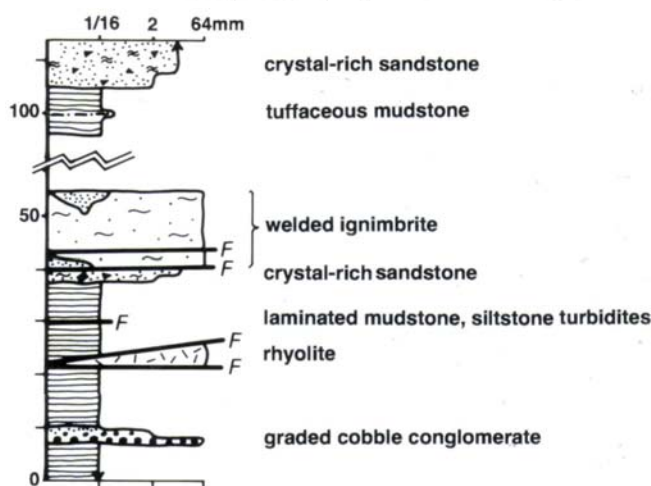
B. Recrystallised welded shards are well preserved in the matrix of the ignimbrite shown in **27.1A**. The shards are deformed, stretched and compacted at the margins of a large quartz crystal fragment and indicate hot, primary emplacement of the volcaniclastic unit even though the depositional setting was below wave base and submarine (**27.1C**). Plane polarised light.

Tyndall Group, Mount Read Volcanics, Cambrian; specimen CT52, Comstock Valley, western Tasmania.



C. The section containing the welded ignimbrite in **27.1A** and **27.1B** is presented here as a graphic log. The occurrence of graded bedded, conglomerate and sandstone turbidites and the absence of tractional sedimentary structures strongly suggest that the ignimbrite was emplaced under water, below wave base. The source vent, however, was probably subaerial and the locality is inferred to have been near the Cambrian basin margin.

Tyndall Group, Mount Read Volcanics, Cambrian; Comstock Valley, western Tasmania.



2. Densely welded, moderately crystal-rich ignimbrite

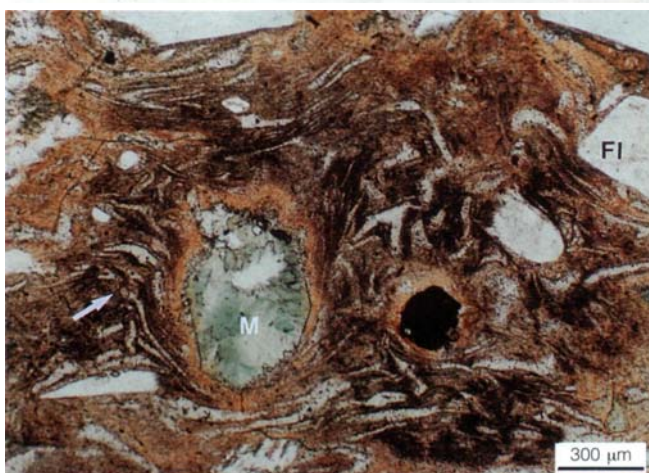
A. The graphic log shows the context of another unit of welded ignimbrite in the Mount Read Volcanics. The section is disrupted by faults and the neither the base nor the top are clearly exposed. The ignimbrite has irregular contacts with crystal-rich sandstone and occurs within a sequence of sandstone and siltstone turbidites and trilobite-bearing mudstone that was clearly deposited below wave base. One possible interpretation is that the ignimbrite is actually a large allochthonous block included in deposits from a giant submarine mass flow. It may have been redeposited from a subaerial, basin-margin site.

Mount Cripps Subgroup, Mount Read Volcanics, Cambrian; Cradle Mountain Link Road, western Tasmania.



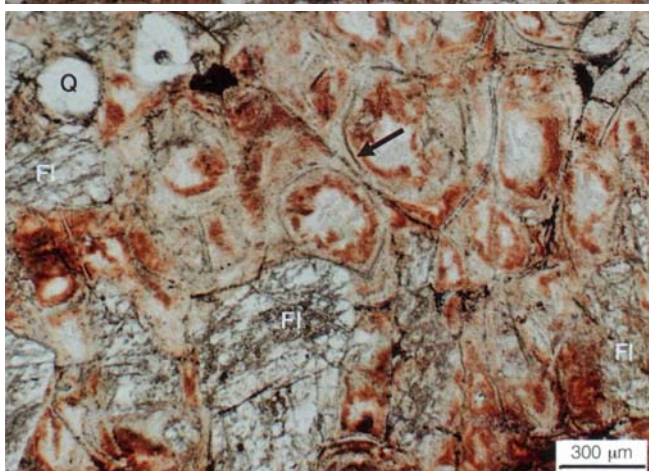
B. Samples of the ignimbrite in the section shown in **27.2A** consist of quartz and feldspar crystal fragments in a dark brown fine matrix in which millimetre-sized relict glass shards can be identified with a hand lens. The ignimbrite is internally massive and contains scattered centimetre-sized lithic fragments.

Mount Read Volcanics, Cambrian; specimen 91-10D, Cradle Mountain Link Road, western Tasmania.



C. In thin-section, recrystallised shards are clearly evident in the matrix of the ignimbrite (**27.2B**). Some shards have recognisable rod and spine shapes, but those at the edges of crystals of quartz, feldspar (**FI**) and a chloritised ferromagnesian phase (**M**; probably amphibole) are strongly deformed (arrow) and indicate significant welding compaction. Plane polarised light.

Mount Read Volcanics, Cambrian; specimen 91-10D, Cradle Mountain Link Road, western Tasmania.



D. Thin-sections also show perlitic fractures (arrow) in the matrix of the ignimbrite (**27.2B**, **27.2C**) and indicate that it was thoroughly welded. Perlite fractures only develop in coherent glass. In pyroclastic deposits, perlitic cracks can form after complete welding compaction of glassy pyroclasts. The formerly glassy, perlitically fractured matrix has subsequently recrystallised to a fine-grained mosaic of quartz and feldspar. Other components are quartz (**Q**) and sericitised feldspar (**FI**) crystal fragments. Plane polarised light.

Mount Read Volcanics, Cambrian; specimen 91-10C, Cradle Mountain Link Road, western Tasmania.

Plate 28 — Subaqueously emplaced pyroclastic flow deposits: northern Wales, UK



1. Shallow marine volcanoclastic sandstone and siltstone below the Lower Rhyolitic Tuff Formation

Steeply dipping strata that underlie pyroclastic deposits from initial eruptions of the Lower Rhyolitic Tuff Formation comprise thinly bedded volcanoclastic sandstone and siltstone (Unit 7 of the Upper Cwm Eigiau Formation — Orton et al., 1990). Sandstone sequences display swaley cross stratification, amalgamated sets of hummocky cross stratification and contain scours (S) that are draped by overlying beds. These bedforms indicate deposition above storm wave base, and storm processes have dominated sediment transport, consistent with an inferred inner submarine shelf setting (Orton et al., 1990).

Unit 7, Upper Cwm Eigiau Formation, Ordovician; Cwm Cneifion, northern Wales, UK.



2. Lower Rhyolitic Tuff Formation: Subaqueously emplaced, non-welded outflow ignimbrite

The outflow facies of the Lower Rhyolitic Tuff Formation comprises a 55 m thick, non-welded, pumiceous pyroclastic flow deposit (P) sourced from a caldera ~6 km to the south (Orton et al., 1990). Weakly developed bedding in the deposit is thought to be due to intraflow shearing during transport, and low angle cross stratification and planar bedding towards the top indicate fractional reworking. The overlying sequence (~100 m) consists predominantly of volcanoclastic turbidites (T) and records resedimentation of more proximal, primary pyroclastic deposits.

Outflow facies of the Lower Rhyolitic Tuff Formation, Ordovician; Idwal Slabs, northern Wales, UK.



3. Shallow submarine volcanoclastic mudstone and sandstone above the outflow Lower Rhyolitic Tuff Formation

This exposure is part of a 20 m thick section generated by shallow submarine reworking of parts of the Lower Rhyolitic Tuff Formation (Howells et al., 1991). Thin- to medium-bedded, coarse, volcanoclastic sandstone (S) is interbedded with planar laminated, shard-rich mudstone (M). Sedimentary structures in sandstone include hummocky cross stratification, small-scale wave-ripple cross lamination, and cut-and-fill structures (arrow) that indicate deposition in a shallow, above-wave-base setting. Mudstone beds comprise ash deposited from suspension and evidently rapidly lithified.

Reworked facies of the Lower Rhyolitic Tuff Formation, Ordovician; Moel Siabod, northern Wales, UK.



4. Pitts Head Tuff: shallow, subaqueous welded ignimbrite

Siliceous nodules are common in ignimbrites emplaced on wet ground or in shallow water. In the Pitts Head Tuff, they form a distinct zone 2-3 m above the base. Slight deformation of the now steeply dipping pumice foliation (F) adjacent to the nodules (N) suggests that they developed during the later stages of welding compaction. Some contain a central vug (arrow), and superficially resemble lithophysae. The nodules may have originally been steam bubbles that formed in hot ignimbrite deposited on a wet substrate and have subsequently been infilled with quartz (Wright and Coward, 1977).

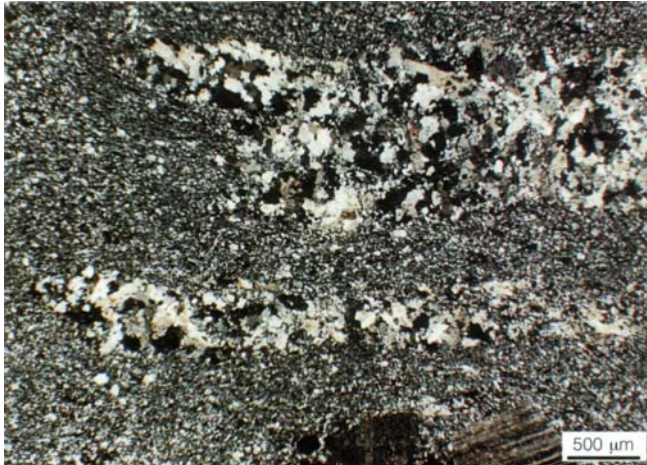
Outflow fades of the Pitts Head Tuff, Ordovician; Llanberis Pass, northern Wales, UK.



5. Pitts Head Tuff: shallow, subaqueous welded ignimbrite

A. Weathered surfaces exhibit dark grey lenses with ragged terminations that define a well-developed foliation. They are interpreted to be recrystallised, originally welded, pumice clasts (fiamme) although vesicular microstructures are not preserved. Other components evident in hand specimen are scattered angular lithic lapilli, crystal fragments and very fine matrix.

Outflow fades of the Pitts Head Tuff, Ordovician; Idwal Syndine,



B. Original vitriclastic textures are only locally preserved in the Pitts Head Tuff. The sample shown in 28.5A is thoroughly recrystallised. Relict pumice(?) lenses consist of interlocking quartz and feldspar. The matrix is a finer felsic mosaic and contains scattered feldspar crystal fragments. Crossed nicols.

Outflow fades of the Pitts Head Tuff, Ordovician; Idwal Syndine, northern Wales, UK.

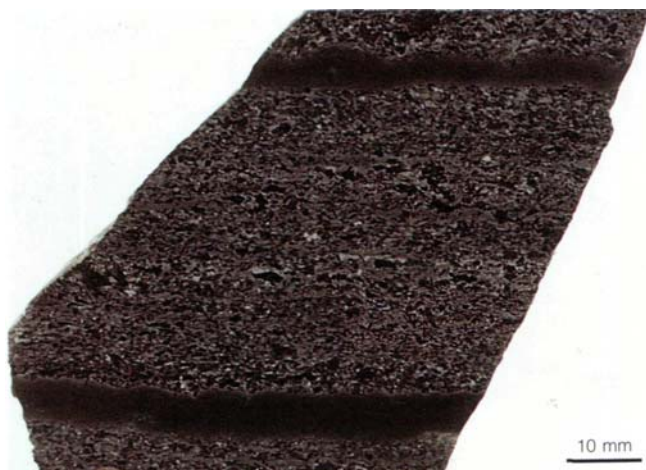


6. Shallow submarine sandstone above the Pitts Head Tuff

Scours, low-angle cross stratification and possible hummocky cross stratification in well bedded, well sorted, brachiopod-bearing sandstone above the Pitts Head Tuff indicate deposition in a high energy environment above storm wave base (Orton et al., 1990). This sequence overlies distal storm beds at the base of the Upper Cwm Eigiau Formation and records the depositional environment which existed following the emplacement of primary and reworked facies of the Pitts Head Tuff Formation.

Upper Cwm Eigiau Formation, Ordovician; Idwal Syndine, northern Wales, UK

Plate 29 — Volcaniclastic turbidites



1. Volcaniclastic sandstone turbidites

A. Thin beds of massive to diffusely laminated, coarse sandstone are interpreted to be deposits from low-density turbidity currents and are interbedded with mudstone probably deposited from suspension. The sandstone consists of black, chlorite-altered, non-vesicular to poorly vesicular, cusped and blocky particles in much finer grained, dark grey mudstone matrix. The sample comes from a Volcaniclastic interval below basaltic pillow lava and fossiliferous black mudstone and was deposited below wave base, in a relatively deep submarine setting.

Mount Read Volcanics, Cambrian; specimen HVS1, Hellyer mine, western Tasmania



B. The chlorite-altered particles have a trachytic texture (arrows) and were originally basaltic. They have both sharp and ragged outlines and may have been produced by quench fragmentation of basaltic lava. Mixing with mud and sparse, rounded, polycrystalline, non-volcanic quartz grains (Q) evidently occurred during mass-flow resedimentation. Plane polarised light.

Mount Read Volcanics, Cambrian; specimen HVS1, Hellyer mine, western Tasmania.



2. Volcaniclastic turbidites and water-settled fall deposits

Laterally continuous, planar thin bedding dominates this exposure of interbedded mudstone, fine sandstone and pebbly sandstone. The main components are crystal and lithic fragments and recrystallised, formerly vitriclastic matrix. The thin beds of fine sandstone and mudstone have been interpreted as water-settled pyroclastic fallout, deposited in water not much deeper than wave base (Kokelaar et al., 1990). Medium to thick, coarse sandstone beds display faint internal lamination, dewatering structures, evidence of substrate erosion and loading, and rare low-angle cross stratification, suggesting rapid deposition from Volcaniclastic turbidities.

Whorneyside Bedded Tuff, Ordovician; Sourmilk Gill, English Lake District, UK



3. Sandy high-density volcanoclastic turbidites

Some beds in this sequence of diffusely stratified and massive bedded, coarse sandstone display normal to reverse grading (cf. S_2 and S_3 turbidite divisions — Lowe, 1982). Siltstone intraclasts (**I**) form lenticular bands within the sandstone beds and lag deposits above erosional basal contacts. Low-angle cross stratification and scour structures also occur and are characteristic of the lower parts of deposits from sandy high-density turbidity currents (cf. S_1 turbidite division — Lowe, 1982; Smith et al., 1990).

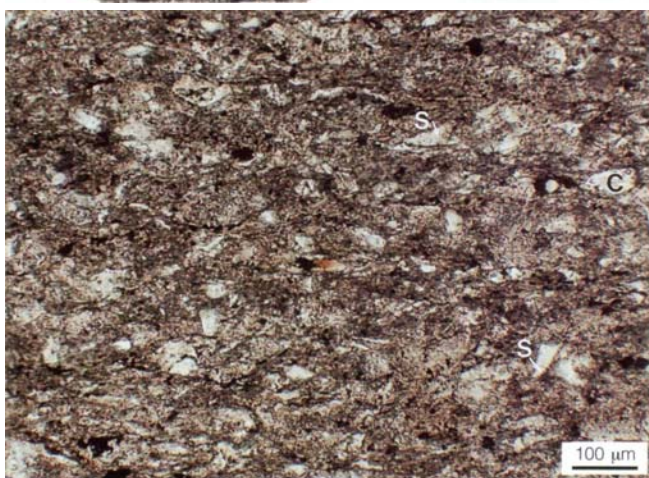
Seathwaite Fell Formation, Ordovician; North Langdale, English Lake District, UK



4. Volcanoclastic megaturbidite

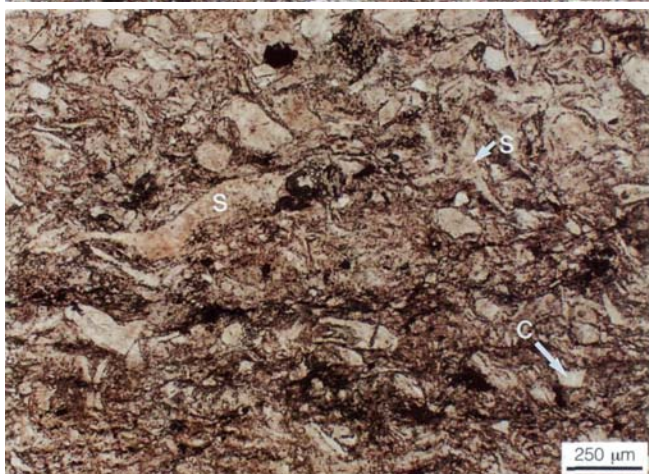
These three samples come from within one very thick (~50 m), graded mass-flow unit comprising crystal-rich sandstone (**C**) overlain by diffusely laminated shard-rich fine sandstone and mudstone (**B** and **A**), interbedded with black laminated mudstone. The components, organisation and context are consistent with deposition from a large volume, syn-eruptive, high-density, volcanoclastic turbidity current. The framework components are largely pyroclasts (shards, relict pumice wisps, crystals).

Mount Read Volcanics, Cambrian; specimens 92-4A, 92-4B, 92-4C, Anthony Road, western Tasmania.



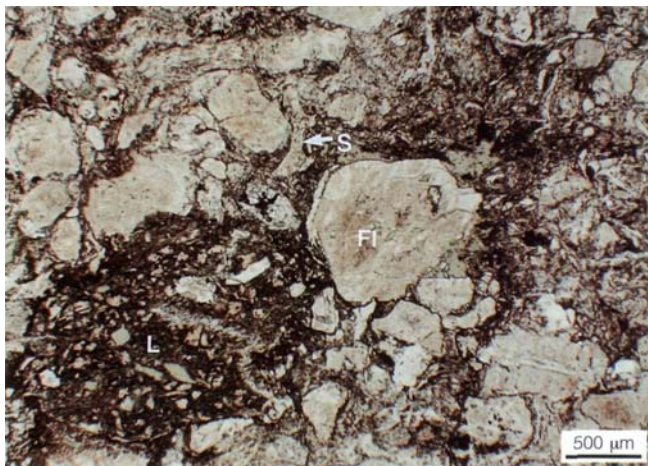
A. In thin-section, the mudstone in the top part of the unit (40 m above the base) is dominated by devitrified shards (**S**) with rod and spike shapes in a very fine, sericitic matrix, accompanied by subordinate feldspar and quartz crystal fragments (**C**). Plane polarised light.

Mount Read Volcanics, Cambrian; specimen 92-4A, Anthony Road, western Tasmania.



B. In thin-section, the middle part of the graded unit (20 m above the base) is composed of undeformed, platy and cusped relict shards (**S**), minor blocky shards and sparse angular crystal fragments (**C**). Diffuse planar lamination in the hand specimen reflects alternating shard-rich and shard-poor, crystal-rich layers. Plane polarised light.

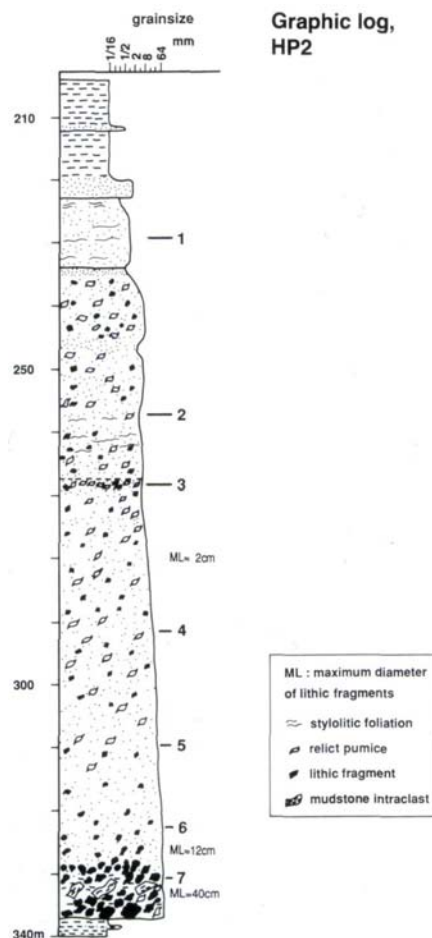
Mount Read Volcanics, Cambrian; specimen 92-4B, Anthony Road, western Tasmania.



C. The base of the thick graded unit (2 m above the base) consists of massive, feldspar (FI) crystal-rich, coarse volcaniclastic sandstone. Other components are formerly glassy and vesicular, trachytic-textured volcanic lithic particles (L), quartzofeldspathic wisps with ragged terminations that may originally have been pumice, and cusped and platy relict shards (S) in much finer matrix. Plane polarised light.

Mount Read Volcanics, Cambrian; specimen 92-4C, Anthony Road, western Tasmania.

Plate 30 — Syn-eruptive submarine volcaniclastic megaturbidite



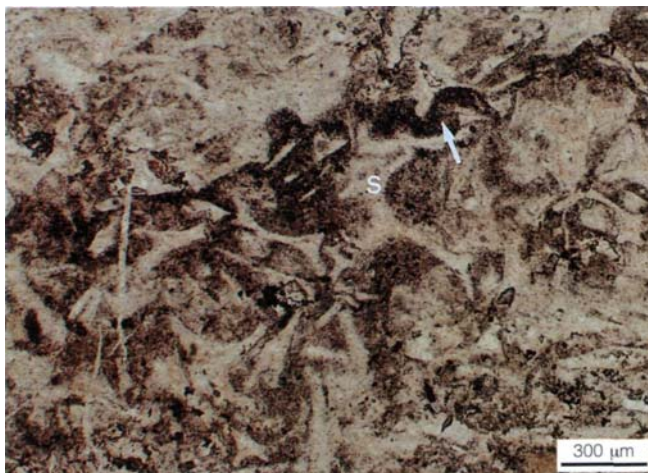
The graphic log shows the grain size variations and sample positions in a 120 m thick, volcaniclastic unit that is inter-bedded with black, laminated mudstone. Subtle changes in grain size and relative proportions of components probably indicate amalgamated subunit boundaries. The principal components are crystal fragments (quartz, feldspar), relict shards, relict tube pumice, volcanic lithic fragments, mudstone intraclasts and fine, unresolvable matrix. The dominance of juvenile pyroclasts, internal organisation and great thickness suggest that the deposit is syn-eruptive, sourced from an explosive, rhyolitic eruption at a subaerial or shallow marine, basin-margin or extrabasinal vent, and was emplaced by large volume, submarine, high-density turbidity currents.

Mount Read Volcanics, Cambrian; DDH HP2, High Point, western Tasmania.



1A. In hand specimen, fine-medium grained volcaniclastic sandstone from the top of the unit (107 m above the base) shows scattered feldspar crystal fragments in finer grey matrix that contains a bedding-parallel, wavy stylolitic foliation (S). The arrow gives the younging direction.

Mount Read Volcanics, Cambrian; DDH HP2 (228.6 m), High Point, western Tasmania.



1B. In thin-section, it is evident that undeformed, bubble-wall and bubble-junction relict shards (**S**) are the dominant component of the fine sandstone at the top of the unit. The formerly glassy shards are recrystallised to a fine quartz-rich mosaic. Other less abundant components are relict pumice (replaced by sericite), black mudstone clasts, feldspar and quartz crystal fragments, and sericite-rich fine matrix. Stylolites (arrow) are defined by concentrations of fine, opaque grains. Plane polarised light.

Mount Read Volcanics, Cambrian; DDH HP2 (228.6 m), High Point, western Tasmania.



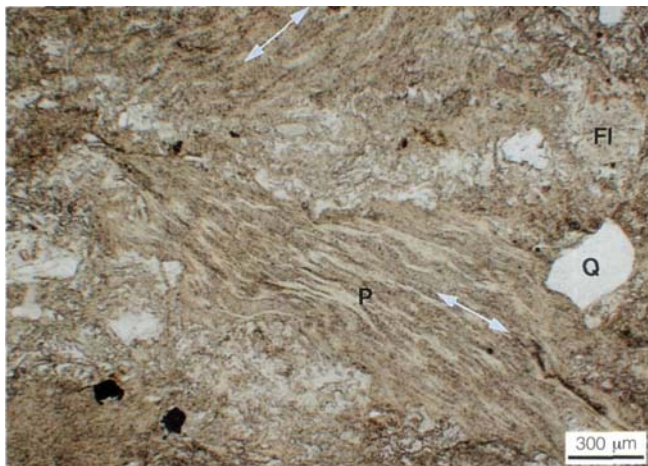
2. This sample from about 79 m above the base is weakly stylolitic, volcaniclastic sandstone composed of scattered feldspar and quartz crystal fragments, sericite-altered pumice wisps (**P**) and abundant shard-rich matrix.

Mount Read Volcanics, Cambrian; DDH HP2 (256.6 m), High Point, western Tasmania.



3A. A 50 cm thick interval about 73 m above the base is crowded with pumice wisps. Although no sharp bedding plane is present, the pumice wisp concentration may mark the top of a 70 m thick subunit. The foliation defined by alignment of the pumice wisps parallel to bedding superficially resembles eutaxitic texture in welded pyroclastic deposits.

Mount Read Volcanics, Cambrian; DDH HP2 (268.3 m), High Point, western Tasmania.

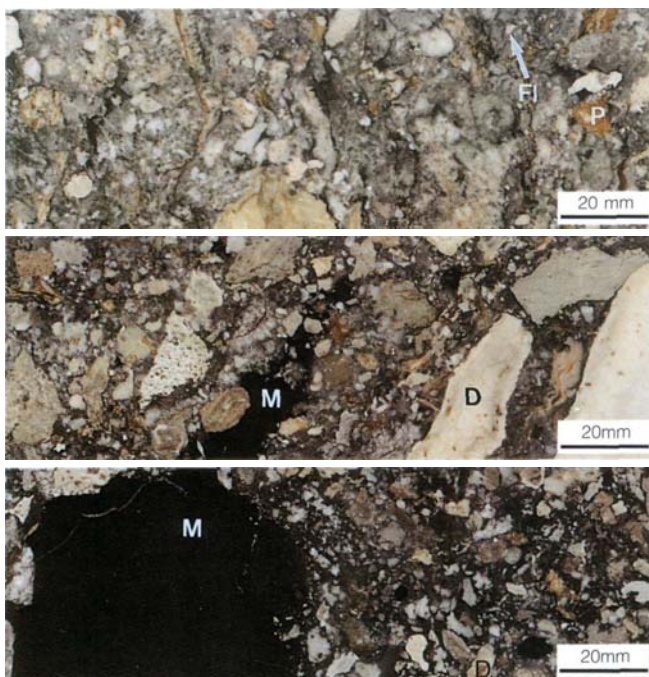


3B. In thin-section, some of the pumice wisps (**P**) show relict tube vesicle texture in random orientations (arrows) and are clearly non-welded. Other components are sparse feldspar (**FI**) and quartz (**Q**) crystal fragments, and undeformed bubble-wall shards. Plane polarised light.

Mount Read Volcanics, Cambrian; DDH HP2 (268.3 m), High Point, western Tasmania.



4. About 44 m above the base, the megaturbidite comprises coarse volcaniclastic sandstone-granule breccia mainly composed of feldspar crystal fragments, dacite clasts and black mudstone intraclasts, together with sparse, ragged, feldspar- and quartz-phyric relict pumice wisps (**P**). *Mount Read Volcanics, Cambrian; DDH HP2 (291.6 m), High Point, western Tasmania.*



5. Lithic-rich and pumiceous breccia from about 26 m above the base of the lowest subunit consists of green, feldspar- and quartz-phyric pumice clasts (**P**) and feldspar crystal fragments (**Fl**) together with abundant pale, volcanic lithic fragments.

Mount Read Volcanics, Cambrian; DDH HP2 (309.7 m), High Point, western Tasmania.

6. Closer to the base of the lowest subunit, the megaturbidite is dominated by lithic fragments. Dacite lava (**D**) and black mudstone (**M**) clasts are abundant in this sample from 13m above the base. Pumice wisps are subordinate to the lithic fragments.

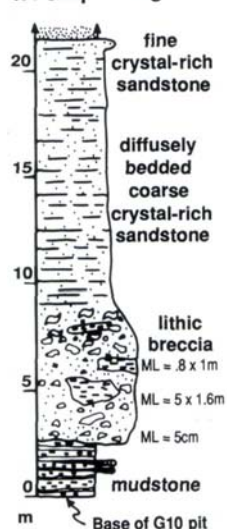
Mount Read Volcanics, Cambrian; DDH HP2 (322.6 m), High Point, western Tasmania.

7. Poorly sorted, polymict, volcaniclastic lithic breccia at the base of the megaturbidite is composed of ragged and angular feldspar-phyric, pale, banded dacite clasts (**D**), sparse basalt lava and pumice fragments, large black mudstone intraclasts (**M**) and dark grey mud-dominated matrix.

Mount Read Volcanics, Cambrian; DDH HP2 (331.1 m), High Point, western Tasmania.

Plate 31 — Volcaniclastic megaturbidites

1A Graphic log :



1. Mudstone intraclast-rich, normally graded, volcaniclastic turbidite

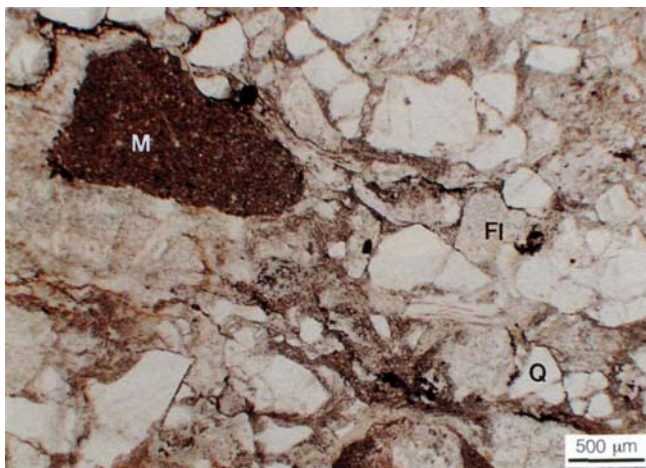
A, B. The graphic log shows a 40 m thick, normally graded unit overlying laminated black mudstone. Poorly sorted, polymict lithic breccia (**Bx**) at the base of the unit includes abundant mudstone intraclasts (**M**), volcanic lithic clasts, relict pumice and rare massive sulfide clasts in crystal-rich sandstone matrix. The finer top of the unit is moderately sorted, diffusely bedded sandstone (**St**), rich in feldspar and quartz crystal fragments (about 30%), relict shards and minor pumice clasts. The internal organisation indicates deposition from a high-density turbidity current which locally eroded the underlying poorly consolidated mud substrate. The grain size range and particle types suggest that the volcanic components were generated by an explosive, silicic eruption and the unit is probably a syn-eruptive deposit.

Mount Read Volcanics, Cambrian; G10 Pit, Hercules mine, western Tasmania.



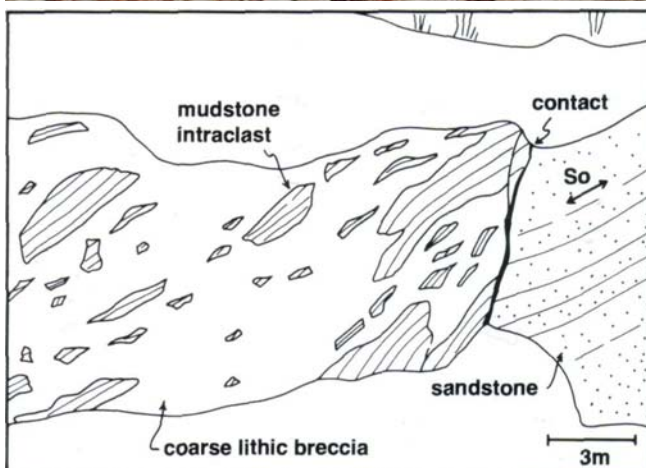
C. Mudstone intraclasts (**M**) in the basal polymict lithic breccia of the unit shown in **31.1A** and **31.1B** have slabby shapes and are preserved in various stages of disintegration. The pale matrix consists of abundant quartz and feldspar crystals, with lesser relict pumice clasts and shards (evident in thin-section).

Mount Read Volcanics, Cambrian; G10 Pit, Hercules mine, western Tasmania.



D. This photomicrograph shows the crystal-rich character of the sandstone matrix of the polymict lithic breccia in **31.1C**. Dominant components are sub-angular feldspar (**Fl**) and quartz (**Q**) crystal fragments, accompanied by black mudstone clasts (**M**) and fine, sericitic interstitial material (altered, formerly glassy shards). Plane polarised light.

Mount Read Volcanics, Cambrian; specimen 91-146, G10 Pit, Hercules mine, western Tasmania.



2. Lithic clast-rich base of a volcanoclastic megaturbidite

A. This field sketch shows coarse, polymict lithic breccia (**31.2B**, **31.2C**) at the base of a ~25 m thick graded unit. Above the lithic-rich base is finer volcanoclastic sandstone rich in pumiceous components. The unit overlies medium bedded, volcanoclastic sandstone. Although partly sheared, the contact truncates the gently dipping bedding in the underlying unit. The breccia is interpreted to be the basal part of a deposit from a high-density volcanoclastic turbidity current that eroded the substrate.

Mount Read Volcanics, Cambrian; Hall Rivulet Canal, western Tasmania.



B. The basal contact (**C**) of the coarse, polymict volcaniclastic lithic breccia truncates bedding (**S₀**) in underlying cream, medium bedded sandstone (**St**). The coarse lithic breccia consists of angular to subangular, feldspar-phyric volcanic lithic fragments, dark grey mudstone clasts (**M**) up to 11 m in length, and a sparse matrix of crystal and pumice fragments. Some mudstone clasts are blocky but others have irregular shapes suggesting that they are intraclasts which were not fully lithified at the time of incorporation into the breccia.

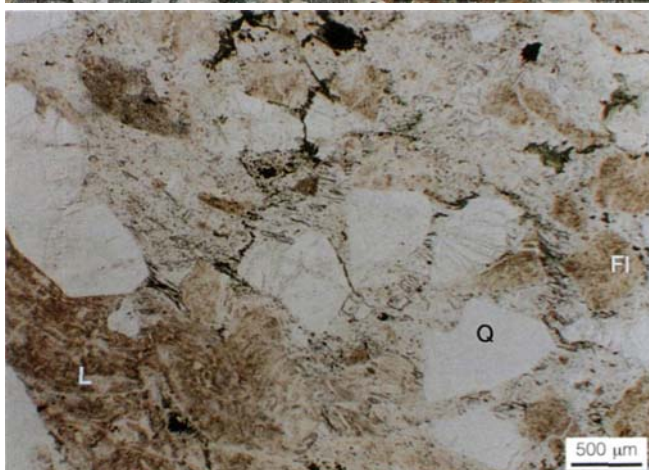
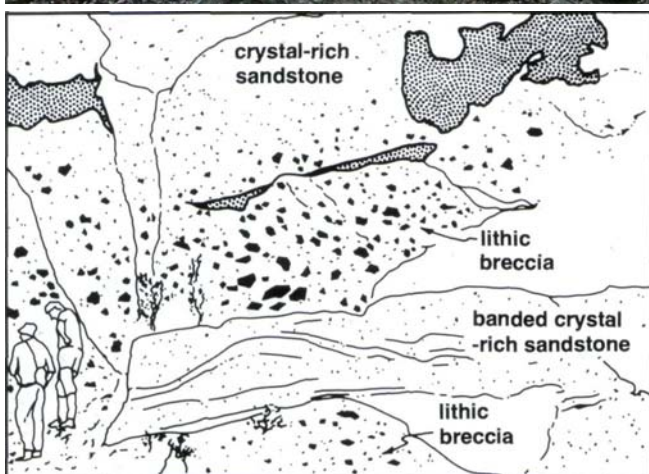
Mount Read Volcanics, Cambrian; Hall Rivulet Canal, western Tasmania.



C. Clasts in the polymict volcaniclastic lithic breccia (**31.28**) are very closely packed. The dominant clast type is pale, angular, feldspar-phyric silicic lava (**V**). Dark grey, irregular mudstone intraclasts (**M**) are also evident.

Mount Read Volcanics, Cambrian; Hall Rivulet Canal, western Tasmania.

Plate 32 — Submarine, lithic-rich, volcaniclastic mass-flow deposits



1. Normally graded, volcaniclastic lithic breccia-sandstone

A, B. Two main lithofacies are evident in this outcrop: (1) a very thick bed graded from volcaniclastic lithic breccia (Bx) at the base to diffusely stratified sandstone (T) at the top; (2) planar bedded, crystal-rich sandstone (St). Pink and green colour banding in the sandstone is defined by alternating pink albite-rich and green chlorite-rich alteration. Both lithofacies are dominated by juvenile volcanic components (angular quartz and feldspar crystals, angular volcanic lithic fragments) that may have been produced by explosive eruptions, but the lithofacies organisation is typical of deposits from successive, subaqueous, high-concentration, volcaniclastic, granular mass flows. The lithofacies are markedly enriched in relatively dense components (crystals, lithic fragments), and depleted in vitric components (pumice, shards) compared with primary pyroclastic flow deposits.

Mount Read Volcanics, Cambrian; Anthony Road, western Tasmania.

2. Polymict, volcaniclastic lithic breccia

A. Lithic breccia at the bases of graded units shown in 32.1 is polymict. The most abundant lithic fragments are dark blue-grey, angular, quartz- and feldspar-bearing, welded ignimbrite and porphyritic lava. They are supported in quartz and feldspar crystal-rich matrix, and surrounded by pinkish haloes of albite alteration.

Mount Read Volcanics, Cambrian; Anthony Road, western Tasmania.

B. A photomicrograph of the crystal-rich matrix of the breccia in 32.2A shows angular quartz (Q) and feldspar (Fl) crystal fragments, and welded ignimbrite lithic (L) fragments separated by fine grained, patchy albite and chlorite (alteration products). Plane polarised light.

Mount Read Volcanics, Cambrian; specimen ARA 4B, Anthony Road, western Tasmania.



3. Chloride clasts in polymict, volcaniclastic lithic breccia

Dark green, very irregularly shaped, ragged chloritic clasts (L) are a minor but conspicuous component of the volcaniclastic lithic breccia shown in 32.1 and 32.2. They contain evenly distributed, euhedral feldspar crystals. The chlorite probably replaces an originally glassy groundmass. Although they may be relict pumice clasts, no vesicular texture is preserved. Instead, they could have been glassy but non-vesicular juvenile clasts (vitriclasts) that have accommodated to the shapes of adjacent rigid lithic fragments after alteration to "weak" chlorite.

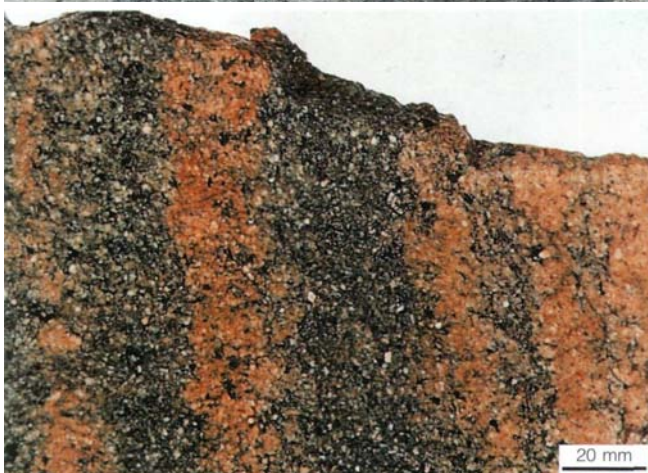
Mount Read Volcanics, Cambrian; Anthony Road, western Tasmania.



4. Pink and green banded, crystal-rich sandstone

In detail, the pink-green banding in the crystal-rich sandstone (St in 32.1) is diffuse and not obviously coincident with grain size or component changes. The bands are commonly but not always parallel to bedding. One interpretation is that albite (pink) and chlorite (green) alteration has accentuated subtle shear-induced primary layering in the sandstone intervals.

Mount Read Volcanics, Cambrian; Anthony Road, western Tasmania.



5. Pink and green banded, crystal-rich sandstone

A. The diffuse banding in this coarse, crystal-rich sandstone is imparted by pink albite-rich and green chlorite-rich bands. The sample comes from a 4 m thick interval that gradation-ally overlies about 10 m of massive, lithic- and crystal-rich volcaniclastic sandstone in the same sequence as that illustrated in 32.1. The marked crystal enrichment in the banded volcaniclastic sandstone may be the result of loss of original vitric components (pumice, shards) by sorting according to density during subaqueous transport.

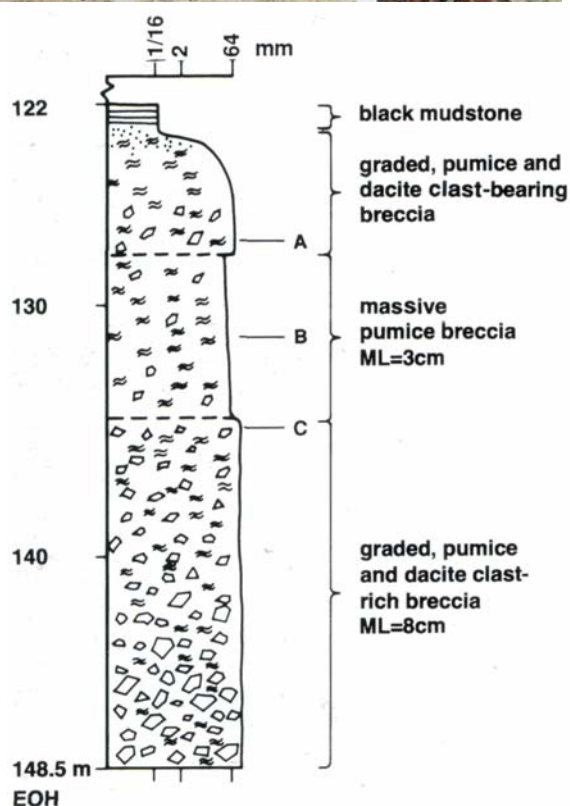
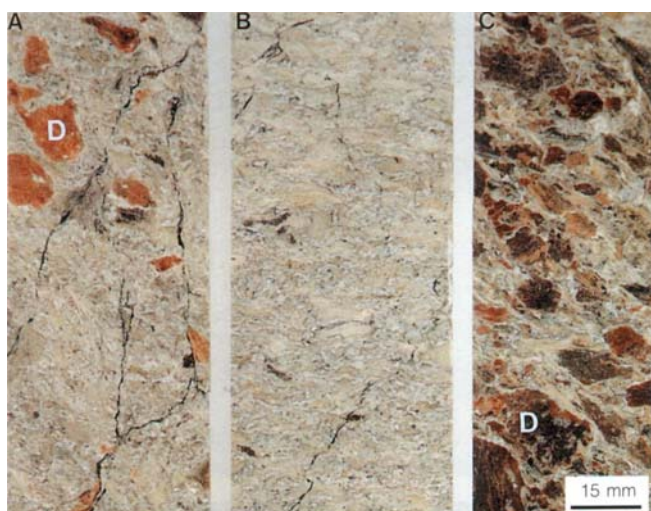
Mount Read Volcanics, Cambrian; specimen 76812, Anthony Road, western Tasmania.



B. A photomicrograph from a green band in 32.5A shows abundant plagioclase and subordinate quartz crystals and crystal fragments, together with sparse volcanic lithic fragments. Chlorite in the dark green bands may be replacing formerly glassy components. In the pink bands interlocking albite occurs between the crystal fragments and completely obscures pre-existing microtextures. Plane polarised light.

Mount Read Volcanics, Cambrian; specimen 76812, Anthony Road, western Tasmania.

Plate 33 — Components in subaqueous, volcanoclastic mass-flow deposits



1. Pumice- and lithic-rich breccia

These three samples come from a thick (>25 m), unstratified, volcanoclastic breccia unit (33.2) in which the dominant component is relict tube pumice. The unit occurs within a submarine, below wave base sequence, and is closely associated with in situ coherent dacite lava. The pumice clasts are not necessarily pyroclasts — they may instead be resedimented from the pumiceous carapace of a nearby submarine lava dome or flow.

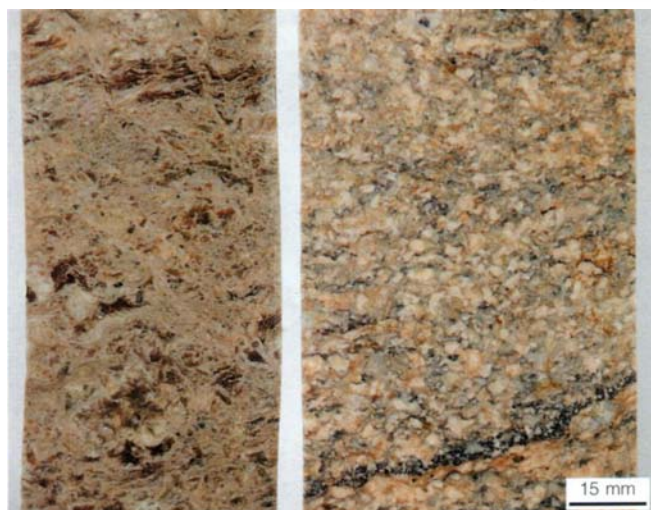
A. Pale green, aphyric relict pumice fragments have ragged margins and undeformed tube vesicle texture. They are closely packed and accompanied by pink, angular, perlitic, dacitic lava clasts (D), and very sparse feldspar crystal fragments.

B. The relict pumice clasts in this pumice breccia show tube vesicle texture in random orientations, and are clearly non-welded.

C. Lower in the unit, angular, pink and brown, perlitically fractured, dacitic lava clasts (D) are much more abundant and occur together with relict pumice clasts.

2. Graphic log of the pumice- and lithic-rich breccia illustrated in 33.1.

Mount Read Volcanics, Cambrian; DDH SCS2 (A, 127.5 m; B, 132 m; C, 134.8 m), Sock Creek South, western Tasmania.



3. Relict sparsely porphyritic tube pumice

Randomly oriented relict pumice clasts have ragged margins and show the fibrous texture characteristic of tube pumice. They occur in a submarine mass-flow deposit and have been resedimented from a subaerial or shallow water source.

Mount Read Volcanics, Cambrian; DDH MAC22 (320 m), Hellyer mine, western Tasmania.

4. Relict coarsely porphyritic pumice

Coarsely quartz- and feldspar-phyric relict pumice clasts are closely packed so that margins of adjacent clasts are indistinct. The strong bedding-parallel foliation is the result of diagenetic compaction, not primary welding, of the pumiceous clasts.

Mount Read Volcanics, Cambrian; DDH HL541

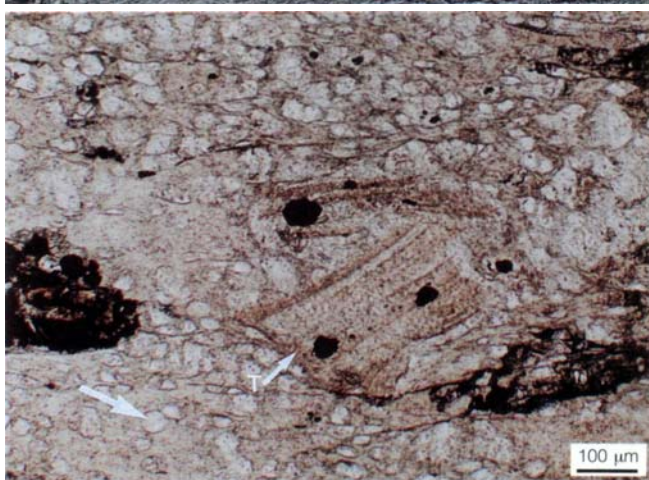


(60.2 m), Hellyer mine, western Tasmania.

5. Altered pumiceous sandstone

A. This grey, non-descript, massive to diffusely layered outcrop occurs at the top of very thick (several tens of metres), feldspar-phyric tube pumice breccia units in the footwall to the Hercules massive sulfide deposit. The pumice clasts are considered to be pyroclasts produced by an explosive silicic eruption in the vicinity, and redeposited by syn-eruptive, submarine, volcanoclastic mass flows (Allen and Hunns, 1990). Millimetre pumice wisps are visible with a hand lens but require a careful search.

Mount Read Volcanics, Cambrian; 4-Level Road, Hercules mine, western Tasmania.



B. Samples from the outcrop in 33.5A are composed of millimetre-sized tube pumice wisps (T), together with minor feldspar crystals. The pumice wisps are variably compacted but are non-welded and have well preserved, undeformed vesicular microtextures. The vesicles (arrow) are now filled with albite(?) and vesicle walls have been replaced by sericite. Plane polarised light.

Mount Read Volcanics, Cambrian; specimen 41971, 4-Level Road, Hercules mine, western Tasmania.



6. Polymict volcanoclastic lithic breccia

This very poorly sorted breccia consists mainly of dacite (D) fragments with minor chert (C) pebbles and mudstone intraclasts. The dacite clasts are feldspar-phyric, flow banded (F), spherulitic and blocky with highly irregular margins. The matrix comprises volcanic lithic granules in dark grey mud and is locally pyritic (P). The breccia is part of a below-wave-base, relatively deep submarine sequence. The dacite clasts probably came from a local, intrabasinal source and may have been generated by quench fragmentation. They have been mixed with other clast types and with the mud matrix during subsequent mass-flow resedimentation.

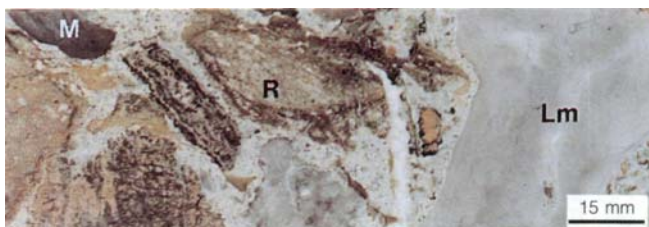
Mount Read Volcanics, Cambrian; specimen HL-2, Hellyer mine, western Tasmania



7. Mixed provenance submarine mass-flow deposits

Rounded non-volcanic clasts of polycrystalline quartz, chert, mudstone and metapelite have been reworked in a subaerial or shoreline environment prior to resedimentation. The pale volcanic clasts probably came from a submarine source.

Mount Read Volcanics, Cambrian; DDHMAC20 (275.5 m), Hellyer mine, western Tasmania.



8. Mixed provenance submarine mass-flow deposits

Trilobite-bearing limestone clasts (Lm) have been rounded in a shallow submarine environment prior to re-sedimentation. Rhyolite clasts (R) came from a submarine lava, and have not been reworked. Mudstone fragments (M) are intraclasts.

Mount Read Volcanics, Cambrian; DDH MAC20 (354 m), Hellyer mine, western Tasmania.

Plate 34 — Deposits from subaqueous volcanoclastic debris flows



1. Subaqueous debris-flow deposits: volcanoclastic breccia and sandstone

Tabular medium and thick beds in this outcrop consist predominantly of angular porphyritic andesite clasts supported in a mud- to sand-sized matrix. Some beds show reverse, coarse-tail grading and pass gradationally or sharply upward into massive or diffusely laminated, poorly sorted sandstone (St). The breccia beds are interpreted to be deposits from submarine debris flows, and the sandstone intervals may comprise sediment settled rapidly from accompanying, more dilute turbulent suspensions (Kokelaar et al., 1990).

Whorneyside Bedded Tuff, Ordovician; Sourmilk Gill area, Borrowdale, English Lake District, UK.



2. Submarine mass-flow deposits: volcanic lithic breccia

The lower 1.5 m thick, tabular bed of volcanoclastic lithic breccia is reversely graded from a matrix-rich base to a coarse clast-rich top. The clasts are dacitic (pale) and andesitic (dark) lava. The lithofacies characteristics suggest deposition from a density-modified grain flow in which matrix strength, clast buoyancy and dispersive pressure probably all contributed to the support of coarse dense clasts (cf. Lowe, 1982). The upper part consists of a 1 m thick bed of a very poorly sorted, matrix-supported, volcanoclastic lithic breccia interpreted to be the deposit from a cohesive debris flow. These beds were deposited in a submarine, below-wave-base setting. Notebook (arrow) for scale.

Green Tuff Belt, Miocene; Suttu Peninsula, Hokkaido, Japan.



3. Submarine mass-flow deposits: reversely graded volcanoclastic lithic breccia

The two mass-flow depositional units in this outcrop show weak reverse grading of angular, andesitic lava clasts. They were deposited in a below-wave-base, submarine setting. The lower clast-rich, clast-supported unit may be a density-modified grain-flow deposit, whereas the upper, matrix-rich unit is interpreted to be a debris-flow deposit. Rucksack for scale.

Green Tuff Belt, Miocene; Kabuto, Shakotan Peninsula, Hokkaido, Japan.

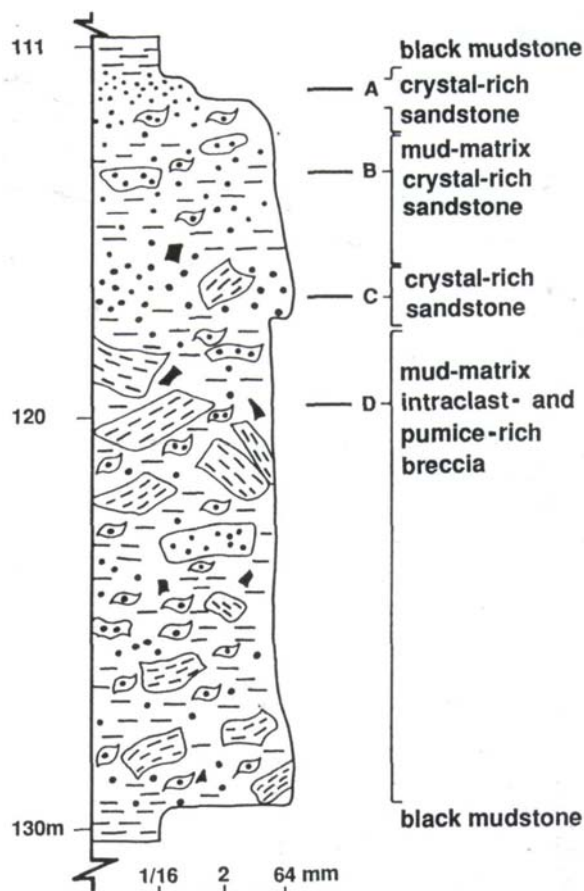


4. Texture of a subaqueous volcanoclastic debris-flow deposit

Poorly sorted, millimetre- to centimetre-sized scoriaceous basalt and white lithic clasts are dispersed in mud-rich matrix. The breccia occurs in a thick, massive unit within a submarine volcanoclastic and mudstone sequence and has textural and lithofacies features consistent with deposition from a submarine debris flow.

Bunga Beds, Late Devonian; Bunga Head, New South Wales.

Graphic log : HP2



5. Submarine syn-eruptive debris-flow deposit: very poorly sorted, mud matrix, volcanoclastic breccia

The graphic log shows part of a texturally complex, 160 m thick, volcanoclastic interval within which the relative proportions and size of the principal components change considerably. The interval occurs within a thick sequence of black, laminated, trilobite-bearing mudstone and was deposited in a submarine, below-wave-base setting. The juvenile volcanic components are feldspar and quartz crystals, feldspar- and quartz-phyric relict pumice clasts, and relict shards. Other components are black mudstone intraclasts, black mud matrix and sparse volcanic lithic clasts. The mudstone intraclasts were clearly unconsolidated when incorporated and their disintegration contributed to the mud matrix. Some mudstone intraclasts are highly contorted and have sharp boundaries. Others contain scattered quartz and feldspar crystals and merge with the mud matrix. The composition and organisation suggest that the interval was deposited from high-concentration, volcanoclastic mass flows, probably debris flows, that incorporated a significant volume of the largely unconsolidated mud substrate during flowage. The volcanic components are juvenile pyroclasts and were generated by an explosive, rhyolitic eruption from a shallow submarine or subaerial vent nearby. Photographs 34.5A to 34.5D show samples from the top half of the graphic log section.

Mount Read Volcanics, Cambrian; DDH HP2, High Point, western Tasmania.



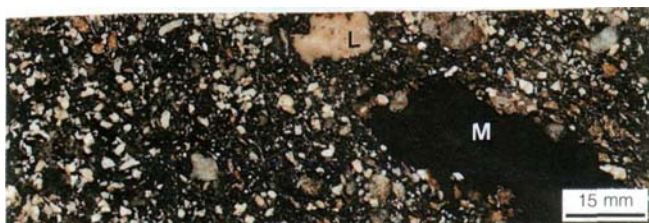
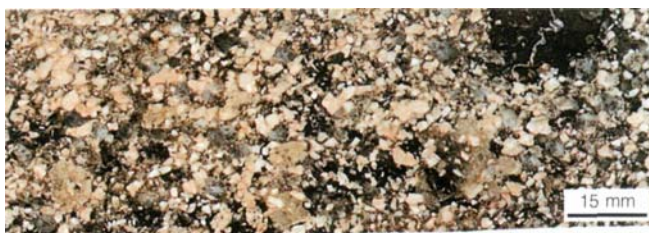
A. Poorly sorted, crystal-rich, coarse sandstone (right) grades into diffusely laminated, crystal-rich, fine sandstone (left). The topmost part of the main debris flow was probably more dilute than the rest, and formed deposits similar to sandy high-density turbidites. The arrow shows the younging direction.

Mount Read Volcanics, Cambrian; DDH HP2 (112 m), High Point, western Tasmania.



B. The pale juvenile volcanic components (crystals, relict pumice wisps) in this poorly-sorted crystal-rich sandstone are thoroughly but inhomogeneously mixed with the black and dark grey mud matrix.

Mount Read Volcanics, Cambrian; DDH HP2 (114 m), High Point, western Tasmania.



C. This part of the unit is markedly crystal-rich and poor in dark grey mud matrix. Coarse quartz and prismatic feldspar crystals dominate over relict pumice, volcanic lithic clasts and mudstone intraclasts.

Mount Read Volcanics, Cambrian; DDH HP2 (117 m), High Point, western Tasmania.

D. Mudstone intraclasts (M) and mud matrix are conspicuous at this level in the unit. Feldspar-bearing volcanic lithic fragments (L) and pumice clasts are also present. Mudstone intraclasts are contorted and some include crystal fragments near their margins.

Mount Read Volcanics, Cambrian; DDH HP2 (119.6 m), High Point, western Tasmania.

Plate 35 — Deposits from subaerial lahars and volcaniclastic debris flows



1. Modern lahar deposits, Armero, Colombia

Melting of snow and ice by deposits of the 13 November 1985 eruption of Nevado del Ruiz volcano initiated dilute floods which rapidly transformed to lahars downstream (Naranjo et al., 1986; Pierson et al., 1990). After flowing about 74 km the lahars emerged from Rio Lagunillas valley and branched into three lobes that inundated an area of 34 km². The smallest lobe (X) followed the SE trend of the Rio Lagunillas, the principal lobe continued directly east (Y) destroying most of Armero and killing 22,000 inhabitants, while the third travelled northward (Z). Armero is built on part of a volcaniclastic fan constructed by older lahar deposits.

View of Armero, Colombia, after the AD 1985 eruption of Nevado del Ruiz volcano.



2. Channelised lahar course, Rio Lagunillas, Colombia

In the Rio Lagunillas valley, vegetation and soil have been scoured from the river bed and walls, and incorporated in lahars sourced at Nevado del Ruiz volcano. Bedrock is exposed in many places, leaving a trim line (T) 20—30 m above normal river level. Deposits along the channel show that the debris flows were inhomogeneous, and varied in rheology and particle concentration both vertically and laterally during flowage. Most of the scoured material was deposited after the debris flows reached the mouth of the valley and spread across the gentle slopes at and beyond Armero (35.1, 35.3). Note person for scale (arrow).

Rio Lagunillas near Armero, Colombia, after the AD 1985 eruption of Nevado del Ruiz volcano.



3. Modern lahar deposit, Rio Lagunillas, Colombia

The 13 November 1985 lahars formed a thick (~5 m) muddy bouldery gravel deposit (D) at the mouth of the Rio Lagunillas valley upstream from Armero. The deposit is very poorly sorted, unstratified and has a tabular bed geometry with a gently sloping upper surface. The post-1985 river (arrow) has cut deeply into the 1985 and older lahar deposits.

Lahar deposits along the Rio Lagunillas, AD 1985; near Armero, Colombia.



4. Debris-flow deposit: poorly sorted volcanoclastic boulder conglomerate

This section exposes a 15 m thick deposit comprising a very poorly sorted mixture of clay, sand and boulders up to 2-3 m across. Slope wash has nearly concealed the basal contact (dashed line). Boulders display crude reverse grading at the base and normal grading towards the top. The conglomerate is interpreted to be the deposit from voluminous volcanoclastic debris flows initiated by avalanches of hydrothermally altered rock from the summit of Mount Rainier triggered by volcanic explosions (Crandell, 1969, 1971).

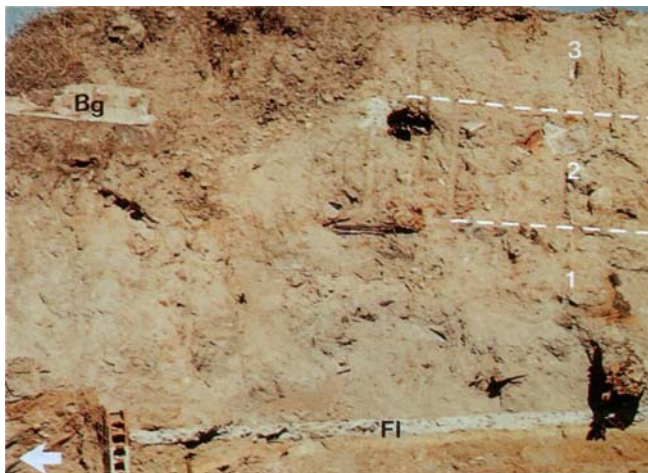
Osceola mud-flow deposit, 5700 a; Inter Fork, Mount Rainier, Washington, USA.



5. Modern volcanoclastic sandy lahar deposit

Primary pyroclastic and volcanic debris-avalanche deposits from the May 18, 1980, eruption of Mount St. Helens have been rapidly resedimented and reworked by fluvial processes and lahars. The fluvial deposits (F) in this exposure are dominated by planar and cross-laminated sand and pebbly sand. They are interbedded with a 60 cm thick, diffusely stratified, poorly sorted sand and granule lahar deposit (L). The bed has a planar, locally erosive base. The top is irregularly incised by an erosion surface and has been fluvially reworked. In this case, the lahars were probably hyperconcentrated flows transitional to debris flows.

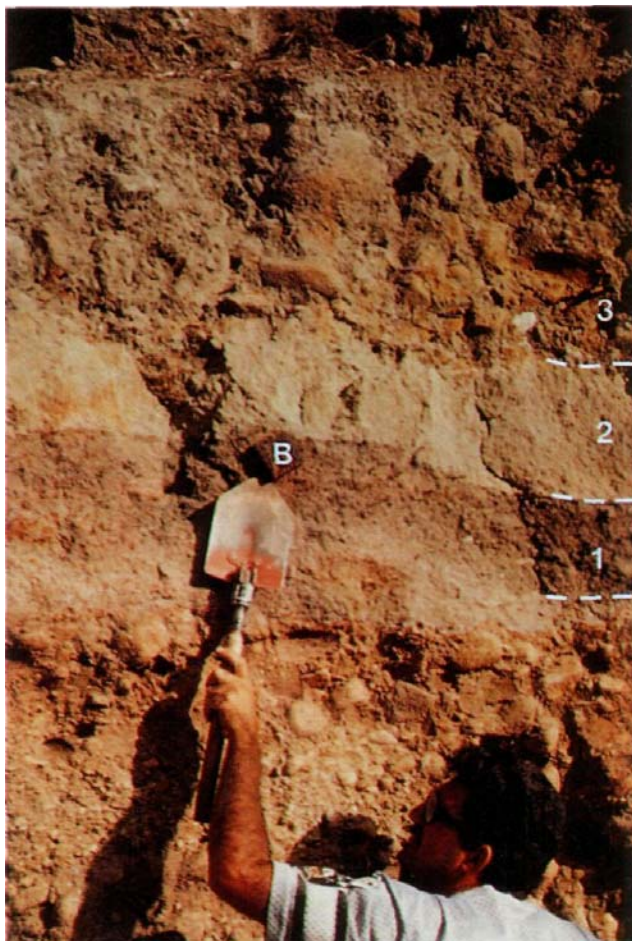
Post-May 1980 fluvial and lahar deposits near Cold Water Creek, Mount St Helens, USA.



6. Modern lahar deposit

The three units (1, 2, 3) evident in this outcrop are deposits from lahars generated by heavy rain on unconsolidated fresh ash and colluviurn at the source volcano. The lowermost unit (1) destroyed and buried a building at this site, the floor (FI) of which remains. The deposits are poorly sorted sand-boulder mixtures comprising abundant anthropogenic clasts (e.g. building fragments, Bg) and minor juvenile basaltic andesite ash. The lahars flowed from right to left (arrow) and originated about 12 km away from this site. The section is about 2.5 m thick.

Lahar deposits generated during the AD 1963–64 eruption of Irazu; Cartega, Costa Rica.



7. Modern lahar deposit

The units labelled 1 to 3 are deposits from rain-triggered lahars, and consist of diverse lithic and anthropogenic fragments (e.g. house brick, B) supported in a sandy matrix. The distinctly rounded clasts in unit 3 have been "recycled" from alluvial deposits traversed en route. Alluvial deposits also occur at the base of the sequence. Although generated on a volcano during an eruptive period, juvenile components (basaltic andesite ash) are minor. The lahars ranged from hyperconcentrated flows to debris flows, and were sourced some 12 km away.

Lahar deposits generated during the AD 1963-64 eruption of Irazu; Cartega, Costa Rica.

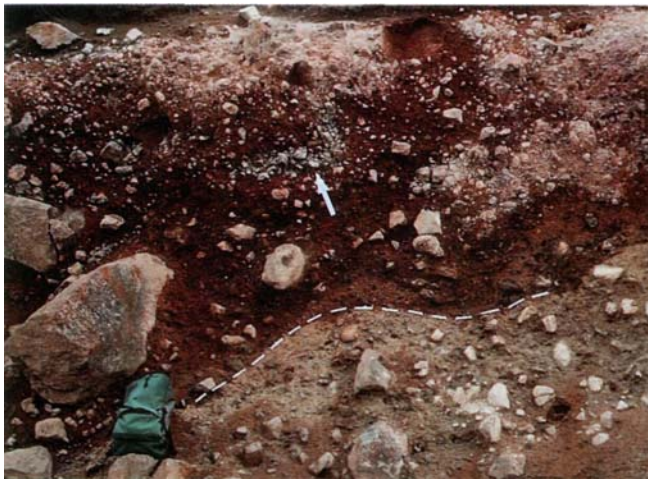
Plate 36 — Subaerial grain-flow and volcanic debris-avalanche deposits



1. Modern volcaniclastic grain-flow deposits

These lenticular beds comprise matrix-poor, clast-supported, granule- to pebble-sized volcanic lithic and pumice fragments. The beds have steep (30°) primary dip and are reversely graded. They are part of a modern scree slope and are typical of deposits emplaced by grain flows in which dispersive pressure and grain interaction contribute to clast support during gravity-driven flowage (Lowe 1982).

Camaldoli Hill, Naples; Campi Flegrei, Italy.



2. Volcanic debris-avalanche deposit: very poorly sorted, volcanic lithic breccia

This cutting exposes the interior of a hummock in a young volcanic debris-avalanche deposit. There is a clear boundary (dashed line) between areas of the deposit in which the colour of the matrix differs. Each area consists of angular lava clasts, some showing jigsaw-fit texture (arrow), supported within sandy matrix. The lava clasts were generated by brittle fracture and dilation of debris avalanche lava blocks, and have progressively mixed with finer components derived from disintegration of softer lithologies during gravity-driven flow.

Murimotu Lahar Formation, 9500 a; western ring plain of Ruapehu volcano, New Zealand.



3. Jigsaw-fit texture in a debris-avalanche deposit

Clusters of clasts within the volcanic debris-avalanche deposit shown in 36.2 display jigsaw-fit texture characteristic of in situ fragmentation. Abundant small fragments of dacite lava can be fitted back together to reconstruct the outline of a larger clast (within dashed line). During flowage in the debris avalanche, pieces of in situ fractured blocks progressively separated and mixed with clasts from adjacent blocks. Fracturing is the result of dilation of blocks at the time of failure and brittle shattering due to collisions during transport (Glicken 1991).

Murimotu Lahar Formation, 9500 a; western ring plain of Ruapehu volcano, New Zealand.



4. Volcanic debris-avalanche deposit and slide blocks

Collapse of the summit area of Socompa (6051 m) generated a vast (600 km²) debris-avalanche deposit and created a 10 km wide amphitheatre that has been partly healed by post-collapse lava flows and domes (F). Large slide blocks (S) form an elongate massif at the mouth of the amphitheatre. Irregular fields and linear trains of red weathering lava boulders (36.6), dominate the subdued hummocky (H) topography of the debris-avalanche deposit (foreground). The "Campo Amarillo" flow deposit (C) mantles the proximal parts of the avalanche deposit and suggests that failure triggered a pyroclastic eruption (Francis et al., 1985; Francis and Wells, 1988).

Socompa volcano and the 7200 a volcanic debris-avalanche deposit, northern Chile.



5. Relict source stratigraphy in a debris avalanche block

This view shows a large debris avalanche block comprising a mound of pumiceous ignimbrite mantled by clasts of grey dacite lava. The ignimbrite plus dacite are allochthonous parts of the original source stratigraphy, and have been transported more or less together and intact by the debris avalanche. The ignimbrite in the blocks is pervasively internally sheared but has behaved in a relatively ductile fashion during flowage, whereas the dacite lava has broken up into abundant separate clasts. Note person for scale (arrow).

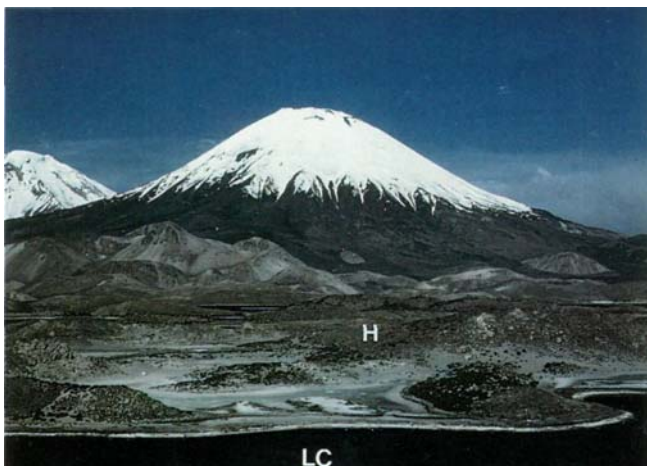
WNW margin of the primary debris avalanche deposit, 7200 a; Socompa volcano, northern Chile.



6. Prismatically jointed dacite lava block in a volcanic debris-avalanche deposit

This large (>20 m) prismatically jointed, glassy dacite lava block occurs within the primary debris-avalanche deposit on Socompa. Such blocks were probably transported hot and developed the pattern of prismatic cooling joints only after deposition. They may have been derived from an active lava flow or dome on the summit of the volcano at the time of collapse (Francis et al., 1985; Francis and Wells, 1988). Most of the joints are curvilinear and divide the block into equant polygons.

Volcanic debris avalanche deposit, 7200 a; Socompa volcano, northern Chile.



7. Hummocky debris-avalanche deposit

Late Pleistocene collapse of the SW sector of Parinacota volcano (6348 m) generated a debris avalanche which altered local hydrology by damming earlier drainages (Francis and Wells, 1988; De Silva and Francis, 1991). Lake Cotocotani (LC) and many small lakes are nested on the hummocky terrane (H) of the debris-avalanche deposit and are maintained by seepages through it. Post-collapse andesitic lava flows have healed the avalanche detachment scarp. The summit of Pomerape, another composite andesitic volcano, is evident in the background.

Volcanic debris avalanche deposit, 13.5 ka; Parinacota volcano, northern Chile.

Plate 37 — Massive sulfide clasts in submarine volcanoclastic mass-flow deposits



1. Normally graded, volcanoclastic lithic breccia—sandstone

This photograph shows part of a 13m thick, graded, polymict, lithic breccia—diffusely bedded, crystal-rich sandstone unit. Clasts in the breccia comprise abundant dacite, and less abundant rhyolite and andesite fragments, together with minor chert, massive sulfide and mudstone clasts. The matrix of the breccia consists of volcanic lithic granules and crystal fragments. The breccia has a sharp basal contact, and the lower parts are clast- to matrix-supported, and reversely graded. Upper parts are dominantly matrix-supported and normally graded. The lithofacies organisation suggests deposition from a high-density, gravelly and sandy turbidity current.

Mount Read Volcanics, Cambrian; Newton Dam Spillway, western Tasmania.



2. Crystal-rich volcanoclastic sandstone

There are scattered dacite clasts (D) up to a metre across in the lower part of the diffusely bedded crystal-rich sandstone shown in 37.1. The sandstone probably accumulated by rapid aggradation at the base of a residual, coarse clast-depleted, sandy high-density turbidity current following deposition of the lithic breccia. The isolated coarse lithic clasts are lags that would have been transported as bedload at the base of the mass flow.

Mount Read Volcanics, Cambrian; Newton Dam Spillway, western Tasmania.



3. Jigsaw-fit texture in clasts in volcanoclastic lithic breccia

Within the lower polymict, volcanoclastic breccia shown in 37.1, groups of dacite clasts locally show jigsaw-fit texture (arrow). Many of the clasts have curvilinear margins. The clasts may have been hot when incorporated in the mass flow and broken in situ by quench fragmentation after deposition, or else were entrained cold but with pre-prepared fractures that progressively opened during transport. In either case, a dacite lava dome or flow contributed most of the clasts, and gravitational collapse, hot or cold, probably initiated the high-density turbidity current.

Mount Read Volcanics, Cambrian; Newton Dam Spillway, western Tasmania.



4. The massive sulfide clasts

The lithic breccia featured in 37.1 and 37.3 contains at least 11 clasts of massive sulfide (C). They are purple-grey, angular to subrounded, and dominated by sphalerite and galena with only minor chalcopyrite and pyrite. Results of lead isotope analyses of galena from one of the clasts illustrated, and four others, fall within the field defined by Cambrian volcanic-hosted massive sulfide deposits in the Mount Read Volcanics (Gibson, 1991). The massive sulfide clasts may have come from the same source as the dacite lava clasts that dominate the lithic breccia (Fig. 53), or else from a separate source traversed en route by the mass flow.

Mount Read Volcanics, Cambrian; Newton Dam Spillway, western Tasmania.



5. Massive sulfide clasts in dacite breccia

The dacite lava breccia shown here occurs at the margin of a submarine dacite lava dome and contains dark grey massive sulfide clasts (arrows). The host breccia is altered (fuchsite) and weathered, but probably originated by resedimentation of dome-derived hyaloclastite. The source of the sulfide clasts may have been a sulfide deposit on the flanks of the dome.

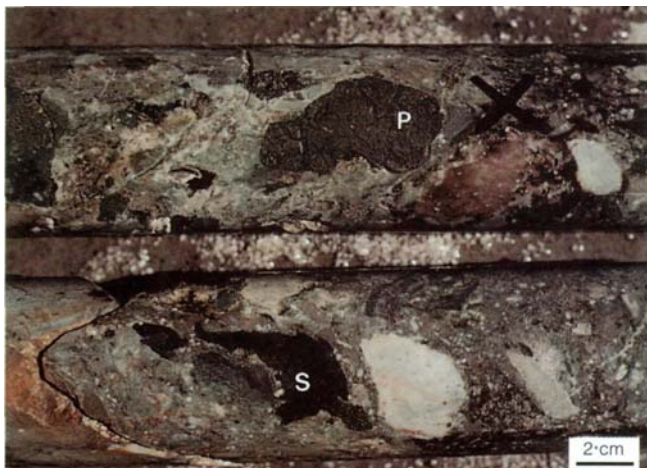
Mount Read Volcanics, Cambrian; Hellyer mine haulage road, western Tasmania.



6. Sulfide clasts in polymict, volcanic breccia

Polymict, volcanic lithic breccia in this outcrop forms the base of a very thick (> 10m) volcanoclastic megaturbidite. Most of the clasts are subrounded quartz- or feldspar-phyric lava and the matrix is crystal-rich sandstone with minor relict pumice shreds. The clast of massive sulfide that occurs beside the hammer head was probably collected en route from a sulfide deposit traversed by the parent submarine mass flow.

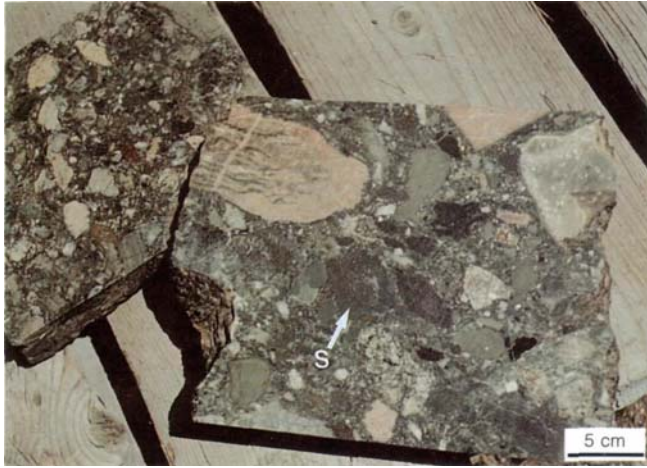
White Spur Formation, Mount Read Volcanics, Cambrian; Howards Road, western Tasmania.



7. Massive sulfide clasts in breccia in drill core

This drill core section of volcanic lithic breccia is texturally similar to that shown in outcrop in 37.6, and also contains massive pyrite (P) and massive sphalerite (S) clasts. The breccia forms the lithic-rich base of a mass-flow unit and consists of pale quartz- and feldspar-phyric lava clasts and pumiceous, crystal-rich sandstone matrix.

White Spur Formation, Mount Read Volcanics, Cambrian; near Howards Road, DDH MR1 (41 m), western Tasmania.



8. Massive sulfide clasts in polymict breccia

Dark grey, massive sulfide (S) and white barite clasts occur together with flow-banded rhyolite, siltstone, granite and altered volcanic lithologies. The breccia is very poorly sorted and matrix supported, and interpreted to be a submarine debris-flow deposit (Binney, 1987). More than 50% of the massive sulfide ore produced at Buchans comes from clasts within mass-flow deposits.

Hangingwall volcanic breccia, Buchans VHMS deposit, Ordovician; Newfoundland, Canada.

Plate 38 — Traction current structures in volcanogenic sediments and pyroclastic surge deposits



1. Reworked accretionary lapilli in volcanogenic sediments

Whole and broken accretionary lapilli (A) occur in planar and cross-laminated (arrow), pumiceous volcanogenic fluviolacustrine sediments generated by reworking of non-welded rhyolitic pyroclastic deposits. Rounding of pumice and abrasion of the outer fine grained rims of some accretionary lapilli, together with the bedforms, are features that indicate fractional transport and reworking.

Modern fluviolacustrine volcanogenic sediments, Taupo Volcanic Centre, Tongariro River Bridge, New Zealand.



2. Cross stratification in fluvial volcanogenic sediments

These volcanogenic sediments were generated by fluvial erosion and reworking of primary, mostly pyroclastic deposits. Granule and pebble components are mainly well rounded, rhyolitic pumice and volcanic lithic clasts. Finer components (sand and silt) consist of quartz and feldspar crystals, pumice and glass shards. The sediments are poorly size sorted: sand- and granule-size lithic and crystal particles occur together with pebble-size pumice. Hydraulic sorting during transport and deposition strongly reflects particle density. Poor size sorting but good density sorting is a common feature of pyroclast-rich sediments which consist of particles that range widely in density.

Hinuera Formation, Late Pleistocene; Daltons Sand Pit, Hauraki Rift, New Zealand.



3. Megaripples in shallow submarine, volcanogenic granule conglomerate

The poorly sorted, medium and thick, granule conglomerate beds (M) are mass-flow deposits, the tops of which have been reworked by storm waves resulting in megaripple bedforms (R) on upper surfaces. The megaripples are draped by normally graded fine sandstone and siltstone deposited from suspension and/or from dilute turbidity currents following storms. The lithofacies association indicates a shallow submarine depositional setting, most probably between fair weather and storm wave base (Kokelaar, 1990). Pen for scale (arrow).

Bedded Pyroclastic Formation, Ordovician; Llanberis Pass, northern Wales, UK.



4. Angle-of-repose cross stratification in shallow submarine pumiceous sandstone

The large scale, angle-of-repose cross stratification in this exposure was formed by a migrating sandwave in a transgressive, tide-dominated, innermost shelf environment. The depositional setting was above wave base and probably in water from 5 to 20 m deep (Abbott and Carter, in press). Thin mud drapes (arrow) separate poorly sorted, uneven to lenticular pebble conglomerate beds. The coarser beds are composed of rounded pumice and greywacke pebbles, transported shelly fossils and crystals (quartz, feldspar). The mud drapes are dominated by glass shards.

Kaimatira Pumice Sand, mid-Pleistocene; junction of State Highway 4 and Kaimatira Road, Wanganui, New Zealand.



5. Cross stratification in pyroclastic surge deposits

The conspicuous tractional structures in this cutting comprise low-angle cross stratification, planar diffuse very thin bedding and low-angle truncations (arrow). The deposit consists predominantly of poorly sorted basaltic lapilli and ash. The tractional structures were produced by primary pyroclastic surges (base surges) in which the interstitial fluid was hot volcanic gas and steam. The uniform dip of the foresets in the deposits indicate transport from right to left. The sequence is part of the rim of a maar volcano and probably accumulated very rapidly from surges generated by numerous successive explosions over a period of hours or days.

Rim beds of Purumbete maar, Tertiary; western Victoria.



6. Cross lamination in pyroclastic surge deposits

This photograph shows in detail the low-angle cross-stratified basaltic pyroclastic surge deposits illustrated in 38.5. Traction currents of volcanic gas (and steam) generated the good bedding and cross stratification. Some very thin beds are very poorly sorted mixtures of fine ash and lapilli. The presence of steam strongly influences the deposition of fine ash. Moisture makes fine ash pyroclasts clump together and adhere to other larger pyroclasts. Deposition of fine ash together with coarser particles results in the relatively poor sorting that characterises surge deposits and helps distinguish them from primary fallout deposits.

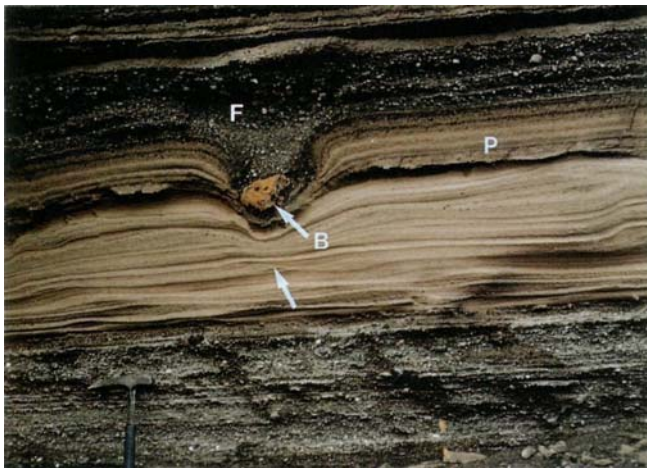
Rim beds of Purumbete maar, Tertiary; western Victoria.



7. Dune bedform in pyroclastic surge deposit

A dune bedform is preserved in this pyroclastic surge (base surge) deposit. The laminae show upward thickening and migration from initially nearly flat beds. A flow direction from left to right is indicated by the asymmetry of the dune. The components are lithic and basaltic ash pyroclasts, and the dune bedform occurs within other more poorly sorted surge deposits in the rim of a small maar volcano.

Ubehebe maar, Holocene; Death Valley, California, USA.



8. Block sag in pyroclastic surge and fallout deposits

The most conspicuous feature is the sag structure caused by impact of a ballistic block (B). The block actually belongs with the dark grey, moderately sorted, planar stratified lapilli fall deposits (F) at the top of the exposure. It has caused deformation of bedding in cream, much finer, stratified ash deposits below. In the lower parts of the cream ash deposits there are subtle unidirectional traction current structures, such as low-angle cross stratification (arrow), attributable to pyroclastic surges. Planar bedded units (P) higher up may be either pyroclastic surge or fall deposits. Dark grey, planar bedded, poorly sorted, lapilli and ash at the base of the exposure are probably pyroclastic surge deposits.

Rim beds of Tower Hill maar, Tertiary; western Victoria.

Plate 39 — Subaerial pyroclastic fall deposits



1. Mantle bedding in subaerial pyroclastic fall deposits

This exposure shows mantle bedding in fallout deposits from several explosive eruptions over a period of 10,000 years. The locality is about 13.5 km from the source. Each fallout layer faithfully mimics the underlying surface. The dark brown intervals are palaeosols that developed in relatively long repose periods between explosive eruptions. The thickness and grain size variations shown by the layers reflect the influence of the size of the eruption, the distance of this locality from the source vent, and prevailing wind directions during fallout. The dashed line marks the base of the pyroclastic fall deposit sequence.

Post-1 Oka fallout deposits from Taupo Volcanic Centre; Rotopuha Road, Taupo, New Zealand.



2. Bedding in subaerial pyroclastic fall deposits

These proximal (less than 2 km from source) fallout deposits show planar, laterally continuous, even bedding. The entire thickness was deposited during plinian phases of one eruption that lasted no more than 60 hours (Fierstein and Hildreth, 1992). The beds are internally massive or weakly graded, clast supported, and composed predominantly of relatively well sorted, angular and ragged dacitic pumice lapilli. Although clast supported, there is very little fine matrix and the pumice lapilli are easily dislodged from the deposit.

Dacitic plinian fallout from the AD 1912 eruption of Novarupta; Valley of Ten Thousand Smokes, Alaska, USA.



3. Pyroclastic fallout: clast-supported pumice lapilli deposit

This fallout deposit comprises well sorted, clast-supported, rhyolitic pumice lapilli. Accessory lithic lapilli (arrow) are markedly finer than the pumice lapilli, reflecting sorting of clasts according to density rather than grain size. Crystal- and shard-rich ash is only very minor at this locality 13.5 km from the source but becomes important in downwind distal deposits. The faint internal stratification can be caused by changes in eruption column height, fragmentation processes or dispersal directions during the eruption. The dark grey layer below the fall deposit is a palaeosol and indicates subaerial deposition.

Waimihia plinian fall deposit, 3.4 ka; Rotopuha Road, Taupo, New Zealand.



4. Proximal fallout: clast-supported pumice lapilli deposit

Closely packed, angular, rhyodacitic pumice lapilli and blocks dominate over much smaller and less abundant lithic lapilli (arrows). The exposure is less than 4 km from the source vent. The larger pumice fragments are pink-brown due to thermal oxidation during relatively slow cooling. Thermal oxidation is normally restricted to juvenile pyroclasts that cool while in contact with air and is a reliable indicator of hot emplacement in a subaerial environment. Some pumice blocks show jigsaw-fit texture (open arrow). In fallout deposits, such fracture patterns result from in situ development of cooling joints or from shattering of clasts on impact with the ground.

Plinian fallout from the 6845 a Mount Mazama eruption; Rim Road, Crater Lake, Oregon, USA.



5. Phreatomagmatic ash fallout: laminated vitric mud

This laminated mud consists almost entirely of glassy ash pyroclasts and was deposited during an explosive, rhyolitic eruption from a vent in a caldera lake. The eruption generated both plinian and phreatoplinian fallout deposits. The phreato-plinian fallout deposits are typically very fine grained. The intraformational gully suggests the presence of abundant surface water during ash deposition. This locality is only 6—7 km from the source, and although very thick (several metres), the entire deposit is very fine grained, indicating that extremely efficient fragmentation processes operated during the eruption. Coin diameter is 28 mm.

Rotongaio Ash, AD 186; Highway 1 cutting, plateau south of Waitahanui, Taupo, New Zealand.



6. Accretionary lapilli-bearing, rhyolitic ash fall deposit

There are abundant, close packed, accretionary lapilli (A) in this ash fall deposit. The bed has diffuse upper and lower contacts and the accretionary lapilli decrease slightly in size from the base to the top. The deposit largely comprises glassy, rhyolitic ash pyroclasts. Abundant accretionary lapilli and fine grain size are typical features of deposits from phreato-magmatic eruptions.

Oruanui Formation, 26.5 ka; Whangamata Road, North Island, New Zealand.



7. Subaerial basaltic fallout: very thick, clast-supported scoria lapilli deposit

This cutting exposes the proximal fallout deposits of a basaltic scoria cone. The principal components are ragged and angular basaltic scoria lapilli, together with minor fluidally-shaped lava bombs (behind the lens cap). The deposit is very thick but only weakly stratified. Locally the scoria pyroclasts display incipient welding. Some scoria lapilli and the rims of the lava bombs are thermally oxidised. These features arise during periods of rapid accumulation in proximal settings that promote effective heat retention.

Mount Eccles scoria cone, Tertiary; western Victoria.



8. Subaerial basaltic fallout: poorly sorted scoria lapilli, bomb and block deposit

Coarse grained, poorly sorted fallout is in most cases confined to relatively proximal settings. This scoria fallout was deposited about 50 m from the vent and forms the rim beds of a scoria cone. Fluidally-shaped lava bombs are separated by closely packed, blocky, angular scoria lapilli. The lava bombs have chilled, poorly vesicular margins, moderately vesicular interiors and are internally jointed. Out of context, the outcrop could be mistaken for pillows and pillow fragment breccia. However, the bombs do not show the distinctive surface textures of pillows, and the blocky scoria lapilli do not have quenched rims.

Eppelsberg scoria cone, Quaternary; Wannenkopfe, Germany.

Plate 40 — Textures and structures in volcanoclastic deposits from suspension, flotation and traction



1. Water-settled accretionary lapilli-bearing fallout deposit

These accretionary lapilli were generated by a large, rhyolitic, phreatomagmatic eruption and fell into a small lake contained in the crater of a scoria cone. They settled through the lake water and have been effectively sorted according to size. The accretionary lapilli rest on an erosion surface (E) in the underlying lacustrine sediments but have not been reworked.

Oruanui Formation, 26.5 ka; Pukeonake, New Zealand.



2. Suspension-settled mudstone associated with volcanoclastic turbidites

Thick beds of massive to weakly graded, shard- and crystal-rich sandstone (St) alternate with laminated black mudstone and very thinly bedded, grey mudstone (M). Stratification in the grey mudstone is largely planar, laterally continuous and even in thickness, although flame structures (F) occur locally. The sandstone beds are interpreted as deposits from low-density turbidity currents. The grey mudstone intervals were formed by sedimentation from dilute suspensions trailing the turbidity currents.

Mount Read Volcanics, Cambrian; Anthony Road, western Tasmania.



3. Flotation: pumiceous rhyolite block in lacustrine sediments

Several metres of thinly bedded, volcanoclastic lacustrine sediments enclose a block of pumiceous rhyolite. Along the base and right hand side of the block are prismatic joints (J) attributable to contraction as those surfaces were rapidly cooled on contact with water. Several similar blocks are exposed in the lacustrine sediments nearby. The blocks were probably spalled from the surface of a sub-lacustrine lava dome, and floated to the edge of the lake where they grounded in near-shore sediments (Wilson and Walker, 1985). Some blocks may simply have settled gently onto the lake floor after becoming water-logged.

Taupo eruption, AD 186; Highway 1, Lake Taupo shore, New Zealand.



4. Suspension and flotation: relict pumiceous clasts in laminated volcanoclastic siltstone

Grey, crystal-rich sandstone (St) is sharply overlain by white, laminated siltstone (Sl). The siltstone occurs at the top of a very thick, volcanoclastic megaturbidite and probably formed by sedimentation from suspension. It contains dark green, evenly porphyritic, blocky and ragged, chloritic (formerly glassy) clasts. The large clasts truncate (arrow) or are mantled by laminae in the siltstone. Although vesicular microstructures are not preserved in the large chloritic clasts, they may be relict pumiceous vitriclasts and have also settled from suspension after flotation.

Mount Read Volcanics, Cambrian; Comstock Valley, western Tasmania.



5. Diverse sedimentation processes: interbedded volcaniclastic mudstone and sandstone

Three lithofacies are present (Smith et al., 1990): (1) planar laminated beds of siltstone and mudstone (M) that were probably deposited from suspension; (2) intervals of coarse grained sandstone with abundant mudstone intraclasts and massive to crudely stratified bases (St) which pass up into planar to low-angle cross-stratified sandstone (P); these probably record rapid deposition from sandy turbidity currents; (3) trough cross-stratified, very coarse sandstone and pebbly sandstone (C), probably generated by tractional reworking of the underlying sediments by currents.

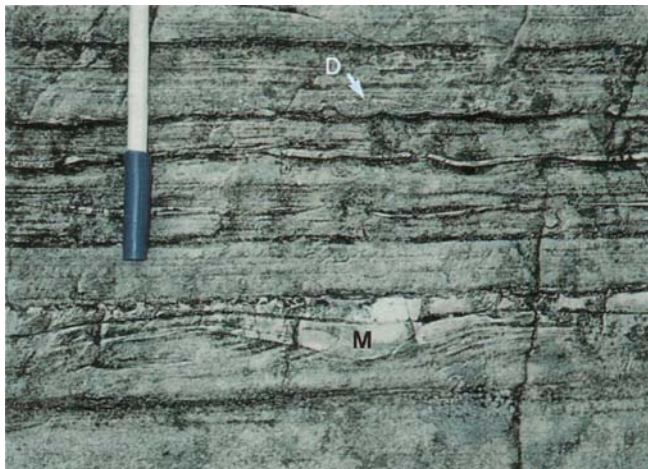
Seathwaite Fell Formation, Ordovician; Lingmoor Fell, English Lake District, UK.



6. Traction and suspension: interbedded volcaniclastic mudstone and sandstone

Two interbedded lithofacies occur in this sequence (Kokelaar et al., 1990): (1) mudstone (M) and sandstone in laterally continuous, even laminae and very thin beds, the tops of which are normally graded; the components are crystal and lithic fragments in a fine-grained, altered, originally vitriclastic matrix; this lithofacies formed by deposition from suspension following fallout of ash onto water; (2) siltstone and sandstone characterised by shallow scours (S) and ripple cross laminae (R) with thin mud drapes; this lithofacies resulted from reworking of suspension sediments by shallow water currents.

Whorneyside Bedded Tuff, Ordovician; Sourmilk Gill, English Lake District, UK.



7. Tractional structures in volcaniclastic sandstone

This sequence has been interpreted as lacustrine, and although deposited mostly below wave base, tractional sedimentary structures are not uncommon (Smith et al., 1990). Graded and diffusely stratified, tabular, thin sandstone beds with sharp bases were probably deposited from low-density turbidity currents. Load structures and dish structures (D) occur in some of the turbidites. The tops of the turbidites were reworked by residual currents, generating tractional bedforms such as ripple cross lamination and planar lamination. Many of the ripples have thin mud drapes (M) which settled from suspension during periods between the influx of turbidity currents.

Seathwaite Fell Formation, Ordovician; North Langdale, English Lake District, UK.

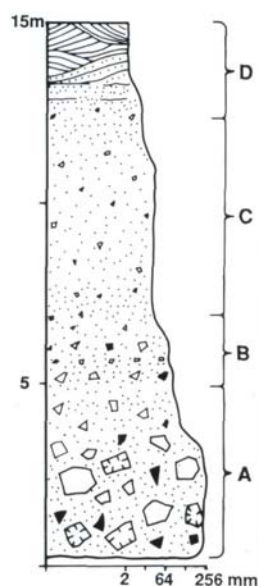


8. Tractional structures in pumiceous sand and gravel

These unconsolidated pumiceous and crystal-rich sand and gravel deposits have been generated by fluvial or lacustrine reworking of subaerial, non-welded, rhyolitic primary pyroclastic deposits. The deposits show delicate ripples, planar lamination and cross bedding. Trains of pumice pebbles occur together with sand-size crystal and lithic particles in some laminae, reflecting hydraulic sorting according to clast density rather than size. The pumice clasts are well rounded, and although poorly sorted, the deposit lacks mud-size components.

Post-AD 186 fluviolacustrine deposits; Highway 1, Lake Taupo shore, New Zealand.

Plate 41 — Syn-eruptive volcanoclastic deposits from shallow submarine explosive activity



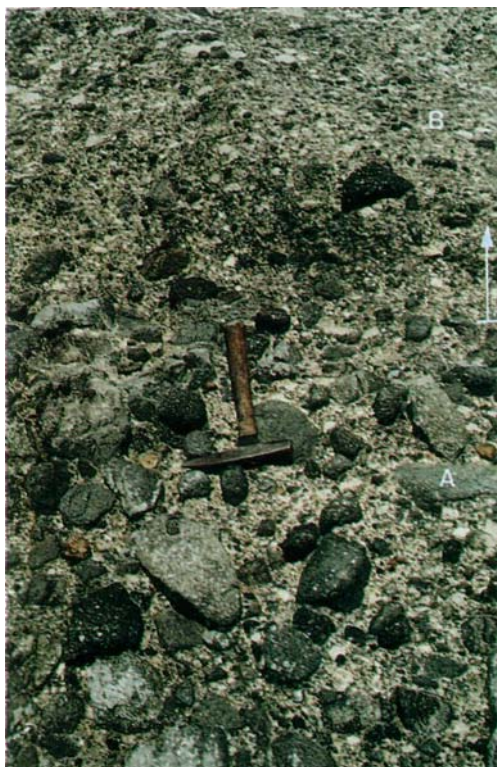
1. Volcaniclastic breccia and stratified—graded pumiceous sandstone

A, B. Part of this section (C; arrow; graded pumiceous sandstone and breccia) is interpreted to be water-settled, pyroclast-rich fallout related to nearby shallow submarine explosive eruptions (Cashman and Fiske 1991). The volcanic breccia at the base (A) has been interpreted to be a debris-flow deposit separated from the water-settled fallout by a "transition zone" (B). Diffusely planar and cross-stratified pumiceous sandstone (D) occurs at the top. The grain size and sorting of the graded pumiceous interval are consistent with fallout from suspension in water. However, such a sedimentation process and the overall context are also consistent with deposition from a submarine, high particle concentration, granular mass flow. Labels 2 and 3 show the approximate positions of 41.2 and 41.3.

Shimhama Group, Miocene-Pliocene; Dogashima, Izu Peninsula, Honshu, Japan.

2. Coarse, graded volcanic breccia

This photograph shows the gradational boundary (arrow) between the dense lava clast-rich basal part (A) and pale pumice-rich transition zone (B) (41.1 A). Juvenile blocks in the breccia have chilled glassy margins and quench fractures, and were derived from disintegration of a submarine lava dome or flow. The matrix consists of coarse pumiceous and crystal-rich sandstone, and is notably poor in finer components.



Shirahama Group, Miocene-Pliocene; Dogashima, Izu Peninsula, Honshu, Japan.



3. Stratified pumiceous sandstone and granule breccia

The top of the section in 41.1 comprises planar and cross-stratified, pumiceous and crystal-rich coarse sandstone. Tractional bedforms indicate reworking, perhaps by residual currents trailing mass flows and/or by above-wave-base currents.

Shirahama Group, Miocene—Pliocene; Dogashima, Izu Peninsula, Honshu, Japan.

Part 5. Alteration: An integral part of textural evolution

After eruption, volcanic deposits are inevitably subject to a sequence of processes: devitrification, hydration, diagenetic and hydrothermal alteration, diagenetic compaction, metamorphism and tectonic deformation. Each process is influenced by the existing deposit texture but also overprints and modifies this texture. Consequently, as these post-eruptive processes take place, the texture evolves along a complex (but predictable) path. We stress the concept that textures in volcanic deposits evolve and should not be considered immutable features once created during eruption, fragmentation and/or flowage, and final emplacement.

Alteration is defined here as a change in the mineralogy and texture of a deposit, facilitated by the action of hot or cold aqueous solutions or gases. Alteration is an integral part of textural evolution and can accompany all the post-eruptive processes listed above. Mineralogical and textural changes that accompany devitrification and hydration of volcanic glass are illustrated in Parts 2-4. In this part, we focus on the style and textural effects of diagenetic and hydrothermal alteration, and overprinting diagenetic compaction and tectonic deformation, using examples from the Mount Read Volcanics. Emphasis is placed on features relevant to the interpretation of textures in volcanic rocks. We do not aim to present a comprehensive account of alteration in volcanic terranes or alteration associated with massive sulfide mineralization.

In many volcanic terranes, diagenetic and hydrothermal alteration are intertwined and inseparable processes. They both involve dissolution, replacement and precipitation of minerals along fluid pathways. Consequently, the distribution of alteration and the textures produced are strongly related to the initial patterns of permeability and compositional contrast formed in volcanic deposits by eruption, fragmentation, devitrification and hydration processes. Some of the results of diagenetic and hydrothermal alteration, such as the formation of mechanically weak phyllosilicate mineral assemblages and mechanically strong quartz-feldspar mineral assemblages, in turn influence the effects of subsequent diagenetic compaction, tectonic deformation and metamorphism. Therefore, the effects of diagenetic and hydrothermal alteration on textures cannot be understood without unraveling the textural effects of all these subsequent processes and considering all the likely earlier processes that generated the pre-alteration texture.

Alteration events in the Mount Read Volcanics

The main alteration events that have affected the Mount Read Volcanics comprise: (1) Cambrian, syn-volcanic

and syn-mineralization alteration that is overprinted by the main regional cleavage and shear zones; (2) lower greenschist grade regional metamorphism; (3) localized syn-tectonic alteration associated with strong cleavage development and shear zones; and (4) localized to widespread post-cleavage alteration zones around Devonian granites. In some areas, such as the Rosebery—Hercules mining area, the volcanics have been affected by all the main alteration events listed above.

Syn-volcanic alteration in the Mount Read Volcanics comprises three main styles: (1) regional diagenetic alteration with various assemblages of white mica, chlorite, plagioclase, quartz, epidote and K-feldspar; (2) localized, zoned hydrothermal alteration, directly associated with massive sulfide mineralization and composed mainly of assemblages of quartz, chlorite, white mica and carbonate; and (3) K-feldspar and chlorite-rich hydrothermal alteration spatially associated with Cambrian granites that intrude the volcanic pile. The mineral assemblages associated with each style are the lower greenschist grade metamorphosed and foliated equivalents of syn-volcanic assemblages which, by analogy with young altered volcanic terranes, probably originally comprised combinations of clays, zeolites, micas, feldspars, quartz and carbonates.

The textural effects of diagenetic and hydrothermal alteration in the Mount Read Volcanics are illustrated using lavas and shallow intrusions as examples of competent, relatively poorly porous rocks, and pumiceous units as examples of incompetent, very porous deposits. These are also the most abundant volcanic rock types in the Mount Read Volcanics and in many other host sequences to massive sulfide deposits.

Alteration of lavas, shallow intrusions and related autoclastic breccias (42-44)

Original texture

Lavas and shallow intrusions are characterized by a porphyritic texture of euhedral or partly resorbed phenocrysts set in a fine-grained or glassy groundmass. Phenocryst size and distribution are almost uniform within each emplacement unit. However, relict primary groundmass textures vary greatly, and indicate that, prior to diagenetic and hydrothermal alteration, the margins of silicic units had glassy groundmasses (commonly perlitic in rhyolitic to andesitic units). These margins graded inwards to cores of: (1) similar glassy texture; (2) glass with scattered spherulites; or (3) mainly crystalline texture (intensely spherulitic, microlitic or granophyric). Most mafic units had thin, sparsely microlitic, glassy margins surrounding intensely microlitic cores. The originally glassy margins

in both the silicic and mafic lavas and shallow intrusions include variable amounts of hyaloclastite and intrusive hyaloclastite (peperite) breccia, whereas the cores are largely coherent.

Glassy margins

The originally glassy, permeable margins show more pervasive, intense and complex textural changes resulting from diagenetic and hydrothermal alteration than do the crystalline, relatively impermeable cores. These differences are attributed to the instability of glass and the influence of permeability on alteration. Most of the originally glassy lavas and shallow intrusions, especially around the ore deposits, display two or more superimposed alteration phases. Each alteration phase consists of an area of rock or a set of domains that can be distinguished by a particular alteration mineral assemblage or by greatly different proportions of minerals in similar mineral assemblages, and also, generally, by different colour and texture. Different alteration phases in the same rock result from different alteration stages, even though the time between stages may be very short. Preservation of overprinting relationships, different stages of textural change and different intensities of alteration, allow reconstruction of the sequence of alteration.

The early alteration resulted in extensive and preferential replacement of glassy parts by a combination of fracture- and/or matrix-controlled alteration, and pervasive alteration. In detail, alteration commenced along permeable fractures (quench, perlitic and hydraulic fractures), and in the matrix of breccias (42, 43). As alteration progressed, alteration fronts moved out from the fractures or matrix toward the centers of unfractured domains. Two situations arose:

(1) In some areas, alteration fronts of the first major alteration stage extended through all glassy parts, including right to the centre of the unfractured glassy domains, and produced one pervasive alteration phase. In these areas, any second alteration stage also generally commenced along fractures and in the matrix of breccias, and extended out from these into the rest of the rock. This alteration was rarely completely pervasive, possibly because the rocks were no longer glassy, and isolated relics of the first pervasive alteration phase remained (42.6).

(2) In other areas, the first alteration stage ceased before complete replacement of the rock, leaving isolated kernels of glass (43.3), that were subsequently altered during a second alteration stage and formed a different alteration phase.

In both situations, incipient alteration, restricted to fractures and matrix, enhanced primary clastic textures by creating a contrast in composition and color between the fractures and matrix and the areas they enclosed.

More advanced alteration produced pseudoclastic textures, comprising isolated domains or pseudoclasts of one alteration phase, enclosed within a continuous interconnected pseudo-matrix domain of a different

alteration phase (42.3-8, 43.2-4). The farther that the prominent fracture- and matrix-controlled alteration phase progressed out from fractures and matrix, the more matrix-rich and matrix-supported was the resultant alteration texture. This two-phase style of alteration was extremely common and has produced pseudo-clastic textures in many units. The pseudoclastic textures can occur at a range of scales in one rock unit, corresponding to the range in types and scales of original fracture networks (compare 42.1, 42.3, 42.6). In outcrop, these altered units resemble coarse-grained, clast- to matrix-supported pseudo-breccias. In hand specimens and thin-sections, original perlitic textures in the coherent glass have been transformed by alteration into aggregates of splintery and arcuate particles that can closely resemble pyroclastic glass shards (Allen, 1988).

Subsequent alteration was (1) mainly restricted to fractures and the matrix of breccias and strongly controlled by fracture and matrix permeability; or (2) overprinted on previously formed alteration domains of similar composition. For example, second-generation phyllosilicate alteration preferentially occurred within previously phyllosilicate-altered domains, and silicification preferentially occurred in existing domains of quartz- or feldspar-rich composition.

The general evolution of alteration style that occurs in many areas, from pervasive to more vein-like, can probably be attributed to the increasing stability of the mineral assemblage and decreasing permeability as alteration progressed. Early pervasive alteration phases now mainly comprise pale feldspar-rich or darker phyllosilicate-rich assemblages. Subsequent overprinting alteration phases are mainly pale quartz-rich or darker phyllosilicate-rich assemblages.

In addition to abundant false clastic textures, this polyphase and domain-controlled alteration style has also produced apparent polymict appearance because:

(1) pseudomatrix and pseudoclast domains appear to have different original composition, due to their different colour and alteration mineralogy (42.4, 43.2, 43.4);

(2) each phase of alteration commonly varies in intensity, and consequently colour, within a single outcrop; originally monomict lava breccia or coherent lava with a uniform texture can assume a polymict appearance, as a result of patchy variation in alteration intensity (42.6, 43.1);

(3) at moderate intensities of alteration, phenocrysts (especially feldspar) are more prominent in dark phyllosilicate domains than in pale siliceous or feldspathic domains (43.1, 43.3), resulting in apparent variation in crystal content between different alteration domains and greatly contributing to clastic, polymict appearance.

In areas of strong tectonic deformation, the phyllosilicate-rich, mechanically weak alteration patches (pseudoclasts) have been flattened and stretched into lenticular shapes (pseudo-fiamme) parallel to

tectonic cleavage and lineation. The alignment of these dark phyllosilicate lenses closely resembles the flattened pumice clast fabric of welded pyroclastic deposits (eutaxitic texture) (42.4, 43.1). Furthermore, in strongly foliated and lineated rocks, phenocrysts and perlitic groundmass have been stretched and partially dismembered into fragments, which further contributes to clastic appearance (Allen, 1988). In altered and deformed volcanic sequences, the relationship of tectonic structures to apparent clast shape and texture must always be evaluated, in order to determine the origin of apparent clastic textures and of foliations that resemble eutaxitic texture.

Mixed glassy and spherulitically devitrified zones

Mixed glassy and spherulitically devitrified zones originally comprised massive coherent volcanic glass with scattered spherulites and lithophysae, or bands of glass alternating with bands of spherulites and lithophysae, or a combination of both (44.3). Diagenetic and hydrothermal alteration of the mixed glassy and devitrified zones in lavas and intrusions was similar to alteration of the totally glassy margins described above, but was also strongly influenced by the compositional domains formed by partial devitrification (compare 44.3, 44.4, 44.7). Bands, nodules and patches of quartzofeldspathic devitrification structures (spherulites, lithophysae) were recrystallized, silicified and/or partially replaced by feldspar during alteration but, in general, maintained a quartzofeldspathic composition (44.4). In contrast, glassy areas between the devitrified domains were replaced mainly by more sericite- or chlorite-rich assemblages (44.4-5, 44.7). Consequently, the glassy domains and devitrified domains now differ in colour and composition, and could be misinterpreted to have been of different original composition. Furthermore, phenocrysts are more prominent in the dark, phyllosilicate-altered, originally glassy domains than in the pale, quartzofeldspathic-altered, spherulitic domains. This results in apparent variation in crystal content between the two domains, and hence polymict clastic appearance.

The original outline or morphology of devitrification bands and nodules has been preserved, except in cases of intense alteration. However, both diagenetic and hydrothermal alteration and subsequent regional metamorphism have recrystallized the original internal fibrous devitrification structure to mosaics of anhedral quartz and feldspar. Intense alteration caused redistribution of the pre-existing compositional domains into massive or weakly banded, irregularly mottled alteration textures (cf. Allen, 1988).

Consequently, diagenetic and hydrothermal alteration have generally imparted a clastic appearance to originally mixed glassy and spherulitically devitrified zones in lavas and intrusions. Spherulites and lithophysae resemble rounded to subrounded volcanic clasts, and strongly spherulitic or lithophysae-rich rocks closely resemble sandy to pebbly, granular volcanoclastic deposits (44.4, 44.6). Altered planar flow-

banded and flow-folded lavas and intrusions resemble thinly bedded and tectonically folded thinly bedded volcanoclastic rocks respectively. Flow banding can, however, be distinguished from bedding due to its characteristic wavy, coarsely to finely bulbous, cauliflower-shaped outline (44.3-4, 44.7). Flow folds can be distinguished from tectonic folds by their irregular distribution and shape, and local areas where tectonic cleavage is not axial planar to the folds.

Spherulitic or microlitic cores of lavas and shallow intrusions

The cores of lavas and shallow intrusions have groundmasses with abundant, small, closely packed spherulites or microlites, and are characterized by massive granular textures, similar to well sorted sandstone (in outcrop, hand specimen and thin-section). Diagenetic and hydrothermal alteration of these rocks generally commenced along cooling joints and hydraulic fractures, producing comparatively simple fracture-controlled vein networks. Moderate to intense alteration resulted in additional patchy (rarely homogeneous) replacement of chemically unstable components between fractures, typically the feldspar microlite-rich groundmass, followed by feldspar phenocrysts. This patchy alteration and resulting compositional contrasts produced false clastic and polymict textures in originally coherent lavas and shallow intrusions in some areas. Furthermore, the widespread recrystallization of spherulites, during alteration and metamorphism, has enhanced the granular texture of these rocks, making the distinction from true volcanoclastic textures particularly difficult.

General trends and implications

In conclusion, diagenetic and hydrothermal alteration caused the textures in both the glassy autoclastic and glassy coherent facies of the lavas and shallow intrusions to evolve toward matrix-supported, monomict and polymict clastic textures typical of volcanoclastic mass-flow deposits including pyroclastic flow deposits. With increasing alteration intensity and deformation, these false clastic textures converged in appearance to resemble the textures of welded pyroclastic flow deposits (42.4, 43.1). Spherulite-defined flow banding is well preserved and even enhanced in weakly altered rocks. However, moderate to strong alteration caused originally flow-banded and nodular devitrified lavas and intrusions to resemble, respectively, thinly bedded and pebbly granular volcanoclastic deposits. The more crystalline cores of the lavas and shallow intrusions are less altered, except near the centre of hydrothermal systems. They are characterized by massive sandy or granular texture, with local areas of fracture-controlled pseudobreccia texture, which comprises granular pseudoclasts in a more altered pseudomatrix.

Consequently, apparent pyroclastic and other volcanoclastic textures must be examined critically, with all likely post-depositional processes in mind, in order to correctly interpret their origin. Furthermore, there

appears to be a broad spatial association between known massive sulfide mineralization, moderate to strong alteration, and increased polyphase alteration style and, hence, pseudoclastic textures. Therefore, recognition of the style of textural modification caused by polyphase alteration in glassy and crystalline volcanic rocks can be a promising sign in exploration for massive sulfide mineralization.

Alteration of pumiceous deposits (45, 46)

Originally glassy and permeable deposits

Pumiceous deposits in the Mount Read Volcanics are mainly rhyolitic to dacitic in composition and comprise non-welded subaqueous mass-flow units ranging up to at least 150 m thick (45.1-2). Relict primary textures indicate that most units are matrix- to clast-supported pumice breccias consisting of abundant non-welded pumice clasts, subordinate lithic clasts and a matrix of finer non-welded pumice shreds and sub-millimeter shards. Consequently, the deposits were originally very porous and permeable aggregates of glassy, incompetent (structurally weak) clasts (pumice and shards). These primary textural characteristics greatly influenced the alteration style.

The originally highly porous, permeable and glassy nature of the deposits allowed rapid, pervasive alteration at the syn-volcanic diagenetic stage. Vast volumes of pumice breccia in the Mount Read Volcanics have been altered without producing distinct hydrothermal veins. Hydrothermal veins are restricted to areas very close to the ore deposits, such as around the Rosebery massive sulfide deposit, and appear to be related to second- and third-order alteration stages that overprint earlier, more pervasive alteration.

Phyllosilicate alteration

In areas of weak to strong phyllosilicate alteration, pumice and shards were replaced by mechanically weak, phyllosilicate-rich mineral assemblages and, consequently, were strongly flattened by diagenetic compaction. The phyllosilicate-altered rocks either comprise very phyllosilicate-rich flattened pumice clasts, set in a matrix of less phyllosilicate-rich and less compacted pumice clasts (45.2-3), or more uniformly altered and compacted pumice clasts in which separate clasts cannot be distinguished (45.4-6). The former have fiamme textures that closely resemble eutaxitic textures in welded ignimbrites. The latter can display a moderately even distribution of euhedral to subhedral phenocrysts and closely resemble coherent, massive altered lavas and shallow intrusions, especially where they are poor in lithic clasts. However, these non-welded pumice breccias can be distinguished from genuine welded pyroclastic deposits and from lavas or shallow intrusions by their lithofacies characteristics, especially the normally graded bedforms, by the compacted nature of pumice clasts, even within the fine-grained graded tops and interbedded suspension-settled shard-rich layers, and by preserved relicts of non-welded pumice and shard textures in outcrop and thin-

section.

In areas of strong tectonic deformation, tube pumice structure, shards and phyllosilicate patches have been flattened, stretched and partly transposed into the cleavage and lineation, resulting in a foliated fabric that mimics eutaxitic texture in welded primary pyroclastic deposits.

Two-phase feldspar and phyllosilicate alteration

A second common alteration style in pumiceous deposits in the Mount Read Volcanics, and well illustrated by the footwall and hangingwall sequences in the Rosebery-Hercules district, is widespread secondary feldspar alteration (K-feldspar and albite — Allen and Cas, 1990). Secondary feldspar nucleated around feldspar phenocrysts and extended outward, filling pore space (mainly vesicles) and replacing the glassy bubble walls of pumice and shards. The feldspar alteration was incomplete and left isolated, diffuse or well-defined, less altered patches, which were subsequently altered to more phyllosilicate-rich compositions (45.1, 45.6-7). Many phyllosilicate-rich patches were flattened during diagenetic compaction and tectonic deformation, with the result that the textures closely resemble eutaxitic texture in welded ignimbrites. However, in the feldspar-rich domains relicts of uncompacted, delicate tube-vesicle and round-vesicle pumice and shard textures (6.4, 46.3-5) indicate that the deposits were originally non-welded and that the feldspar alteration occurred very early, prior to tectonic foliation, and prior to or during the onset of diagenetic compaction (Allen, 1990; Allen and Cas, 1990).

The distribution of secondary feldspar alteration does not have a clear stratigraphic control, and it is uncertain whether feldspar was the first alteration mineral or, instead, replaces even earlier minerals such as zeolites. Components (K, Na, Al, SiO₂) necessary to form the enormous volume of secondary feldspar, may have been derived from the dissolution of volcanic glass at clast contacts during diagenetic compaction, and from the upward migration of components (K, Na, SiO₂) liberated by diagenetic or hydrothermal leaching of glass deeper in the volcanic pile. Important textural evidence that supports early leaching and dissolution of glassy clasts in the volcanic pile is the widespread occurrence of a bedding-parallel, spaced, stylolitic dissolution foliation in many pumiceous rocks in the Mount Read Volcanics (46.1). The bedding-parallel foliation is composed of phyllosilicate and opaque minerals and pre-dates regional cleavage. The foliation partly overprints syn-volcanic feldspar and phyllosilicate alteration. However, phyllosilicate-altered fiamme are commonly aligned along this foliation, indicating a spatial and possibly temporal association between formation of the fiamme and the stylolitic foliation. The bedding-parallel foliation is interpreted as a diagenetic compaction fabric, or a combination of a diagenetic compaction fabric and very early bedding-parallel tectonic fabric (Allen, 1990; Allen and Cas, 1990).

In areas of moderate to strong tectonic deformation, the bedding-parallel foliation is irregularly and coarsely crenulated. Bedding-parallel phyllosilicate fiamme are also coarsely crenulated and have developed cusps which are strongly aligned along the regional cleavage (46.1). Tube pumice and shards in the feldspar-rich matrix domains are more strongly transposed into the regional cleavage and lineation than are the bedding-parallel foliation and fiamme. This strong alignment of tube pumice structure and shards superficially resembles a eutaxitic welding fabric (45.1, 46.4). However, in addition to the relict non-welded texture of many pumice clasts, this false welding fabric can be distinguished from true welding by its orientation: it is parallel to cleavage and oblique to the bedding-parallel foliation and fiamme; a genuine welding fabric would be parallel to fiamme, and oblique to and crenulated by the regional cleavage.

In areas of intense cleavage, the bedding-parallel foliation and fiamme are almost completely transposed into the regional cleavage and lineation (45.1). Intense foliation overprinting very competent feldspar- and quartz-rich alteration has produced augen schists (46.6). The augen are pumice clasts extensively replaced by feldspar and quartz. The anastomosing phyllosilicate cleavage that wraps around the augen represents the transposed fiamme and bedding-parallel foliation.

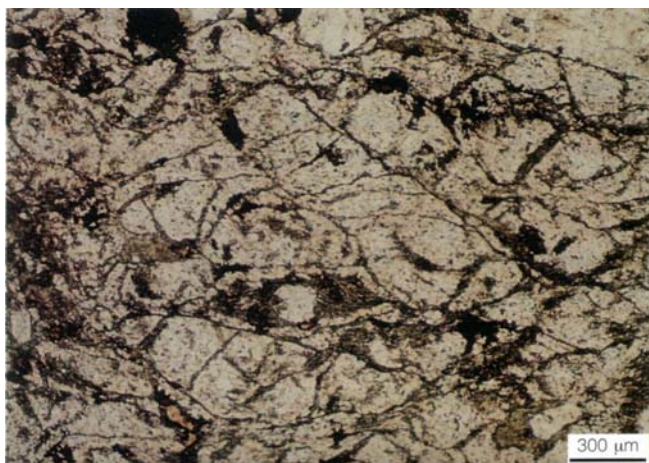
Two-phase feldspar and phyllosilicate alteration of pumiceous deposits and the resultant fiamme textures are widespread in the Mount Read Volcanics. They occur in zones up to at least 25 km in strike extent and 2 km in stratigraphic thickness. The fiamme are mainly sericite-rich except close to mineralization, where they are commonly chlorite-rich. In the Rosebery—Hercules

mining district, where these textures have been most closely studied, the boldness of the fiamme texture increases within 1 km of the ore bodies. This change is due to increased colour contrast between the dark fiamme and the light matrix domain, which, in turn, is due to enrichment of dark phyllosilicate in the fiamme and feldspar and/or quartz in the matrix domain. Locally (for example, at Rosebery) or over extensive areas (for example, around Hercules) within 50—1000 m of the ore bodies, the sericite fiamme are replaced by chlorite and the matrix domain is silicified, resulting in further enhancement of the fiamme texture (45.7). Within 50–100 m of the ore bodies, strong silicification, carbonate alteration, and sericite or chlorite alteration, form irregular zones with mottled to nodular to locally massive alteration textures (46.7). These alteration textures thoroughly overprint and obscure primary textures and fiamme.

General trends and implications

With very careful observation, relicts of primary non-welded pumice texture can be identified in most of the altered and deformed pumiceous deposits, including the augen schists and intensely altered rocks adjacent to the ore bodies. In general, alteration has caused the non-welded pumiceous deposits to evolve in texture toward that of matrix-supported, welded pyroclastic deposits and especially welded pyroclastic flow deposits. The implications of these alteration effects are similar to those for the altered lavas, shallow intrusions and related breccias: all post-depositional processes must be carefully considered when interpreting textures in volcanic rocks, and recognition of the textures produced by polyphase alteration in pumiceous volcanoclastic rocks can be a guide to mineralization.

Plate 42 — Altered coherent lava and related breccia



1. Incipient alteration of perlitic fractures in thin-section

Perlitic fracture texture is well developed in this formerly glassy dacite. The fractures are accentuated by fine-grained green chlorite resulting from incipient alteration. Plane polarized light.

Mount Read Volcanics, Cambrian; Mackintosh Bridge, western Tasmania.



2. Incipient stage alteration of in situ rhyolitic hyaloclastite

Subpolygonal blocky rhyolite clasts are defined mainly by broadly curved fractures and show jigsaw-fit texture with local rotation of faintly flow-banded clasts. Brecciation was probably caused by quench fracturing of a formerly glassy, coherent lava or intrusion, producing in situ hyaloclastite. Intense silicification (white) is confined to the fracture network and is prominent along the main fractures, but poorly developed along minor fractures. Weak to moderate phyllosilicate-quartz alteration occurs between the fractures.

Mount Read Volcanics, Cambrian; Mount Read, western Tasmania.



3. Intermediate stage alteration of in situ rhyolitic hyaloclastite

This breccia is strictly monomict, comprising blocky clasts of altered, formerly glassy rhyolite that range from millimetre to decimetre dimensions. The clasts locally display jigsaw-fit texture (arrow) and many have curvilinear outlines. The breccia is matrix poor and clast supported. However an apparent matrix has formed by strong silicification that has spread out up to 10 mm from original quench fractures, thereby replacing the margins of larger clasts and completely replacing some small clasts. Areas between silicified fractures have weak to moderate phyllosilicate-quartz alteration.

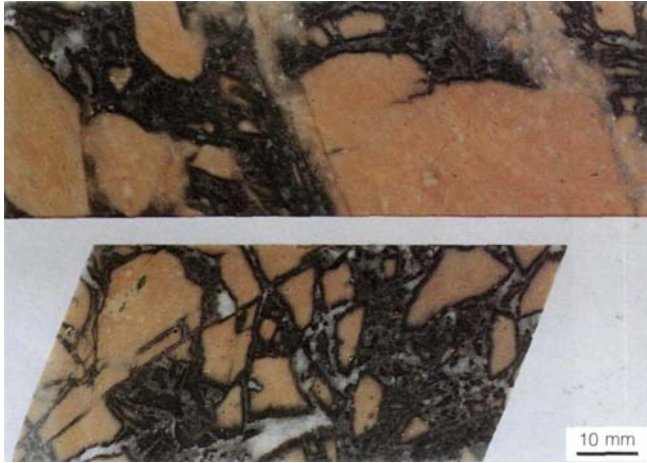
Mount Read Volcanics, Cambrian; Mount Read, western Tasmania.



4. Advanced stage alteration of in situ rhyolitic hyaloclastite

Intense silicification of this breccia has formed an extensive, fine-grained pseudomatrix (white) by replacing the margins of all larger clasts and completely replacing many small clasts. Silicification moved outward 5-20 mm from all fractures, reducing the apparent size of the clasts, and changing the original clast-supported breccia texture to an apparent matrix-supported texture. Areas enclosed by the silicified domain have moderate to strong chlorite-quartz alteration (dark grey). Subsequent strong tectonic foliation and lineation has stretched the chlorite-rich domains into elongate pseudoclasts, which resemble pumice fiamme in welded pyroclastic deposits.

Mount Read Volcanics, Cambrian; Mount Read, western Tasmania.



5. Altered in situ breccia in dacite

This breccia consists of angular, blocky to cuneiform clasts of altered, fine-grained dacite. The breccia is strictly monomict and jigsaw-fit texture between groups of clasts occurs locally. Although the breccia closely resembles in situ hyaloclastite, it lacks clasts with quenched margins or "tiny normal joints" and is confined to a fracture zone, suggesting instead that hydraulic fracturing was important. Strongly fracture-controlled silicification (dark) overprints more pervasive K-feldspar-sericite alteration (pale orange). Silicification has spread out 1-2 mm from fractures, thereby forming a dark siliceous pseudomatrix domain.

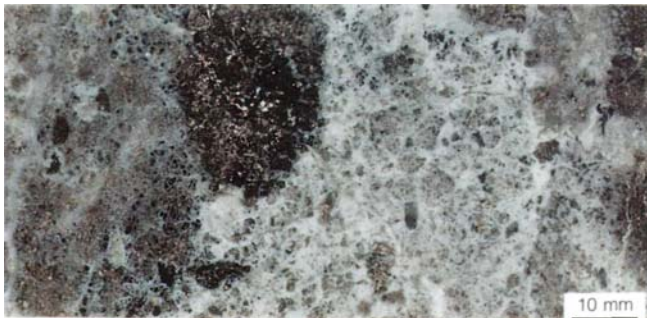
Mount Read Volcanics, Cambrian; DDH QR793 (63.96 m), Que River mine, western Tasmania.



6. Altered perlitic rhyolite

Large diameter perlitic fractures (macro-perlite) are evident in this coherent rhyolite. Chlorite-epidote alteration (dark green-grey) along and adjacent to the perlitic fractures overprints earlier, pervasive feldspar alteration (pale grey). In areas where chlorite-epidote alteration is narrowly confined to the perlitic fractures (centre of photograph), the arcuate character of the fracture network is faintly preserved. However, in areas where chlorite-epidote alteration has advanced farther out from the fractures (top right), the rock has a matrix-supported breccia texture consisting of pale, feldspar altered pseudoclasts in a dark, chlorite-epidote altered pseudomatrix.

Mount Read Volcanics, Cambrian; Pieman Road, western Tasmania.



7. Altered perlitic dacite

The formerly glassy groundmass is cut by arcuate and concentric perlitic fractures. Fluids responsible for strong silicification (white) have used the perlitic fractures as channel ways and silicification has completely replaced the fractures in most of the rock, thereby forming a continuous pseudo-matrix domain. Silicified domains enclose large irregular patches and small kernels of darker, less silicified, more chloritic dacite that form pseudoclasts.

Mount Read Volcanics, Cambrian; DDH HL304 (95.6 m), Hellyer mine, western Tasmania.



8. Calcite-flooded basaltic hyaloclastite

Centimeter-sized clasts in in situ basaltic hyaloclastite are separated by a finely comminuted matrix of the same composition. The porous breccia matrix has been partially flooded with calcite alteration (white). Larger clasts remain relatively unaltered.

Mount Read Volcanics, Cambrian; DDH HL52 (156.43 m), Hellyer mine, western Tasmania.



1. Pseudobreccia in altered, in situ rhyolitic hyaloclastite

These six samples are from an altered, quench fragmented rhyolitic sill in the Rosebery mine hangingwall. Weakly quench brecciated rhyolite (core **A**) has relatively homogeneous feldspar-minor sericite-chlorite alteration. Strongly quench fragmented rhyolite (all other cores) has heterogeneous sericite-chlorite (dark green) and feldspar-rich (pink to brown) alteration. Most of the hyaloclastite has been replaced by secondary feldspar (pink to brown pseudomatrix domain) and original clast outlines are faint or obscured. The apparent matrix-supported, dark green pseudoclasts (**P**) are relicts of earlier pervasive phyllosilicate alteration and range from discrete, strongly phyllosilicate altered clasts (core **E**) to phyllosilicate patches within clasts incompletely overprinted by feldspar alteration (core **F**). Phyllosilicate-rich pseudoclast domains were flattened and stretched by tectonic deformation and resemble welded pumice fiamme in pyroclastic rocks (core **C** and **E**). Pale grey, silicified mudstone matrix locally present between clasts (core **D**) was incorporated while still unconsolidated during intrusion and fragmentation of the rhyolite (intrusive hyaloclastite or peperite).

Mount Read Volcanics, Cambrian; DDH 101R (20-50 m), Rosebery mine, western Tasmania.



2. Altered andesitic hyaloclastite

This in situ andesitic hyaloclastite breccia has a fine-grained volcaniclastic sediment matrix (pale grey; **M**). The clasts (dark grey; **C**) are hornblende-phyric andesite and have been pervasively weakly chlorite-epidote altered. Subsequent silicification preferentially replaced the more porous sediment matrix and encroached on the margins of andesite clasts. Alteration of the clast margins (white; **A**) has partly obscured the original hyaloclastite clast shapes and has created a more extensive apparent matrix domain.

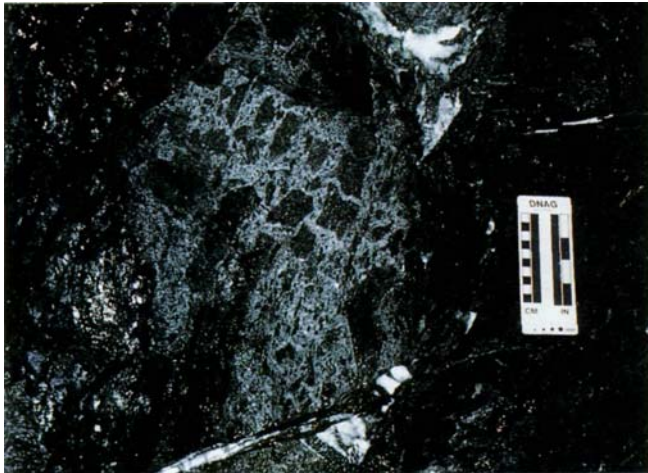
Mount Read Volcanics, Cambrian; Anthony Road, western Tasmania.



3. Altered rhyolitic autoclastic breccia

Although strictly monomict, the clasts in this autoclastic breccia are various shades of grey or black. The breccia originally comprised clast-supported blocks of flow-banded, glassy, perlitic rhyolite but the texture has been modified as a result of alteration. Clast margins, fractures and flow bands have been altered to clay mineral assemblages, creating a pale green and cream apparent matrix domain and imparting an apparent matrix-supported breccia texture.

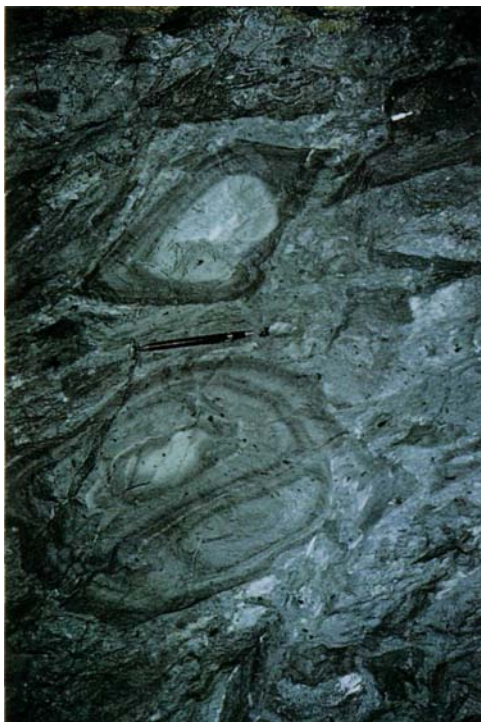
Shinzan Rhyolite, Miocene; Oga Peninsula, Japan.



4. Pseudobreccia in altered andesite

False breccia textures commonly result from overprinting of alteration phases. In the footwall alteration zone of the Hellyer massive sulfide deposit, intense silicification overprints earlier pervasive chlorite alteration. Silicified domains form a pseudomatrix and enclose remnants of the darker chlorite alteration that appear to be clasts. As silicification advances, apparent clasts become smaller and ultimately, a massive, fine-grained siliceous rock devoid of primary textures is formed.

Mount Read Volcanics, Cambrian; Hellyer mine, western Tasmania.



5. Altered polymict volcanic breccia

Clasts in this mass-flow-emplaced volcanic breccia are predominantly andesitic and dacitic lava. The breccia occurs in the outer alteration shell in the footwall of the Hellyer massive sulfide deposit. The matrix and all but the cores of the largest clasts have been replaced by strong quartz-sericite-minor chlorite alteration (grey). Alteration of the clasts is concentrically zoned and remnants of an earlier, pervasive quartz-sericite-chlorite alteration (pale green) occur in the cores of the largest clasts. The second, strong alteration phase commenced in the porous breccia matrix and spread into the relatively impermeable clasts as a series of replacement fronts. In this exposure, the original character of the breccia can still be recognized. However, elsewhere in the footwall the clast margins in the breccia are indistinct and an apparent matrix-rich, matrix-supported texture occurs.

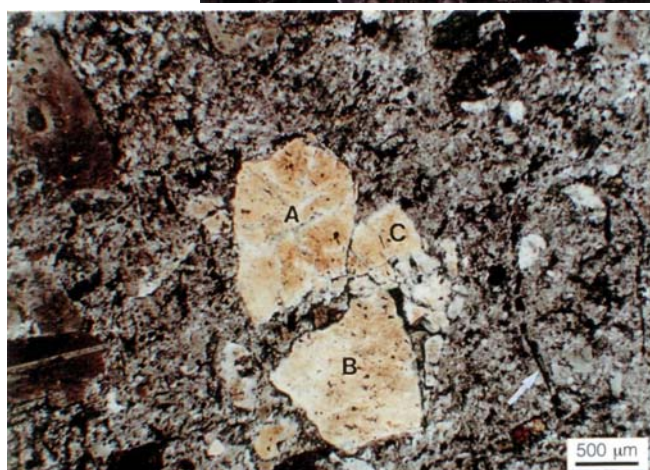
Mount Read Volcanics, Cambrian; 360 level, Hellyer mine, western Tasmania.



1. False polymict breccia texture in altered coherent dacite

Overprinting of alteration phases commonly results in false polymict breccia textures. Heterogeneous feldspar-quartz (orange and pink) and chlorite-epidote (dark green) alteration of this coherent dacite (lava or sill) has been strongly influenced by perlitic fracturing in the formerly glassy groundmass. Relicts of early, feldspar-rich alteration (orange) in least fractured areas form pseudoclasts, enclosed by a pseudomatrix domain of subsequent feldspar-quartz alteration (pink) that mainly affected more strongly fractured areas. Chlorite-epidote alteration has overprinted feldspar-quartz alteration in some strongly fractured areas, forming irregular pseudoclasts of superficially more mafic composition.

Mount Read Volcanics, Cambrian; Pieman Road, western Tasmania.



2. Fragmented phenocrysts in thin-section

Although coherent lavas and intrusions are characterized by euhedral phenocrysts, in situ fractured and fragmented crystals can occur, especially in deformed sequences. The sericitized feldspar phenocryst fragments (**A**, **B**, **C**) in this example show jigsaw-fit texture and are set in a formerly glassy ground-mass with relict perlitic fractures (arrow) defined by chlorite and/or opaque phases. Crossed nicols.

Mount Read Volcanics, Cambrian; Murchison Highway, western Tasmania.



3. Spherulitically devitrified rhyolitic lava

The flow foliation in this rhyolitic lava is defined by alternating black, glassy bands (obsidian) and grey spherulitic bands. Large lithophysae (pale pink; **L**) occur in concentrations along particular flow bands and as isolated structures (compare with **44.4**).

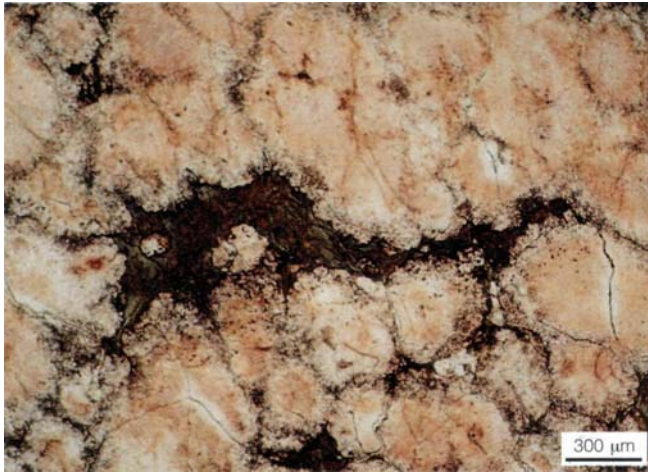
Obsidian Cliff rhyolite lava flow, 0.18 Ma; Yellowstone National Park, Wyoming, USA.



4. Altered, flow-banded and nodular devitrified rhyolite

Flow foliation in altered rhyolitic lava is defined by alternating siliceous and phyllosilicate-rich bands. Siliceous laminae comprise abundant, small (mm) spherulites. Larger nodular siliceous structures are interpreted as lithophysae (compare with 44.3). The nodules are concentrated in bands (top and centre) or are isolated (arrow). Intervening sericitic bands (dark grey) may have been formerly glassy. Alteration was strongly influenced by the pre-existing pattern of devitrification: spherulitic bands and lithophysae (quartzofeldspathic devitrified) were replaced by quartz-albite (white) and glassy bands were replaced by sericite-quartz (dark green).

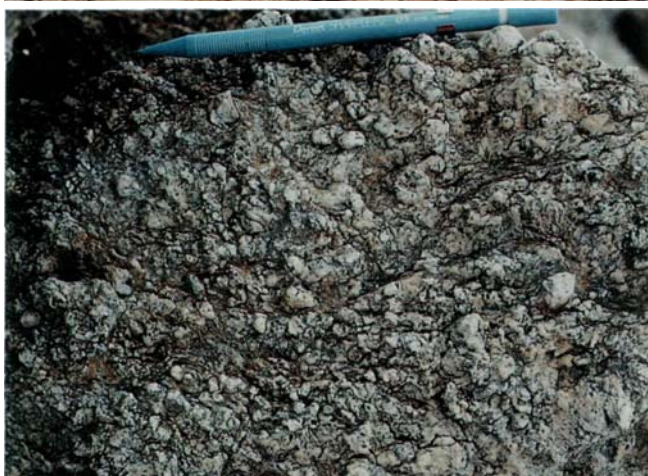
Mount Read Volcanics, Cambrian; Mount Read, western Tasmania.



5. Altered spherulitic rhyolitic lava in thin-section

Spherulites have been partially recrystallized to pink feldspar-quartz mosaics in which only faint relict radial fibrous structure is preserved. Formerly glassy domains between the spherulites have been replaced by sericite (dark green). Such sericitic lenses can be mistaken for flattened pumice fiamme that occur in a variety of pumice-rich volcanoclastic deposits. Plane polarized light.

Mount Read Volcanics, Cambrian; Winter Brook area, western Tasmania.



6. Altered, strongly cleaved, spherulitic rhyolitic lava

Texturally and mineralogically contrasting domains have been accentuated by weathering. Silicified spherulite nodules are resistant and prominent, whereas sericite-altered, originally glassy areas are recessive. The resulting very uneven outcrop surface contributes to a false clastic appearance. The trace of a strong cleavage is approximately parallel to the pen.

Mount Read Volcanics, Cambrian; Mount Read, western Tasmania.



7. Devitrified, flow-banded dacite

A, B. Both these samples come from a devitrified, altered dacitic intrusion with well-developed flow banding and evenly porphyritic texture. Phenocrysts of feldspar are chloritized and appear as dark spots. In A, flow laminae are defined by alternating chloritic (grey) and siliceous (cream) layers. In B, siliceous and chloritic flow banding wraps around a large patch of coalesced spherulites (S) with bulbous margins (cf. 44.3). The flow banding is locally accentuated by hematite alteration (arrow).

Mount Windsor Volcanics, Cambrian; DDH REW803 (A, 60.4 m; B, 62.1 m), Reward prospect, northern Queensland.

Plate 45 — Altered pumiceous volcaniclastic deposits



1. Altered rhyolitic pumice-rich breccia

These samples are from the base (A) through to the top (D) of a 190 m thick, rhyolitic pumice-rich, subaqueous mass-flow deposit affected by feldspar and sericite alteration. A and B contain tightly packed, white, feldspar-altered pumice clasts (8 mm), feldspar crystals with secondary feldspar overgrowths, dark green relict pumice lenses, and lithic clasts (L). Relict pumice clasts are transposed into a strong tectonic cleavage. C is from the normally-graded upper part of the unit and consists mainly of smaller (3 mm) pumice clasts. D comprises sericitic, pumiceous sandstone and dark green relict pumice clasts interpreted to be suspension-settled pumice and ash.

Mount Read Volcanics, Cambrian; DDH H1175 (270-467 m), Hercules South prospect, western Tasmania.



2. Diagenetically compacted altered pumice

Parts of two normally graded, rhyolitic pumice-rich, subaqueous mass-flow units can be seen in this outcrop. Relict pumice clasts (pale green; P) have been extensively replaced by sericite and subsequently flattened parallel to bedding (S_0), now steeply dipping, by diagenetic load compaction. Although the breccia units were originally non-welded, the pumice lenses define a foliation similar to eutaxitic texture.

Mount Read Volcanics, Cambrian; Hellyer mine haulage road, western Tasmania.



3. Diagenetically compacted, altered pumice breccia

These two drillcore samples are composed almost entirely of rhyolitic pumice clasts. However, alteration is not uniform in intensity, composition or colour. Least altered pumice is grey and poorly compacted, whereas strongly phyllosilicate altered pumice clasts (grey-green) have been thoroughly compacted and appear as dark grey-green wavy streaks. Alignment of compacted altered pumice defines a bedding-parallel diagenetic compaction foliation.

T₁ Tuffs, Otaki Formation, Miocene; Hokuroku district, Japan.



4. Diagenetically compacted, altered pumice breccia

Rhyolitic pumice clasts (pale grey) have been almost uniformly altered to clays and subsequently strongly compacted. In contrast, lithic clasts (dark; **L**) are unaltered and uncompacted. Pumice compaction has produced weakly defined, bedding-parallel foliation. The samples come from a non-welded, pumice-rich, submarine mass-flow deposit.

T₂ Tuffs, Otaki Formation, Miocene; Hokuroku district, Japan.



5. Foliated, compacted, sericite-altered pumice breccia

Pumice clasts in this rhyolitic pumice breccia have been strongly altered, compacted and deformed, forming an almost homogeneous mass of foliated sericite. White spots are feldspar crystals (within pumice clasts). Their apparently even distribution imparts a porphyritic texture resembling a deformed coherent lava or intrusion.

Mount Read Volcanics, Cambrian; Rosebery mine footwall, western Tasmania.



6. Heterogeneously altered pumice breccia

Green and pink colour mottling here is the result of heterogeneous alteration of rhyolitic pumice breccia, and imparts a pseudobreccia texture overprinting the original clastic texture. Discontinuous chlorite-epidote alteration domains (green) resemble large scattered clasts and the continuous feldspar-rich domain (pink and grey) resembles a finer grained clastic matrix of different composition. The pumice clasts are feldspar-phyric (small white spots).

Mount Read Volcanics, Cambrian; near Howards Road, DDH MR1 (82 m), western Tasmania.



7. Altered pumice breccia with prominent fiamme

The dark grey fiamme are chlorite-altered pumice that has been strongly compacted parallel to bedding. Some fiamme are single altered pumice clasts and others comprise two or more pumice clasts. The fiamme are separated by a pseudo-matrix (white) comprising largely uncompacted relict pumice clasts, indicating that the pumice breccia was originally non-welded. Early feldspar alteration in the pseudomatrix and sericite alteration in the fiamme have been overprinted by silicification and chlorite alteration respectively. The pumice breccia occurs in the footwall alteration zone of the Hercules massive sulfide ore body.

Mount Read Volcanics, Cambrian; Hercules mine

Plate 46 — Altered and deformed pumiceous volcanoclastic deposits



1. Foliated, strongly quartz-sericite altered tube pumice breccia

This rhyolitic pumice breccia has undergone early heterogeneous feldspar and sericite alteration and an overprinting quartz and sericite alteration stage (cf. 45.7). Flattened sericite-altered pumice clasts (fiamme) are associated with and aligned along a spaced stylolitic foliation (S_1) which is crenulated by the steep regional cleavage (S_2). Some sericite-altered pumice clasts are transposed into the tectonic cleavage.

Mount Read Volcanics, Cambrian; Hercules mine footwall, western Tasmania.



2. Relict fiamme in altered rhyolitic pumice breccia

The prominent dark green lenses (**L**) in this outcrop are relict fiamme and consist of phyllosilicate-altered, diagenetically compacted pumice. The relict fiamme have highly irregular, cusped terminations and are feldspar-phyric. Feldspar crystals are equally abundant in the intervening pale feldspathic domains but much less obvious. Pumice clasts in the feldspathic domains display unflattened round and tubular vesicles in random orientations (46.3, 46.4), indicating that the unit is non-welded.

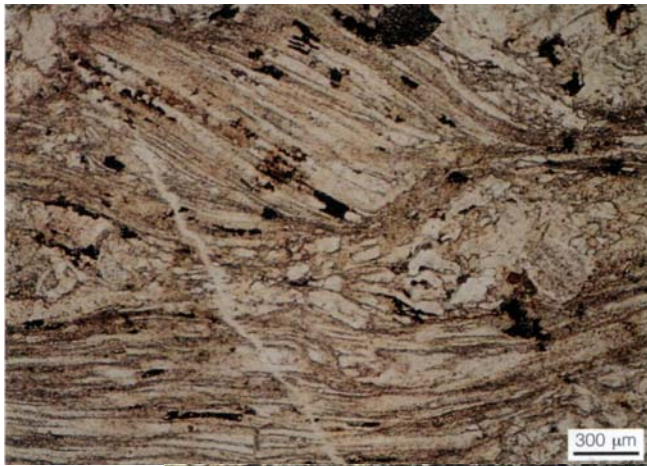
Mount Read Volcanics, Cambrian; Hercules mine haulage road, western Tasmania.



3. Altered tube pumice breccia in thin-section

Thin-sections of feldspathic domains in rhyolitic pumice breccia such as that shown in 46.2 reveal unflattened tube pumice clasts in various orientations, indicating that the deposit is non-welded. Pumice preservation is due to replacement of vesicle walls and infilling of vesicles by feldspar soon after deposition. Pumice which was not replaced by feldspar was phyllosilicate-altered and readily flattened by diagenetic or early tectonic compaction, generating the relict fiamme conspicuous in outcrops shown in 45.7 and 46.2. Plane polarized light.

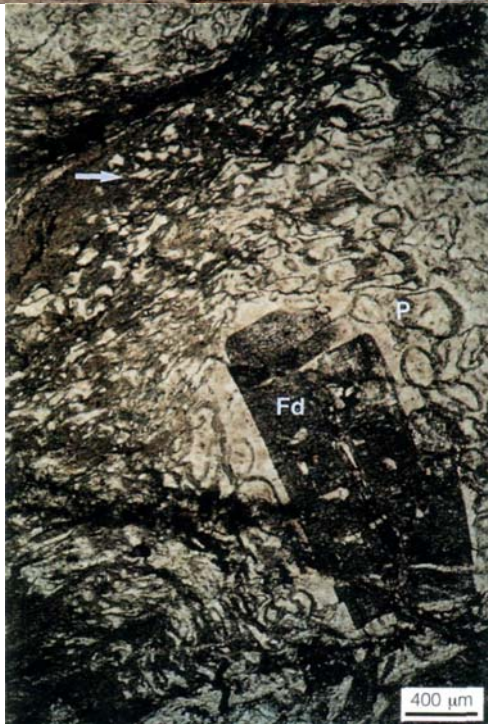
Mount Read Volcanics, Cambrian; Hercules South prospect hangingwall, western Tasmania.



4. Strongly deformed, altered tube pumice breccia in thin-section

Tube vesicles in pumice clasts in this thin-section of pumice breccia are clearly defined and have been replaced mainly by secondary feldspar. After feldspar alteration and during strong tectonic deformation, the initially randomly oriented pumice clasts were realigned subparallel to the regional tectonic cleavage. Plane polarized light.

Mount Read Volcanics, Cambrian; Hercules South prospect hangingwall, western Tasmania.



5. False shard texture in altered rhyolitic pumice in thin-section

This photomicrograph shows an altered pumice clast in non-welded rhyolitic pumice breccia. Round vesicles (**P**) that surround a sericite-altered feldspar crystal (**Fd**) have been replaced by secondary feldspar (white to pale brown). Subsequent sericite alteration (green-grey) has partially replaced the margins of the pumice clast, resulting in a false shard texture (arrow) comprising relict segments of the original feldspar-altered pumice clast, enclosed by sericite. Plane polarized light.

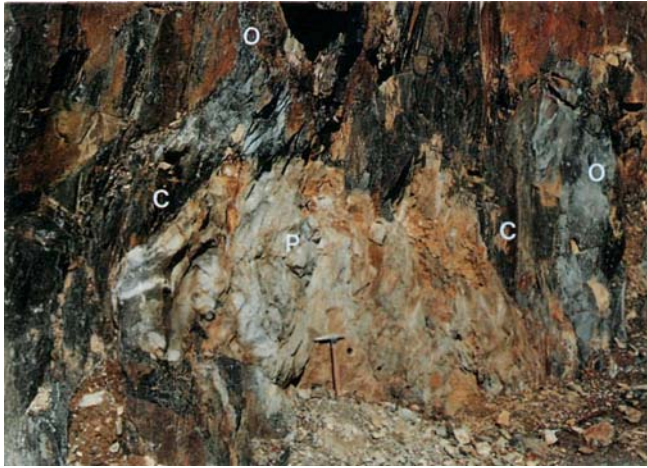
Mount Read Volcanics, Cambrian; DDH LB271 (130.5 m), Rosebery mine footwall, western Tasmania.



6. Augen schist texture in deformed, altered rhyolitic pumice breccia

The progressive development (**A** to **C**) of augen schist texture is shown by these core samples of deformed and altered rhyolitic pumice breccia. Augen schist texture has resulted from strong cleavage superimposed on competent feldspar-and quartz-rich alteration assemblages. In **A**, feldspar-altered pumice clasts have been silicified and the larger pumices form prominent white siliceous patches. Core **B** shows the same rock and alteration type with slightly stronger cleavage causing incipient augen texture. In areas of stronger deformation (core **C**), cleavage anastomoses around the competent silicified pumice clasts resulting in augen schist texture. Relict fibrous tube pumice textures are preserved in some siliceous augen and can be identified with a hand lens but require a careful search.

Mount Read Volcanics, Cambrian; DDH DP259 (220-330 m), Rosebery-Hercules footwall, western Tasmania.



7. Mineralized and altered pumice breccia

Relict primary textures can be preserved even in extremely altered volcanic rocks. At the margin of a massive sulfide lens at Hercules, massive chlorite (black; **C**), massive pods of quartz-sericite-carbonate (cream; **P**) and semi-massive spotty galena-sphalerite (pale grey; **O**) have replaced diffusely planar stratified pumiceous rocks. Relict tube pumice textures are locally preserved in the altered and mineralized pumiceous host rocks in both outcrop and thin-section.

Mount Read Volcanics, Cambrian; 4-Level road, Hercules mine, western Tasmania.

References

- Abbott ST and Carter (in press) The sequence architecture of Mid-Pleistocene (c. 1.1-0.4 Ma) cyclothems from New Zealand: facies development during a period of orbital control on sea-level cyclicity. In de Boer PL and Smith DG (eds), *Orbital forcing and cyclic sequences*. IAS Spec Pub.
- Allen JRL 1985 *Principles of physical sedimentology*. Allen and Unwin, London 272 pp.
- Allen RL 1988 False pyroclastic textures in altered silicic lavas, with implications for volcanic-associated mineralization. *Econ Geol* 83: 1424-1446.
- Allen RL 1990 Subaqueous welding, or alteration, diagenetic compaction and tectonic dissolution? IAVCEI International Volcanological Congress, Mainz, Germany, Abstracts.
- Allen RL 1992 Reconstruction of the tectonic, volcanic and sedimentary setting of strongly deformed Zn-Cu massive sulfide deposits at Benambra, Victoria. *Econ Geol* 87: 825-854.
- Allen RL and Gas RAF 1990 The Rosebery controversy: distinguishing prospective submarine ignimbrite-like units from true subaerial ignimbrites in the Rosebery-Hercules ZnCuPb massive sulphide district, Tasmania. *Geol Soc Aust Abs* 25: 31-32.
- Allen RL and Hunns SR 1990 *Excursion Guide El. The Mount Read Volcanics and related ore deposits*. 10th Aust Geol Conv, Hobart: 15-27.
- Anderson JE Jr 1969 Development of a snowflake texture in a welded tuff, Davis Mountains, Texas. *Geol Soc Am Bull* 80: 2075-2080.
- Applegate B and Embley RW 1992 Submarine tumuli and inflated tube-fed lava flows on Axial Volcano, Juan de Fuca Ridge. *Bull Volcanol* 54: 447-458.
- Bacon CR 1983 Eruptive history of Mount Mazama and Crater Lake caldera, Cascade Range, USA. *J Volcanol Geotherm Res* 18: 57-115.
- Baldwin B 1971 Ways of deciphering compacted sediments. *J Sediment Petrol* 41: 29-301.
- Ballard RD and Moore JG 1977 *Photographic atlas of the Mid-Atlantic Ridge Rift Valley*. Springer-Verlag, New York 114 pp.
- Ballard RD, Holcomb RT and van Andel TH 1979 The Galapagos Rift at 86°W: 3. Sheet flows, collapse pits and lava lakes of the rift valley. *J Geophys Res* 84: 5407-5422.
- Basaltic Volcanism Study Project 1981 *Basaltic Volcanism on the Terrestrial Planets*. Pergamon Press Inc, New York 1286 pp.
- Bateson JH 1965 Accretionary lapilli in a geosynclinal environment. *Geol Mag* 102: 1-7.
- Benson GT and Kittleman LR 1968 Geometry of flow layering in silicic lavas. *Am J Sci* 266: 265-276.
- Bergh SG and Sigvaldason GE 1991 Pleistocene mass-flow deposits of basaltic hyaloclastite on a shallow submarine shelf, South Iceland. *Bull Volcanol* 53: 597-611.
- Bevins RE and Roach RA 1979 Pillow lava and isolated-pillow breccia of rhyodacitic composition from the Fishguard Volcanic Group, lower Ordovician, SW Wales, United Kingdom. *J Geol* 87: 192-201.
- Binney WP 1987 A sedimentological investigation of Maclean channel transported sulphide ores. In Kirkham (ed) *Buchans Geology*, Newfoundland. *Geol Survey of Canada Paper* 86-24: 107-147.
- Blackburn EA, Wilson L and Sparks RSJ 1976 Mechanisms and dynamics of strombolian activity. *J Geol Soc London* 132: 429-440.
- Bonnichsen B and Kauffman DF 1987 Physical features of rhyolite lava flows in the Snake River Plain volcanic province, southwestern Idaho. *Geol Soc Am Spec Pap* 212: 119-145.
- Bouma AH 1962 *Sedimentology of some flysch deposits*. Elsevier, Amsterdam 168 pp.
- Branney MJ and Suthren RJ 1988 High-level peperitic sills in the English Lake District: distinction from block lavas, and implications for Borrowdale Volcanic Group stratigraphy. *Geol J* 23: 171-187.
- Branney MJ and Sparks RSJ 1990 Fiamme formed by diagenesis and burial-compaction in soils and subaqueous sediments. *J Geol Soc London* 147: 919-922.
- Branney MJ and Kokelaar P 1992 A reappraisal of ignimbrite emplacement: progressive aggradation and changes from particulate to non-particulate flow during emplacement of high-grade ignimbrite. *Bull Volcanol* 54: 504-520.
- Brooks ER, Wood MM and Garbutt PL 1982 Origin and metamorphism of peperite and associated rocks in the Devonian Elwell Formation, northern Sierra Nevada, California. *Geol Soc Am Bull* 93: 1208-1231.
- Bryan WB 1972 Morphology of quench crystals in submarine basalts. *J Geophys Res* 72: 5812-5819.
- Bull SW and Cas RAF 1989 Volcanic influences in a storm and tide dominated shallow marine depositional system: the Late Permian Broughton Formation, southern Sydney Basin, Kiama,

- NSW, Australia. *Aust J Earth Sci* 36: 569-584.
- Bull SW and Cas RAF 1991 Depositional controls and characteristics of subaqueous bedded volcanoclastics of the Lower Devonian Snowy River Volcanics. *Sedimentary Geology* 74: 189-215.
- Burnham CW 1983 Deep submarine pyroclastic eruptions. *Econ Geol Mon* 5: 142-148.
- Bursik MI, Sparks RSJ, Gilbert JS and Carey SN 1992 Sedimentation of tephra by volcanic plumes: I. Theory and its comparison with a study of the Fogo A plinian deposit, San Miguel (Azores). *Bull Volcanol* 54: 329-344.
- Busby-Spera CJ 1984 Large-volume rhyolite ash flow eruptions and submarine caldera collapse in the lower Mesozoic Sierra Nevada, California. *J Geophys Res* 89: 8417-8427.
- Busby-Spera CJ 1986 Depositional features of rhyolitic and andesitic volcanoclastic rocks of the Mineral King submarine complex, Sierra Nevada, California. *J Volcanol Geotherm Res* 27: 43-76.
- Busby-Spera CJ and White JDL 1987 Variation in peperite textures associated with differing host-sediment properties. *Bull Volcanol* 49: 765-775.
- Carey S and Sparks RSJ 1986 Quantitative models of the fallout and dispersal of tephra from volcanic eruption columns. *Bull Volcanol* 48: 109-126.
- Carey S and Sigurdsson H 1989 The intensity of plinian eruptions. *Bull Volcanol* 51: 28-40.
- Carlisle D 1963 Pillow breccias and their aquagene tuffs, Quadra Island, British Columbia. *J Geol* 71: 48-71.
- Carmassi M, De Rita D, Di Filippo M, Funicello R and Sheridan MF 1983 Geology and volcanic evolution of the island of Ponza, Italy. *Geol Rom* 22: 211-232.
- Cas RAF 1978 Silicic lavas in Paleozoic flysch-like deposits in New South Wales, Australia: behaviour of deep subaqueous silicic flows. *Geol Soc Am Bull* 89: 1708-1714.
- Cas RAF 1983 Submarine 'crystal tuffs': their origin using a lower Devonian example from southeastern Australia. *Geol Mag* 120: 471-486.
- Cas RAF and Wright JV 1991 Subaqueous pyroclastic flows and ignimbrites: an assessment. *Bull Volcanol* 53: 357-380.
- Cas RAF, Allen RL, Bull SW, Clifford BA and Wright JV 1990 Subaqueous, rhyolitic dome-top cones: a model based on the Devonian Bunga Beds, southeastern Australia and a modern analogue. *Bull Volcanol* 52: 159-174.
- Cashman KV and Fiske RS 1991 Fallout of pyroclastic debris from submarine volcanic eruptions. *Science* 253: 275-279.
- Chapin CE and Lowell GR 1979 Primary and secondary flow structures in ash flow tuffs of the Gribbles Run paleovalley, central Colorado. *Geol Soc Am Spec Pap* 180: 137-153.
- Christiansen RL and Lipman PW 1966 Emplacement and thermal history of a rhyolite lava flow near Fortymile Canyon, southern Nevada. *Geol Soc Am Bull* 77: 671-684.
- Christiansen RL and Hildreth W 1989 Voluminous rhyolitic lavas of broad extent on the Yellowstone Plateau. IAVCEI General Assembly, Santa Fe, USA, Abstracts: 52.
- Clough BJ, Wright JV and Walker GPL 1981 An usual bed of giant pumice in Mexico. *Nature* 289: 49-50.
- Cole PD 1991 Migration direction of sand-wave structures in pyroclastic surge deposits: implications for depositional processes. *Geology* 19: 1108-1111.
- Collinson JD and Thompson DB 1989 *Sedimentary Structures*. 2nd ed. Unwin Hyman Ltd, London 207 pp.
- Corbett KD 1992 Stratigraphic-volcanic setting of massive sulfide deposits in the Cambrian Mount Read Volcanics, Tasmania. *Econ Geol* 87: 564-586.
- Corbett KD and Komysan P 1989 Geology of the Hellyer-Mt Charter area. Tasmania Dept Mines, Geological Report 1, Mt Read Volcanics Project 48 pp.
- Cousineau P and Dimroth E 1982 Interpretation of the relations between massive, pillowed and brecciated facies in an Archean submarine andesitic volcano - Amulet Andesite, Rouyn-Noranda, Canada. *J Volcanol Geotherm Res* 13: 83-102.
- Cox KG, Bell JD and Pankhurst RJ 1979 The interpretation of igneous rocks. Unwin Hyman, London 450 pp.
- Crandell DR 1969 Surficial geology of Mount Rainier National Park, Washington. *US Geol Surv Bull* 1288: 25-26.
- Crandell DR 1971 Postglacial lahars from Mount Rainier volcano, Washington. *US Geol Surv Prof Pap* 677: 24-30.
- Crandell DR, Mullineaux DR, Sigafos RS and Rubin M 1974 Chaos Crag eruptions and rock-fall avalanches, Lassen Volcanic National Park, California. *US Geol Surv J Res* 2: 45-59.
- Crandell DR, Miller CD, Glicken HX, Christiansen RL and Newhall CG 1984 Catastrophic debris avalanche from ancestral Mount Shasta volcano, California. *Geology* 12: 143-146.
- Crawford AJ, Corbett KD and Everard JL 1992 Geochemistry of the Cambrian volcanic-hosted massive sulfide-rich Mount Read Volcanics, Tasmania, and some tectonic implications. *Econ Geol* 87: 597-619.
- Crowe BM and Fisher RV 1973 Sedimentary structures in base surge deposits with special reference to cross bedding, Ubehebe craters, Death Valley, California. *Geol Soc Am Bull* 84: 663-682.
- Dadd KA 1992 Structures within large volume rhyolite lava flows of the Devonian Comerong Volcanics, southeastern Australia, and the Pleistocene Ngongotaha lava dome, New Zealand. *J Volcanol Geotherm Res* 54: 33-53.
- Davies DK, Almon WR, Bonis SB and Hunter BE 1978 Deposition and diagenesis of Tertiary-Holocene volcanoclastics, Guatemala. In Scholle PA and Schluger PR (eds) *Aspects of Diagenesis*. SEPM Spec Pub 26: 281-306.
- De Rosen-Spence AF, Provost G, Dimroth E, Gochner K and Owen V 1980 Archean subaqueous felsic flows, Rouyn-Noranda, Quebec, Canada and their Quaternary equivalents. *Precambrian Res* 12: 43-77.
- De Silva SL and Francis PW 1991 *Volcanoes of the Central Andes*. Springer-Verlag, Berlin 216 pp.
- Dewit MJ and Stern C 1978 Pillow talk. *J Volcanol Geotherm Res* 4: 55-80.
- Dimroth E and Yamagishi H 1987 Criteria for the recognition of ancient subaqueous pyroclastic rocks. *Geol Surv Hokkaido Rep* 58: 55-88.
- Dimroth E, Cousineau P, Leduc M and Sanschagrin Y 1978 Structure and organisation of Archean basalt flows, Rouyn-Noranda area, Quebec, Canada. *Can J Earth Sci* 15: 902-918.
- Doloz MB and Ayres LD 1991 Early Proterozoic, basaltic andesite tuff breccia: downslope, subaqueous mass transport of phreatomagmatically-generated tephra. *Bull Volcanol* 53: 477-495.
- Dott RH Jr and Bourgeois J 1982 Hummocky stratification: significance of its variable bedding sequences. *Geol Soc Am Bull* 93: 663-680.
- Druitt TH 1992 Emplacement of the 18 May 1980 lateral blast ENE of Mount St. Helens, Washington. *Bull Volcanol* 54: 554-572.
- Druitt TH and Sparks RSJ 1982 A proximal ignimbrite breccia facies on Santorini, Greece. *J Volcanol Geotherm Res* 13: 147-171.
- Duffield WA and Dalrymple GB 1990 The Taylor Creek Rhyolite of New Mexico: a rapidly emplaced field of lava domes and flows. *Bull Volcanol* 52: 475-87.

- Duke WL, Arnott RWC and Cheel RJ 1991 Shelf sandstones and hummocky cross-stratification: New insights on a stormy debate. *Geology* 19: 625-628.
- Easton RM and Johns GW 1986 Volcanology and mineral exploration: the application of physical volcanology and facies studies. *Ontario Geol Surv Misc Pap* 129: 2-40.
- Eichelberger JC and Westrich HR 1981 Magmatic volatiles in explosive rhyolitic eruptions. *Geophys Res Lett* 8: 757-760.
- Eichelberger JC, Carrigan CR, Westrich HR and Price RH 1986 Non-explosive silicic volcanism. *Nature* 323: 598-602.
- Einsele G 1986 Interaction between sediments and basalt injections in young Gulf of California-type spreading centres. *Geol Rund* 75: 197-208.
- Ekren EB, McIntyre DH and Bennett EH 1984 High-temperature, large volume, lava-like ash-flow tuffs without calderas in southwestern Idaho. *US Geol Surv Prof Pap* 1272.
- Farrand WH and Singer RB 1992 Alteration of hydrovolcanic basaltic ash: observations with visible and near-infrared spectrometry. *J Geophys Res* 97: 17393-17408.
- Fierstein J and Hildreth W 1992 The plinian eruptions of 1912 at Novarupta, Katmai National Park, Alaska. *Bull Volcanol* 54: 646-684.
- Fink JH 1980 Gravity instability in the Holocene Big and Little Glass Mountain rhyolitic obsidian flows, northern California. *Tectonophysics* 66: 147-166.
- Fink JH 1983 Structure and emplacement of a rhyolite obsidian flow: Little Glass Mountain, Medicine Lake Highland, northern California. *Geol Soc Am Bull* 94: 362-380.
- Fink JH and Fletcher RC 1978 Ropy pahoehoe: surface folding of a viscous fluid. *J Volcanol Geotherm Res* 4: 151-170.
- Fink JH and Pollard DD 1983 Structural evidence for dikes beneath silicic domes, Medicine Lake Highland volcano, California. *Geology* 11: 458-461.
- Fink JH and Manley CR 1987 Origin of pumiceous and glassy textures in rhyolitic flows and domes. *Geol Soc Am Spec Pap* 212: 77-88.
- Fink JH, Anderson SW and Manley CR 1992 Textural constraints on effusive silicic volcanism: beyond the permeable foam model. *J Geophys Res* 97: 9073-9083.
- Fisher RV 1960 Classification of volcanic breccias. *Geol Soc Am Bull* 71: 973-982.
- Fisher RV 1961 Proposed classification of volcanoclastic sediments and rocks. *Geol Soc Am Bull* 72: 1409-1414.
- Fisher RV 1966a Mechanism of deposition from pyroclastic flows. *Am J Sci* 264: 350-363.
- Fisher RV 1966b Rocks composed of volcanic fragments. *Earth Sci Rev* 1: 287-298.
- Fisher RV 1968 Puu Hou littoral cones, Hawaii. *Geol Rundsch* 57: 837-864.
- Fisher RV 1979 Models for pyroclastic surges and pyroclastic flows. *J Volcanol Geotherm Res* 6: 305-318.
- Fisher RV 1983 Flow transformations in sediment gravity flows. *Geology* 11: 273-274.
- Fisher RV 1984 Submarine volcanoclastic rocks. In Kokelaar BP and Howells MF (eds) *Marginal Basin Geology*. *Geol Soc Spec Pub* 16: 5-28.
- Fisher RV and Waters AC 1970 Base surge bed forms in maar volcanoes. *Am J Sci* 268: 157-180.
- Fisher RV and Heiken G 1982 Mt Pelee Martinique: May 8 and 20, 1902, pyroclastic flows and surges. *J Volcanol Geotherm Res* 13: 339-371.
- Fisher RV and Schmincke H-U 1984 *Pyroclastic rocks*. Springer-Verlag, Berlin 472 pp.
- Fisher RV, Smith AL and Roobol MJ 1980 Destruction of St Pierre, Martinique by ash cloud surges, May 8 and 20, 1902. *Geology* 8: 472-476.
- Fiske RS 1963 Subaqueous pyroclastic flows in the Ohanapcosh Formation, Washington. *Geol Soc Am Bull* 74: 391-406.
- Fiske RS and Matsuda T 1964 Submarine equivalents of ash flows in the Tokiwa Formation, Japan. *Am J Sci* 262: 76-106.
- Fornari DJ 1986 Submarine lava tubes and channels. *Bull Volcanol* 48: 291-298.
- Francis EH and Howells MF 1973 Transgressive welded ash-flow tuffs among the Ordovician sediments of NE Snowdonia, N Wales. *J Geol Soc London* 129: 621-641.
- Francis PW and Baker MCW 1978 Sources of two large ignimbrites in the central Andes: some LANDSAT evidence. *J Volcanol Geotherm Res* 4: 81-87.
- Francis PW and Wells GL 1988 Landsat Thematic Mapper observations of debris avalanche deposits in the Central Andes. *Bull Volcanol* 50: 258-278.
- Francis PW, Gardeweg M, Ramirez CF and Rothery DA 1985 Catastrophic debris avalanche deposit of Socoma volcano, northern Chile. *Geology* 13: 600-603.
- Freundt A and Schmincke H-U 1986 Emplacement of small volume pyroclastic flows at Laacher See (East Eifel, Germany). *Bull Volcanol* 48: 39-60.
- Freundt A and Schmincke H-U 1990 The densely Welded basaltic ignimbrite PI on Gran Canaria. IAVCEI International Volcanological Congress, Mainz, Germany Abstracts.
- Freundt A and Schmincke H-U 1992 Mixing of rhyolite, trachyte and basalt magma erupted from a vertically and laterally zoned reservoir, composite flow PI, Gran Canaria. *Contrib Mineral Petrol* 112: 1-9.
- Fridleifsson IB, Furnes H and Atkins FB 1982 Subglacial volcanics on the control of magma chemistry on pillow dimensions. *J Volcanol Geotherm Res* 13: 84-117.
- Friedman GM and Sanders JE 1978 *Principles of sedimentology*. John Wiley and Sons, New York 792 pp.
- Friedman I 1989 Are extrusive rhyolites produced from permeable foam eruptions? *Bull Volcanol* 51: 69-71.
- Friedman I and Smith RL 1958 The deuterium content of water in some volcanic glasses. *Geochim Cosmochim Acta* 15: 218-228.
- Friedman I and Long W 1976 Hydration rate of obsidian. *Science* 191: 347-352.
- Friedman I, Smith RG and Long WD 1966 Hydration of natural glass and formation of perlite. *Geol Soc Am Bull* 77: 323-328.
- Furnes H, Fridleifsson IB and Atkins FB 1980 Subglacial volcanics on the formation of acid hyaloclastites. *J Volcanol Geotherm Res* 8: 95-110.
- Gemmell JB and Large RR 1992 Stringer system and alteration zones underlying the Hellyer volcanic-hosted massive sulfide deposit, Tasmania, Australia. *Econ Geol* 87: 620-649.
- Gibson RG and Naney MT 1992 Textural development of mixed, finely porphyritic silicic volcanic rocks, Inyo Domes, eastern California. *J Geophys Res* 97: 4541-4559.
- Gibson RP 1991 The geology of the Mount Read Volcanics in the Anthony Road—Newton Creek area, western Tasmania. Unpubl. BSc Hons thesis, University of Tasmania.
- Gilbert JS, Lane SJ, Sparks RSJ and Koyaguchi T 1991 Charge measurements on particle fallout from a volcanic plume. *Nature* 349: 598-600.
- Gill J and twelve others 1990 Explosive deep water basalt in the Sumisu backarc rift. *Science* 248: 1214-1217.
- Glazner AF, Nielson JE, Howard KA and Miller DM 1986 Correlation of the Peach Springs Tuff, a large volume Miocene ignimbrite sheet in California and Arizona. *Geology* 14: 840-843.

- Glicken H 1991 Sedimentary architecture of large volcanic-debris avalanches. In Fisher RV and Smith GA (eds) *Sedimentation in Volcanic Settings*. SEPM Spec Pub 45: 99-106.
- Godinot A 1988 Comment on 'Pipe vesicles in Hawaiian basaltic lavas: their origin and potential as paleoslope indicators'. *Geology* 16: 90.
- Green GR, Solomon M and Walshe JL 1981 The formation of the volcanic hosted massive sulfide ore deposit at Rosebery, Tasmania. *Econ Geol* 76: 304-338.
- Green JC and Fitz TJ 1993 Extensive felsic lavas and rhyolinites in the Keweenaw Midcontinent Rift plateau volcanics, Minnesota: petrographic and field recognition. *J Volcanol Geotherm Res* 54: 177-196.
- Griffiths RW and Fink JH 1992 Solidification and morphology of submarine lavas: a dependence on extrusion rate. *J Geophys Res* 97: 19729-19737.
- Guest JE and Sanchez J 1969 A large dacite lava flow in northern Chile. *Bull Volcanol* 33: 778-790.
- Hanson RE 1991 Quenching and hydroclastic disruption of andesitic to rhyolitic intrusions in an submarine island-arc sequence, northern Sierra Nevada, California. *Geol Soc Am Bull* 103: 804-816.
- Hanson RE and Schweickert RA 1982 Chilling and brecciation of a Devonian rhyolitic sill intruded into wet sediments, northern Sierra Nevada, California. *J Geol* 90: 717-724.
- Hanson RE and Wilson TJ 1993 Large-scale rhyolite peperites (Jurassic, southern Chile). *J Volcanol Geotherm Res* 54: 247-264.
- Hargreaves R and Ayres LD 1979 Morphology of Archean metabasalt flows, Utik Lake, Manitoba. *Can J Earth Sci* 16: 1452-1466.
- Hausback BP 1987 An extensive, hot, vapor-charged rhyodacite flow, Baja California, Mexico. *Geol Soc Am Spec Pap* 212: 111-118.
- Head JW and Wilson L 1986 Volcanic processes and landforms on Venus: Theory, predictions, and observations. *J Geophys Res* 91: 9407-9446.
- Hedenquist JW and Henley RW 1985 Hydrothermal eruptions in the Waiotapu Geothermal System, New Zealand: their origin, associated breccias, and relation to precious metal mineralization. *Econ Geol* 80: 1640-1668.
- Heiken GH 1972 Morphology and petrology of volcanic ashes. *Geol Soc Am Bull* 83: 1961-1988.
- Heiken GH 1974 An atlas of volcanic ash. *Smithsonian Cont Earth Sci* 12: 1-101.
- Heiken GH and Wohletz K 1985 Volcanic ash. University of California Press, Berkeley 246 pp.
- Heiken GH and Wohletz K 1987 Tephra deposits associated with silicic domes and lava flows. *Geol Soc Am Spec Pap* 212: 55-76.
- Heiken GH and Wohletz K 1991 Fragmentation processes in explosive volcanic eruptions. In Fisher RV and Smith GA (eds) *Sedimentation in Volcanic Settings*. SEPM Spec Pub 45: 19-26.
- Heinrichs T 1984 The Umsoli Chert, turbidite testament for a major phreatoplinian event at the Onverwacht/Figtree transition (Swaziland Supergroup, Archaean, South Africa). *Precambrian Res* 24: 237-283.
- Henry CD and Wolff JA 1992 Distinguishing strongly rheomorphic tuffs from extensive silicic lavas. *Bull Volcanol* 54: 171-186.
- Henry CD, Price JG, Rubin JN, Parker DF, Wolff JA, Self S, Franklin R and Barker DS 1988 Widespread, lava-like silicic volcanic rocks of Trans-Pecos Texas. *Geology* 16: 509-512.
- Henry CD, Price JG, Rubin JN and Laubach SE 1990 Case study of an extensive lava: the Bracks Rhyolite, Trans-Pecos Texas. *J Volcanol Geotherm Res* 43: 113-132.
- Hildreth W 1979 The Bishop Tuff: evidence for the origin of compositional zonation in silicic magma chambers. In Chapin CE and Elston WE (eds) *Ash-Flow Tuffs*. *Geol Soc Am Spec Pap* 180: 43-75.
- Hildreth W 1983 The compositionally zoned eruption of 1912 in the Valley of Ten Thousand Smokes, Katmai National Park, Alaska. *J Volcanol Geotherm Res* 18: 1-56.
- Honnorez J and Kirst P 1975 Submarine basaltic volcanism: morphometric parameters for discriminating hyaloclastites from hyalotuffs. *Bull Volcanol* 39: 441-465.
- Houghton BF and Hackett WR 1984 Strombolian and phreatomagmatic deposits of Ohakune Craters, Ruapehu, New Zealand: a complex interaction between external water and rising basaltic magma. *J Volcanol Geotherm Res* 21: 207-231.
- Houghton BF and Wilson CJN 1989 A vesicularity index for pyroclastic deposits. *Bull Volcanol* 51: 451-62.
- Howells MF, Leveridge BE Addison R, Evans CDR and Nutt MJC 1979 The Capil Curig Volcanic Formation, Snowdonia, North Wales; variations in ash-flow tuffs related to emplacement environment. *Geol Soc London Spec Pub* 8: 611-618.
- Howells MF, Campbell SDG and Reedman AJ 1985 Isolated pods of subaqueous welded ash-flow tuff: a distal facies of the Capel Curig Volcanic Formation (Ordovician), North Wales. *Geol Mag* 122: 175-180.
- Howells MF, Reedman AJ and Campbell SDG 1986 The submarine eruption and emplacement of the Lower Rhyolitic Tuff Formation (Ordovician), N Wales. *J Geol Soc London* 143: 411-423.
- Howells MF, Reedman AJ and Campbell SDG 1991 Ordovician (Caradoc) marginal basin volcanism in Snowdonia (northwest Wales). *British Geological Survey, London* 191 pp.
- Hulme G 1974 The interpretation of lava flow morphology. *Geophys J R Astr Soc* 39: 361-383.
- Huppert HE, Shepherd JB, Sigurdsson H and Sparks RSJ 1982 On lava dome growth, with application to the 1979 lava explosion of the Soufriere of St Vincent. *J Volcanol Geotherm Res* 14: 199-222.
- Jaggard TA and Finch RH 1924 The explosive eruption of Kilauea in Hawaii. *Am J Sci Fifth Series* 8: 353-374.
- Jakobsson SP and Moore JG 1986 Hydrothermal minerals and alteration rates at Surtsey volcano, Iceland. *Geol Soc Am Bull* 97: 648-659.
- Jones JG 1969 Pillow lavas as depth indicators. *Am J Sci* 267: 181-195.
- Jones JG and Nelson PHH 1970 The flow of basalt lava from air into water - its structural expression and stratigraphic significance. *Geol Mag* 107: 13-19.
- Joplin GA 1971 A petrography of Australian igneous rocks. Angus and Robertson, Sydney 253 pp.
- Kano K 1990 An ash-flow tuff emplaced in shallow water, Early Miocene Koura Formation, southwest Japan. *J Volcanol Geotherm Res* 40: 1-9.
- Kano K 1991 Miocene pillowed sills in the Shimane Peninsula, SW Japan. *J Volcanol Geotherm Res* 48: 359-366.
- Kano K, Takeuchi K, Yamamoto T and Hoshizumi H 1991 Subaqueous rhyolite block lavas in the Miocene Ushikiri Formation, Shimane Peninsula, SW Japan. *J Volcanol Geotherm Res* 46: 241-253.
- Kano KI 1989 Interactions between andesitic magma and poorly consolidated sediments: examples in the Neogene Shirahama Group, South Izu, Japan. *J Volcanol Geotherm Res* 37: 59-75.
- Kato Y 1987 Woody pumice generated with submarine eruption.

- J Geol Soc Japan 93: 11-20.
- Kato Y 1988 Woody pumice - an indicator of submarine eruption. *Proceedings Kagoshima International Conference on Volcanoes*: 143-146.
- Kawachi Y and Pringle IJ 1988 Multiple-rind structure in pillow lava as an indicator of shallow water. *Bull Volcanol* 50: 161-168.
- Kokelaar BP 1982 Fluidization of wet sediments during emplacement and cooling of various igneous bodies. *J Geol Soc London* 139: 21-33.
- Kokelaar BP 1983 The mechanism of Surtseyan volcanism. *J Geol Soc London* 140: 939-944.
- Kokelaar P 1986 Magma-water interactions in subaqueous and emergent basaltic volcanism. *Bull Volcanol* 48: 275-291.
- Kokelaar P 1990 Excursion L: Marine volcanogenic sedimentary records of rifting and volcanotectonism during basaltic volcanism at the site of a rhyolitic caldera — the Bedded Pyroclastic Formation on Snowdon. In *Volcanogenic Sedimentation in Ancient Terrains, Field Guide II, IAVCEI/IAS Field Workshop 1990*: L1-L12.
- Kokelaar P and Busby C 1992 Subaqueous explosive eruption and welding of pyroclastic deposits. *Science* 257: 196-201.
- Kokelaar BP, Howells MF, Bevins RE and Roach RA 1984 Volcanic and associated sedimentary and tectonic processes in the Ordovician marginal basin of Wales: a field guide. In Kokelaar BP and Howells MF (eds) *Marginal Basin Geology*. *Geol Soc Spec Pub* 16: 291-322.
- Kokelaar P, Branney M and Suthren R 1990 Excursion A: Shallow basinal sedimentation during a phreatoplinian eruption - The Whorrieside Formation at Sourmilk Gill. In *Volcanogenic Sedimentation in Ancient Terrains, Field Guide I, IAVCEI/IAS Field Workshop 1990* A1-A15.
- Kuenzi WD, Horst OH and McGehee 1979 Effect of volcanic activity on fluvial-deltaic sedimentation in a modern arc-trench gap, southwestern Guatemala. *Geol Soc Am Bull* 90: 827-838.
- Large RR 1992. Australian volcanic-hosted massive sulfide deposits: features, styles and genetic models. *Econ Geol* 87: 471-510.
- Ledbetter MT and Sparks RSJ 1979 Duration of large-magnitude explosive eruptions deduced from graded bedding in deep-sea ash layers. *Geology* 7: 240-244.
- Lipman PW 1965 Chemical comparison of glassy and crystalline volcanic rocks. *US Bull* 1201-D: 24 pp.
- Lipman PW 1976 Caldera collapse breccias in the western San Juan Mountains, Colorado. *Geol Soc Am Bull* 87: 1397-1410.
- Lipman PW, Normark WR, Moore JG, Wilson JB and Gutmacher CE 1988 The giant submarine Alike debris slide, Mauna Loa, Hawaii. *J Geophys Res* 93 B5: 4279-4299.
- Lofgren G 1970 Experimental devitrification rate of rhyolite glass. *Geol Soc Am Bull* 81: 553-560.
- Lofgren G 1971a Spherulitic textures in glassy and crystalline rocks. *J Geophys Res* 76: 5635-5648.
- Lofgren G 1971b Experimentally produced devitrification textures in natural rhyolitic glass. *Geol Soc Am Bull* 82: 111-124.
- Lofgren G 1974 An experimental study of plagioclase crystal morphology: isothermal crystallisation. *Am J Sci* 274: 243-273.
- Lonsdale P 1977 Abyssal pahoehoe with lava coils at the Galapagos Rift. *Geology* 5: 147-152.
- Lonsdale P and Batiza R 1980 Hyaloclastite and lava flows on young seamounts examined with a submersible. *Geol Soc Am Bull* 91: 545-554.
- Lorenz V 1973 On the formation of maars. *Bull Volcanol* 37: 183-204.
- Lorenz V 1974 Vesiculated tuffs and associated features. *Sedimentology* 21: 273-291.
- Lowe DR 1976 Grain flow and grain flow deposits. *J Sediment Petrol* 46: 188-199.
- Lowe DR 1979 Sediment gravity flows: their classification and some problems of application to natural flows and deposits. *SEPM Special Publication* 27: 75-82.
- Lowe DR 1982 Sediment gravity flows: II. Depositional models with special reference to the deposits of high density turbidity currents. *J Sediment Petrol* 52: 279-297.
- Macdonald GA 1953 Pahoehoe, aa and block lava. *Am J Sci* 251: 169-191.
- Macdonald GA 1968 Composition and origin of Hawaiian lavas. *Geol Soc Am Bull* 116: 477-522.
- Macdonald GA 1972 *Volcanoes*. Prentice Hall, New Jersey 510 pp.
- Mahood GA 1984 Pyroclastic rocks and calderas associated with strongly peralkaline magmatism. *J Geophys Res* 89: 8540-8552.
- Major JJ and Newhall CG 1989 Snow and ice perturbation during historical volcanic eruptions and the formation of lahars and floods. A global review. *Bull Volcanol* 52: 1-27.
- Mangan MT, Cashman KV and Newman S 1993 Vesiculation of basaltic magma during eruption. *Geology* 21: 157-160.
- Manley CR 1992 Extended cooling and viscous flow of large, hot rhyolite lavas: implications of numerical modeling results. *J Volcanol Geotherm Res* 53: 27-46.
- Marshall RR 1961 Devitrification of natural glass. *Geol Soc Am Bull* 72: 1493-1520.
- McArthur GJ and Dronseika EV 1990 Que River and Hellyer zinc-lead deposits. *Australasian Inst Mining Metallurgy Mon* 14: 1331-1339.
- McBirney AR 1963 Factors governing the nature of submarine volcanism. *Bull Volcanol* 26: 455-69.
- McBirney AR and Murase T 1970 Factors governing the formation of pyroclastic rocks. *Bull Volcanol* 34: 372-334.
- McPhie J 1986 Primary and redeposited facies from a large-magnitude, rhyolitic, phreatomagmatic eruption: Cana Creek Tuff, Late Carboniferous, Australia. *J Volcanol Geotherm Res* 28: 319-350.
- McPhie J 1987 The Hianana Volcanics: remnants of a Late Permian tuff ring and lava flow, Coombadjha Volcanic Complex, northeastern New South Wales. *Aust J Earth Sci* 34: 417-433.
- McPhie J 1993 The Tennant Creek porphyry revisited: a syn-sedimentary sill with peperite margins, early Proterozoic, Northern Territory. *Aust J Earth Sciences* (in Press).
- McPhie J and Allen RL 1992 Facies architecture of mineralised submarine volcanic sequences: Cambrian Mount Read Volcanics, western Tasmania. *Econ Geol* 87: 587-596.
- McPhie J, Walker GPL and Christiansen RL 1990 Phreatomagmatic and phreatic fall and surge deposits from explosions at Kilauea volcano, Hawaii, 1790 AD: Keanakakoi Ash Member. *Bull Volcanol* 52: 334-354.
- Mellors RA, Waitt RB and Swanson DA 1988 Generation of pyroclastic flows and surges by hot-rock avalanches from the dome of Mount St. Helens volcano, USA. *Bull Volcanol* 50: 14-25.
- Minakami T, Ishikawa T and Yagi K 1951 The 1944 eruption of Volcano Usu in Hokkaido, Japan. *Bull Volcanol* 11: 45-160.
- Moore HJ, Arthur DWG and Schaber GG 1978. Yield strengths of flows on the Earth, Mars and the Moon. *Proc 9th Lunar Planet Conference*: 3351-3378.
- Moore JG 1964 Giant submarine landslides on the Hawaiian Ridge. *US Geol Surv Prof Pap* 501D: D95-D98.
- Moore JG 1965 Petrology of deep-sea basalt near Hawaii. *Am J Sci*

- 263: 40-52.
- Moore JG 1967 Base surge in recent volcanic eruptions. *Bull Volcanol* 30: 337-363.
- Moore JG 1975 Mechanisms of formation of pillow lava. *Am J Sci* 63: 269-277.
- Moore JG 1985 Structure and eruptive mechanisms at Surtsey Volcano, Iceland. *Geol Mag* 122: 649-661.
- Moore JG and Peck DL 1962 Accretionary lapilli in volcanic rocks of the western continental United States. *J Geol* 70: 182-193.
- Moore JG and Schilling JG 1973 Vesicles, water and sulphur in Reykjanes Ridge basalts. *Contrib Mineral Petrol* 41: 105-118.
- Moore JG, Phillips RL, Grigg RW, Peterson DW and Swanson DA 1973 Flow of lava into the sea, 1969-1971, Kilauea Volcano, Hawaii. *Geol Soc Am Bull* 84: 537-546.
- Moore JG, Lipman PW, Swanson DA and Tau Rho Alpha 1981 Growth of lava domes in the crater, June 1980-January 1981. *USGS Prof Pap* 1250: 541-547.
- Muffler LJP, White DE and Truesdell AH 1971 Hydrothermal explosion craters in Yellowstone National Park. *Geol Soc Am Bull* 82: 723-740.
- Nairn IA and Self S 1978 Explosive eruptions and pyroclastic avalanches from Ngauruhoe in February 1975. *J Volcanol Geotherm Res* 3: 39-60.
- Nairn IA and Wiradirdja S 1980 Late Quaternary hydrothermal explosion breccias at Kawerau Geo thermal Field, New Zealand. *Bull Volcanol* 43: 1-13.
- Naranjo JL, Sigurdsson H, Carey SN and Fritz W 1986 Eruption of Nevado del Ruiz volcano, Colombia, on 13 November 1985: tephra fall and lahars. *Science* 233: 961-963.
- Nelson SA 1981 The possible role of thermal feedback in the eruption of siliceous magmas. *J Volcanol Geotherm Res* 11: 127-137.
- Newhall CG and Melson WG 1983 Explosive activity associated with the growth of volcanic domes. *J Volcanol Geotherm Res* 17: 111-131.
- Ninkovich D, Sparks RSJ and Ledbetter MT 1978 The exceptional magnitude and intensity of the Toba eruption, Sumatra: an example of the use of deep-sea tephra layers as a geological tool. *Bull Volcanol* 41: 286-298.
- Noble DC 1967 Sodium, potassium and ferrous iron contents of some secondarily hydrated natural silicic glasses. *Am Mineral* 52: 230-285.
- Ocean Drilling Program Leg 139 Scientific Drilling Party 1992 Hot rocks and massive sulfide: northern Juan de Fuca Ridge. *EOS* 73: 193-198.
- Orsi G, D'Antonio M, de Vita S and Gallo G 1992 The Neopolitan Yellow Tuff, a large magnitude trachytic phreatoplinian eruption: eruptive dynamics, magma withdrawal and caldera collapse. *J Volcanol Geotherm Res* 53: 275-287.
- Orton G, Howells M and Fritz B 1990 Excursion F: Cwm Eigiau, Pitts Head Tuff, Lower Rhyolitic Tuff and Bedded Pyroclastic Formations-shallow marine volcanoclastic sedimentation about primary extrusive volcanic rocks, Cwm Bochlywyd-Cwm Cneifion-Cwm Idwal. In *Volcanogenic Sedimentation in Ancient Terrains, Field Guide II, IAVCEI/IAS Field Workshop 1990*: 47-58.
- Palmer BA, Alloway BV and Neall VE 1991 Volcanic-debris-avalanche deposits in New Zealand—lithofacies organisation in unconfined, wet-avalanche flows. In Fisher RV and Smith GA (eds) *Sedimentation in Volcanic Settings*. *SEPM Spec Pub* 45: 89-98.
- Peacock MA and Fuller RR 1928 Chlorophaeite, sideromelane and palagonite from the Columbia River Plateau. *Am Mineral* 13: 360-383.
- Perret FA 1937 The eruption of Mt Pelee 1929-1932. *Carnegie Inst Wash Pub* 458: 1-126.
- Peterson DW and Tilling RJ 1980 Transition of basaltic lava from pahoehoe to aa, Kilauea Volcano, Hawaii: field observations and key factors. *J Volcanol Geotherm Res* 7: 271-293.
- Philpotts A and Lewis C 1987 Pipe vesicles — an alternative model for their origin. *Geology* 15: 971-974.
- Pichler H 1965 Acid hyaloclastites. *Bull Volcanol* 28: 293-310.
- Pierson TC and Scott KM 1985 Downstream dilution of a lahar: transition from debris flow to hyperconcentrated streamflow. *Water Resources Research* 21: 1511-1524.
- Pierson TC, Janda RJ, Thouret JC and Borrero CA 1990 Perturbation and melting of snow and ice by the 13 November 1985 eruption of Nevado del Ruiz, Colombia, and consequent mobilization, flow and deposition of lahars. *J Volcanol Geotherm Res* 41: 17-66.
- Ragan DH and Sheridan MF 1972 Compaction of the Bishop Tuff, California. *Geol Soc Am Bull* 83: 95-106.
- Reading HG (ed) 1986 *Sedimentary environments and facies*. 2nd ed Blackwell Scientific Publications, Oxford: 615 pp.
- Reedman AJ, Howells MF, Orton G and Campbell SGD 1987 The Pitts Head Tuff Formation: a subaerial to submarine welded ash-flow tuff of Ordovician age, North Wales. *Geol Mag* 124: 427-439.
- Reimer TO 1983 Accretionary lapilli in volcanic ash falls: physical factors governing their formation. In Peryt TM (ed) *Coated Grains*. Springer, Berlin 56-68.
- Reynolds MA and Best JG 1976 Summary of the 1953-57 eruption of Tulum Volcano, Papua New Guinea. In Johnson RW (ed) *Volcanism in Australasia*. Elsevier, Amsterdam 287-296.
- Reynolds MA, Best JG and Johnson RW 1980 1953-57 eruption of Tulum volcano: rhyolitic volcanic activity in the northern Bismarck Sea. *Geol Surv Papua New Guinea Mem* 7: 44 pp.
- Riehle JR 1973 Calculated compaction profiles of rhyolite ash flows. *Geol Soc Am Bull* 84: 2193-2216.
- Rittmann A 1962 *Volcanoes and their activity*. John Wiley and Sons, New York 305 pp.
- Rose WI, Newhall CG, Bornhorst TJ and Self S 1987 Quaternary silicic pyroclastic deposits of Atitlan caldera, Guatemala. *J Volcanol Geotherm Res* 33: 57-80.
- Rosi M 1992 A model for the formation of vesiculated tuff by the coalescence of accretionary lapilli. *Bull Volcanol* 54: 429-34.
- Ross CS and Smith RL 1955 Water and other volatiles in volcanic glasses. *Am Mineral* 40: 1071-1089.
- Ross CS and Smith RL 1961 Ash flow tuffs: their origin, geologic relations and identification. *US Geol Surv Prof Pap* 366: 81 pp.
- Rowland SK and Walker GPL 1987 Toothpaste lava: characteristics and origin of a lava structural type transitional between pahoehoe and aa. *Bull Volcanol* 49: 631-641.
- Rowland SK and Walker GPL 1988 Mafic-crystal distributions, viscosities and lava structures of some Hawaiian lava flows. *J Volcanol Geotherm Res* 35: 55-66.
- Rowland SK and Walker GPL 1990. Pahoehoe and aa in Hawaii: volumetric flow rate controls the lava structure. *Bull Volcanol* 52: 615-628.
- Ryan MP and Sammis CG 1978 Cyclic fracture mechanisms in cooling basalt. *Geol Soc Am Bull* 89: 1295-1308.
- Sahagian DL, Anderson AT and Ward B 1989 Bubble coalescence in basalt flows: comparison of a numerical model with natural examples. *Bull Volcanol* 52: 46-56.
- Sampson DE 1987 Textural heterogeneities and vent area structures in the 600-year-old lavas of the Inyo volcanic chain, eastern California. *Geol Soc Am Spec Pap* 212: 89-102.
- Sato H, Fujii T and Nakada S 1992 Crumbling of dacite dome lava

- and generation of pyroclastic flows at Unzen Volcano. *Nature* 360: 664-666.
- Schmidt R 1981 Descriptive nomenclature and classification of pyroclastic deposits and fragments: recommendations of the IUGS Subcommission on the Systematics of Igneous Rocks. *Geology* 9: 41-43.
- Schmincke H-U 1967 Fused tuff and peperites in south central Washington. *Geol Soc Am Bull* 78: 319-330.
- Schmincke H-U 1974 Volcanological aspects of peralkaline silicic welded ash-flow tuffs. *Bull Volcanol* 38: 594-636.
- Schmincke H-U and Swanson DL 1967 Laminar viscous flowage structures in ash-flow tuffs from Gran Canaria, Canary Islands. *J Geol* 75: 641-664.
- Schmincke H-U, Fisher RV and Waters AC 1973 Amidune and chute and pool structures in base surge deposits of the Laacher See area, Germany. *Sedimentology* 20: 553-574.
- Schmincke H-U, Robinson PT, Ohrmacht W and Flower, MFJ 1978 Basaltic hyaloclastites from Hole 396B, DSDP Leg 46. In Dmitriev L, Heimler J et al. (eds) Initial Reports, Deep Sea Drilling Project 46: 341-355.
- Schumacher R and Schmincke H-U 1991 Internal structure and occurrence of accretionary lapilli — a case study at Laacher See volcano. *Bull Volcanol* 53: 612-634.
- Self S 1983 Large scale phreatomagmatic silicic volcanism: A case study from New Zealand. *J Volcanol Geotherm Res* 17: 433-469.
- Self S and Sparks RSJ 1978 Characteristics of widespread pyroclastic deposits formed by the interaction of silicic magma and water. *Bull Volcanol* 41: 196-212.
- Self S and Rampino M 1981 The 1883 eruption of Krakatau. *Nature* 292: 699-704.
- Self S, Sparks RSJ, Booth B and Walker GPL 1974 The 1973 Heimaey Strombolian scoria deposit, Iceland. *Geol Mag* 111: 539-548.
- Self S, Wilson L and Nairn IA 1979 Vulcanian eruption mechanisms. *Nature* 277: 440-443.
- Setterfield T 1987 Massive and brecciated dikes in the McDougall and Despina Faults, Noranda, Quebec, Canada. *J Volcanol Geotherm Res* 31: 87-97.
- Settle M 1978 Volcanic eruption clouds and the thermal power output of explosive eruptions. *J Volcanol Geotherm Res* 3: 309-324.
- Sheridan MF 1979 Emplacement of pyroclastic flows: a review. *Geol Soc Am Spec Pub* 180: 125-136.
- Sheridan MF and Updike RG 1975 Sugarloaf Mountain tephra—a Pleistocene rhyolitic deposit of base-surge origin in northern Arizona. *Geol Soc Am Bull* 86: 571-581.
- Sheridan MF and Wohletz KH 1981 Hydrovolcanic explosions: the systematics of water-pyroclast equilibration. *Science* 212: 1387-1389.
- Siebert L 1984 Large volcanic debris avalanches: characteristics of source areas, deposits and associated eruptions. *J Volcanol Geotherm Res* 22: 163-197.
- Siebert L, Glicken H and Ui T 1987 Volcanic hazards from Bezymianny- and Bandai-type eruptions. *Bull Volcanol* 49: 435-459.
- Sigurdsson H and Carey S 1989 Plinian and co-ignimbrite tephra fall from the 1815 eruption of Tambora volcano. *Bull Volcanol* 51: 243-270.
- Sigurdsson H, Grey S, Mandeville C and Bronto S 1991 Pyroclastic flows of the 1883 Krakatau eruption. *EOS* 72: 377-381.
- Silvestri SC 1963 Proposal for a genetic classification of hyaloclastites. *Bull Volcanol* 25: 315-321.
- Smith GA 1986 Coarse grained nonmarine volcanoclastic sediment: terminology and depositional processes. *Geol Soc Am Bull* 97: 1-10.
- Smith GA and Katzman D 1991 Discrimination of eolian and pyroclastic surge processes in the generation of cross-bedded tuffs, Jemez Mountains volcanic field, New Mexico. *Geology* 19: 465-468.
- Smith GA and Lowe DR 1991 Lahars: volcano-hydrologic events and deposition in the debris-flow-hyperconcentrated flow continuum. In Fisher RV and Smith GA (eds) *Sedimentation in Volcanic Settings*. SEPM Spec Pub 45: 59-70.
- Smith RCM 1991 Landscape response to a major ignimbrite eruption, Taupo Volcanic Centre, New Zealand. In Fisher RV and Smith GA (eds) *Sedimentation in Volcanic Settings*. SEPM Spec Pub 45: 123-138.
- Smith RL 1960a Ash flows. *Geol Soc Am Bull* 71: 795-842.
- Smith RL 1960b Zones and zonal variations in welded ash flows. *US Prof Pap* 354F: 149-159.
- Smith RL and Bailey RA 1966 The Bandelier Tuff: A study of ash-flow eruption cycles from zoned magma chambers. *Bull Volcanol* 29: 83-103.
- Smith R, Kokelaar P, McConnell B, Branney M and Kneller B 1990 Excursion B: Sedimentation in a complex piecemeal caldera — the Seathwaite Fell Formation in Langdale. In *Volcanogenic Sedimentation in Ancient Terrains*, Field Guide I, IAVCEI/IAS Field Workshop 1990: B1-B17.
- Smith TL and Batiza R 1989 New field and laboratory evidence for the origin of hyaloclastite flows on seamount summits. *Bull Volcanol* 51: 96-114.
- Snyder GL and Fraser GD 1963a Pillowed lavas I: Intrusive layered lava pods and pillowed lavas, Unalaska Island, Alaska. *US Prof Pap* 454-B: B1-B23.
- Snyder GL and Fraser GD 1963b Pillowed lavas, II: A review of selected recent literature. *US Prof Pap* 454-C: C1-C7.
- Solomon M 1989 The mineral deposits of the Mt Read Volcanics. *Geol Soc Aust Spec Pub* 15: 119-125.
- Sparks RSJ 1976 Grain size variations in ignimbrites and implications for the transport of pyroclastic flows. *Sedimentology* 23: 147-188.
- Sparks RSJ 1978 The dynamics of bubble formation and growth in magmas: a review and analysis. *J Volcanol Geotherm Res* 3: 1-38.
- Sparks RSJ 1986 The dimensions and dynamics of volcanic eruption columns. *Bull Volcanol* 48: 3-15.
- Sparks RSJ and Walker GPL 1973 The ground surge deposit: a third type of pyroclastic rock. *Nature* 241: 62-64.
- Sparks RSJ and Walker GPL 1977 The significance of vitric-enriched airfall ashes associated with crystal-enriched ignimbrites. *J Volcanol Geotherm Res* 2: 329-341.
- Sparks RSJ and Wilson L 1976 A model for the formation of ignimbrite by gravitational column collapse. *J Geol Soc London* 132:441-451.
- Sparks RSJ and Wright JV 1979 Welded air fall tuffs. *Geol Soc Am Spec Pub* 180: 155-166.
- Sparks RSJ and Huang TC 1980 The volcanological significance of deep-sea ash layers associated with ignimbrites. *Geol Mag* 117: 425-36.
- Sparks RSJ, Moore JG and Rice CJ 1986 The initial giant umbrella cloud of the May 18, 1980 explosive eruption of Mount St Helens. *J Volcanol Geotherm Res* 28: 257-274.
- Sparks RSJ, Self S and Walker GPL 1973 Products of ignimbrite eruptions. *Geology* 1: 115-118.
- Sparks RSJ, Pinkerton H and Hulme G 1976 Classification and formation of lava levees on Mt Etna, Sicily. *Geology* 4: 269-271.
- Sparks RSJ, Sigurdsson H and Carey SN 1980a The entrance of pyroclastic flows into the sea I. Oceanographic and geologic

- evidence from Dominica, Lesser Antilles. *J Volcanol Geotherm Res* 7: 87-96.
- Sparks RSJ, Sigurdsson H and Carey SN 1980b The entrance of pyroclastic flows into the sea, II. Theoretical considerations on subaqueous emplacement and welding. *J Volcanol Geotherm Res* 7: 97-105.
- Sparks RSJ, Wilson L and Hulme G 1978 Theoretical modelling of the generation, movement, and emplacement of pyroclastic flows by column collapse. *J Geophys Res* 83: 1727-1739.
- Sparks RSJ, Bursik MI, Ablay GJ, Thomas RME and Carey SN 1992 Sedimentation of tephra by volcanic plumes. Part 2: controls on thickness and grain size variations of tephra fall deposits. *Bull Volcanol* 54: 685-695.
- Spry AH 1962 The origin of columnar jointing particularly in basalt flows. *J Geol Soc Aust* 8: 191-216.
- Staudigel H and Schmincke H-U 1984 The Pliocene seamount series of La Palma, Canary Islands. *J Geophys Res* 89: 11195-11215.
- Steven TA and Lipman PW 1976 Calderas of the San Juan volcanic field, southwestern Colorado. *US Prof Pap* 958 35 pp.
- Stow DAV 1986 Deep clastic seas. In Reading HG (ed) *Sedimentary Environments and Facies*. 2nd ed, Blackwell Scientific Publications, Oxford: 399-444.
- Sundell KA 1983 The Castle Rocks chaos: a gigantic Eocene landslide-debris flow within the Absaroka volcanic sequence, northwestern Wyoming. *Geol Soc Am Abst Prog* 15: 332.
- Suzuki-Kamata K 1988 The ground layer of Ata pyroclastic flow deposit, southwestern Japan — evidence for the capture of lithic fragments. *Bull Volcanol* 50: 119-129.
- Swanson DA 1973 Pahoehoe flows from the 1969-71 Mauna Ulu eruption, Kilauea volcano, Hawaii. *Geol Soc Am Bull* 84: 815-826.
- Swanson DA, Wright TL and Helz RT 1975 Linear vent systems (and estimated rates of magma production and eruption) for the Yakima Basalt of the Columbia Plateau. *Am J Sci* 275: 877-905.
- Swanson DA, Dzurisin D, Holcomb RT, Iwatsubo EY, Chadwick WW, Casadevall TJ, Ewert JW and Heliker CC 1987 Growth of the lava dome at Mount St Helens, Washington (USA), 1981-1983. *Geol Soc Am Spec Pap* 212: 1-16.
- Swanson SE, Naney MT, Westrich HR and Eichelberger JC 1989 Crystallization history of Obsidian Dome, Inyo Domes, California. *Bull Volcanol* 51: 161-176.
- Tamura Y, Koyama M and Fiske RS 1991 Paleomagnetic evidence for hot pyroclastic debris flow in the shallow submarine Shirahama Group (Upper Miocene-Pliocene), Japan. *J Geophys Res* 96: 21779-21787.
- Taylor BE, Eichelberger JC and Westrich HR 1983 Hydrogen isotopic evidence of rhyolitic degassing during shallow intrusion and eruption. *Nature* 306: 541-545.
- Thomas RME and Sparks RSJ 1992 Cooling of tephra during fallout from eruption columns. *Bull Volcanol* 54: 542-553.
- Thy P 1992 Petrology of basaltic sills from Ocean Drilling Program sites 794 and 797 in the Yamato Basin of the Japan Sea. *J Geophys Res* 97: 9027-9042.
- Tribble GW 1991 Underwater observations of active lava flows from Kilauea volcano, Hawaii. *Geology* 19: 633-636.
- Ui T 1983 Volcanic dry avalanche deposits—identification and comparison with nonvolcanic debris stream deposits. *J Volcanol Geotherm Res* 18: 135-150.
- Ui T and Glicken H 1986 Internal structural variations in a debris-avalanche deposit from ancestral Mount Shasta, California, USA. *Bull Volcanol* 48: 189-194.
- Ui T, Metsugi H, Suzuki K and Walker GPL 1983 Flow lineations of Koya low aspect-ratio ignimbrite, south Kyushu, Japan. *EOS* 64: 876.
- Valentine GA 1987 Stratified flow in pyroclastic surges. *Bull Volcanol* 49: 616-630.
- Vessell RK and Davies DK 1981 Nonmarine sedimentation in an active fore arc basin. *SEPM Spec Pub* 31: 31-45.
- Voight B, Glicken H, Janda RJ and Douglass PM 1981 Catastrophic rockslide avalanche of May 18. In Lipman PW and Mullineaux DR (eds) *The 1980 Eruption of Mount St Helens, Washington*. *US Prof Pap* 1250: 347-377.
- Walker GPL 1970 Compound and simple lava flows and flood basalts. *Bull Volcanol* 35: 579-590.
- Walker GPL 1971 Grain-size characteristics of pyroclastic deposits. *J Geol* 79: 696-714.
- Walker GPL 1972 Crystal concentration in ignimbrites. *Contrib Mineral Pet* 36: 135-146.
- Walker GPL 1973a Explosive volcanic eruptions — a new classification scheme. *Geol Rund* 62: 431-446.
- Walker GPL 1973b Lengths of lava flows. *Phil Trans R Soc London* 274: 107-118.
- Walker GPL 1979 A volcanic ash generated by explosions where ignimbrite entered the sea. *Nature* 281: 642-646.
- Walker GPL 1981a Plinian eruptions and their products. *Bull Volcanol* 44: 223-240.
- Walker GPL 1981b Generation and dispersal of fine ash and dust by volcanic eruptions. *J Volcanol Geotherm Res* 11: 81-92.
- Walker GPL 1981 c Volcanological applications of pyroclastic studies. In Self S and Sparks RSJ (eds), *Tephra Studies*. D Reidel Publishing Co, Holland 391-404.
- Walker GPL 1983 Ignimbrite types and ignimbrite problems. *J Volcanol Geotherm Res* 17: 65-88.
- Walker GPL 1984 Characteristics of dune bedded pyroclastic surge bedsets. *J Volcanol Geotherm Res* 20: 281-296.
- Walker GPL 1985 Origin of coarse lithic breccias near ignimbrite source vents. *J Volcanol Geotherm Res* 25: 157-171.
- Walker GPL 1987a Pipe vesicles in Hawaiian basaltic lavas: their origin and potential as paleoslope indicator. *Geology* 15: 84-87.
- Walker GPL 1987b The dike complex of Koolau Volcano, Oahu: internal structure of a Hawaiian rift zone. *US Prof Pap* 1350: 961-993.
- Walker GPL 1989a Gravitational (density) controls on volcanism, magma chambers and intrusions. *Aust J Earth Sci* 36: 149-165.
- Walker GPL 1989b Spongy pahoehoe in Hawaii: a study of vesicle distribution patterns in basalt and their significance. *Bull Volcanol* 51: 199-209.
- Walker GPL 1991 Structure, and origin by injection of lava under surface crust, of tumuli, "lava rises", "lava-rise pits", and "lava-inflation clefts" in Hawaii. *Bull Volcanol* 53: 546-558.
- Walker GPL 1992 Morphometric study of pillow-size spectrum among pillow lavas. *Bull Volcanol* 54: 459-474.
- Walker GPL and Croasdale R 1970 Two plinian-type eruptions in the Azores. *J Geol Soc London* 127: 17-55.
- Walker GPL and Croasdale R 1972 Characteristics of some basaltic pyroclastics. *Bull Volcanol* 35: 303-317.
- Walker GPL, Wilson L and Bowell ELG 1971 Explosive volcanic eruptions — I. The rate of fall of pyroclasts. *Geophys J R Astron Soc* 22: 377-383.
- Walker GPL, Heming RF and Wilson CJN 1980 Low-aspect ratio ignimbrites. *Nature* 283: 286-287.
- Walker GPL, Wilson CN and Froggatt PC 1981a An ignimbrite veneer deposit: the trail marker of a pyroclastic flow. *J Volcanol Geotherm Res* 9: 409-421.
- Walker GPL, Self S and Froggatt PC 1981b The ground layer of the Taupo Ignimbrite: a striking example of sedimentation

- from a pyroclastic flow. *J Volcanol Geotherm Res* 10: 1-11.
- Walker RG 1979 Shallow marine sands. In Walker (ed) *Facies Models*. Geological Association of Canada, Geoscience Canada Reprint series 1: 75-89.
- Watanabe KK and Katsui Y 1976 Pseudo-pillow lavas in the Aso Caldera, Kyushu, Japan. *J Jap Assoc Min Pet Econ Geol* 71: 44-49.
- Waters AC 1960 Determining direction of flow in basalts. *Am J Sci* 258A: 350-366.
- Waters AC and Fisher RV 1971 Base surges and their deposits: Capelinhos and Taal volcanoes. *J Geophys Res* 76: 5596-5614.
- Waters JC and Wallace DB 1992 Volcanology and sedimentology of the host succession to the Hellyer and Que River volcanic-hosted massive sulfide deposits, northwestern Tasmania. *Econ Geol* 87: 650-666.
- Weaver SD, Gibson IL, Houghton BF and Wilson CJN 1990 Mobility of rare earth and other elements during crystallization of peralkaline silicic lavas. *J Volcanol Geotherm Res* 43: 57-70.
- Wells G, Bryan WB and Pearce TH 1979 Comparative morphology of ancient and modern pillow lavas. *J Geol* 87: 427-440.
- Wentworth CK and Macdonald GA 1953 Structures and forms of basaltic rocks in Hawaii. *USGS Bull* 994: 1-98.
- White JDL and Busby-Spera CJ 1987 Deep marine arc apron deposits and syndepositional magmatism in the Alistos group at Punta Cono, Baja California, Mexico. *Sedimentology* 34: 911-927.
- Whitham AG and Sparks RSJ 1986 Pumice. *Bull Volcanol* 48: 209-224.
- Williams H and McBirney AR 1979 *Volcanology*. Freeman, Cooper and Company, San Francisco 397 pp.
- Wilmoth RA and Walker GPL 1993 P-type and S-type pahoehoe: a study of vesicle distribution patterns in Hawaiian lava flows. *J Volcanol Geotherm Res* 55: 129-142.
- Wilson CJN 1980 The role of fluidisation in the emplacement of pyroclastic flows: an experimental approach. *J Volcanol Geotherm Res* 8: 231-249.
- Wilson CJN 1985 The Taupo eruption, New Zealand. II. The Taupo ignimbrite. *Phil Trans R Soc. London* 314: 229-310.
- Wilson CJN 1988 Comment on "Stratified flow in pyroclastic surges", by GA Valentine. *Bull Volcanol* 50: 350-351.
- Wilson CJN and Walker GPL 1981 Violence in pyroclastic flow eruptions. In Self S and Sparks RSJ (eds) *Tephra Studies*. D Reidel Publishing Company, Holland 441-48.
- Wilson CJN and Walker GPL 1982 Ignimbrite depositional facies: the anatomy of a pyroclastic flow. *J Geol Soc London* 139: 581-592.
- Wilson CJN and Walker GPL 1985 The Taupo eruption, New Zealand. I. General aspects. *Phil Trans R Soc London* 314: 199-228.
- Wilson L 1972 Explosive volcanic eruptions — II. The atmospheric trajectories of pyroclasts. *Geophys J R Astron Soc* 30: 381-392.
- Wilson L 1976 Explosive volcanic eruptions — III. Plinian eruption columns. *Geophys J R Astron Soc* 45: 543-556.
- Wilson L 1980 Relationships between pressure, volatile content and ejecta velocity in three types of volcanic explosion. *J Volcanol Geotherm Res* 8: 297-313.
- Wilson L and Head JW 1981 Ascent and eruption of basaltic magma on the earth and moon. *J Geophys Res* 86: 2971-3001.
- Wilson L and Walker GPL 1987 Explosive volcanic eruptions — VI. Ejecta dispersal in plinian eruptions: the control of eruption conditions and atmospheric properties. *Geophys J R Astron Soc* 89: 657-679.
- Wilson L, Sparks RSJ, Huang TC and Watkins ND 1978 The control of volcanic column heights by eruption energetics and dynamics. *J Geophys Res* 83: 1829-1836.
- Wilson L, Sparks RSJ and Walker GPL 1980 Explosive volcanic eruptions — IV. The control of magma properties and conduit geometry on eruption column behaviour. *Geophys J R Astron Soc* 63: 117-148.
- Wilson L, Pinkerton H and Macdonald R 1987 Physical processes in volcanic eruptions. *Ann Rev Earth Planet Sci* 15: 73-95.
- Wohletz KH 1983 Mechanisms of hydrovolcanic pyroclast formation: grain size, scanning electron microscopy, and experimental studies. *J Volcanol Geotherm Res* 17: 31-63.
- Wohletz KH 1986 Explosive magma-water interactions: thermodynamics, explosion mechanisms, and field studies. *Bull Volcanol* 48: 245-264.
- Wohletz KH and Sheridan MF 1979 A model of pyroclastic surge. *Geol Soc Am Spec Pap* 180: 177-194.
- Wolff JA and Wright JV 1981 Rheomorphism of welded tuffs. *J Volcanol Geotherm Res* 10: 13-34.
- Woods AW 1988 The fluid dynamics and thermodynamics of eruption columns. *Bull Volcanol* 50: 169-193.
- Woods AW and Bursik MI 1991 Particle fallout, thermal disequilibrium and volcanic plumes. *Bull Volcanol* 53: 559-570.
- Wormald PJ 1992 Sub-volcanic facies analysis within an intensive breccia and igneous complex (hosting the Mt Leyshon gold mine, NW Qld). *Geol Soc Aust Abst* 32: 134-135.
- Wright FE 1915 Obsidian from Hrafninnuhryggur, Iceland: Its lithophysae and surface markings. *Geol Soc Am Bull* 26: 255-286.
- Wright JV 1980 Stratigraphy and geology of the welded airfall tuffs of Pantelleria, Italy. *Geol Rund* 69: 263-291.
- Wright JV and Coward MP 1977 Rootless vents in welded ash-flow tuffs from northern Snowdonia, North Wales, indicating deposition in a shallow water environment. *Geol Mag* 114: 133-140.
- Wright JV and Walker GPL 1977 The ignimbrite source problem: significance of a co-ignimbrite lag-fall deposit. *Geology* 5: 729-732.
- Wright JV and Mutti E 1981 The Dali Ash, Island of Rhodes, Greece: a problem in interpreting submarine volcanogenic sediments. *Bull Volcanol* 44: 153-168.
- Wright JV and Walker GPL 1981 Eruption, transport and deposition of ignimbrite: a case study from Mexico. *J Volcanol Geotherm Res* 9: 111-131.
- Wright JV, Smith AL and Self S 1980 A working terminology of pyroclastic deposits. *J Volcanol Geotherm Res* 8: 315-336.
- Yamada E 1984 Subaqueous pyroclastic flows: their development and their deposits. In Kokelaar BP and Howells MF (eds) *Marginal Basin Geology*. *Geol Soc Spec Pub* 16: 29-36.
- Yamagishi H 1979 Classification and features of subaqueous volcanoclastic rocks of Neogene age in southwest Hokkaido. *Geol Surv Hokkaido Rep* 51: 1-20.
- Yamagishi H 1985 Growth of pillow lobes — evidence from pillow lavas of Hokkaido, Japan, and North Island, New Zealand. *Geology* 13: 499-502.
- Yamagishi H 1987 Studies on the Neogene subaqueous lavas and hyaloclastites in southwest Hokkaido. *Rep Geol Surv Hokkaido* 59: 55-117.
- Yamagishi H 1991 Morphological features of Miocene submarine coherent lavas from the "Green Tuff" basins: examples from basaltic and andesitic rocks from the Shimokita Peninsula, northern Japan. *Bull Volcanol* 53: 173-181.
- Yamagishi H and Dimroth E 1985 A comparison of Miocene and

- Archean rhyolite hyaloclastites: Evidence for a hot and fluid rhyolite lava. *J Volcanol Geotherm Res* 23: 337-355.
- Yamagishi H and Goto Y 1991 Trachyandesite pillow lava from the Abashiri area, northeast Hokkaido, Japan. *Bull Volcanol Soc Japan* 36: 177-181.
- Yamagishi H and Goto Y 1992 Cooling joints of subaqueous rhyolite lavas at Kuroiwa, Yaumo, southern Hokkaido, Japan. *Bull Volcanol Soc Japan* 37: 205-207.
- Yamagishi H, Sakamoto I and Ishii J 1989 Internal structures of pillow lobes of Cenozoic and Mesozoic pillow lavas in and around Hokkaido. *Proceedings Hokkaido Tokai Univ Science and Engineering* 2: 107-118.
- Yamamoto T, Takarada S and Suto S 1993 Pyroclastic flows from the 1991 eruption of Unzen Volcano, Japan. *Bull Volcanol* 55: 166-175.
- Yamazaki T, Kato I, Muroi I and Abe M 1973 Textural analysis and flow mechanisms of the Donzurubo subaqueous flow deposits. *Bull Volcanol* 37: 231-244.

Index

- Text, *figure*, Table, plate
- a'a (*see also* lava) 27, 54, 69-70, 34, 19.7
- accessory lithic pyroclast *see* lithic fragment
- accidental lithic clast *see* lithic fragment
- accretionary lapilli 15, 29-30, 96, 100, 118, 121, 3, 9, Table 2, 7.6-7, 22.6, 38.1, 39.6, 40.1
- achnelith (*see also* bomb) 27-28
- agglomerate 120, Table 3
- agglutinate 28, 120
- agglutination of pyroclasts (*see also* welding) 28, 103
- alteration 165-169, 32, 42, 43, 44, 45, 46
- definition 165
 - diagenetic 23-24, 121, 165
 - fracture- or matrix-controlled 166, 42-43
 - hydrothermal 8, 23-24, 54, 165
 - mineral assemblage 8, 12, 165, Table 1, Table 2
 - Mount Read Volcanics 165-169
 - of glass 23-24, 28, 165-167, 168-169, 44, 45
 - of lavas, intrusions and autoclastic deposits 57, 166-168, 10.1, 10.3, 12, 13.2, 42, 43, 44
 - of pumiceous deposits 22, 27, 29, 30, 168-169, 6.3-4, 26.7, 45, 46
 - phase 166
 - stage 166
 - texture 3, 165-166, 42, 43, 44, 45, 46
 - two phase 166-169, 43.4-5, 45.6-7, 46.1, 46.6
- amygdale (*see also* vesicle) 22, Table 1, 2.3-4, 12.8, 17.4
- angular fragment breccia *see* hyaloclastite andesite (*see also* lava)
- hyaloclastite 11.4, 11.8, 12.1-5, 13.2-7, 43.2
 - pillowed 60, 23, 24, 25, 15.1, 16.2, 17.6
 - subaerial 71, 36", 10.5-6, 19.5
 - subaqueous 71, 19, 25, 9.2-3, 11.4, 15.1, 16.2, 17.6
- angular fragment breccia *see* hyaloclastite
- aphanitic texture 3, 31, 53, 61, 2, Table 1
- aphyric texture 3, 53, Table 1
- apparent texture
- bedding 31, 167, 168.8.4
 - coherent texture 3, 7, 168, 1.4, 45.5
 - matrix-supported 42.4, 43.1
 - polymict 113, 167, 10.3, 44.1
 - porphyritic texture (*see also* apparent coherent texture) 22, 27, 168, 1.4, 45.5-6
 - pseudobreccia 43.1, 43.4, 45.6
 - pyroclastic texture (*see also* apparent volcaniclastic texture) 22, 26, 166-169, 46.5
 - shards 26, 166, 15, 46.5
 - volcaniclastic texture 3, 7, 54, 57, 113, 166-169, 42.6-7, 44.2, 44.6, 46.5
- armoured lapilli 29-30, 118, 7.8
- armoured mud ball 29 ash 28-29, 6, Table 3
- ash cloud surge *see* pyroclastic surge deposit
- ash fall deposit *see* pyroclastic fall deposit
- augen schist 169, 46.6
- autobreccia 53-54, 68-69, 94, 166, 2, 33, 36, Table 3, 10.1-3, 10.5, 19.1, 43.3
- autobrecciation 28, 53-54, 58, 65, 71, 94
- autoclastic deposit (*see also* autobreccia, hyaloclastite, lava, peperite) 1, 8, 22, 18, 31, 33, 53-71, 94, 166-168, 1, 33, Table 3
- autoclastic fragmentation (*see also* autobrecciation, quench fragmentation) 27
- avalanche *see* debris-avalanche deposit axiolitic devitrification (*see also* devitrification) 24, 28, 14, 23.3-4, 25.4
- basaltic glass 23, 59, 2.2, 2.5
- basalt (*see also* lava)
- continental flood basalt province 70
 - hyaloclastite 60-61, 12.8, 42.8
 - pillow lava 58-61 9.4, 14.5-6, 15.2-7, 16.1, 17.2-4
 - subaerial 23, 69-70, 17, 34, 35, 9.5, 19.3, 19.6-7
 - subaqueous 23, 60-61, 25, 35, 2.2, 9.4, 15.2-7, 16.1, 17.2-4
- basaltic glass (*see also* sideromelane) 23, 59, 2.2, 2.5
- base surge *see* pyroclastic surge deposit
- bedding-parallel foliation 27, 30, 103, 169, 33.4, 45.2^, 45.7, 46.1-2
- bedload (*see also* traction transport and deposits) 111, 112, 117, 120, 37.2
- bed thickness Table 2
- block 27-28, 95, 118, 120, 6, Table 3, 6.8, 38.8
- block and ash flow *see* pyroclastic flow deposit

block fades (*see also* debris-avalanche deposit) 115-116, 52, 36.5-6
 block lava *see* lava blocky peperite *see* peperite
 bomb 27-28, 61, 95, 118, 120, 6, Table 3, 6.8, 39.7-8
 breadcrust texture 27, 6.8
 Bunga Beds, New South Wales 65, 18
 caldera 105, 107, 114
 Chao dacite lava flow, Chile 66, 19.4
 chisel mark 31
 classification 1, 3, 94, 1, 6, Table 3
 clinker 69, 34, 10.5, 19.7
 coalescence of pyroclasts (*see also* welding) 103
 cognate lithic pyroclast *see* lithic fragment
 coherent texture 1-3, 7, 21, 28, 53, 54, 61, 64, 67, 2, 9, 1.1-2
 co-ignimbrite fall deposit *see* pyroclastic fall deposit
 colonnade 32, 17, 9.5
 columnar joint *see* joint
 compositional zonation (*see also* pyroclastic flow deposit) 22, 102, 105, 41, 26.2
 compound cooling unit concentric joint *see* joint
 concentric pillow *see* hyaloclastite
 confining pressure 23, 57, 63, 64, 65, 96
 cored lapilli 29-30, 118, 7.8
 corrugation 58, 23
 co-surge fall deposit *see* pyroclastic fall deposit
 critical pressure of water 57
 cross stratification (*see also* sedimentary structure) 15, 117-118, 54, 55, 28.6, 38.1-2, 38.4-6, 40.5, 40.8, 41.3
 cryptodome, partly extrusive (*see also* lava dome) 1, 2, 27, 58, 64, 66, 2, 29, 31, 32, 18
 crystal, crystal fragment 22, 102, Table 2, 1.3
 dacite (*see also* lava)
 hyaloclastite 11.5-7, 12.6-7
 subaerial 66-69, 33, 10.4, 19.4
 subaqueous 66, 31, 32, 8.4-5, 8.7, 11.5-7, 42.7, 44.1, 44.7
 debris-avalanche deposit (*see also* mass-flow deposit) 114-116, 48, 52, 36.2-7
 debris-flow deposit (*see also* mass-flow deposit) 100, 108, 112-113, 46, 47, 48, 50, 18.4, 34, 35
 degassing of magma 53, 69, 96
 density current *see* mass-flow deposit
 density-modified grain-flow deposit (*see also* grain-flow deposit) 55, 114, 51, 34.2-3
 devitrification 15, 22, 23, 24-25, 28, 30, 68-69, 103, 165, 167, 14, 33, 42, 3, 8.5, 23.3-4, 44.3-7
 granophyric texture 24, 69, 103, 166, 24.3-4, 28.5
 in pyroclastic flow deposits 103, 42, 3.7, 24.3-4, 25, 28.5
 lithophysae 3, 15, 24, 25, 69, 103, 167, 2, 9, 3.7, 25.1, 44.3-4
 micropoikilitic texture 3, 15, 24-25, 69, 103, 2, 4
 microspherulitic texture 3, Table 1, 3.2-3
 spherulite 24-25, 69, 103, 166-167, 2, 9, Table 1, 3.1-6, 8.1-2, 25.2-3, 44.3-7
 diagenetic alteration *see* alteration
 diagenetic compaction 15, 22, 27, 30, 165, 168-169, 33.4, 45.2-5, 45.7, 46.1-3
 dome *see* lava dome dyke *see* feeder dyke
 effusive eruption 1, 2, 53-54, 61, 69, 1
 en masse freezing 100, 113, 115
 entablature 32, 17, 9.5
 epiclast 29, 97
 epiclastic deposit *see* volcanogenic sedimentary deposit
 eutaxitic texture 30, 103, 24, 25.3, 26.1
 explosive eruption 1, 2, 22, 27, 28, 29, 30, 69, 95-96, 118, 120, 1, 3
 subaqueous 97, 107-108, 109, 121, 45, 18.5-7, 41
 explosive magmatic eruption (*see also* explosive eruption) 27
 feeder dyke 1, 2, 23, 30, 31, 32, 33, 54-56, 58, 61-63, 64-65, 2, 18, 20, 21, 8.3, 8.6, 11.1, 13.3, 13.6-7
 fiamme 15, 30, 103, 168-169, 9, 44, Table 2, 1.4, 22.4, 24, 26.5, 28.5, 45.1-5, 45.7, 46.1-2
 flamme-like lens *see* pseudo-fiamme
 fire-fountain *see* lava fountain
 flotation 27, 65, 121, 48, 40.3-4
 flow banding *see* flow foliation
 flow fold *see* flow foliation
 flow foliation 3, 15, 25, 27, 28, 30-31, 54, 55, 61, 66, 167, 9, 16, 21, 33, 2.1, 2.3, 3.1, 3.6, 5.2, 8, 11.2-3, 20.2, 20.4, 26.3-4, 43.3, 44.3-7
 fluidisation
 in pyroclastic flows 99
 of sediment 57, 30, 46
 fountain-fed lava flow *see* lava fountain
 genetic interpretation 3, 12, 15, 169
 glass 15, 21, 23-24, 27, 28-29, 55-56, 68-69, 103, 19, 33, Table 1, 2.1-2, 2.5-6, 6.1-2, 20
 alteration of glass 23-24, 28, 165-167, 168-169, 44, 45
 devitrification 24-25, 3, 4, 20
 hydration 25-26, 5, 42.1, 42.6
 obsidian 24, 25, 26, 63, 68-69, 33, 2.1, 3.2-3, 20.2-3, 44.3
 palagonite 23, 28, 2.5, 7.3, 16.1
 sideromelane 23, 28, 59, 2.5, 16.1
 tachylite 23, 59, 16.1
 glass shard *see* shard
 glassy globule 56
 globular peperite *see* peperite
 glomeroporphyritic texture 21
 grade *see* pyroclastic flow deposit
 graded bedding (*see also* sedimentary structure) 15, 108, 109, 114, 120-122, 44, 45, 49, 51, 29.3-4, 30, 31, 32.1, 34, 37.1, 41.1-2, 45.1
 grain-flow deposit (*see also* mass-flow deposit) 54, 55, 114, 46, 47, 48, 51, 11.8, 36.1
 grain size 6, Table 2, Table 3
 granophyric texture (*see also* devitrification) 24, 69, 103, 166, 24.3-4, 28.5
 granular texture 25, 167, 168, 4.1
 graphic logging 12, 7, 8, 9
 gravitational collapse 29, 60-61, 65, 69, 71, 99, 114-115, 122
 ground layer *see* pyroclastic flow deposit
 groundmass 21, 25, 28, 53, Table 1
 ground surge *see* pyroclastic surge deposit
 hawaiian eruption (*see also* explosive eruption) 95
 heat retention 94, 102, 105, 118, 26, 39.4
 Hellyer mine 17, 53, 12
 high-temperature devitrification *see* devitrification
 hummocky cross stratification (*see also* sedimentary structure) 117-118, 122-123, 55, 28.1

- hyaloclastite 15, 22, 27, 28, 32-33, 54-57, 60, 61, 166, 2, Table 3, 11, 12, 13
- angular fragment breccia 55, 63, 65, 17.7
- concentric pillow 32, 56, 65, 13.3-4
- in situ 55-57, 61-66, 71, 4, 19, 21, 26, 27, 28, 29, 31, 32, 11.1-7, 12, 13.5, 13.7, 42.2-4, 42.8, 43.2
- intrusive (*see also* peperite) 53, 55, 57-58, 64-66, 166, 22, 26, 29, 30, 14, 18.3, 43.1
- pillow fragment breccia 56, 61, 2, 25, 15.4, 17.1
- resedimented 55-56, 61-66, 4, 20, 26, 28, 29, 31, 32, 11.8, 37.5
- hydration (*see also* perlite) 15, 22, 23, 25-26, 68-69, 97, 165, 5, 12.5, 24.1, 42.1, 42.6
- hydraulic fracture 166, 42.5
- hydraulic sorting 65, 18.7, 32.5, 38.2, 40.8
- hydroclastic breccia 56-57, 58
- hydrothermal alteration *see* alteration
- hydrovolcanic 95
- hyperconcentrated flow 113, 35.5, 35.7
- ignimbrite (*see also* pyroclastic flow deposit) 30, 31, 99, 102, 3, 40, 41, 42, 43, 1.4, 2.6, 7.2, 21.5-7, 22, 23, 24, 25, 26, 27, 28
- lava-like 3, 15, 22, 30-31, 104, 3
- Mount Read Volcanics 27
- rheomorphic 3, 15, 22, 30-31, 104, 26.3-5
- welded 102-104, 1.4, 2.6, 3.7, 22.3-4, 24, 25, 26.1, 27, 28.4-5
- ignimbrite veneer (*see also* pyroclastic flow deposit) 104, 43, 22.7
- indurated sediment 58, 60, 61, 64, 13.6, 14.4, 14.9
- in situ fragmentation 22, 27, 29, 30, 54, 36.2-3, 36.6, 37.3, 42.2-3, 42.5, 44.2
- intraclast 29, 4, 9, 44, 30.6-7, 31, 34.5
- isolated pillow breccia 56
- jigsaw-fit texture 22, 54, 56, 57, 115, 2, 9, 11.1-7, 12, 14.8-9, 36.2-3, 37.3, 39.4, 42.2-3, 42.5, 44.2
- joint 24, 31-33, 66, 71, 17, 18, Table 1, Table 2
- columnar 15, 31-32, 71, 17, 19, 36, 9.1-3, 9.5, 13.7, 19.2, 26.1-2
- concentric 32, 56, 59, 13.3-4
- platy 71, 36
- prismatic 22.2, 36.7, 40.3
- radial columnar 32, 59, 9.3-4, 15.7, 16.1, 17.6
- "tiny normal joints" 28, 33, 54, 56, 2, 18, 9.6, 17.7
- tortoise shell 32, 59, 18, 9.7, 15.2, 17.4, 17.7
- Juan de Fuca Ridge 53, 60
- juvenile clast 27-28, 30, 33, 105, 113, 115, 116, 3, 4, 9
- Krakatau, Indonesia 106
- lahar (*see also* mass-flow deposit) 97, 113-114, 35
- lapilli 6, Table 3
- lapillistone 6, Table 3
- lapilli-tuff 6, Table 3
- lava (*see also* autoclastic deposit, coherent texture) 1, 2, 3, 7, 15, 21, 22, 23, 24, 25, 26, 27-28, 29, 53-71, 99, 1, 2, Table 1
- a'a 27, 54, 69-70, 34, 19.7
- alteration 166-168, 3.5-6
- andesitic 60, 71, 19, 22, 24, 25, 361.2, 9.2-3, 10.5-6, 15.1, 16.2, 17.6, 19.5
- basaltic 60-61, 69-70, 17, 25, 34, 35.2.2, 8.8, 9.4-5, 15.2-7, 16.1, 17.2-4, 19.3, 19.6-7
- block lava 54, 60, 10.6
- chemical composition 7, 12, 21, 9, Table 1
- dacitic 66-69, 31, 32, 33, 36, 1.1, 8.4-5, 8.7, 9.1, 10.4, 19.4, 42.7, 44.1, 44.7
- degassing of 27
- flow foliation 30-31, 8, 44.3-7
- jointing 31-33, 9
- on graphic logs 12
- pahoehoe 23, 60, 69-70, 34, 35, 19.6-7
- pillow lava 56, 58-61, 2, 23, 25, 34, 9.4, 14.5-6, 15, 16, 17
- pumiceous 27, 54, 65, 66-69, 33, 2.1, 20
- psuedo-pillow 33, 56, 18, 9.6, 17.7
- rhyolitic 61-69, 26, 27, 28, 29, 30, 33, 3.1-6, 4, 5.1, 7.5, 8.1-2, 11.1-3, 18, 19.1-2, 20, 44.3-6
- sheet 60
- silicic (*see also* dacitic, rhyolitic) 27-28, 61-64, 65-69, 26, 27, 28, 33, 3, 4, 18, 19.1-2, 19.4, 20
- younging indicator 22-23, 59, 34, 17.2, 17.5
- lava delta 59
- lava dome (*see also* cryptodome) 1, 2, 27-28, 29, 30, 53-58, 61-69, 71, 99, 121, 26, 29, 31, 32, 33, 38, 10.4, 18, 19.1, 33.1-2, 41
- lava fountain 28, 53, 61, 95, 13.1
- lava levee 69
- lava-like ignimbrite *see* ignimbrite lava lobe 32, 33, 55-56, 58, 60, 61-64, 19, 27, 13.5
- lee-side lense (*see also* pyroclastic flow deposit) 22.7
- lithic fragment 29, 96, 100, 115, 3, 9, Table 2, 7.4-5, 22.3-5, 25.4
- accessory lithic pyroclast 27, 29, 95, 96, 105
- accidental lithic clast 29, 105
- cognate lithic pyroclast 29, 25.4
- in fall deposits 39.4
- in mass-flow deposits 7.4, 31.2, 33.6-8, 37
- in pyroclastic flow deposits 100, 105, 1.4, 22.3-5, 25.4
- provenance 108, 33.6-8, 37
- lithophysae (*see also* devitrification) 3, 15, 24, 25, 69, 103, 167, 2, 9, Table 1, 3.3, 3.7, 25.1, 44.3-4
- Little Glass Mountain rhyolite flow, USA 68-69, 2.1, 20
- Lower Rhyolitic Tuff Formation, UK 107, 28.2
- macro-perlite (*see also* perlite) 26, 42.6
- magma mixing 21, 23, 27, 69, 105, 6.5
- mantle bedding (*see also* sedimentary structure) 120, 58, 39.1
- mass-flow deposit 15, 22, 98-116, 121, 122, 5, 37, 46, 47, 48, 49, 50, 51, 52, 59, Table 4, 18.1, 18.4-6, 29, 30, 31, 32, 33, 34, 35, 36, 37, 45, 46
- internal facies 98, 37
- massive sulfide clasts 116, 53, 37
- particle support 97-98, 108, 46, 47, 48
- pumiceous 96-97, 106-107, 37, 44, 45, 29A, 30, 33.1-5, 45.46
- subaerial 7.7, 35, 36
- subaqueous 18.4-6, 29, 30, 31, 32, 33, 34, 37, 45, 46
- types 98
- massive sulfide clasts 116, 53, 37
- megaturbidite *see* turbidite
- microlite (*see also* quench crystal) 23, 166-167, 20
- micropoikilitic texture (*see also* devitrification) 3, 15, 24-25, 69, 103, 2, 4
- microspherulitic texture (*see also* devitrification) 3, Table 1, 3.2-3
- mixed facies (*see also* debris-avalanche deposit) 115-116, 52, 36.2

- Mount Read Volcanics 15-17, 165-169, 10, 11, 12, 13, 44
- mudflow deposit *see* debris-flow deposit
- multiple-crust structure (*see also* pillow lava) 58, 60, 23, 16
- multiple-rind structure (*see also* pillow lava) 59-60, 16
- non-particulate flow 31, 104, 120, 26.3-4
- nuee ardente *see* pyroclastic flow deposit
- obsidian 24, 25, 26, 63, 68-69, 33, 2.1, 3.2-3, 20.2-3, 44.3
- Oshinkoshin Dyke, Japan 18, 9.7, 17.7
- pahoehoe lava (*see also* basalt) 23, 59, 60, 69-70, 34, 35, 19.6-7
- channel 60
 - shelly 47, 69
 - spongy 23, 69, 19.6
 - tube 60, 61, 69, 35, 19.6
 - tumuli 60, 70
- palagonite 23, 28, 2.5, 7.3, 16.1
- particle transport *see* transport and deposition
- peperite (*see also* intrusive hyaloclastite) 15, 53, 57-58, 60, 61, 64-66, 166, 22, 26, 29, 30, 14, 18.3, 43.1
- perlite 15, 23, 24, 25-26, 55, 69, 166, 75 2.6, 5, 12.5, 24.1, 27.2, 42.1, 42.6-7
- phenocryst (*see also* crystal) 21-22, 26, 27, 69, 166, 167, 168, 9, Table 1, 1.1-2, 6.2, 6.4, 8.1, 20.1, 44.1
- phreatic deposit *see* pyroclastic deposit
- phreatic eruption 96, 118
- phreatomagmatic deposit *see* pyroclastic deposit
- phreatomagmatic eruption 27, 58, 96, 118
- phreatoplinian eruption 96
- pillowed sill (*see also* pillow lava) 60, 24
- pillow fragment breccia *see* hyaloclastite pillow lava 15, 23, 32, 33, 56, 58-60, 61, 2, 23, 25, 34, 9.4, 14.5-6, 15, 16, 17
- facies 59-60, 25
 - multiple-crust structure 58, 60, 23, 16
 - multiple-rind structure 59-60, 16
- pipe in pyroclastic flow deposit 30, 103, 40, 22.5-6, 26.6-7
- pipe vesicle 23, 58-59, 69-70, 34, 16.1, 17.2
- Pitts Head Tuff Formation, UK 28.4-5
- planar bedding (*see also* sedimentary structure) 117-118, 120, 121, 54, 29.2, 38.8, 39.2, 40.5-7
- platy jointing *see* joint
- plinian eruption (*see also* explosive eruption) 95, 99, 102
- Ponza, Italy 56, 5.1, 11.1-3
- porphyridic texture 3, 15, 21-22, 53, 61, 166, 2, 9, Table 1, 1.1-2, 6.2, 6.4, 20.1, 44.7
- primary dip 55, 59, 4, 36.1
- primary volcanoclastic deposit (*see also* autoclastic deposit, pyroclastic deposit) 1, 94, 96, 106
- progressive aggradation (*see also* pyroclastic flow deposit) 99-100, 113, 117, 121, 39, 22.7, 37.1-2
- proximal coarse lithic breccia (*see also* pyroclastic flow deposit) 105
- pseudobreccia *see* apparent texture
- pseudofiamme (*see also* alteration) 15, 30, 167-169, 42.4, 43.1, 44.5
- pseudo-pillow 33, 56, 18, 9.6, 17.7
- pumice 15, 23, 27, 95, 96, 121, 9, 6.1-5, 18.5-6, 20.1, 20.4, 22.7, 33.1-5, 39.3-i
- alteration 168-169, 23.5, 45, 46
 - flotation 121, 40.3-4
 - tube pumice 27, 168-169, 6.1-3, 23.1, 30.3, 33.1-3, 33.5-6, 46.1-4, 46.6-7
- pumice concentration zone (*see also* pyroclastic flow deposit) 102, 37, 102
- pumice flow deposit *see* ignimbrite
- pyroclast
- block 27-28, 6.8
 - bomb 27-28, 6.8
 - crystal 22
 - juvenile fragment 27-28, 6
 - lithic fragment 29
 - pumice 27, 6.5
 - scoria 27, 6.6
 - shard 28-29, 7.1-3
- pyroclastic breccia 6, Table 3
- pyroclastic deposit 1, 2, 3, 8, 22, 29, 94-96, 7, 3
- explosive magmatic 28, 95, 3
 - grain size terms 6, Table 3
 - phreatic 96, 3
 - phreatomagmatic 28, 29, 96, 3
 - rheomorphic 30-31
 - welded 7, 24, 25, 26, 27, 28, 3
- pyroclastic fall deposit 95, 120-121, 58, 6.8, 19.3, 38.8, 39
- characteristics 120-121
 - co-ignimbrite 29, 30, 102, 120-121, 40, 41
 - co-surge 29, 30, 118, 120
 - mantle bedding 120, 58, 39.1
 - phreatoplinian 30, 39.5-6
 - plinian 121, 39.2-4
 - proximal 28, 120, 121, 39.2, 39.4, 39.7-8
- pumice fall deposit 3, 39.2-4
- scoria fall deposit 3, 6.6, 39.7-8
 - water-settled 30, 121, 168, 59, 18.7, 41
 - welded 120, 3
- pyroclastic flow deposit (*see also* ignimbrite) 29, 30, 95, 98, 99-105, 113, 118, 122, 3, 37, 38, 40, 59, Table 4, 21, 22, 23, 24, 25, 26, 27, 28
- aspect ratio 104
- block and ash flow deposit 69, 99-102, 106, 3, 38, 40, 21.1-2
- characteristics 100-105
 - components 100, 102, 105, 40, 21.6, 22.3-7
 - compositional zoning 102, 105, 41, 26.2
 - devitrification 103, 42, 23.3-4, 24.3-4, 25
 - dimensions 105
 - facies 102-104, 105, 37, 41, 42, 43, 21.5, 21.6
 - geometry 104, 43, 22.1-2
 - grade 103-104, 26.3-5
 - ground layer 102, 40
 - pipe 30, 103, 40, 22.5-6, 26.6-7
 - scoria and ash flow deposit 95, 99, 102, 40, 21.3-4
 - subaqueous emplacement 106-108, 44, 45, 27, 28
 - transport and deposition 99-100, 39
 - vapour-phase crystallisation 31, 103, 42, 22.2, 23, 26.7
 - welding 102-104, 42, 24, 25, 26.1, 26.3-5, 27, 28.2
- pyroclastic surge deposit 29, 30, 95, 117, 118-119, 122, 3, 56, 57, 7.8, 38.5-7
- ash cloud surge deposit 118-119, 40
 - base surge deposit 96, 118-119, 38.5-7
 - dimensions 119
 - ground surge deposit 102, 118-119, 40
- pyroclast-rich deposit (*see also* resedimented syn-eruptive volcanoclastic deposit) 28, 30, 56, 94-97, 168-169, Table 3
- subaqueous 29.4, 30, 31, 32, 33, 34.5, 45, 46

quench crystal 21, 23, 24, 69, 20
 quench fracture 24, 26, 31, 33, 56, 166
 quench fragmentation 22, 27, 28, 53, 54-56, 57, 58, 61, 65, 96
 radial columnar joint *see* joint
 ramp structure 66
 reaction rim 21
 resedimented syn-eruptive volcanoclastic deposit 1, 2, 3, 8, 22, 28, 94, 96-97, 98, 114, 1, 4, 59, Table 4, 29.4, 30, 31, 33.1-2, 34.5, 41
 definition 94, 1
 resedimented autoclastic 54, 55, 65-66, 97, 4, 31, 32, Table 3, 11.8, 18.4, 37.1-5
 resedimented pyroclastic 28, 29, 30, 56, 65, 96-97, 105, 107-108, 4, 44, Table 3, 7.7, 29, 30, 31, 33.5, 34.5, 41
 resorption of phenocryst 21, 166
 reticulite 27
 rheomorphic *see* pyroclastic deposit
 rhyolite (*see also* lava)
 flow direction 16
 hyaloclastite 11.1-3, 42.2-4, 43.1
 subaerial 66-69, 33, 2.1, 3.1-3, 8.2, 19.1-2, 20, 44.3
 subaqueous 61-65, 26, 27, 28, 29, 30, 4, 5.1, 8.1, 11.1-3, 18, 44.4-6
 rhyolitic glass *see* silicic glass rind 59, 15.7, 16.1, 17.2
 ropy wrinkle 58, 23, 15.2-3, 15.7, 16.2
 Rosebery-Hercules mineralisation 17, 165, 168-169, 13, 46.6
 saltation (*see also* traction transport and deposits) 111, 117, 120
 scoria 27, 96, 6.6-7, 39.7-8
 scoria and ash flow deposit *see* pyroclastic flow deposit
 scoria fall deposit *see* pyroclastic fall deposit
 sedimentary structure 15, 97, 117-118, 119, 122, 54, 55, 57, 59, Table 2, 38, 40
 cross stratification 15, 117-118, 54, 55, 28.6, 38.1-2, 38.4-6, 40.5, 40.8, 41.3
 graded bedding 15, 108, 109, 114, 120-122, 44, 45, 49, 51, 29.3-4, 30, 31, 32.1, 34, 37.1, 41.1-2, 45.1
 hummocky cross stratification 117-118, 122-123, 55, 28.1
 mantle bedding 120, 58, 39.1
 planar bedding 117-118, 120, 121, 54, 29.2, 38.8, 39.2, 40.5-7
 ripple 117, 54, 28.3, 38.3, 40.6-7
 sandwave 117, 5457, 38.7
 tractional 117-119, 5, 54, 55, 57, 38
 sedimentation
 environments 97, 105, 113, 118, 119, 120, 122-123, 59
 transport and deposition 94, 97, 109, 117-118, 122-123, 46, 47, 48, 59, Table 4
 sediment gravity flow *see* mass flow deposit
 shard 15, 28-29, 96, 168-169, 3, Table 2, 2.5-6, 7.1-3, 23.1-4, 24.4, 25.3-6, 27, 29.4, 30.1
 sheet flow *see* lava
 shelly pahoehoe *see* pahoehoe
 sideromelane 23, 28, 59, 2.5, 16.1
 siliceous nodule 28.4 silicic glass (*see also* obsidian) 24, 25
 silicic lava (*see also* dacite, lava, rhyolite)
 subaerial 66-69, 33
 subaqueous 61-66, 26, 27, 28, 29, 31, 32
 sill 1, 23, 30, 31, 32, 53, 57-58, 60, 64-65, 2, 22, 24, 30
 simple cooling unit 103, 42
 slide deposit 114-115, 36.4
 snowflake texture *see* micropoikilitic texture
 Sock Creek South, western Tasmania 66, 31, 32, 33.1-2
 Socompa volcano, Chile 114-115, 36.4-6
 spatter 95
 spherulite (*see also* devitrification) 3, 15, 24-25, 69, 103, 166-167, 2, 9, Table 1, 3.1-6, 8.1-2, 25.2-3, 44.3-7
 spinifex texture 23
 spreading crack 58, 23, 15.3, 15.7, 17.1
 steam explosion (*see also* phreatic eruption) 57, 58
 strombolian eruption (*see also* explosive eruption) 95
 stylolitic dissolution foliation (*see also* diagenetic compaction) 169, 30.1, 46.1
 subaerial lava
 andesitic 71, 36, 10.5-6, 19.5
 basaltic 23, 69-70, 17, 34, 35, 9.5, 19.3, 19.6-7
 dacitic 66-69, 33, 10.4, 19.4
 rhyolitic 66-69, 33, 2.1, 3.1-3, 8.2, 19.1-2, 20, 44.3
 silicic (*see also* dacite, rhyolite) 66-69, 33
 subaerial mass-flow deposit *see* mass-flow deposit
 subaqueous lava
 andesitic 71, 19, 25, 9.2-3, 11.4, 15.1, 16.2, 17.6
 basaltic 23, 60-61, 25, 35, 2.2, 9.4, 15.2-7, 16.1, 17.2-4
 dacitic 66, 31, 32, 8.4-5, 8.7, 11.5-7, 42.7, 44.1, 44.7
 rhyolitic 61-65, 26, 27, 28, 29, 30, 4, 5.1, 8.1, 11.1-3, 18, 44.4-6
 silicic (*see also* dacite, rhyolite) 26, 61-66, 26, 27, 28, 29, 31, 32
 subaqueous mass-flow deposit *see* mass-flow deposit
 subaqueous pyroclastic flow deposit *see* pyroclastic flow deposit
 surge *see* pyroclastic surge deposit
 suspension transport and deposits 15, 98, 117, 120-122, 48, 58, 59, Table 4, 39, 40.1-2, 40.4-7, 41
 associated with subaqueous mass flow 121-122, 29.1, 40.2, 40.4
 pyroclastic fall deposit 120-121, 58, 39
 water-settled 30, 121, 168, 48, 59, 18.7, 28.3, 29.1, 40.1, 40.6, 41, 45.1
 syn-sedimentary sill 57-58, 60, 64-65, 22, 24, 30
 syn-volcanic intrusion (*see also* sill, feeder dyke, cryptodome) 2, 3, 7, 12, 15, 21, 22, 24, 25, 26, 53-71, 1, 2, 29, 30
 alteration 166-168
 tachylite 23, 59, 16.1
 talus 54, 61, 69, 71, 114, 33, 36, 48, 10.4, 10.6, 19.1-2
 tectonic deformation 22, 30, 165, 167-169
 tensional crack 58, 23, 17.1
 terminology 7, 94
 descriptive Table 1, Table 2
 genetic 7, 94, Table 3
 lithofacies 7, 12, Table 1, Table 2
 lithological 7, 12
 textural evolution 1, 165-166
 thermal oxidation 100, 6.6, 10.5, 19.3, 39.4, 39.7
 "tiny normal joint" *see* joint
 toothpaste lava 70
 tortoise shell joint *see* joint
 trachytic texture 2.4, 8.8, 29.2
 traction transport and deposits 15, 28, 98, 111-112, 117-120, 122, 59, Table 4, 38, 40.5-8
 tractional sedimentary structure *see* sedimentary structure
 transport and deposition (*see also* sedimentation) 94, 97, 109, 117-118, 122-123, 46, 47, 48, 49, 59, Table 4
 tube pumice *see* pumice

- tuff 8, 6, Table 3
- tuff-breccia 6, Table 3
- tuffaceous 8, Table 3
- tumuli 60, 70
- turbidite (*see also* mass-flow deposit) 15, 99, 108, 111-112, 46, 47, 48, 49, 18.1, 29, 30, 31
 - facies 111-112, 49, 30, 31.1, 32.1, 37.1-4
 - lithic-rich 31.2, 32.1-3, 37.6-7
 - megaturbidite 108, 109, 29.4, 30, 31, 37.1-4, 37.6-7
 - pumiceous 112, 30
 - shard and crystal-rich 29.4, 31.1
- turbidity current *see* turbidite
- valley pond (*see also* pyroclastic flow deposit) 104, 43, 22.2
- vapour-phase crystallisation (*see also* pyroclastic flow deposit) 31, 103, 42, 22.2, 23, 26.7
- vesicle (*see also* amygdale, pipe vesicle) 3, 15, 22-23, 27, 28, 30, 53, 56, 58-59, 63, 66, 69-70, 34, Table 1, 2.1-5, 6, 15.6, 16.1, 17.4, 19.6, 20
- vesicular ash 29, 118
- vesicular sediment 58 vitriclast Table 2, 25.6, 32.3, 40.4
- vitriclastic texture 22, 28-29, 102, 121, 23.1-4, 24.1-2, 25.3, 27, 29.4, 30.1-3
- volcanic glass *see* glass
- volcanic-hosted massive sulfide deposit 8, 15, 17, 116, 165, 168, 5
- volcaniclastic deposit (*see also* autoclastic, pyroclastic, resedimented syn-eruptive, volcanogenic sedimentary deposits) 1, 2, 3, 7, 8, 22, 29, 94-123, 1, 3, 4, 5, Table 2
 - autoclastic 53-71, 94, 3
 - components 94, Table 2
 - definition 3, 94
 - grain size classification Table 2, Table 3
 - on graphic logs 12, 9
 - pyroclastic 94, 95-96, 99-105, 118-119, 120-122
 - resedimented syn-eruptive 94, 96-97, 107-108
 - texture 1-3, 1.3, 2.5
- volcanogenic sedimentary 94, 97, 117-118, 120, 122-123
- volcaniclastic mass-flow deposit *see* mass-flow deposit
- volcaniclastic turbidite *see* turbidite
- volcanogenic sedimentary deposit 1, 3, 7, 8, 22, 27, 28, 29, 94, 97, 98, 117, 119, 122-123, 1, 5, 59, Table 3, Table 4, 38.1-4, 40.3, 40.5, 40.7-8
- vug 25
- vulcanian eruption (*see also* explosive eruption) 95, 99
- Wadaira Tuff, Japan 108, 45
- welding 3, 15, 22, 28, 30, 102-104
 - in pyroclastic flow deposits 102-104, 106-107, 24, 25, 26.1, 26.3-5, 27, 28.2
- woody pumice 27
- xenocryst 21